NASA Contractor Report 3603

Crashworthy Airframe Design Concepts
Fabrication and Testing

J. D. Cronkhite and V. L. Berry

CONTRACT NAS1-14890
SEPTEMBER 1982

NASA

NASA Contractor Report 3603

Crashworthy Airframe Design Concepts
Fabrication and Testing

J. D. Cronkhite and V. L. Berry
Bell Helicopter Textron, Inc.
Fort Worth, Texas

Prepared for
Langley Research Center
under Contract NAS1-14890

National Aeronautics
and Space Administration

**Scientific and Technical
Information Branch**

1982

CONTENTS

ILLUSTRATIONS

ILLUSTRATIONS (Continued)

ILLUSTRATIONS (Concluded)

1. FOREWORD

Bell Helicopter Textron (BHT), Fort Worth, Texas, prepared this report, "Crashworthy Airframe Design Concepts Fabrication and Testing", for the National Aeronautics and Space Administration, Langley Research Center, Hampton, Virginia, under contract NAS1-14890. Mr. Huey D. Carden was the contracting officer's technical representative and also directed the static and dynamic testing done by NASA.

Technical tasks in this program were conducted under the direction of Mr. James D. Cronkhite, BHT Project Engineer. Principal investigators at BHT were:

Design	R. Mort
NASTRAN and KRASH analyses	V. Berry
Stress analysis	T. Haas
Fabrication	Spinks Industries - Ft. Worth, Texas

Those at BHT wish to express their appreciation of Mr. Carden's assistance and support in the performance of this work and especially in the conduct of the static and dynamic testing at NASA.

2. SUMMARY

The results of a research program directed toward the investigation of crashworthy concepts applicable to metal airframe structures of general aviation aircraft are discussed. The program consisted of three phases as follows:

(1) development of concepts
(2) design, fabrication, and testing of full-scale floor sections
(3) modification of full-scale aircraft structure

In the first phase, several crashworthy concepts of energy-absorbing lower fuselage structure were developed and design support tests conducted to determine the performance of the concepts. The five most promising concepts were then selected for the design of full-scale floor sections.

In the second phase, full-scale floor sections were designed that featured a high-strength structural platform supported by crushable underfloor structure. The platform provided structural integrity for the attachment of crashworthy, energy-attenuating seats. The subfloor structure utilized the crashworthy concepts to provide a crush zone for crash impact energy-absorption and load control. Mathematical analyses used to verify the floor section designs included the NASTRAN computer program for the static load conditions and the KRASH computer program for the dynamic crash impact load conditions.

Following the design effort, eighteen floor sections, (three or four sections for each of the five concepts) were fabricated. Static tests were then conducted at NASA Langley Research Center to determine the load-deflection characteristics of each type of concept and dynamic drop tests were done to determine the crash impact response of the floor sections. After evaluation of the floor test results, two concepts were selected for incorporation into a full fuselage.

In phase three, two twin-engine airplane fuselages were modified by incorporating crashworthy floor sections. The modified fuselages will be tested at NASA Langley Research Center in the future and compared with earlier test results of unmodified fuselages.

The results of this research program indicate that several of the crashworthy structure concepts that were investigated may be applicable to future airframe designs of general aviation aircraft.

3. INTRODUCTION

Preventing the occurrence of accidents has been, and probably will continue to be, the number one objective of general aviation manufacturers. However, even with intensive studies of accidents, technological advancements, increased reliability, and improved pilot training, accidents do occur. To reduce the risk of injury and death in an accident, design techniques are being investigated in a joint NASA/FAA program directed toward improving the survivability and crashworthiness of general aviation aircraft.

Crashworthiness is a complex subject involving human tolerance, the crash environment (impact surface, terrain, aircraft velocities and attitudes), seats and restraints, cabin environment, post-crash fire, emergency egress, landing gear, and the airframe structure. In addition, the type of aircraft will affect the crashworthiness design approach. For example, to provide control of decelerative loads of seated occupants in a vertical impact, a different design approach would probably be used for a large transport aircraft compared to a light fixed-wing general aviation aircraft or a helicopter (Fig. 1). The large transport structure having considerable depth of crushable structure may not require energy-absorbing landing gear and seats. On the other hand, light fixed-wing aircraft and helicopters having relatively little crushable airframe structure would require energy absorption in the landing gear and seats, as well as the fuselage structure, to prevent injury to occupants in potentially survivable crashes.

When designing a crashworthy airframe structure, there are many factors to consider (Fig. 2). Of prime importance is the design of the airframe to maintain structural integrity and a livable space for the occupants. Results of accident investigations have shown that a protective structure around the occupant, along with adequate restraint, improves the occupant crash protection in agricultural aerial application airplanes (Ref. 1). The airframe structure should incorporate a high-strength protective shell or cage around the occupants. This structure should provide rollover strength, a strong support structure for restraint of large mass items and seats, as well as maintain the integrity of the normal exits for emergency egress. The forward fuselage structure should be designed to minimize plowing and to absorb energy during longitudinal impacts. In addition, the crushable structure in an aircraft should be dual purpose; that is, it should be designed to carry normal airframe loads as well as absorb as much energy as possible in a crash; otherwise, a weight penalty will be paid. If the seat support structure is allowed to crush, it must maintain enough structural capability to support the seat loads. If the seats are energy-absorbing, the crushing structure must not interfere with the stroking seats.

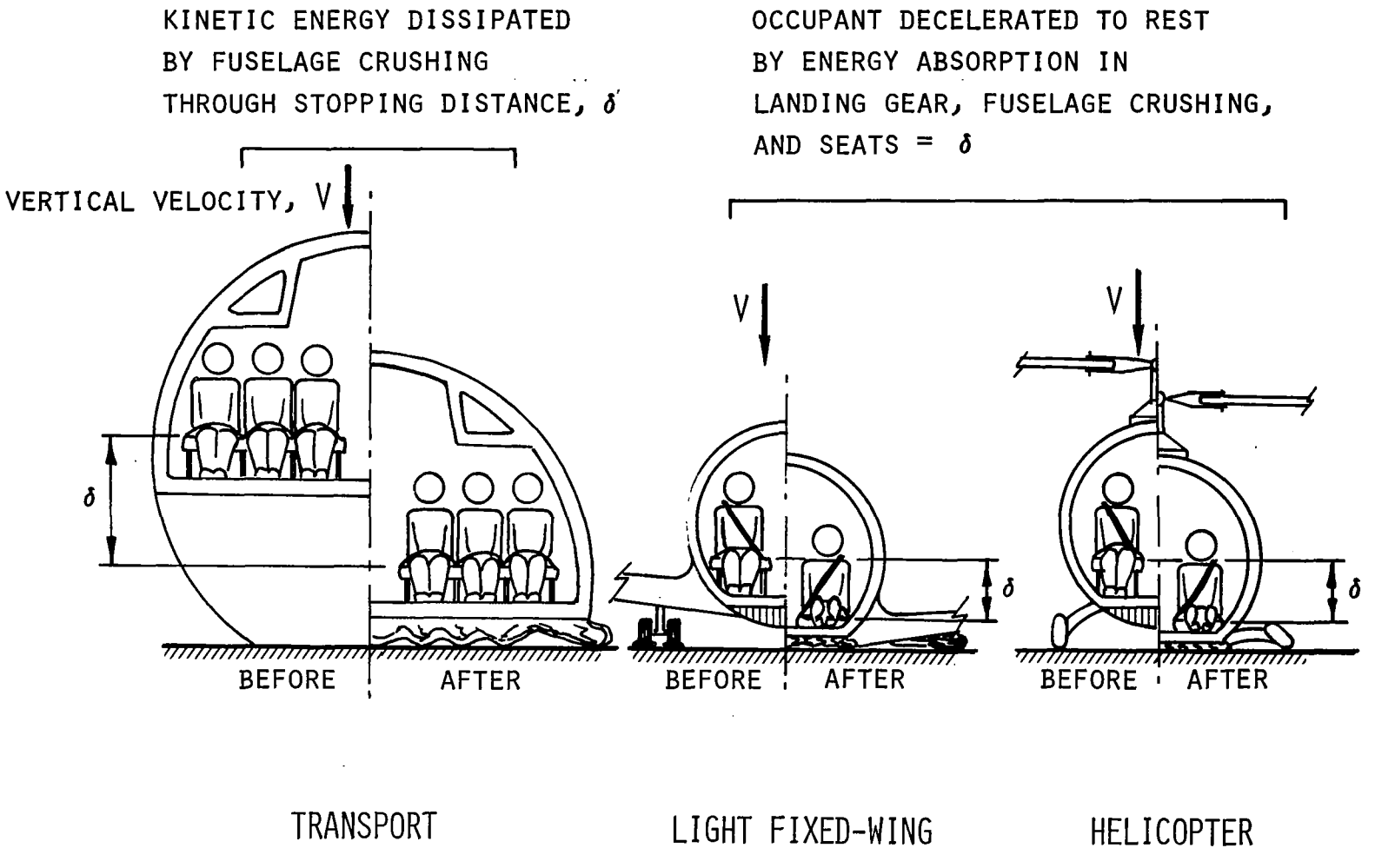

Figure 1. Crash energy absorption design approaches for various types of aircraft.

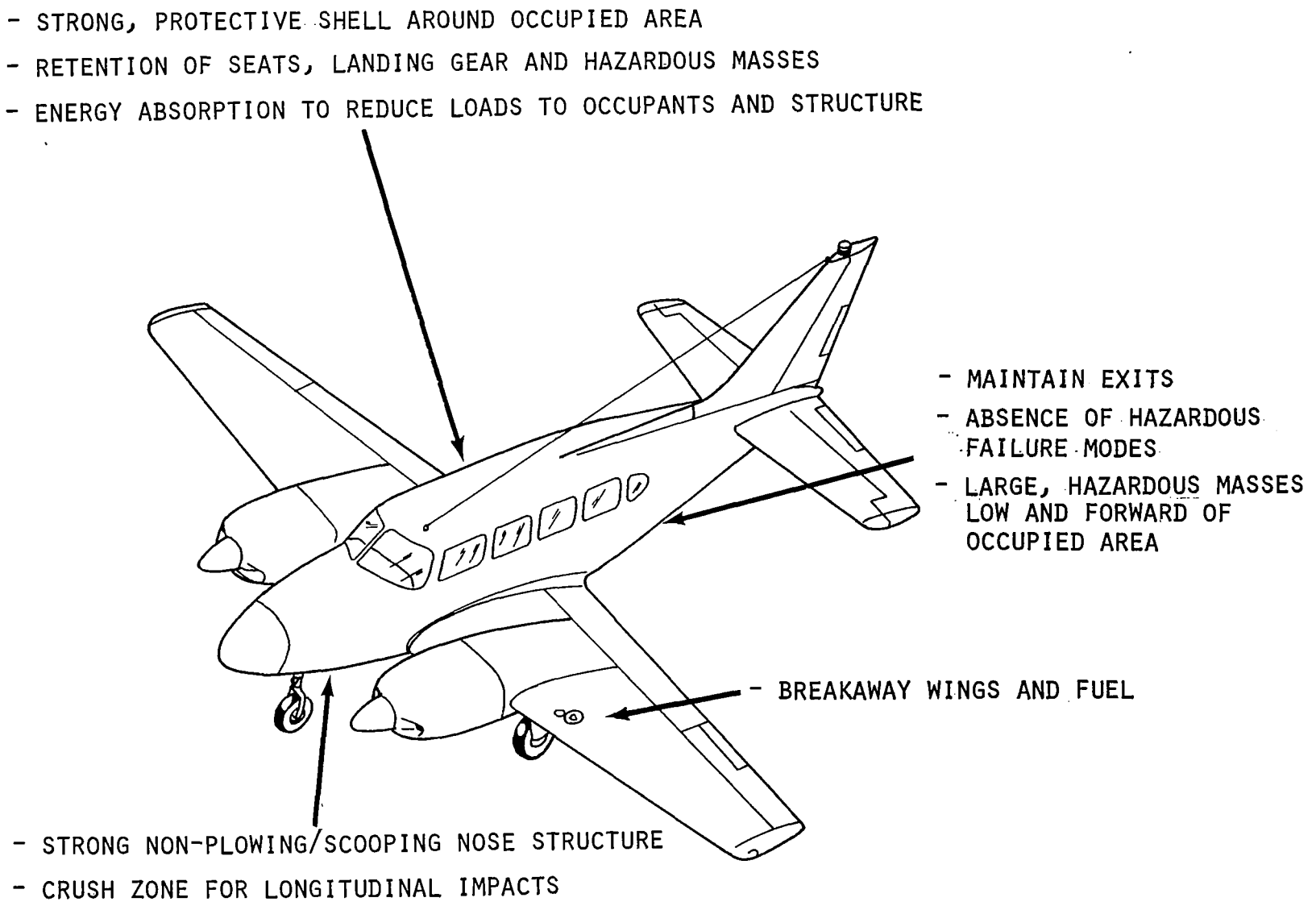

Figure 2. Airframe structure crashworthiness design considerations.

At NASA-Langley Research Center, full-scale testing of light fixed-wing aircraft is being conducted to study the crash-worthiness of airframe structures and seating systems (Ref. 2). NASA observed that for some of the tests that resulted in high vertical floor loading, severe floor distortions and loss of integrity of the airframe structure occurred such as shown in Fig. 3. Similar results have been observed in actual crashes with high vertical floor loading combined with longitudinal loads as shown in Figs. 4(a) and (b). The interior view of the airplane reveals that the floor is wavy and separated, seat rails are broken, and floor structure is crumpled under the front seat legs. The intersections of the longitudinal keel beams and the lateral bulkheads formed "hard points" of stiff columns that did not allow crushing of the subfloor structure.

To study the airframe structure in more detail, NASA conducted drop tests of smaller fuselage sections (Fig. 5) with loading from seats and dummies. This report describes the development of test floor sections compatible with the NASA section that would improve the floor structural integrity and energy-absorption of the fuselage in a crash. The results of NASA's static and dynamic tests of the floor sections are described in a paper by Carden and Hayduk (Ref. 3).

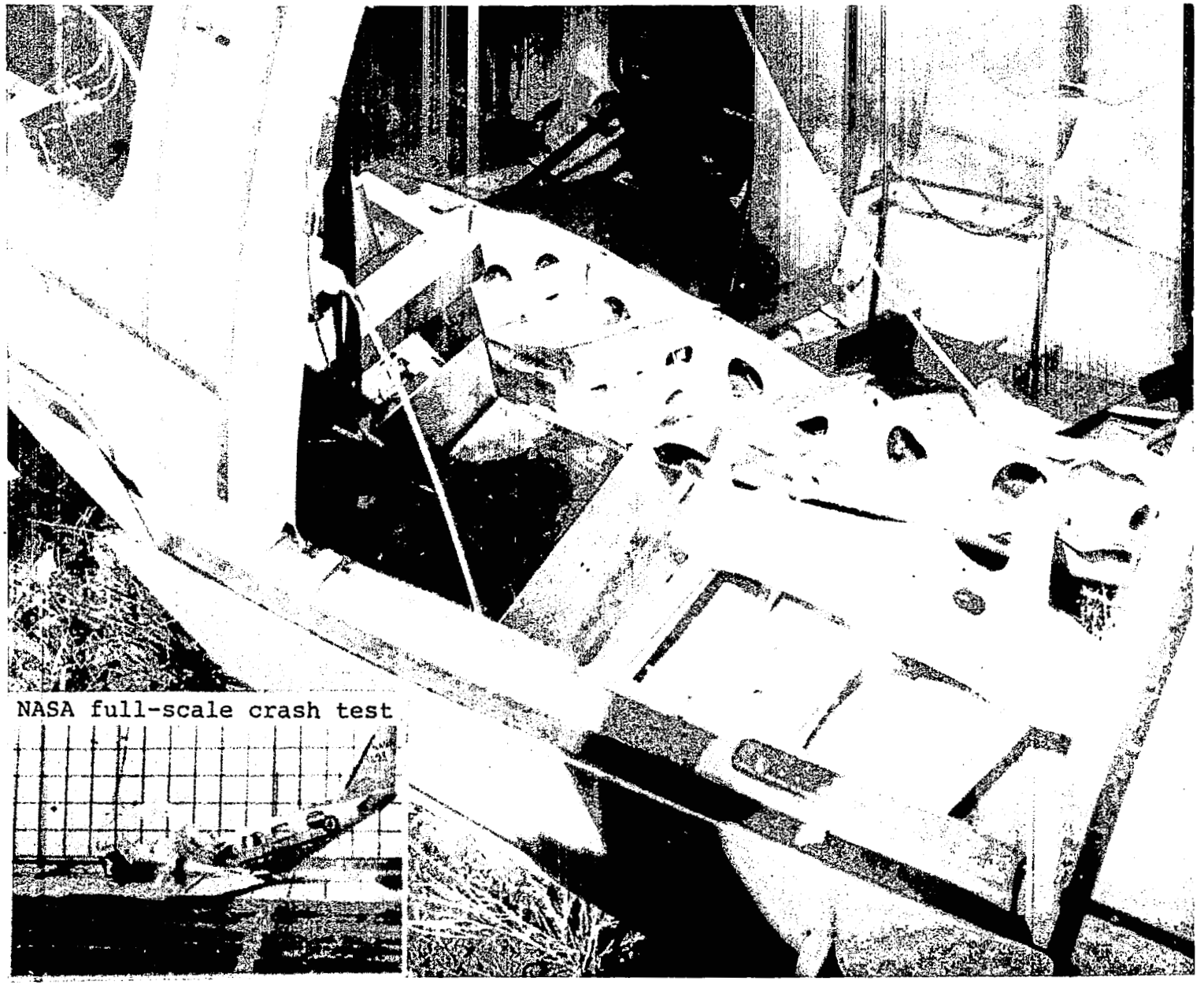

Figure 3. Floor damage in twin-engine aircraft tested at NASA-Langley.

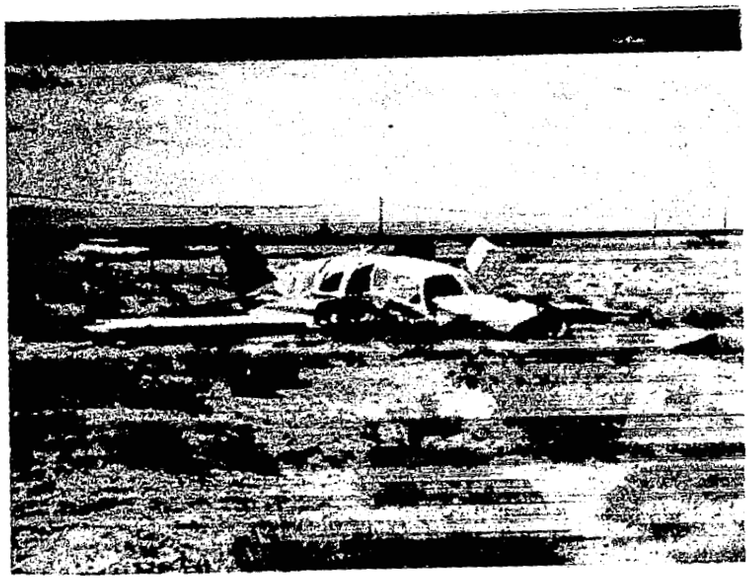

(a) Exterior view

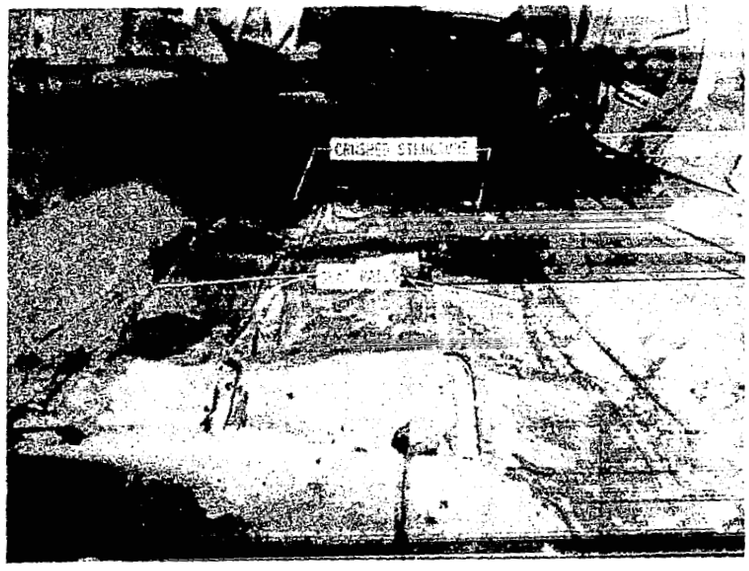

(b) Interior view

Figure 4. Post-crash condition of a twin-engine airplane.

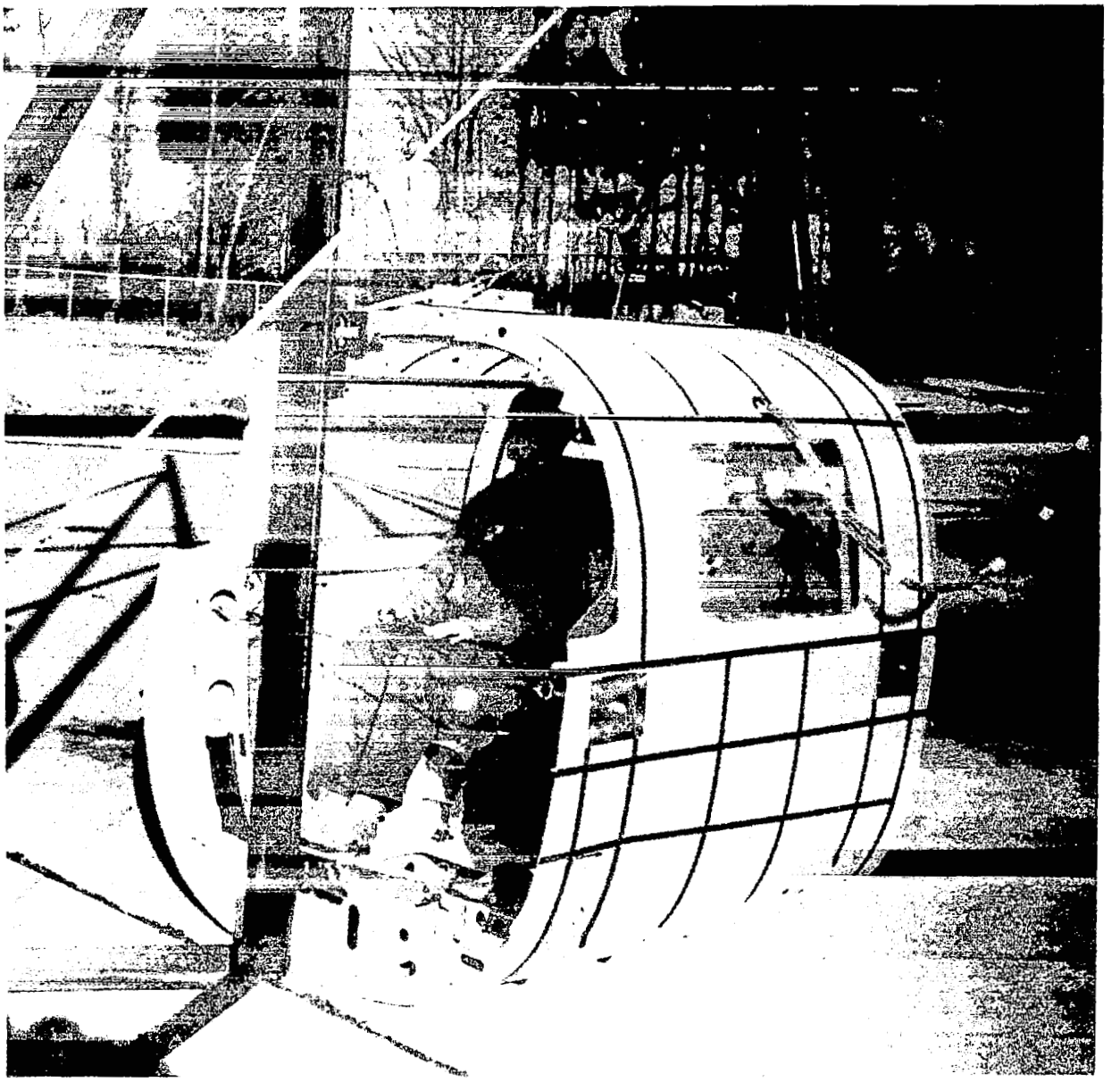

Figure 5. NASA fuselage test section.

4. DEVELOPMENT OF CONCEPTS

4.1 TEST SECTION DESCRIPTION AND DESIGN PHILOSOPHY

The primary objective of the study was to develop crashworthy design concepts suitable for the floor sections of light aircraft such as the twin-engine airplanes being tested at NASA. The floor structure of the NASA fuselage test section (Fig. 5) was used as a basis for the design of the crashworthy floor sections and is shown in Fig. 6 with floor panels removed for clarity. The structure consists of twin longitudinal keel beams about 39 cm (15.5 in.) apart with a depth of about 20 cm (8 in.) and lateral bulkheads spaced between 20 cm (8 in.) and 30.5 cm (12 in.) apart. There are two rows of seat tracks each spaced about 28 cm (11 in.) apart.

The strengths of the floor and the seat tracks were increased to be compatible with floor-mounted crashworthy seats that NASA was developing (Ref. 2). The primary emphasis in designing the floor structure was to ensure that structural integrity was maintained so that the seats and occupants would be retained and a protective shell would be provided in a crash. This would prevent severe floor damage such as that shown in Figs. 3 and 4(b). Floor damage with loss of structural integrity may result in the seats coming loose during a crash, subjecting the occupants to secondary impact with the structure that could result in major injuries or fatalities.

The general design philosophy chosen for the floor sections is shown in Fig. 7 and consists of a strong structural floor with a crush zone underneath. The structural floor is a 5 cm (2 in.) deep platform designed to carry loads and moments imposed by the seat/occupant and to maintain seat-to-structure integrity without breaking up, heaving, or decreasing the cabin volume. The energy-absorbing subfloor or crush zone, which is about 15.2 cm (6 in.) deep, is designed to distribute the loads to the upper floor as uniformly as possible and to collapse in a controlled manner to absorb as much impact energy as possible at or near human tolerance levels.

When designing the crush zone, it is important that the crushing load developed during a crash not exceed the structural capability yet be sufficiently high so that maximum energy is absorbed. As shown in Fig. 7, the load-deflection curve for a conventional structure is generally characterized by a high peak load that will tend to heave up and destroy the floor structural integrity.

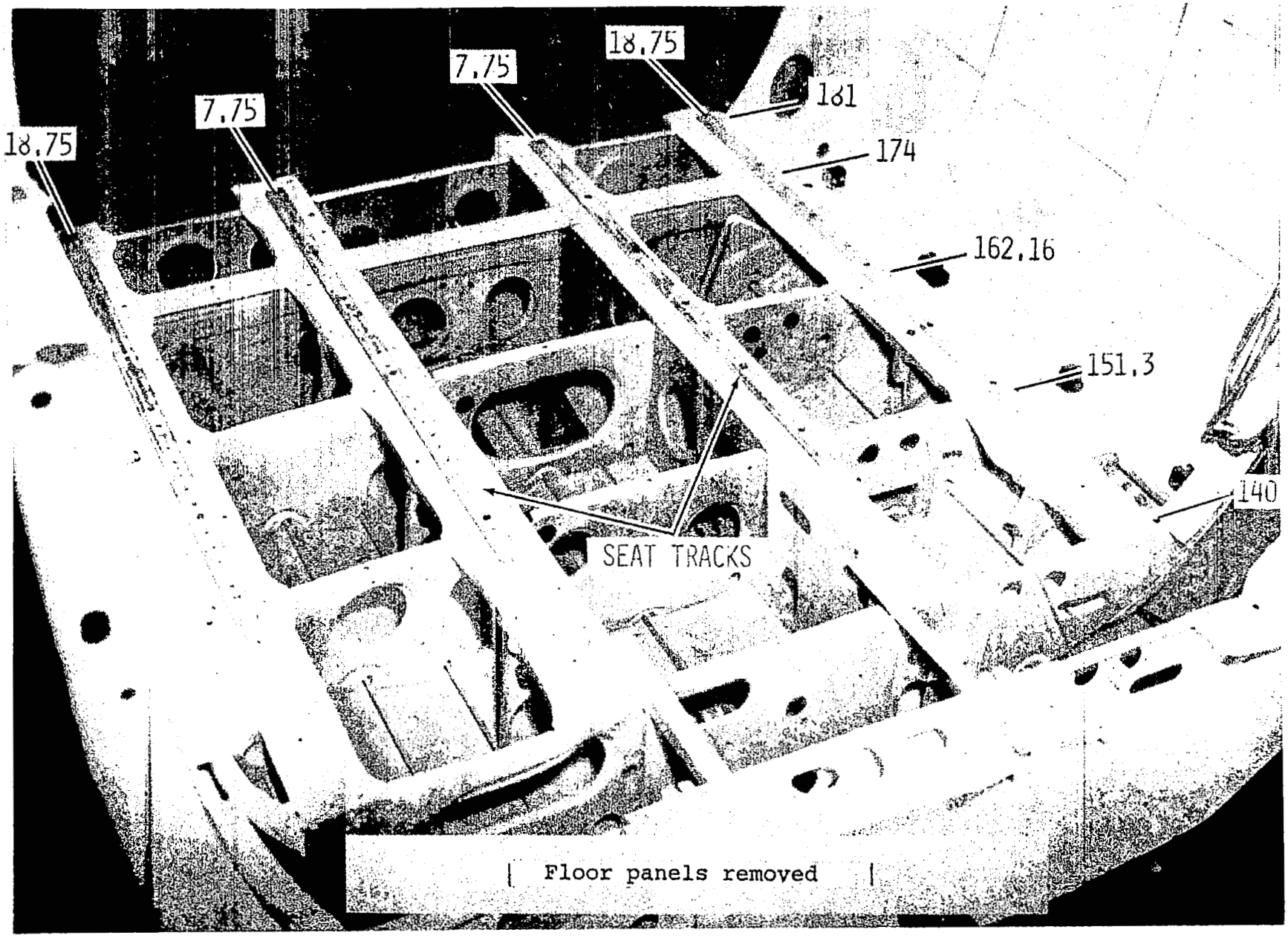

Figure 6. Floor of NASA fuselage test.

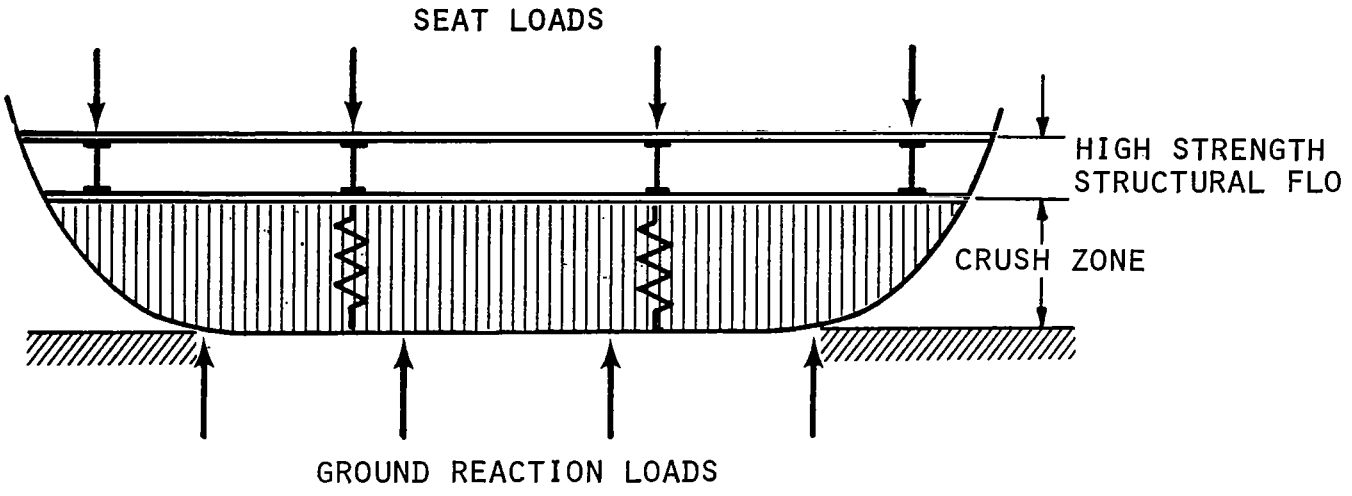

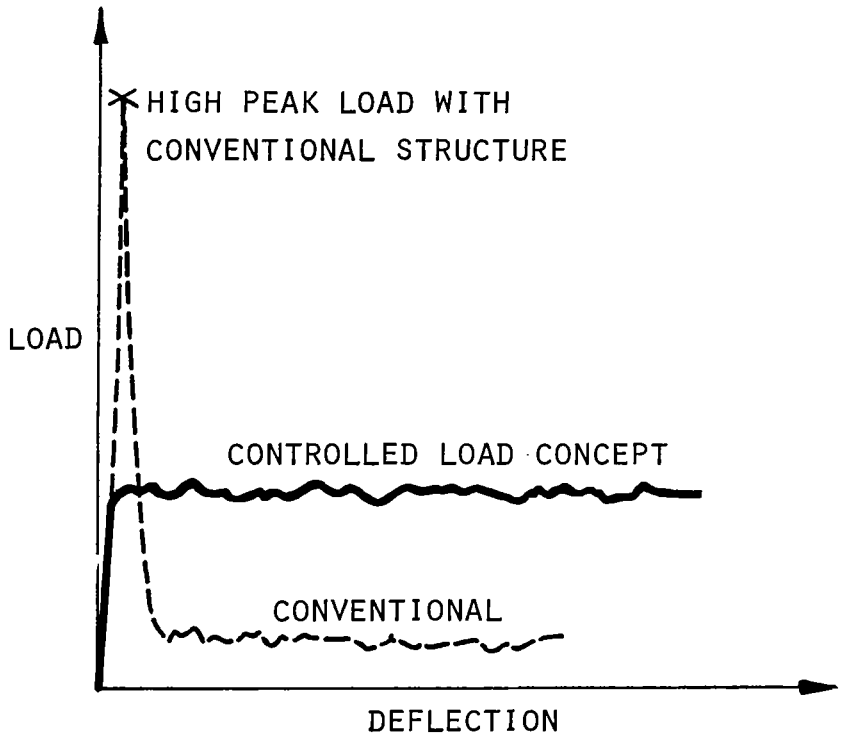

CRUSH ZONE LOAD-DEFLECTION CHARACTERISTICS

Figure 7. Lower fuselage design philosophy.

The high peak load is followed by a sharp drop in load, normally following a stability failure; this results in low energy absorption (area under the load-deflection curve). On the other hand, the ideal crush would have a controlled peak load that is within the capability of the structural floor and is rectangular-shaped for maximum energy absorption as shown by the "controlled load concept" curve.

As previously mentioned, crash impact loads on the occupant are controlled to within human tolerance by energy absorption in the seats, fuselage structure and landing gear (Fig. 1). Often, for aircraft impacts at highly oblique angle attitudes or on rough or soft terrain, the landing gear may fail, leaving the fuselage structure and seat to absorb the kinetic energy and to control the g-loads (forces normalized by the gravitational constant) on the occupants. Since the decelerative g-loads on the occupant are inversely proportional to the stopping distance, a reinforced structure designed to minimize structural deformations will result in increasing g-loads on the structure and occupants. Thus, the structure should be designed to have a zone that is intended to be crushed. This deformation should be restricted to areas outside the livable volume, and it should be controlled.

Although the work described herein deals primarily with future metal airframe designs, future airframes constructed of composite materials deserve special attention. When considering the application of composites to a crashworthy airframe structure, it is known that these materials generally exhibit a low strain-to-failure characteristic behavior compared to metals. Ductile metals, such as 2024 aluminum, can tolerate rather large strains, deform plastically, and absorb considerable energy without fracture or separation. Because of this low strain-to-failure characteristic of composites, energy absorption will probably not come through an inherent stress-strain behavior as it can with metals, but rather through innovative design configurations. These configurations will provide for energy absorption and force attenuation by other means; for example, the protective structural shell can be surrounded by a crushable material such as foam, honeycomb, or a crushable composite concept. The crushable material in the lower fuselage should be designed to attenuate crash forces, absorb and dissipate energy, and distribute loads to the stronger primary structural shell. Some energy-absorbing concepts that can be applied to the lower fuselage structure of composite structures have been described by Cronkhite, et. al. (Ref. 4). However, work on crashworthy composite structures deserves further study.

4.2 ENERGY-ABSORBING SUBFLOOR CONCEPTS

Several energy-absorbing crush zone concepts were considered in this investigation. A good example of a crush zone design approach is presented in the Army Crash Survival Design Guide (Ref. 5), and is shown in Fig. 8. More conventional concepts such as honeycomb, foam, closed cells with orifices, etc., were also evaluated. However, material deformation concepts that utilized the existing structure required for flight and landing loads were considered the most attractive since redundant weight would be minimized.

Besides energy absorption, there are several practical design considerations for the subfloor concepts. First, the concept should be multipurpose (used for airframe strength and stiffness as well as energy absorption) so that the weight penalty would be minimized. In addition, room for routing controls, wiring, and plumbing should be available. Furthermore, the concept should perform well under combined loading with various aircraft pitch and roll attitudes at impact while maintaining a protective shell and reacting concentrated loads from seats and large masses. Finally, the concepts should be practical from a cost/producibility standpoint.

After reviewing available energy-absorbing concepts and considering their incorporation into a fuselage structure, five concepts were initially selected. (Note that these were not the final five concepts that were fabricated.) The five concepts are shown in Fig. 9. From left to right, the concepts shown in the figure are described as follows:

1. Formable Keel Web - This concept absorbs energy by plastic forming of the keel beam web similar to that shown in Fig. 8.
2. Corrugated Sandwich Web - This concept absorbs energy by deforming preformed corrugated webs plus crushing of the foam filler.
3. Corrugated Web/Notched Corners/Foam - This concept absorbs energy primarily by crushing foam and has structurally tailored notched corners to reduce load spikes at the intersections of longitudinal keel beams and lateral bulkheads.
4. Corrugated Half-Shell - This concept absorbs energy by bending deformation of a curved corrugated shell.
5. Foam-Filled Cylinder - This concept absorbs energy by crushing foam with the cylinder walls needed primarily for web shear strength.

Note that many of these concepts used foam that was later discarded because it was mostly add-on weight and relatively heavy compared to metal-forming concepts.

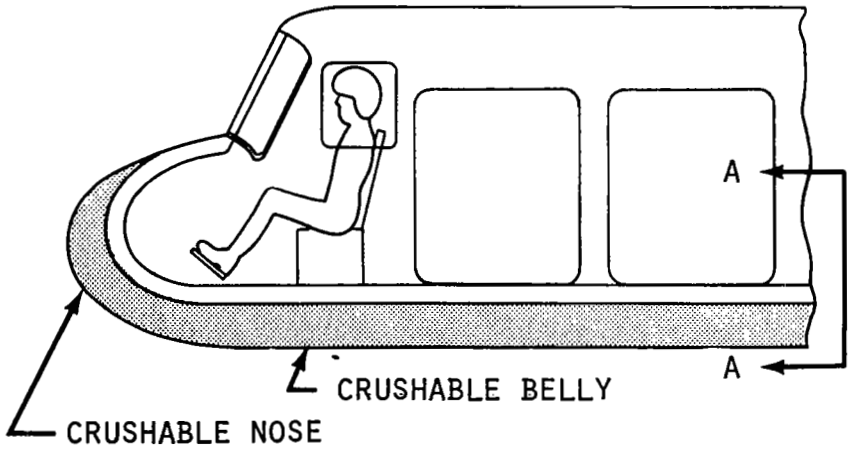

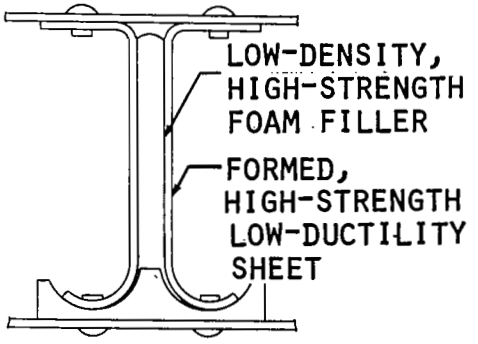

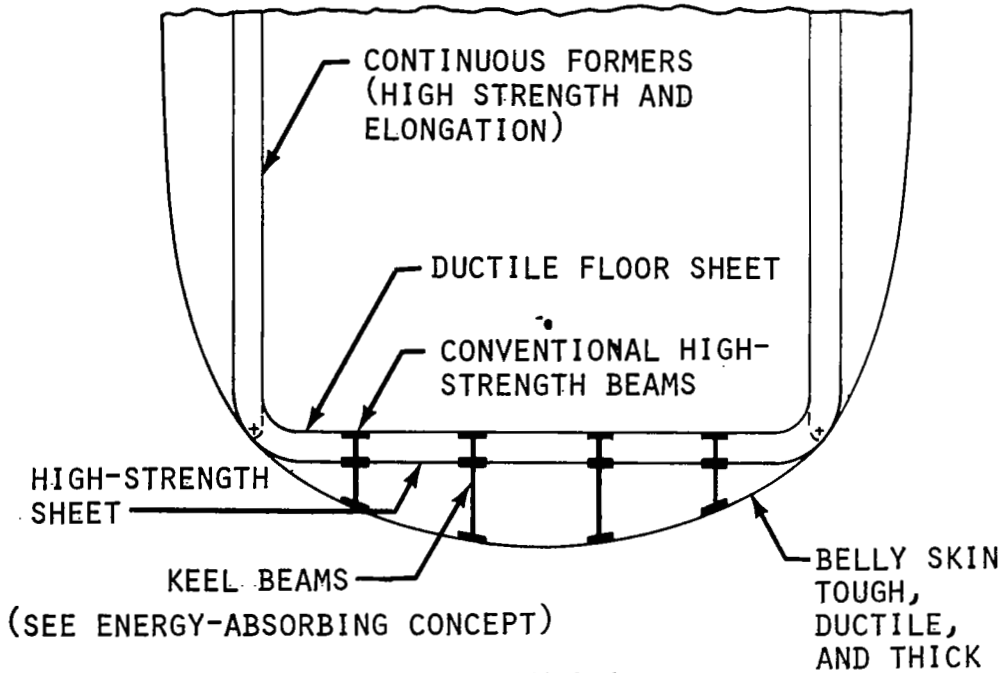

VIEW A-A

ENERGY-ABSORBING KEEL BEAM CONCEPT

Figure 8. Fuselage structure energy-absorbing concept for Army helicopter (Ref. 5).

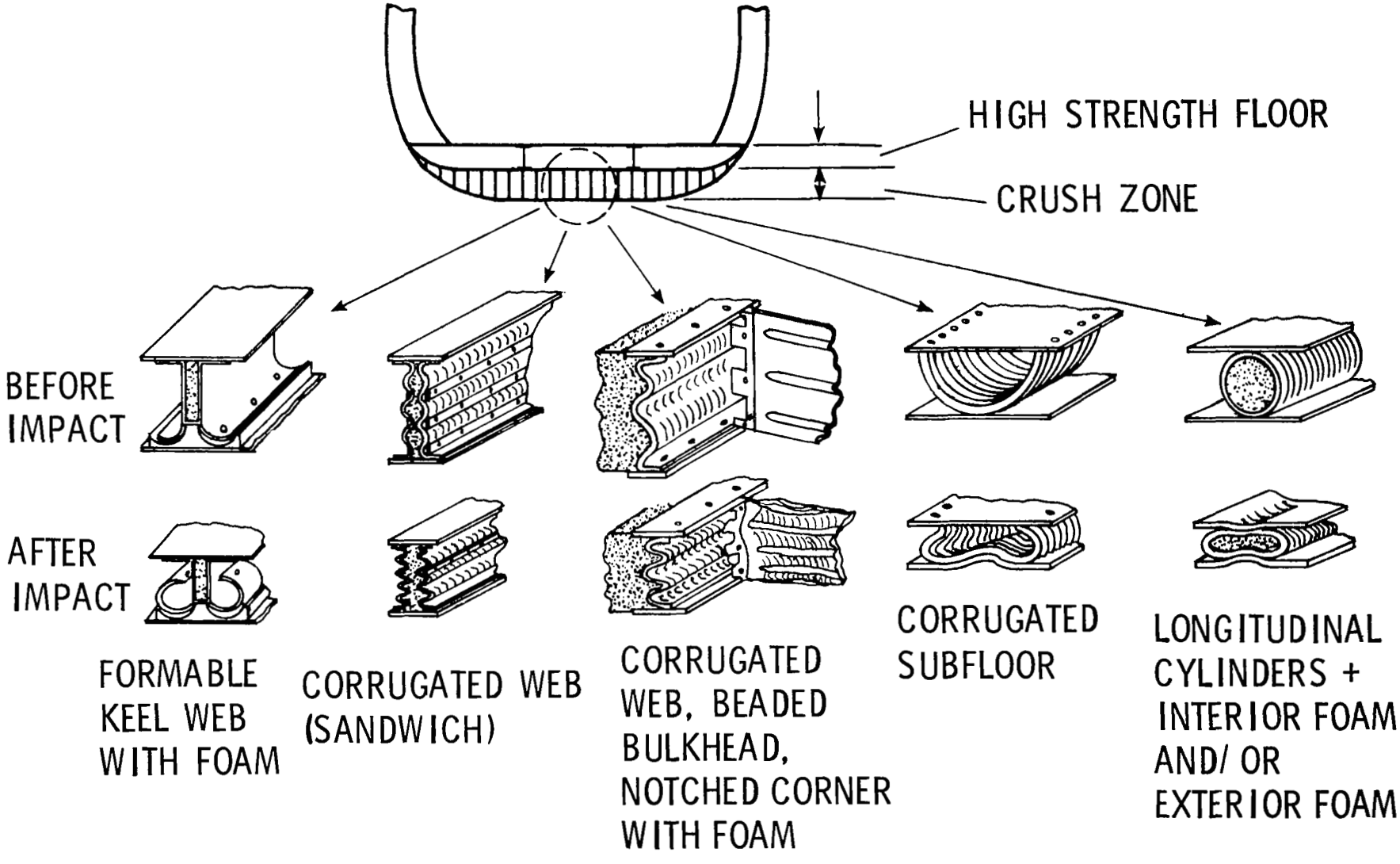

Figure 9. Lower fuselage load-limiting, energy-absorbing concepts.

For most of the subfloor concepts, design data such as load-deflection were not available so that design support testing was required to develop the concepts further.

4.3 DESIGN SUPPORT TESTING

Design data for the various energy-absorbing concepts were developed by static and dynamic compression testing in order to provide load-deflection data and evaluate the effect of rate of loading. By varying some critical parameters such as thickness, geometry, bend radius, etc., a set of data could be generated from which a designer could size the energy absorber to give the desired stroking load.

Initially, one might attempt to design the crushing structure stroking load at 14.5 g's, the vertical stroking load that has been widely accepted for attenuating seats (Ref. 5). However, since the floors were designed to be drop tested at approximately 9.1 m/sec (30 ft/sec) and there is only 15.2 cm (6 in.) of depth, the ideal g-loading becomes about twice this 14.5 g stroking load. This is quite acceptable since the most important design consideration for the crush zone structure is that the crush loads be controlled to within the strength capability of the structural floor that must react these loads. The vertical g-loads to the occupants are best controlled by the seats while the airframe structure's most important role is to retain the seats so they can function and to maintain a livable volume for the occupants.

Samples of design support test load-deflection data are shown in Fig. 10. A complete set of load-deflection data is presented in Appendix A. Results of the design support tests are summarized in the following paragraphs.

1. Formable Keel Web - Fig. 11 graphically compares the energy absorbed with the formable keel web by varying certain parameters such as bend radius and foam density. The formable keel web performed very well giving a nice flat rectangular load-deflection curve for about 8 cm (3 in.) out of a 13 cm (5.25 in.) length. The poor stroke-to-length ratio was due to the high density foam core that was used. The performance would have been much better had the facesheets been thicker and had the core material been much lower density. This concept was eliminated, however, because the webs could not be fastened with rivets and still be used structurally without creating an initial peak load that was much too high.
2. Corrugated Keel Web - Fig. 12 compares the energy absorbed by the corrugated keel web with two different skin thicknesses. This concept had excellent performance both in rectangular-shaped load deflection and stroke-to-length ratio. The stroking load was relatively low compared to some of the other concepts, but in combination with the required notched corners used

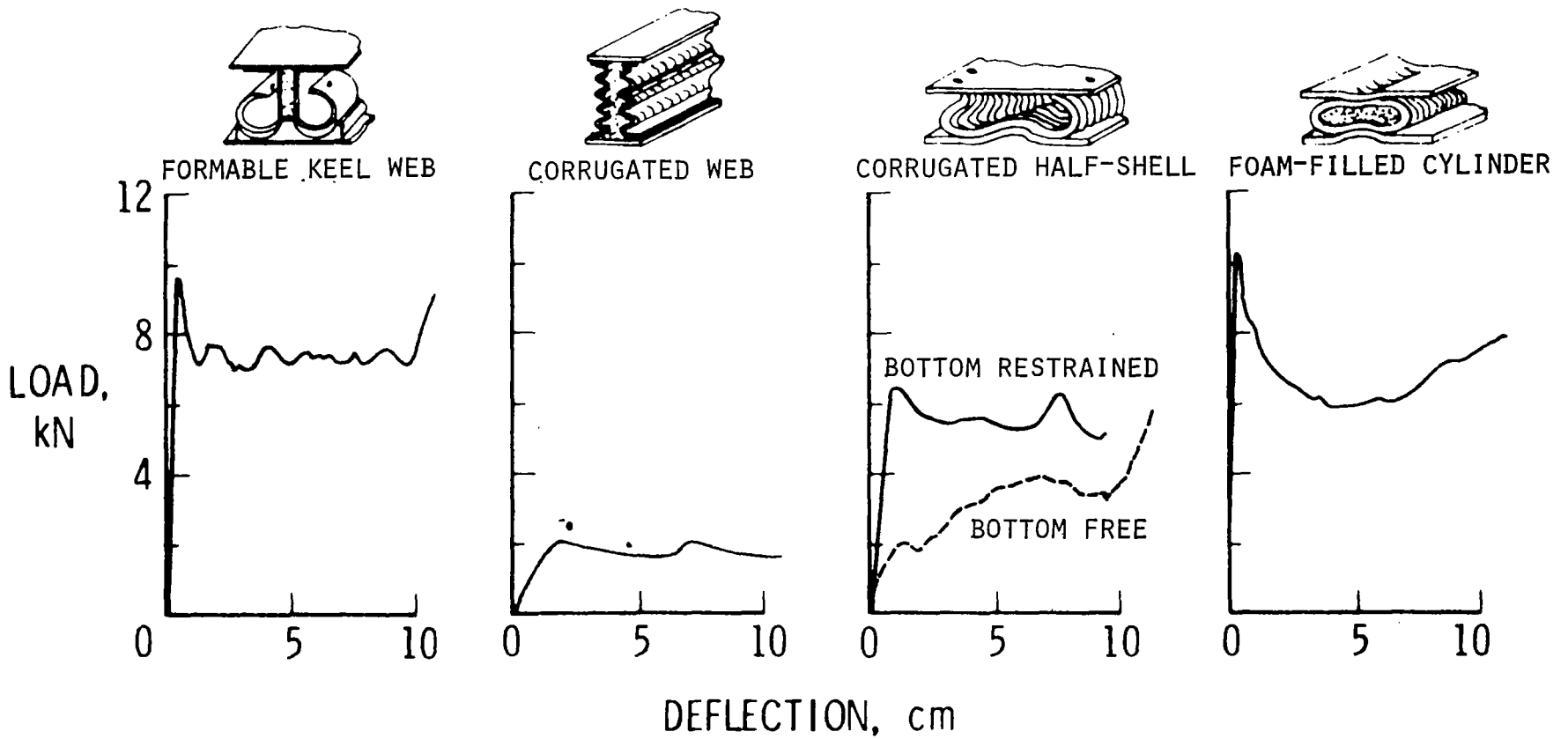

Figure 10. Samples of load-deflection curves from design support tests.

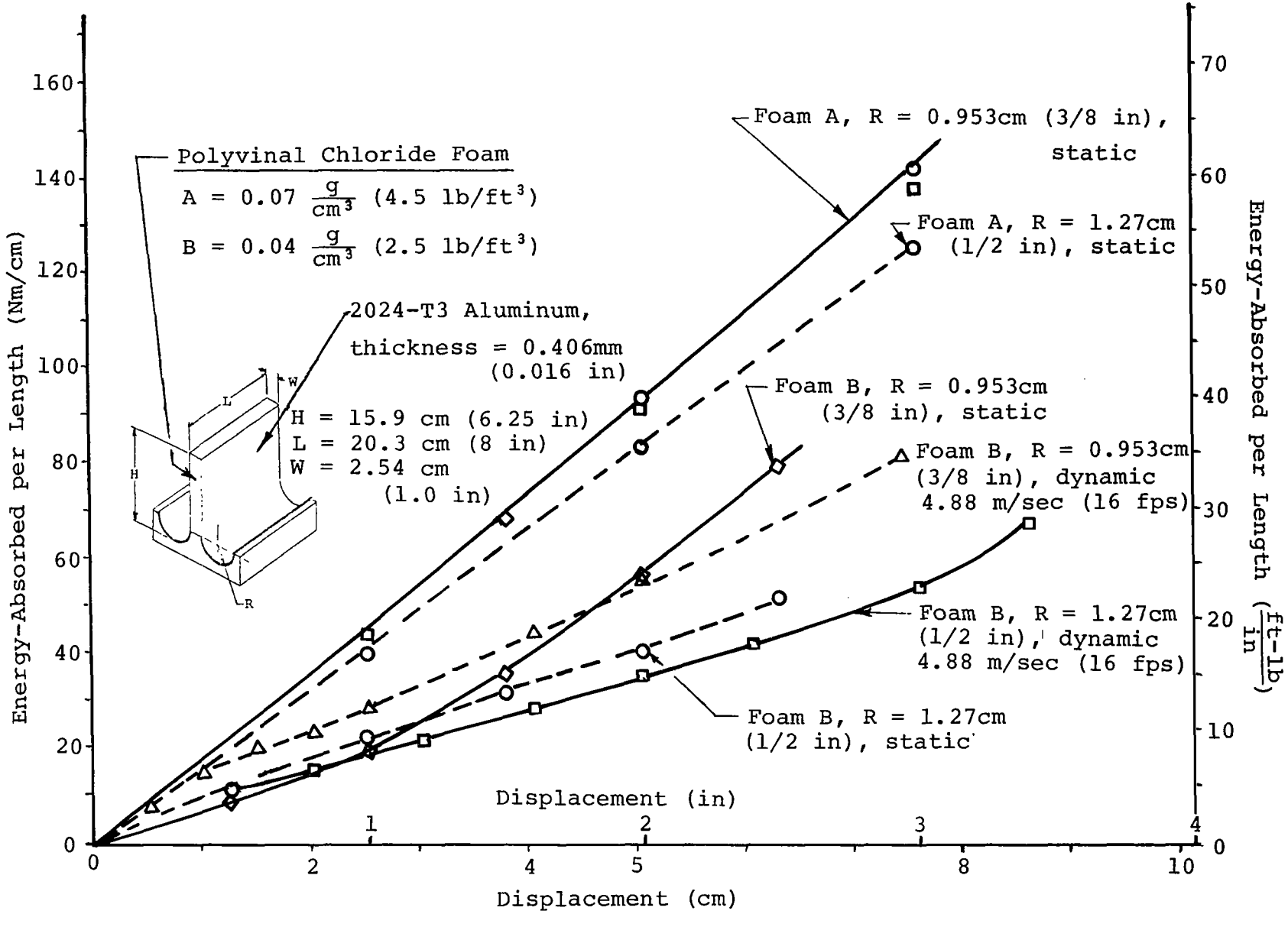

Figure 11. Formable keel web energy-absorption test data.

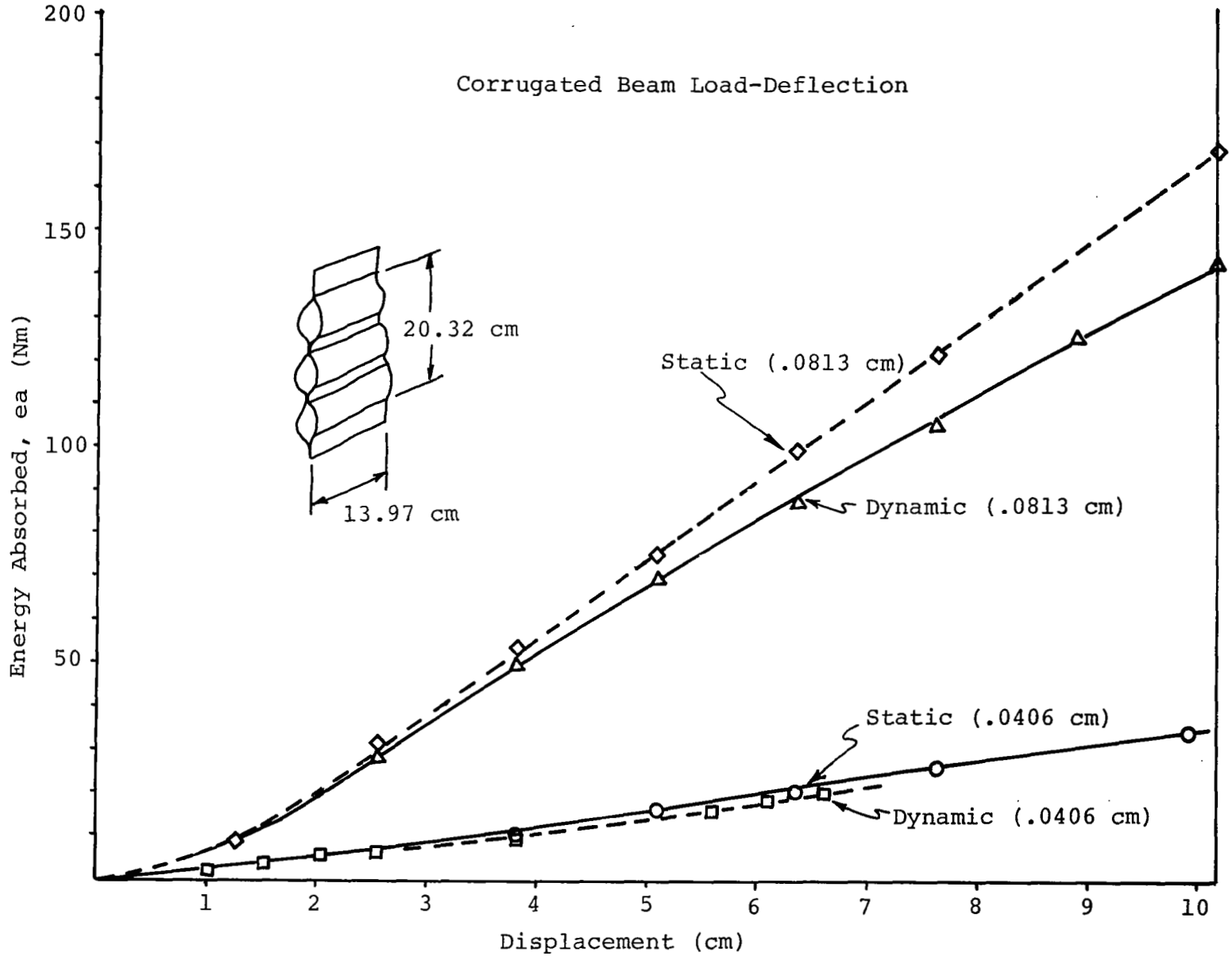

Figure 12. Corrugated keel web energy-absorption test data two different thickness webs.

for attaching the keel beams and bulkheads, the energy absorption was acceptable. Another advantage of the corrugated web concept is that it can be used to carry structural loads while giving low compression loads, making it useful in tailoring with other concepts such as foam or notched corners.

3. Notched Corners - This concept was used to control the crushing load at beam/bulkhead intersections that can be extremely stiff hardpoints and "spear" up through the structural floor if not designed properly. The notched angle serves as shear ties between the keel beam webs and bulkhead webs while having low compression load capability. This concept was used extensively in conjunction with all of the concepts except the corrugated half-shell and the foam-filled cylinders. Fig. 13 compares the energy absorbed for various sheet metal thicknesses utilized in a box with notched corners and in a cruciform with notched corners.
4. Corrugated Half-Shell - This concept exhibits good load control and energy absorption. It loses some efficiency initially by having a relatively low load and then develops a load spike at about 10 cm (4 in.), at which point a fold on the sides of the shell bottoms out on the lower surface of the test machine. When the bottom centerline of the shell is fastened down, the initial load is increased significantly and improves the performance. Fig. 14 relates the energy absorbed to displacement in the corrugated half-shell for both the dynamic and static conditions.
5. Rigid PVC Foam - Rigid Polyvinyl Chloride (PVC) foam was tested at both low -54C and high +74C temperatures because of the concern that temperature would affect the load-deflection characteristics. It was found that for low density foam, temperature had little effect. The energy-absorption was good with about an 80 percent stroke-to-length ratio before bottoming-out occurred. A 0.032 g/cm^3 (2.0 pcf) foam that was tested showed only about a 15 percent increase in load under dynamic loading. However, higher density foams that were tested, 0.056 g/cm^3 (3.5 pcf) and higher, were highly rate sensitive. Fig. 15 shows a comparison of energy absorption for test specimens constructed of .04 gm/cm^3 (2.5 pcf) PVC foam with various thickness Kevlar composite and aluminum tubes. Note that the tubes were hollow with the foam on the outside, whereas the foam would be on the inside of the tube when incorporated into the floor sections.

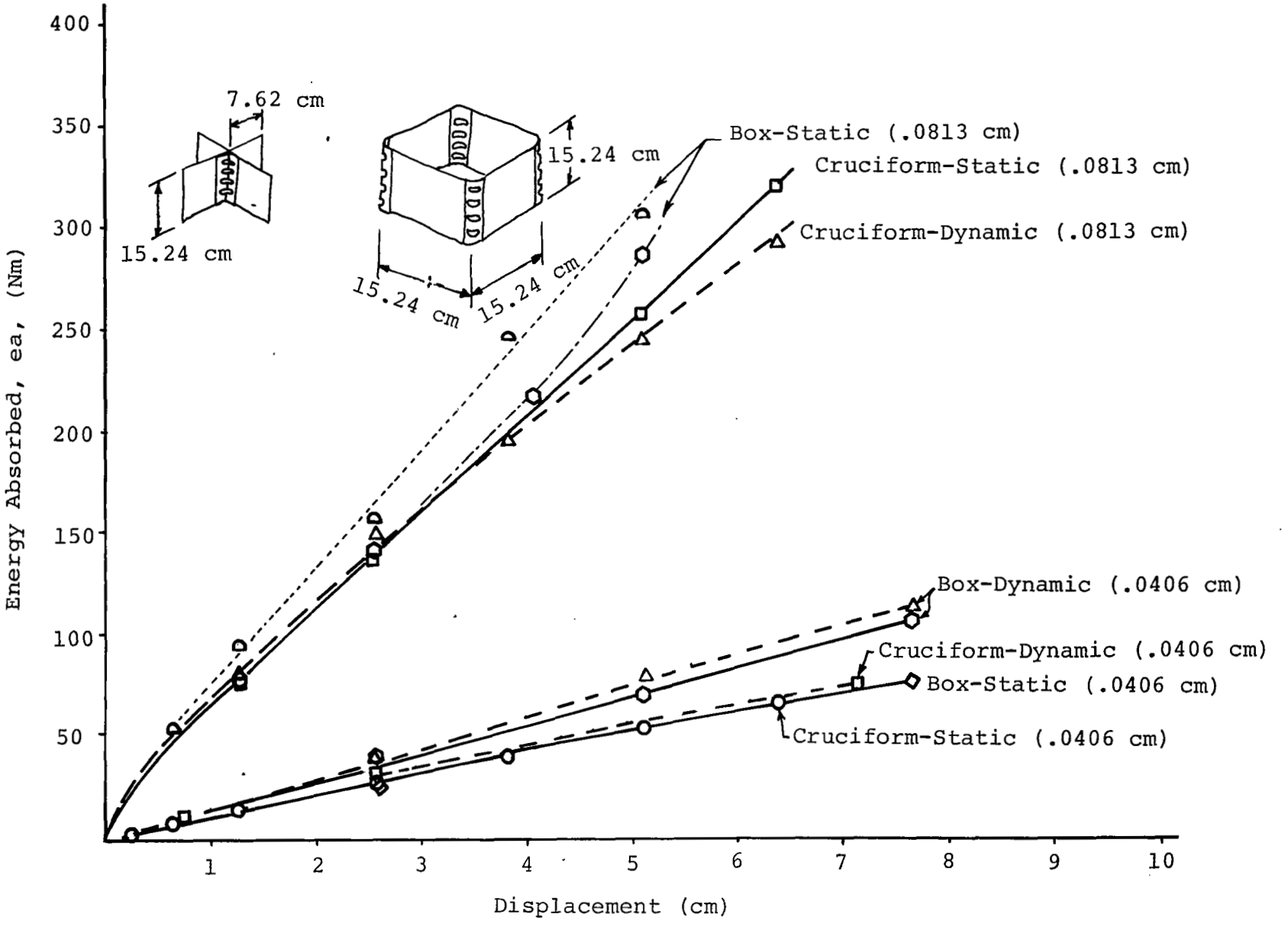

Figure 13. Notched-corner box and cruciform energy-absorption test data two different thicknesses.

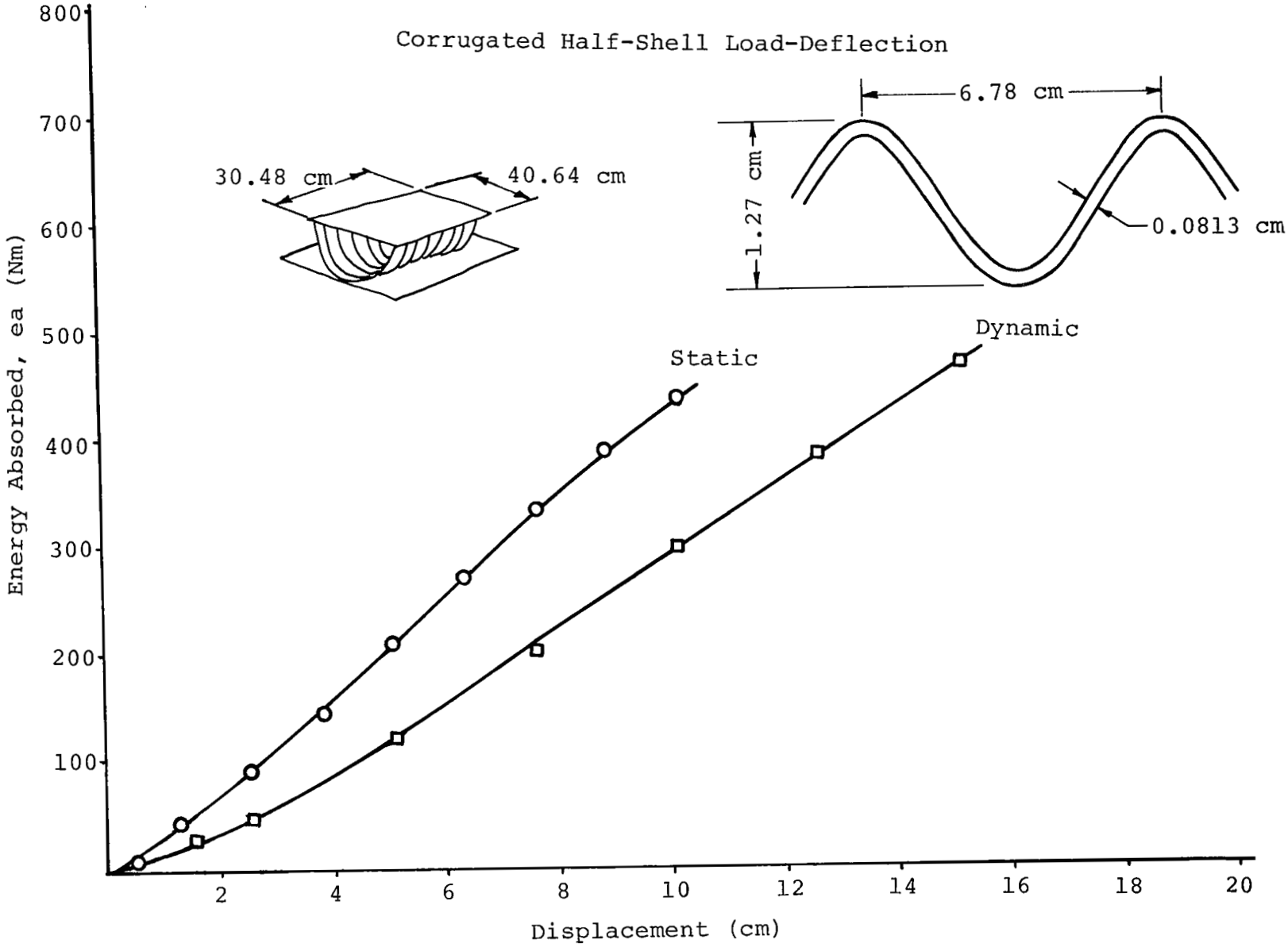

Figure 14. Corrugated half-shell energy-absorption test data.

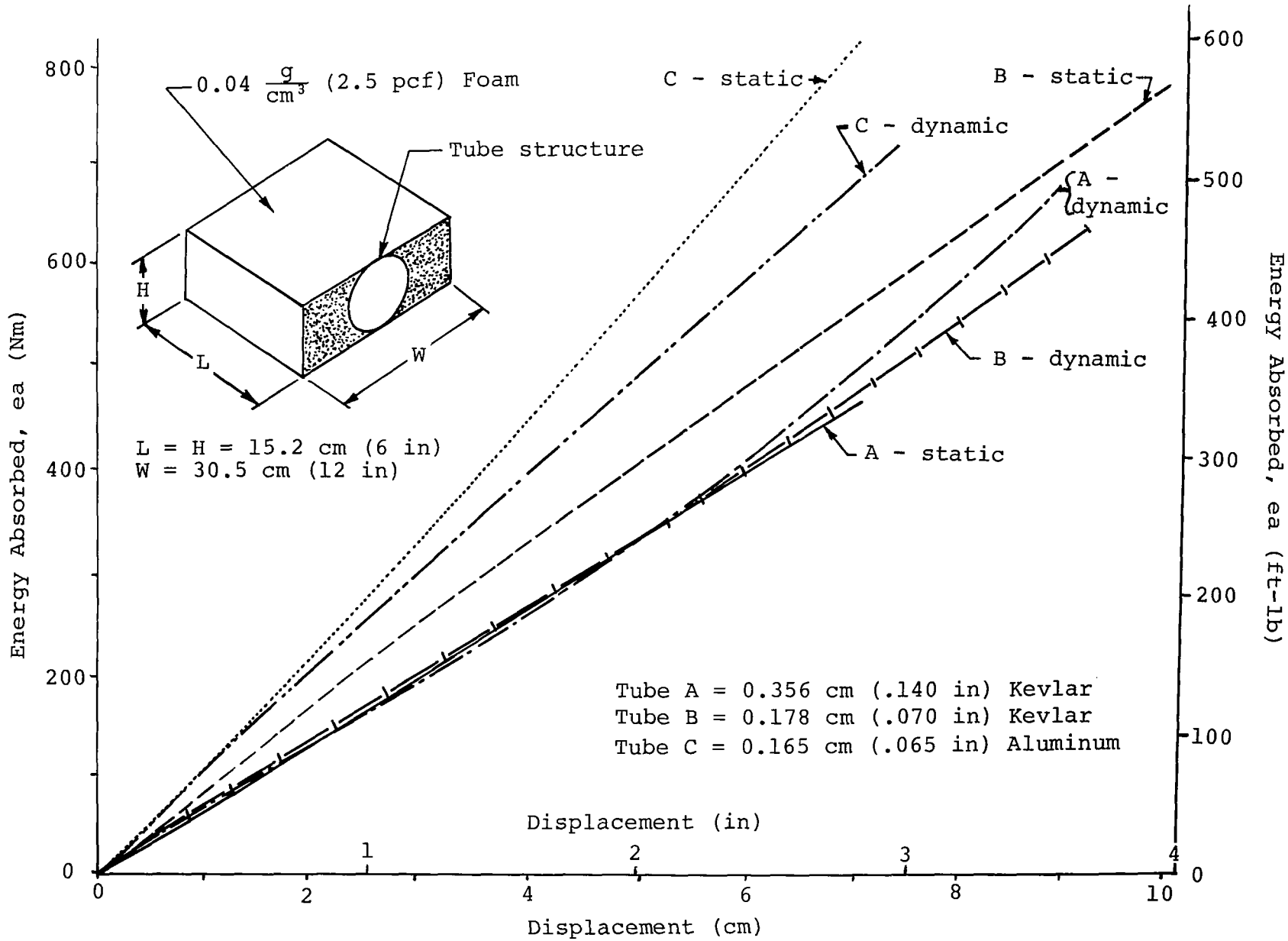

Figure 15. Foam and tube energy-absorption test data.

5. DESIGN, FABRICATION, AND TESTING OF FULL-SCALE FLOOR SECTIONS

5.1 DESIGN CONDITIONS AND ANALYSIS OF FLOOR SECTIONS

The floor sections were designed using the NASTRAN (Ref. 6) and KRASH (Ref. 7) computer programs. NASTRAN was used for sizing the structural floor to react the seat loads, while KRASH was used to evaluate the effects of dynamic loading of the seat on the structure for a vertical drop test condition. The results of the design support testing were used to develop the ground reaction loads for the KRASH analysis.

The seat that was used for design of the floor section was a floor-mounted, stroking seat being developed by NASA and is shown in Fig. 16. The two crash load conditions, 30° nose down pitch and longitudinal, are also shown in Fig. 16. The NASTRAN deformed plots are shown in Fig. 17. Note that on Fig. 17, front view, the ground reaction load from the keel beam located under the inboard seat rail forms a couple with the seat reaction of the outboard rail causing severe bending in the lateral floor member. If the lateral members were made continuous rather than the longitudinal, the lateral members would probably form plastic hinges at beam flange crippling locations, if overloaded, but remain continuous with good residual strength. As will be discussed later, this in fact did happen with some of the sections during NASA's testing (Ref. 3) and was considered a good fail-safe design with adequate residual strength to retain the seats. The static derivation of external loads and structural analysis is found in Appendix B.

The KRASH analysis was used as a check on the NASTRAN static analysis to ensure that the floor structure would be adequate for a dynamic crash impact type of loading. The KRASH model used for the floor section analysis is shown in Fig. 18. The crushable subfloor spring load-deflection data were developed from the design support test data. The floor structure was found to be adequate for a vertical drop since the forward static condition (longitudinal impact) put a more severe loading into the floor than the simulated 9.1 m/sec (30 ft/sec) dynamic drop test condition. A comparison of the response of the seat mass between KRASH and test for a drop test condition with a lumped seat mass is presented in Section 5.6. The KRASH model is documented in Appendix C.

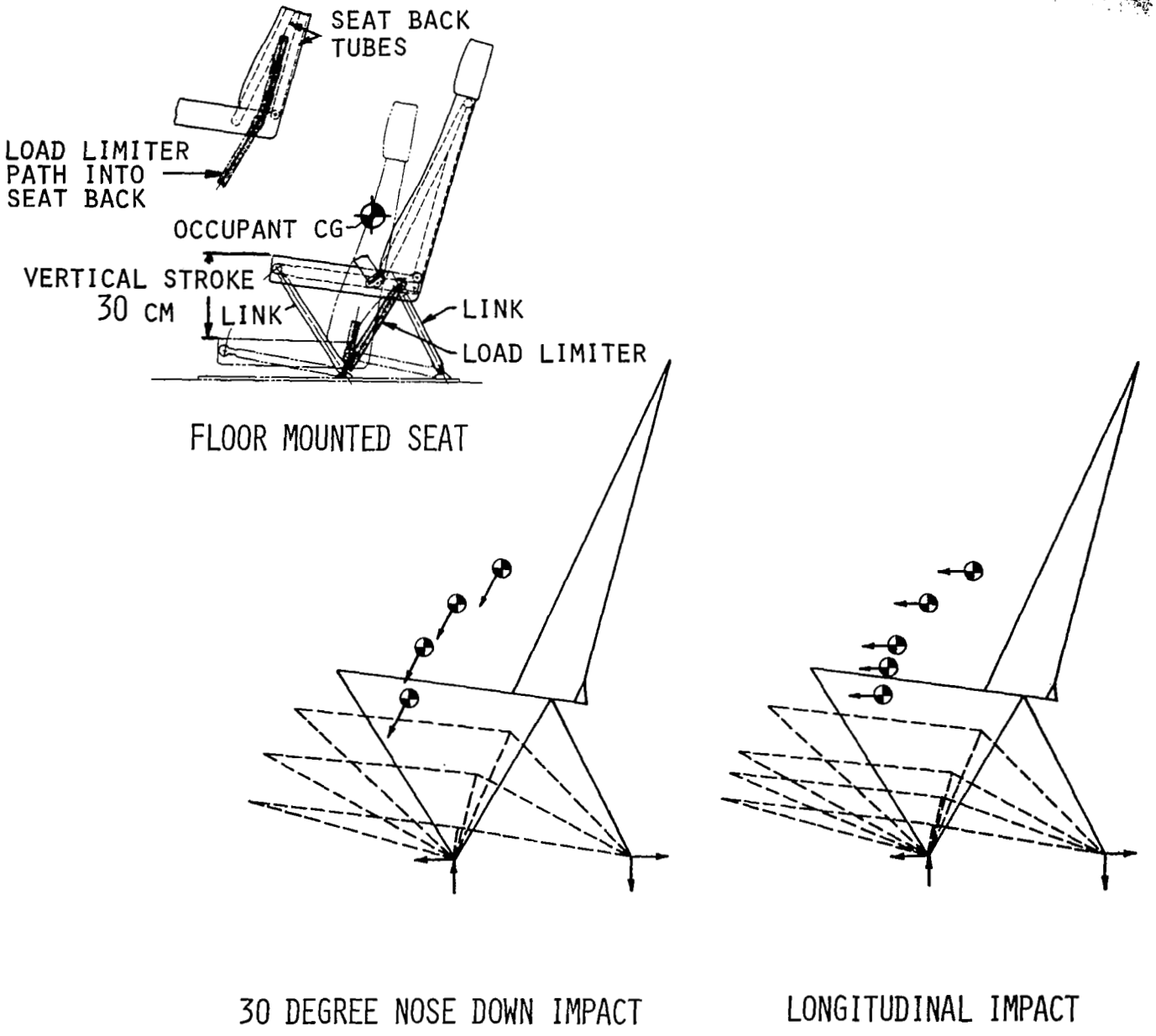

Figure 16. NASA general aviation floor-mounted passenger seat design load conditions.

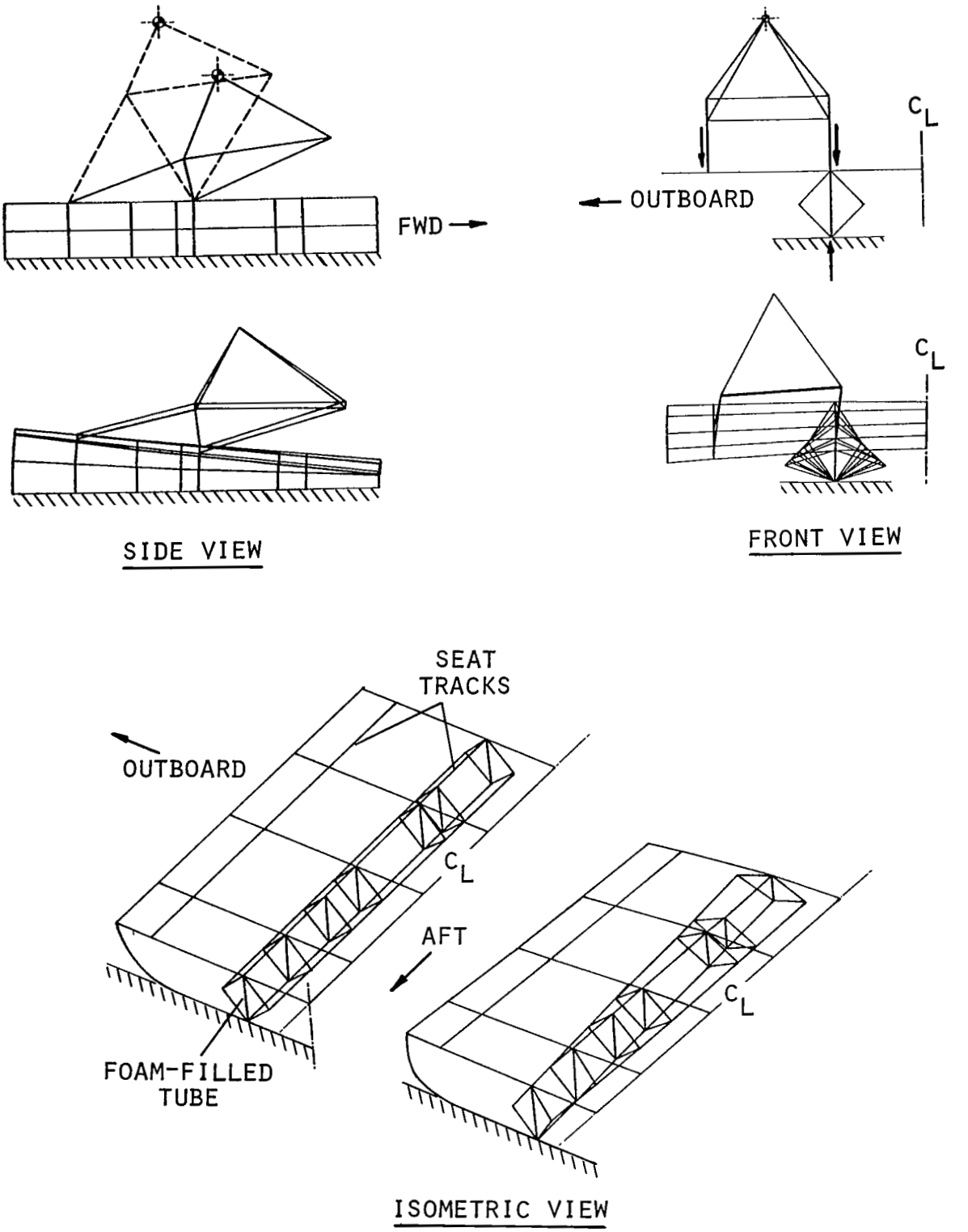

Figure 17. NASTRAN static loads model of floor section and seat, 30° impact condition.

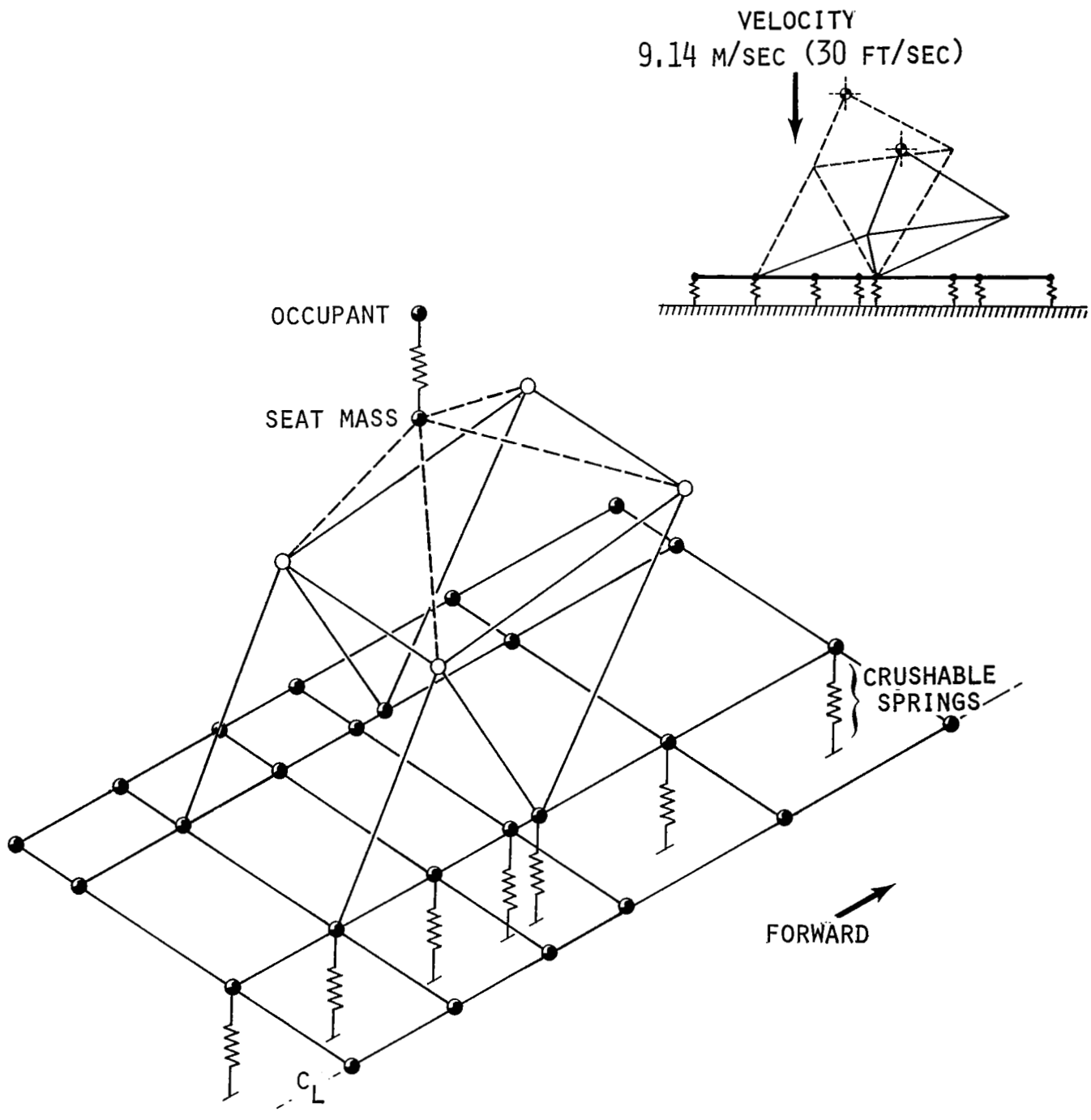

Figure 18. KRASH dynamic model of floor section, vertical drop condition.

5.2 FINAL CONCEPT SELECTION

Design goals for the crashworthy fuselage floor concepts were as follows:

- Control crash impact loads while maintaining an integral structural floor which is needed for seat retention and for providing a protective shell around the occupied area.
- Exhibit rectangular load-deflection characteristics for maximum energy absorption in the crush zone.
- Be lightweight and dual purpose, that is, serving as load-carrying structure under normal design conditions while providing occupant protection and energy absorption under crash impact conditions.
- Be inexpensive and practical for production.

After considering the design goals, the results of the design support testing and the application to an actual aircraft fuselage structure, the following concepts were selected to be incorporated into floor test sections and fabricated (these are shown schematically in Fig. 19):

1. The corrugated web with notched-corner intersections.
2. The corrugated half-shell.
3. Notched corner intersections with conventional webs.
4. The foam-filled cylinder.
5. Canted bulkheads with conventional intersections.

The third and fifth concepts are considered minimum modifications to conventional structures (Fig. 20) while the first, second, and fourth concepts are more unconventional. This section could represent a "minimum modification" to existing construction techniques for floor structure. For example, the addition of an angle near the top of the longitudinal beam (forming a channel with existing flanges) could form a stronger upper structure out of the original floor and be similar to the shallow 5.08 cm (2 inch) platform of the energy absorbing subfloors. The use of notched corners (angles) for attaching the bulkheads with larger flange radius would complete the modification to the load-limiting subfloor lower zone.

The floor section assembly is shown in Figs. 21 and 22. The completed floor sections are shown in Figs. 22(c) and 23. The design drawings are included in Appendix D. The structural floor that was identical for all of the floor test sections is shown in Figs. 21 and 22(a). Note that the lateral structural floor channel members are continuous and the bending continuity of the longitudinal members is provided by the seat tracks above the floor and the straps outboard and energy-absorbing keel beams inboard below the floor. In addition, the belly skin and contour were identical in all five types of sections. The bulkhead

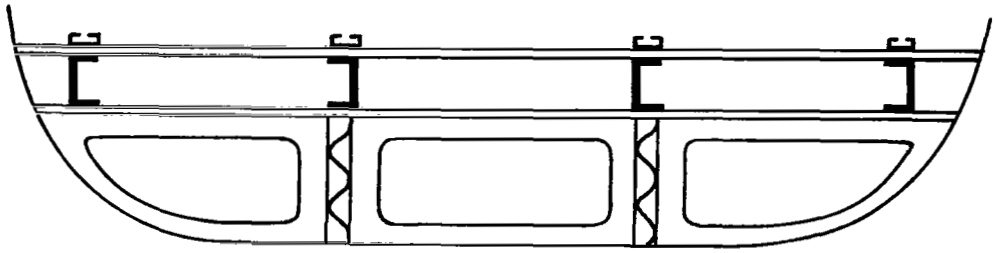

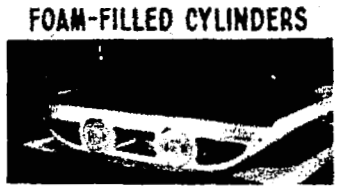

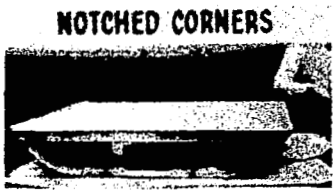

Figure 19. Five energy-absorbing subfloor concepts selected for fabrication.

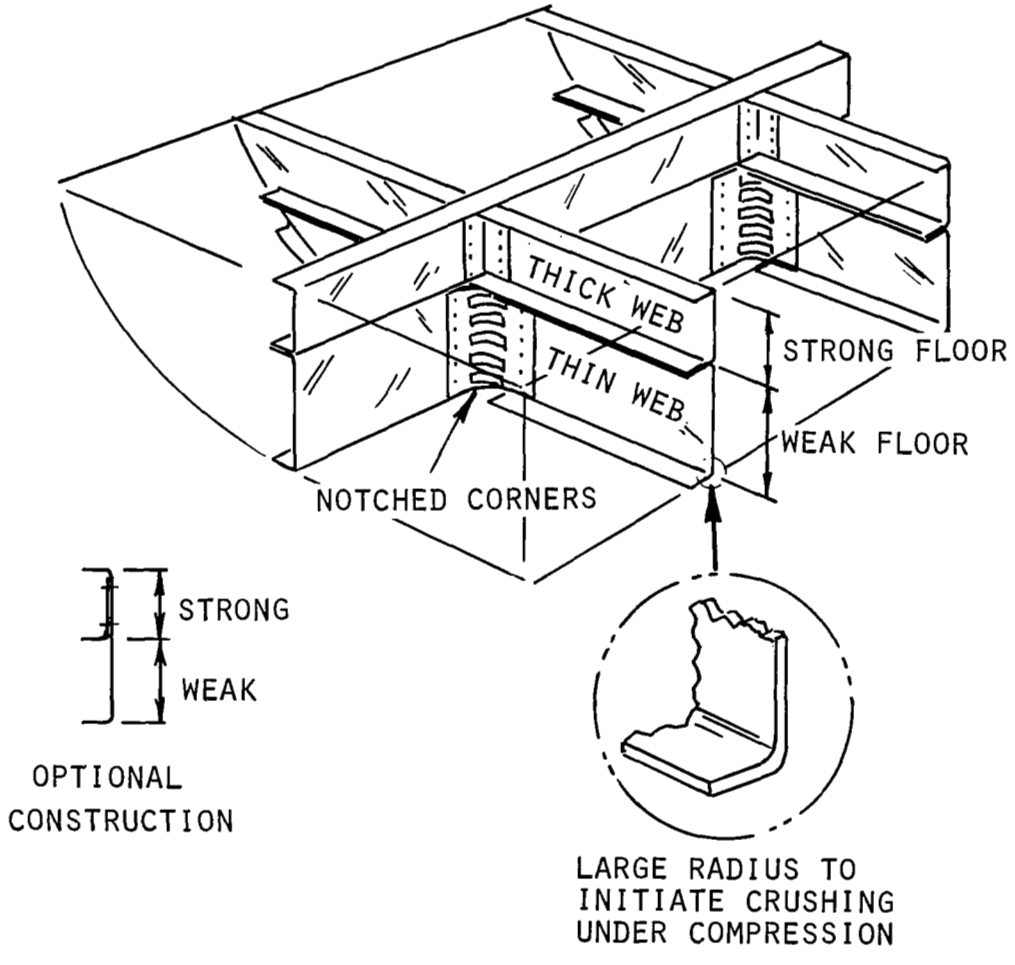

Figure 20. Notched corner minimum-modification ("mini-mod") concept.

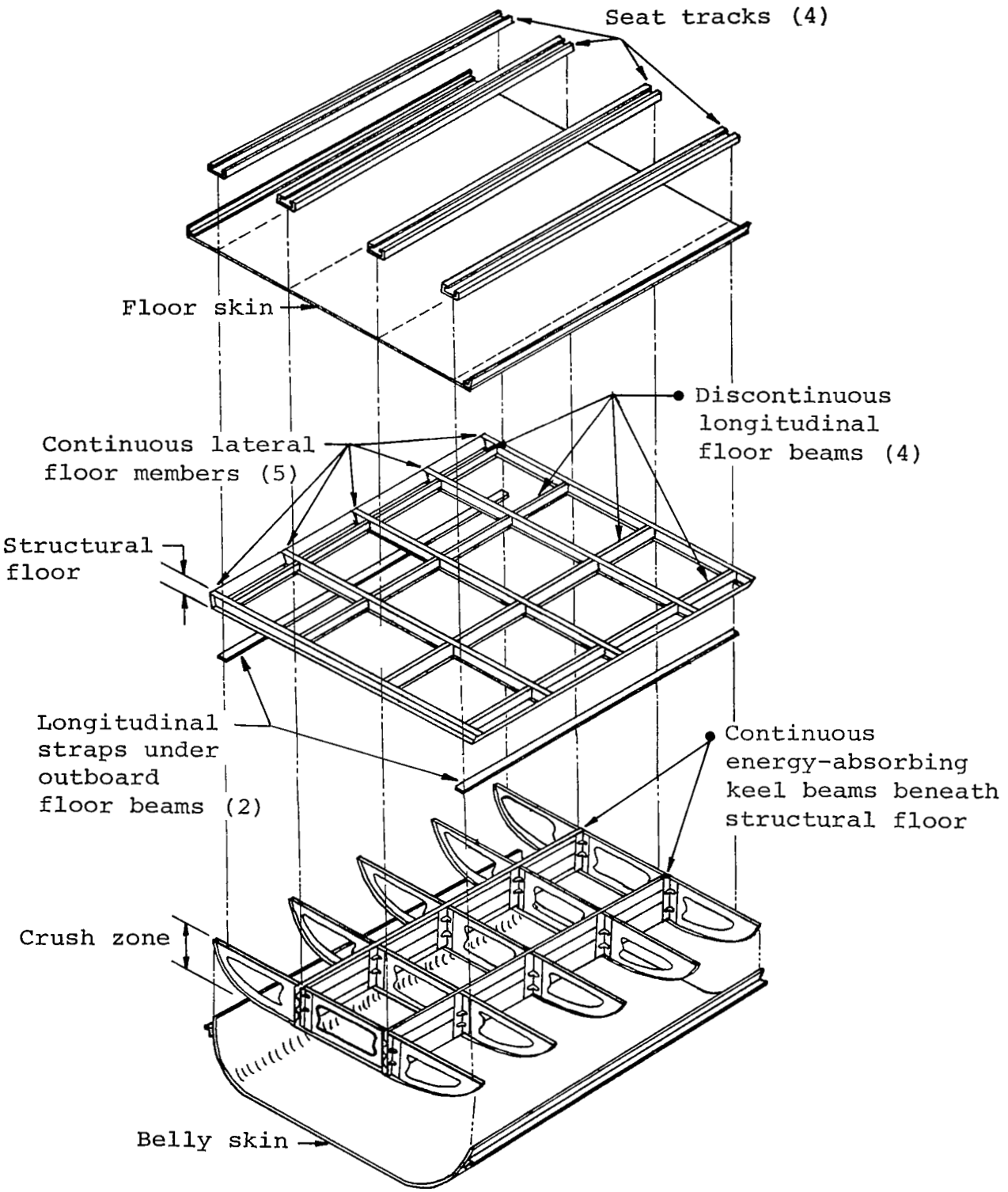

Figure 21. Floor section assembly.

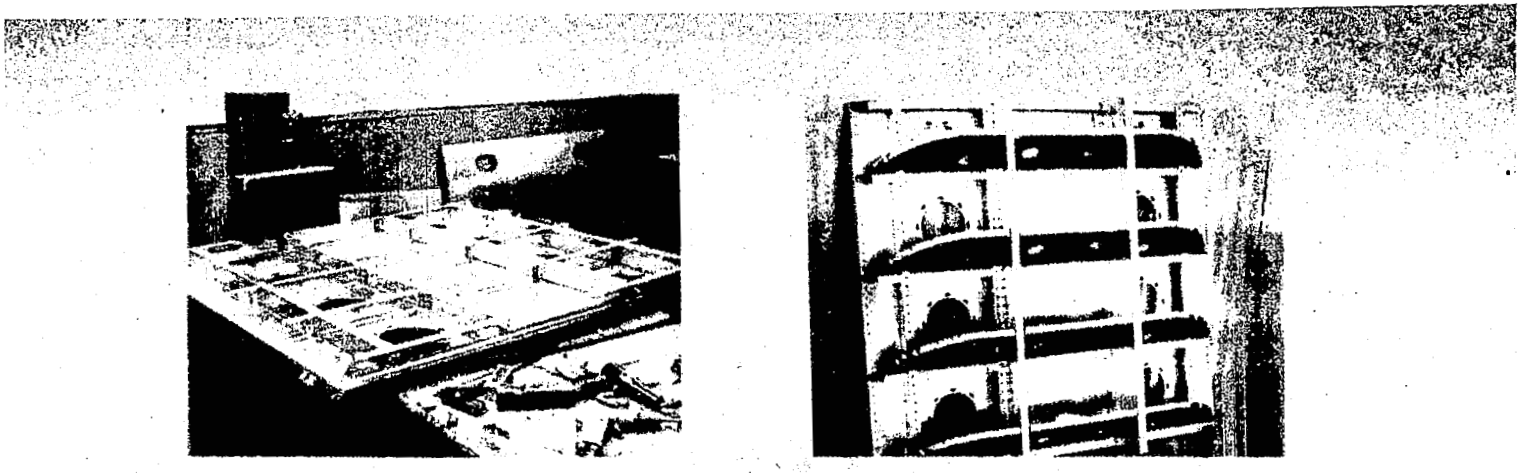

(A) STRUCTURAL FLOOR (UPSIDE DOWN)

(B) CANTED BULKHEADS AND KEEL BEAMS (BELLY SKIN REMOVED)

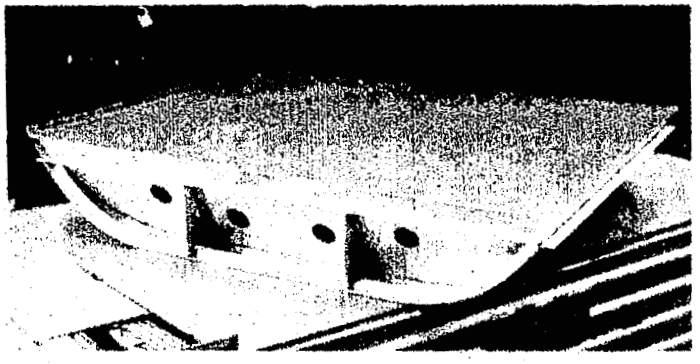

(C) COMPLETED SECTION

Figure 22. Fuselage floor test section assembly.

longitudinal spacing is 27.9 cm (11 inch) for all the test sections. Features of each of the final five concepts are described below (design drawings are included in Appendix D):

1. The corrugated beam floor test section resembles conventional airframe structure with sheet metal skins, beams, frames, and stringers except for the configuration of the longitudinal beams. The beam web material has been longitudinally corrugated to promote controlled collapse during the crush stroke. The corrugation pitch is 5.8 cm (2 inch) while the amplitude of the corrugation is 2.3 cm (.90 inch). "Notched corner" (Fig. 13) or structurally tailored shear clips are also incorporated in this configuration. (See Fig. 23(c)).
2. The corrugated half-shell floor test section differs considerably from conventional structure. The primary fore-aft structural member resembles one-half of a large corrugated sewer pipe with a 36.83 cm (14.50 inch) diameter. It, and outboard frames, supports the exterior belly skin (see Fig. 23(d)). The corrugations run circumferentially with a corrugation pitch in the longitudinal direction of 6.78 cm (2.67 inch).
3. The "mini-mod" notched corner floor test section incorporates conventional metal airframe structure with sheet metal skins, beams, frames, and stringers. The shear clips that tie the beams to the frame members have been structurally tailored to reduce their column stiffness and promote an accordion-style buckling mode for the longitudinal beams and frame members during the crush stroke. (See Figs. 20 and 23(a)).
4. The foam-filled cylinder floor test section uses two longitudinal cylinders with 15.3 cm (6 inch) diameter for primary fore-aft structure. The cylinders are filled with PVC foam material appropriately vented for absorbing energy. The cylinders and outboard frames support the exterior skin. (See Fig. 23(b)).
5. The "mini-mod" canted bulkhead specimen incorporates conventional metal airframe structure with sheet metal skins, beams, frames, and stringers except that all frames are canted at an angle of 30° from vertical to promote their collapse for vertical impacts and help prevent plowing for longitudinal impacts. (See Fig. 22(c)).

To obtain a relative comparison of the various concepts, comparable bulkhead and web sizes were used based on strength requirements and what was observed in the NASA fuselage test sections. The lower bulkheads on all test sections were the same basic .064 cm (.025-in) sheet. The webs of all the crashworthy concepts were .081 cm (.032-in) sheet except the foam-filled cylinders that have .051 cm (.020-in) skins. The shear clips or

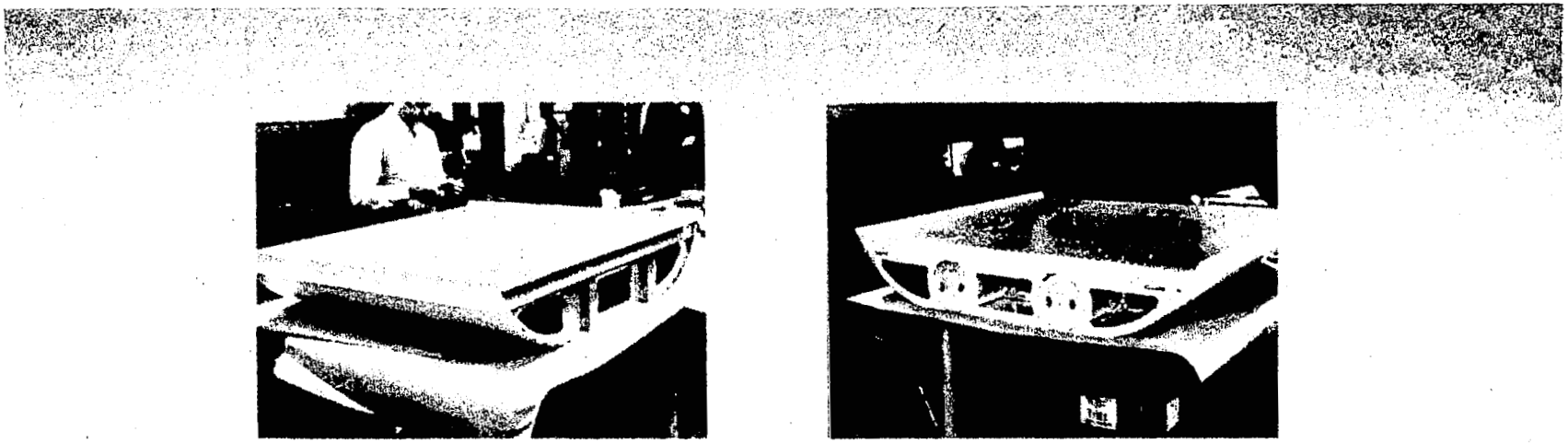

(A) NOTCHED CORNERS

(B) FOAM-FILLED CYLINDERS

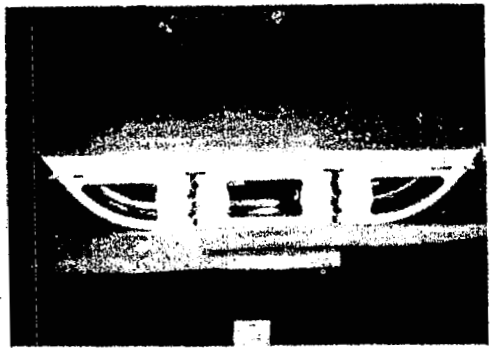

(C) CORRUGATED WEBS

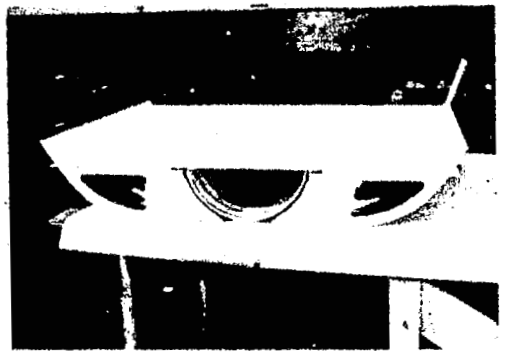

(D) CORRUGATED HALF-SHELL

Figure 23. Completed fuselage floor test sections.

angles which include the notched corners that tie the keel webs to the bulkheads were all .081cm (.032-in) sheet. The structural material that was used throughout was 2024-T3 aluminum.

The final assembly weights of the test sections were as follows:

1. Corrugated web section 15.1 kg (35.5 lb)
2. Corrugated half-shell 16.6 kg (36.6 lb)
3. Notched corner section 15.7 kg (34.5 lb)
4. Foam-filled cylinder 17.7 kg (39.0 lb)
5. Canted bulkhead section 15.9 kg (35.0 lb)

The structural floor assembly and access panels for each section weighed 8.9 kg (19.5 lb). It should be noted that the screw and nut plates used on the access panels added 1.1 kg (2.5 lb) to the section weight that is not representative of lightweight aircraft construction. Note also that most of the concepts were relatively close to the same weight (within 2 lb) except for the foam-filled cylinder. This is because the foam weight is strictly add-on weight over what is required for structural purposes. The other concepts take advantage of the structure that is required for basic strength and is reconfigured to make it crushable. The weight penalty for adding crashworthiness features to all of the floor test sections except the foam-filled cylinder is estimated to average 2.5 kg (5.5 lb). For a 2724 kg (6000 lb) airplane with a floor about three times the length of the test sections, this would be a penalty of about .3 percent of the aircraft gross weight. For the foam-filled cylinder concept, the penalty would be considerably higher (0.5 percent gross weight). In all, eighteen of the floor sections were fabricated with 3 or 4 sections of each of the five concepts. The floor sections were to be used for static and dynamic test evaluation at NASA Langley Research Center that is discussed in Sections 5.3 and 5.4.

5.3 STATIC TESTS (Ref. 3)

Static compression testing was conducted at NASA Langley Research Center in order to determine the static crushing and load-deflection characteristics of each type of floor section.

A typical experimental setup for the static testing of the five subfloor concepts is shown in Fig. 24. A subfloor is shown with two loading platforms attached to the rails at seat leg spacing of approximately 40.6 cm (16 inches) to transfer loads to the test section. Conical rollers on the top of the loading platforms allowed the platform to tilt or roll during the crushing process. The machine head and platen of the 4.5 MN (1.2 million-pound force) loading machine used to obtain load-deflection (crush) and strain gauge data on the subfloors are also shown. Loading rate for each test was 0.64 cm/minute (1/4 inch/minute).

Strain gauge rosettes shown in Fig. 25 at various locations in the subfloor crush zone were used to measure strain distribution beneath the subfloors. The various rosettes were connected to junction boxes (Fig. 24) that were in turn connected to Beckman data acquisition system for recording at a sampling rate of 1 sample/second.

Lateral separation of the platforms and vertical crush of the subfloors were measured with deflectometers shown in Fig. 24. Sixteen millimeter cameras running at 8 pictures/ second provide photographic coverage of each test.

Static test results for the five load-limiting subfloor concepts are presented in Figs. 26 through 30. Shown on the left of each figure are photographs of the subfloor "before" testing and "after" testing, whereas on the right of the figures are the load-deflection (crush) results from the static loading tests. Loads and displacements are given in both SI and English units.

Several important points may be deduced from these results. First, as evident in the after-test photographs, none of the five subfloors broke apart but remained structurally intact and had residual strength after collapse of the lower crush zone. Second, under the static loads, the load platforms rolled outward (except for the corrugated beam-notched corner section) as plastic hinges formed either at the inner rail location or in the center of the subfloor. Third, the formation of plastic hinges was as designed to help prevent loss of structural integrity and to maintain seat-to-structure integrity in the event of overload conditions on the floor. Fourth, although all five subfloor sections performed well in that no break-up (structurally) occurred, some collapsed with a more constant load with displacement than others. Compare, for example, Figs. 26 and 27 with Figs. 28 through 30.

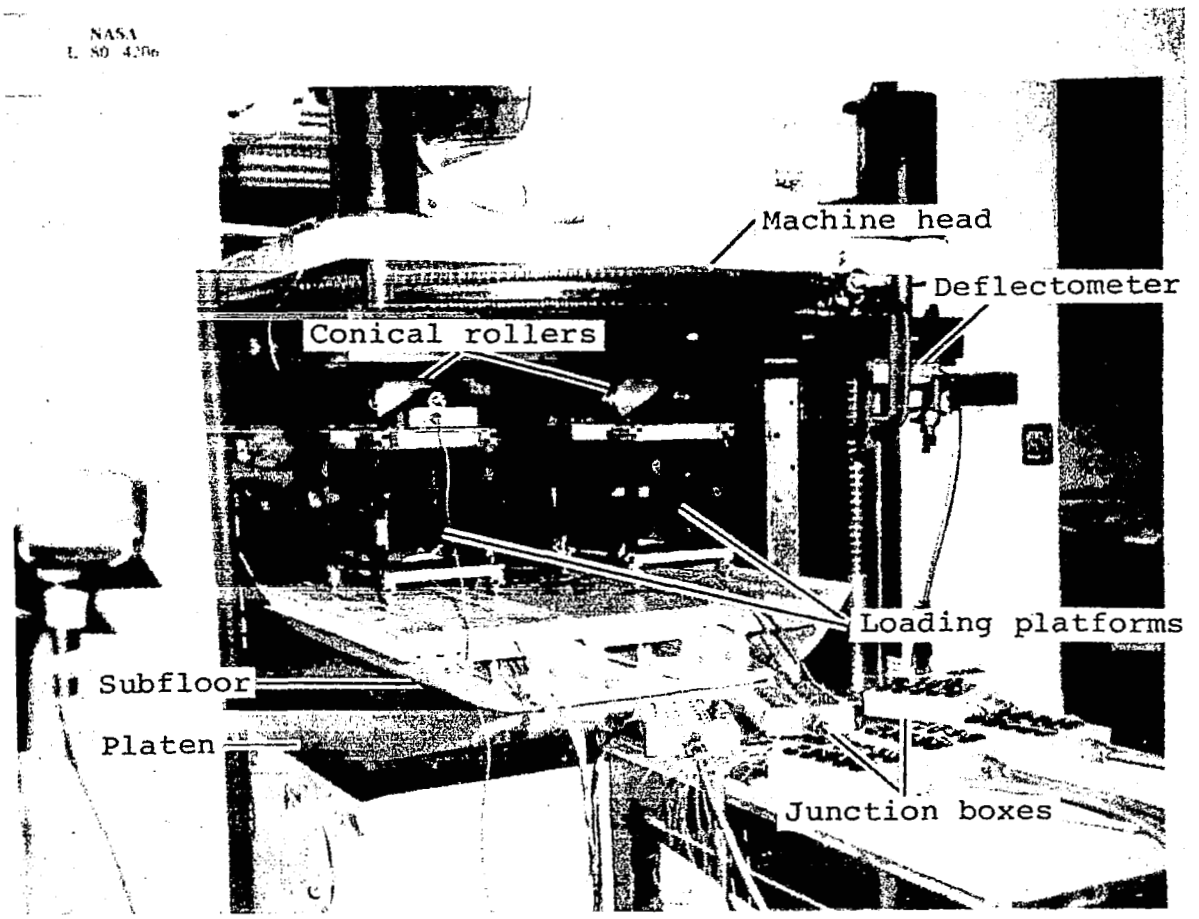

Figure 24. Typical experimental set-up for static testing of fuselage floor sections.

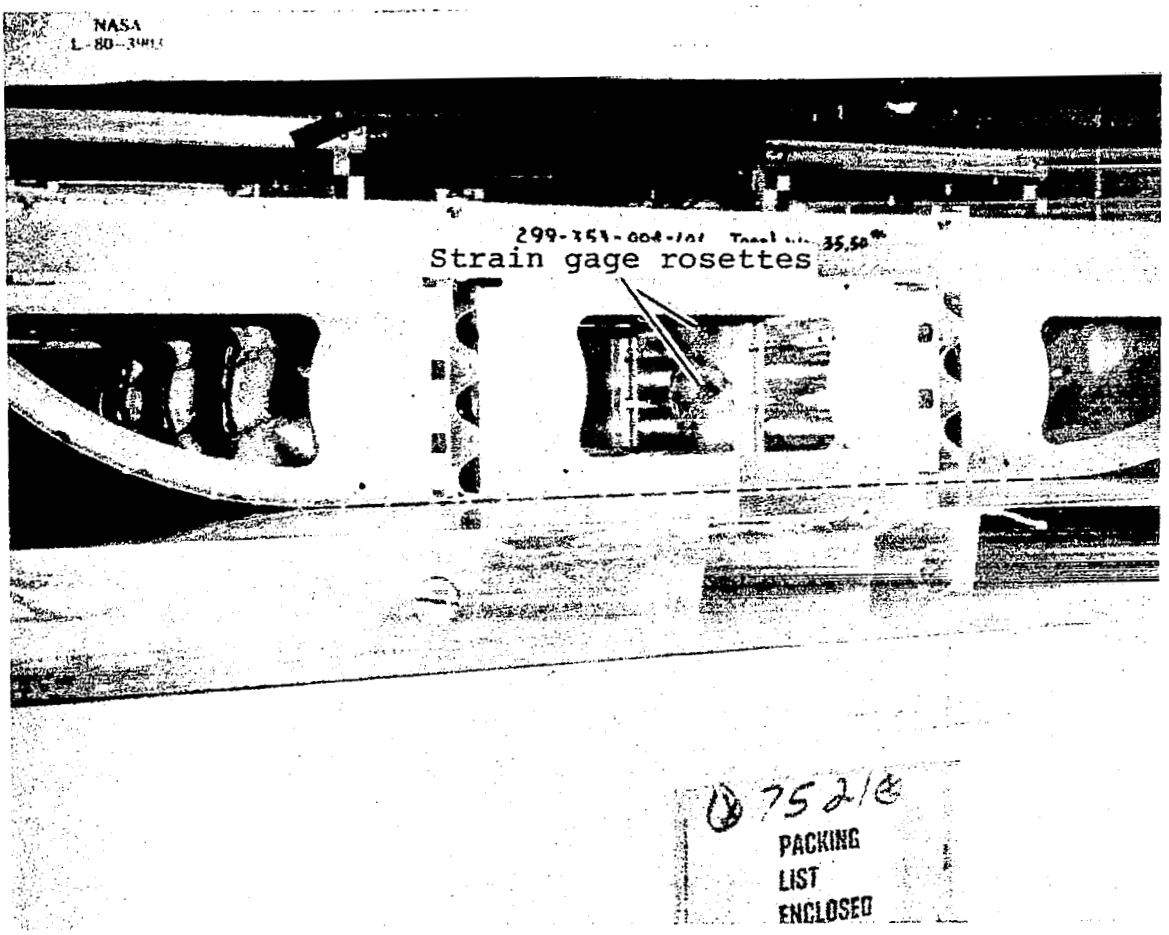

Figure 25. Typical strain gage instrumentation.

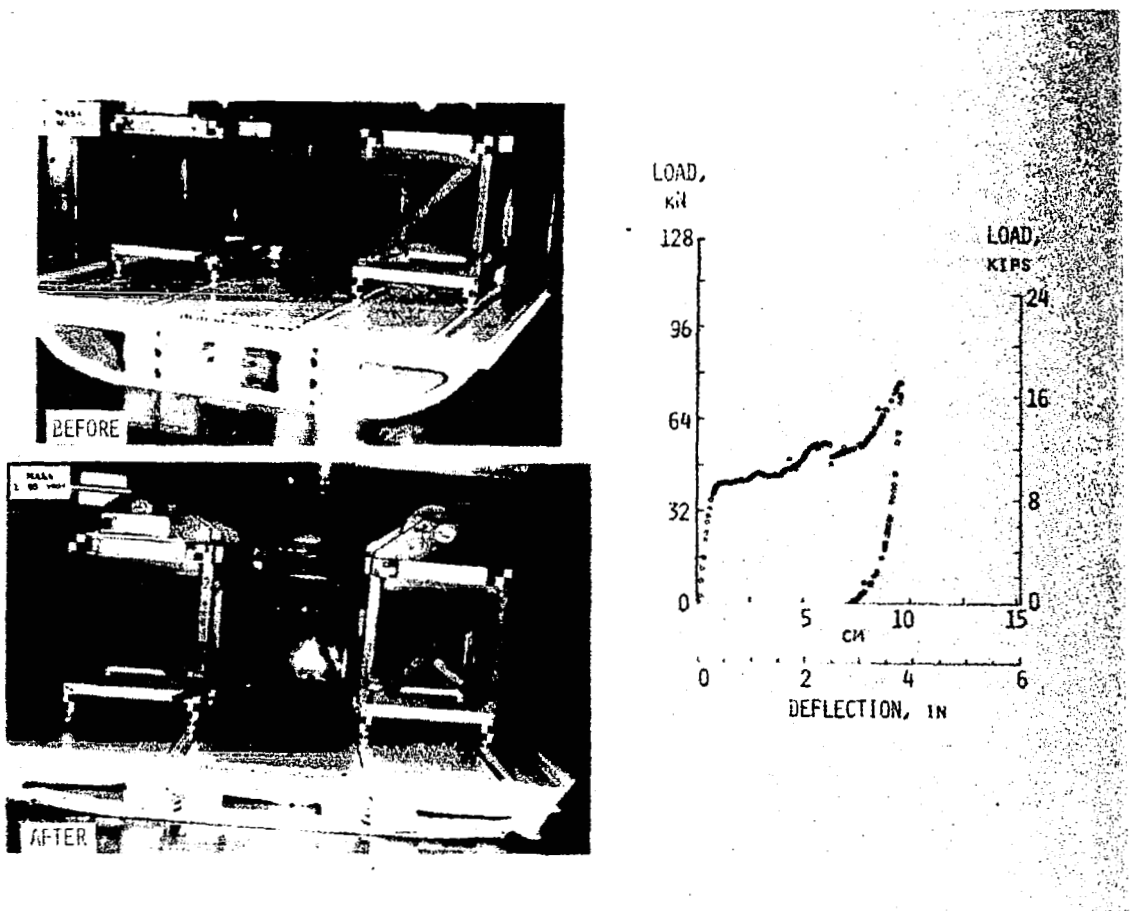

Figure 26. Static test results for corrugated web concept.

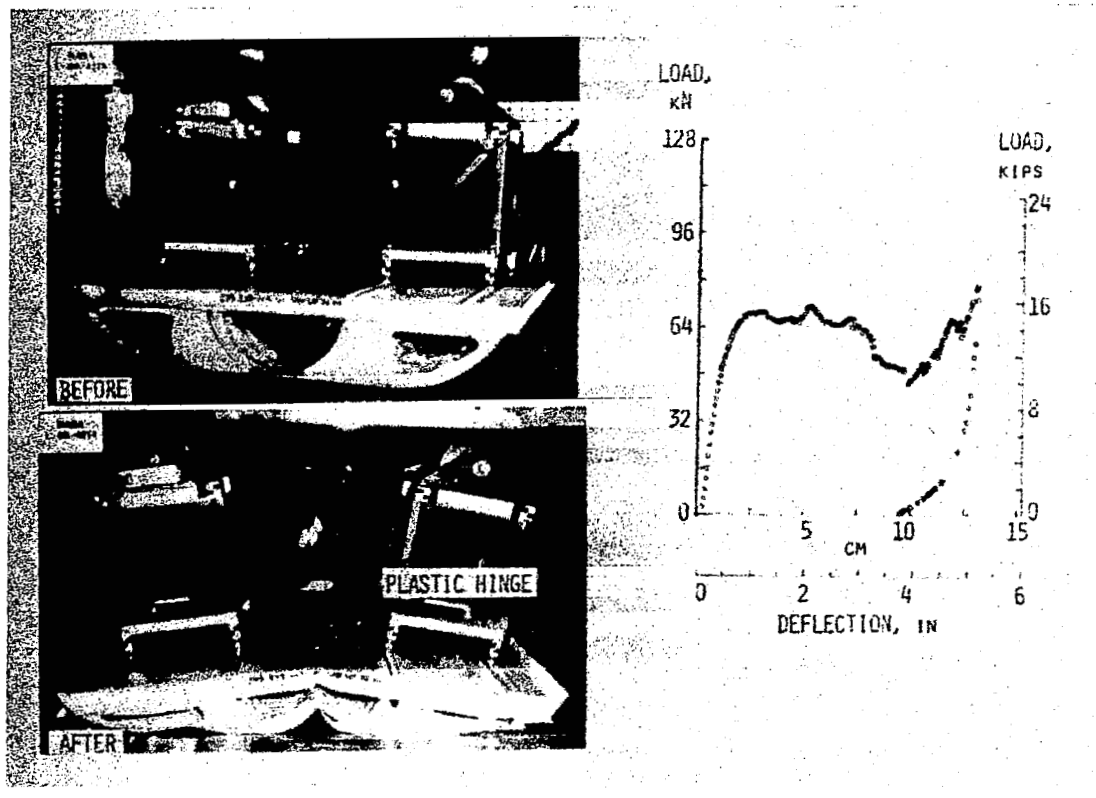

Figure 27. Static test results for corrugated half-shell concept.

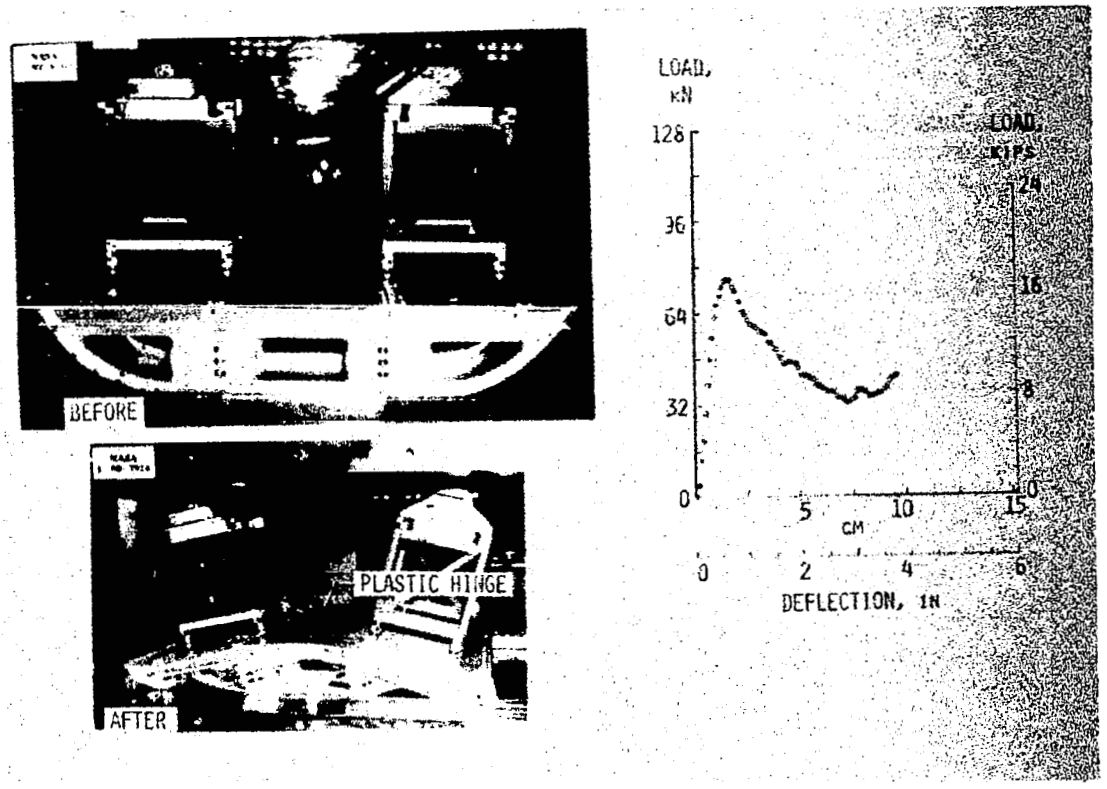

Figure 28. Static test results for notched-corner "mini-mod" concept.

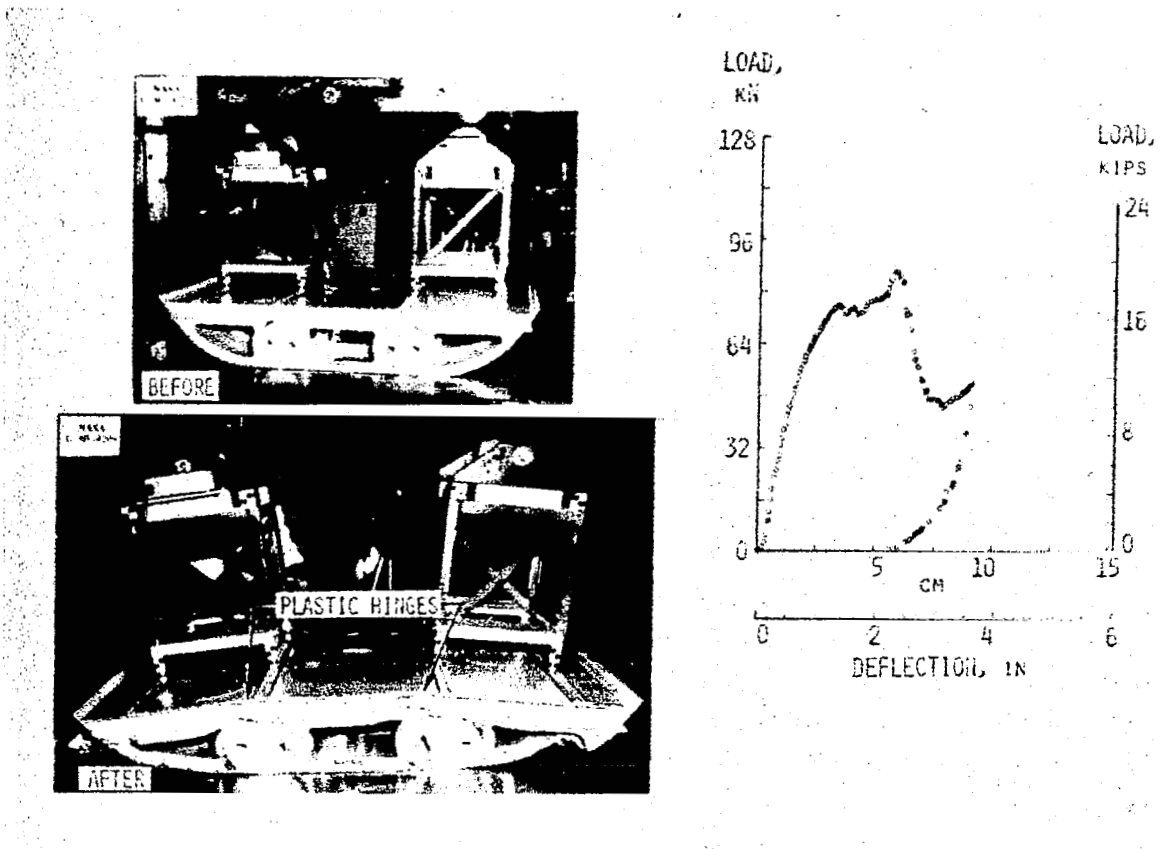

Figure 29. Static test results for foam-filled cylinder concept.

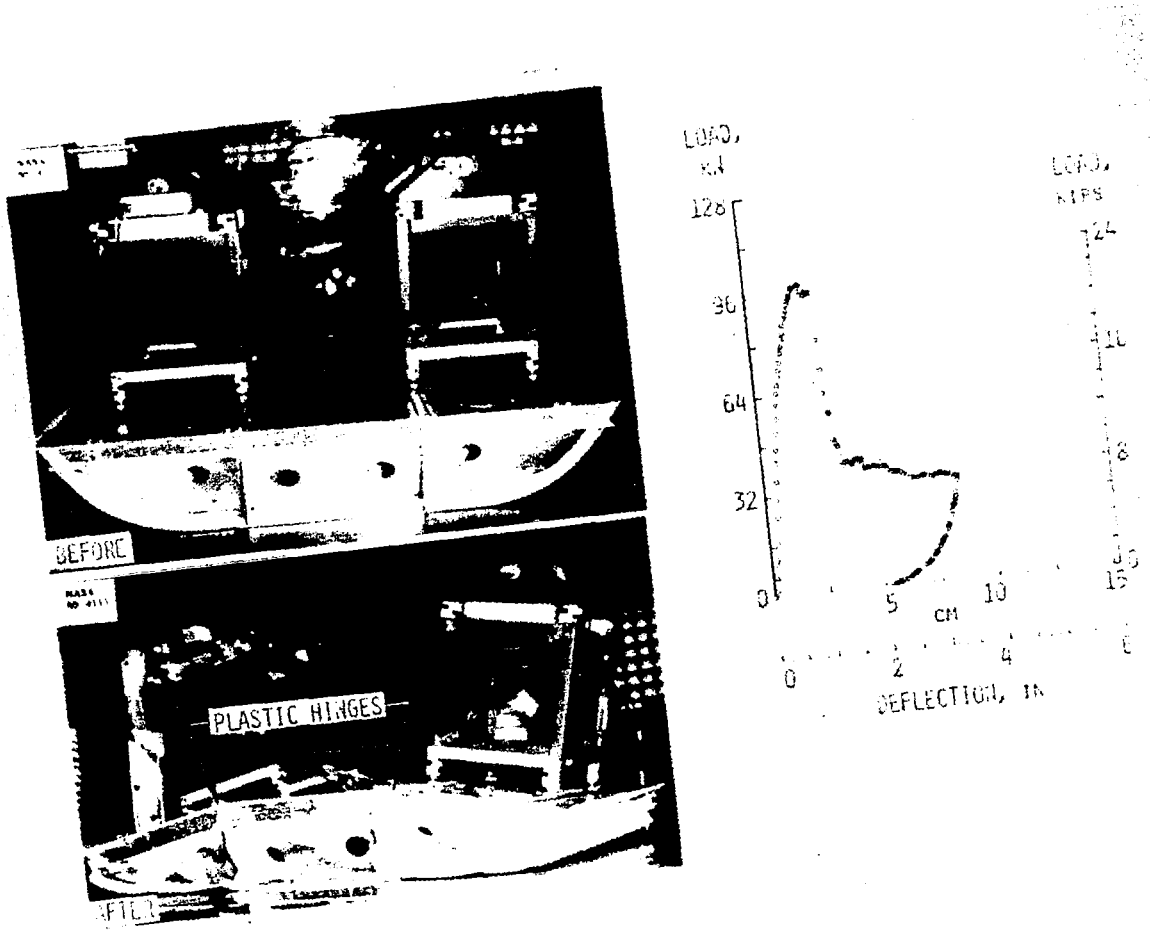

Figure 30. Static test results for canted bulkhead concept.

The crushing load was more desirable for the corrugated beam-notched corner and corrugated half-shell since the load remained relatively uniform in magnitude throughout the loading cycle compared to the notched corners, foam filled cylinders and canted bulkhead subfloors.

A design iteration on the latter three subfloors discussed above could eliminate some of the unwanted behavior noted with these approaches in the lower zone of the subfloors. For example, the high peak load on both the notched corner and canted bulkhead subfloors could possibly be reduced by providing a larger radius on the top and bottom flanges of the longitudinal beams to initiate buckling more readily. For the foam-filled cylinders, removal of the foam probably would result in improved static load-crush behavior since the foam compression in the confinement of the cylinders limited the available vertical crush distance and increased the load which caused the formation of the plastic hinge noted in Fig. 29.

Photographs of the static test results for the corrugated web and foam-filled cylinder concepts are compared in Fig. 31. Note that the corrugated web concept performed excellently with no noticeable floor distortion, while the foam-filled cylinder concept had noticeable deformation of lateral members with plastic hinges formed above the cylinder locations. However, the structural floor for the foam-filled cylinder section remains intact with excellent residual strength for seat retention. This appears to support the design decision to use continuous lateral floor beams that was discussed earlier. It should be noted that the foam-filled cylinder section did not have any noticeable floor distortion in the NASA dynamic test as it did in the static test. The difference was the result of the method of applying the static load which introduced a lateral outboard load component to the seat. The component increased with increasing floor bending so that once the floor starts bending, the applied load aggravates the bending. For the dynamic drop test condition, however, the inertial loads developed on the seat mass give an inboard reaction load that acts to keep the seat upright.

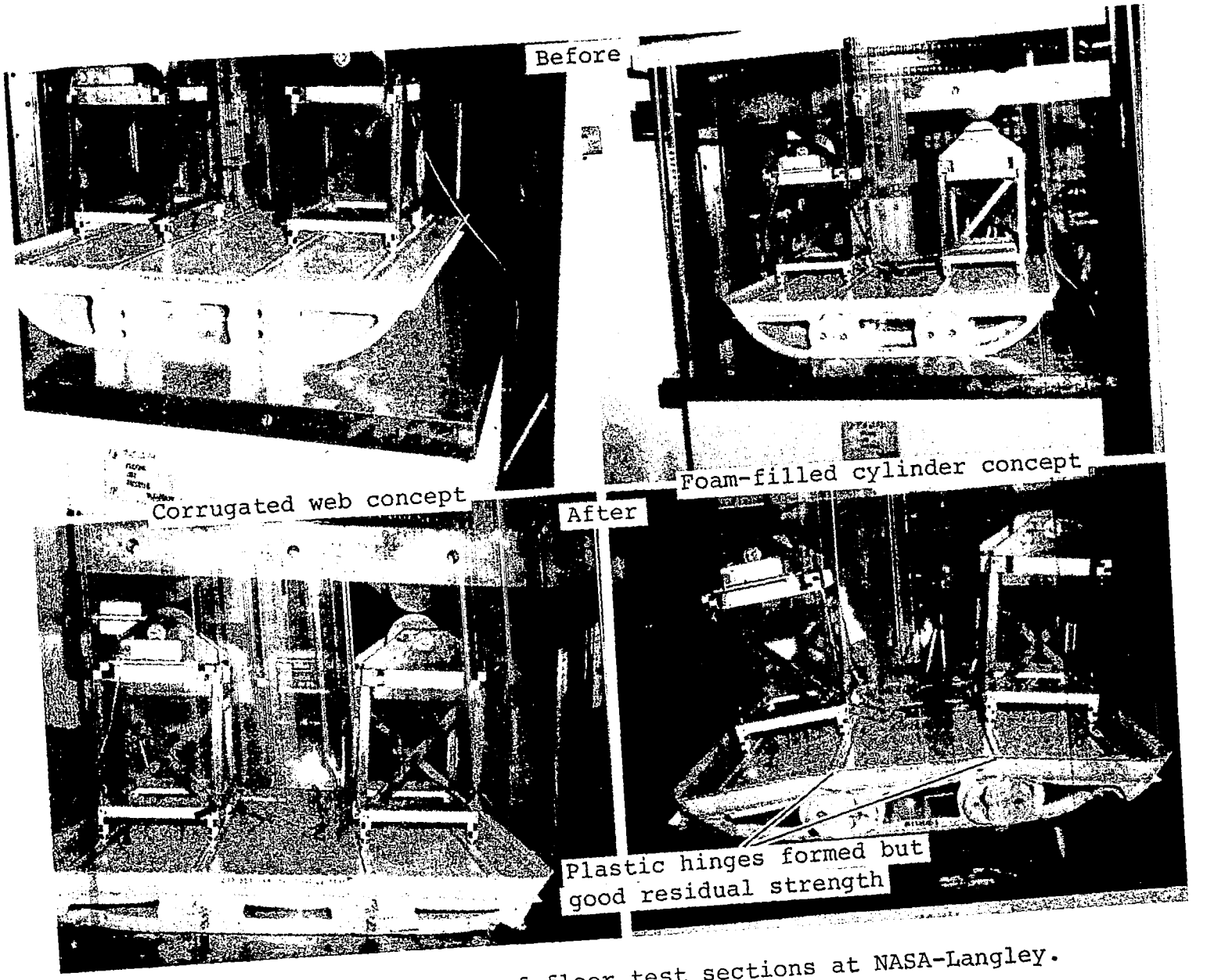

Figure 31. Static tests of floor test sections at NASA-Langley.

5.4 DYNAMIC TESTS (Ref. 3)

Dynamic drop tests were conducted at NASA Langley Research Center to evaluate the response of the floor sections to crash impact type loading and to define loading rate effects on the energy-absorbing concepts.

A typical experimental setup for the dynamic testing of the five subfloor concepts is shown in Fig. 32. The foam-filled cylinder subfloor section shown in the figure had two loading platforms ballasted to approximately the total mass of two conventional seats and two dummies each of 75 kg (165 lbm) mass. Total mass of the assembly was approximately 198 kg (435 lbm).

The deceleration responses of the subfloors to vertical loading at an impact velocity of 7.3 m/s (24 fps) onto a concrete surface were measured. The D.C. strain-gauge type accelerometers (response flat from D.C. to 2000 Hz) were mounted at each loading platform, at the upper mass c.g. locations, and at the center of the subfloor. In addition to the vertical decelerations, longitudinal and lateral responses also were measured at the upper mass c.g. locations and at the center of the subfloor and only additional lateral responses were measured at the two outside corners of each loading platform. Data signals were transmitted from the subfloor through an umbilical cable to a near-by control room where the signals were conditioned, amplified and recorded on FM-multiplex tape recorders. 600-Hz low pass filters were used with the recording system.

The test procedures involved leveling the subfloor prior to raising the section by electric hoist to the desired drop height of 2.7 m (9 ft.). The tape recorders and three cameras were started. One camera provided overall coverage at 400 pictures/second and two other cameras at 1000 pictures/second provided closeup front and side views of the subfloor impact. Finally, the cargo hook was electrically activated to allow the subfloor to fall to the impact surface. Post-test photographs were then made to supplement the pretest photographs of each subfloor.

Data from the FM tape recorders were digitized at 4000 samples/second and converted by calibration factors to engineering units from which deceleration curves were plotted (Figs. 33 to 37).

Dynamic responses to impact loading on each of the five subfloor sections at a vertical impact velocity of 7.3 m/s (24 fps) with 0° pitch and roll angles are presented in Figs. 33 through 37. Photographs of the subfloor "before" and "after" the impact tests are included on the left along with experimental and analytical responses of the upper lead mass c.g. (top right) and only experimental response on the floor at the corner of the loading platform (bottom right).

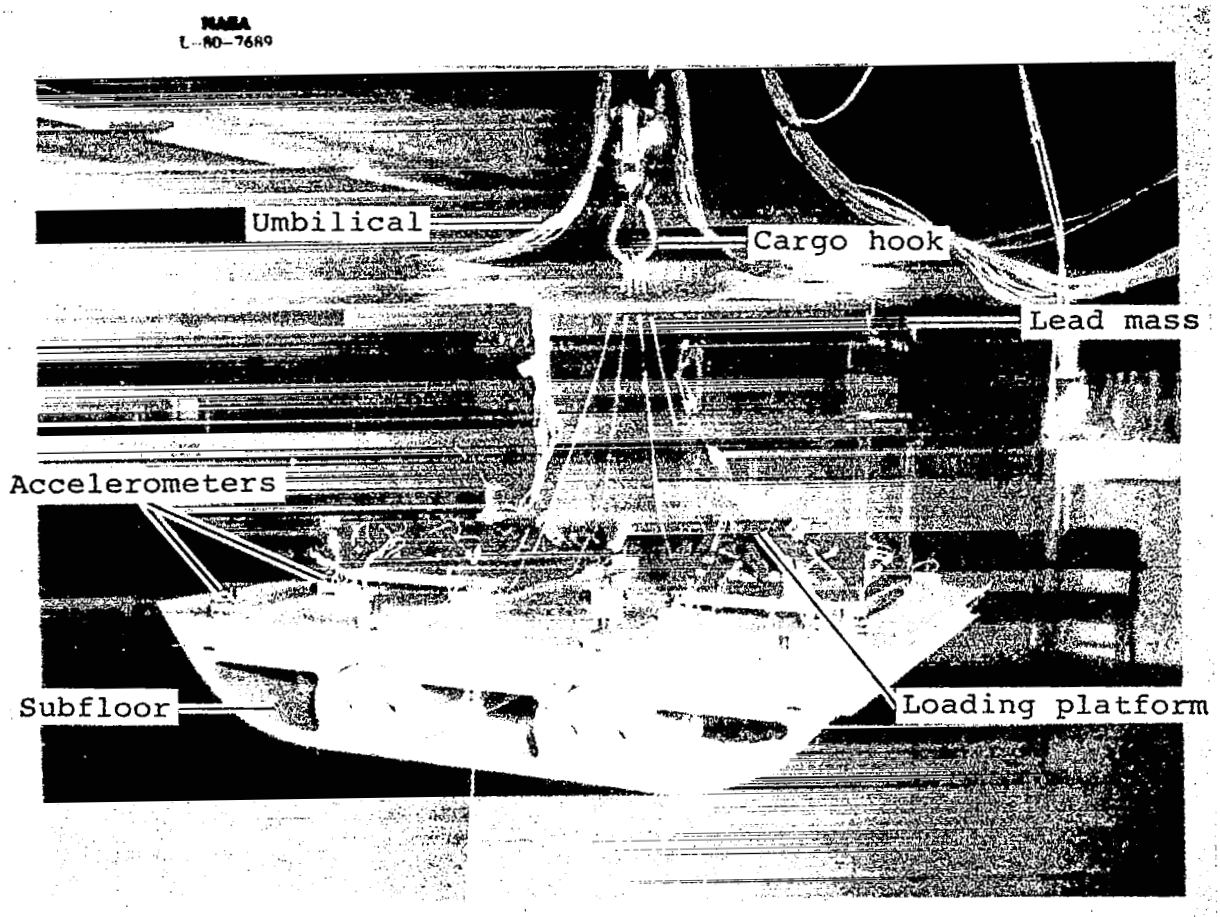

Figure 32. Typical experimental set-up for dynamic testing of fuselage floor sections.

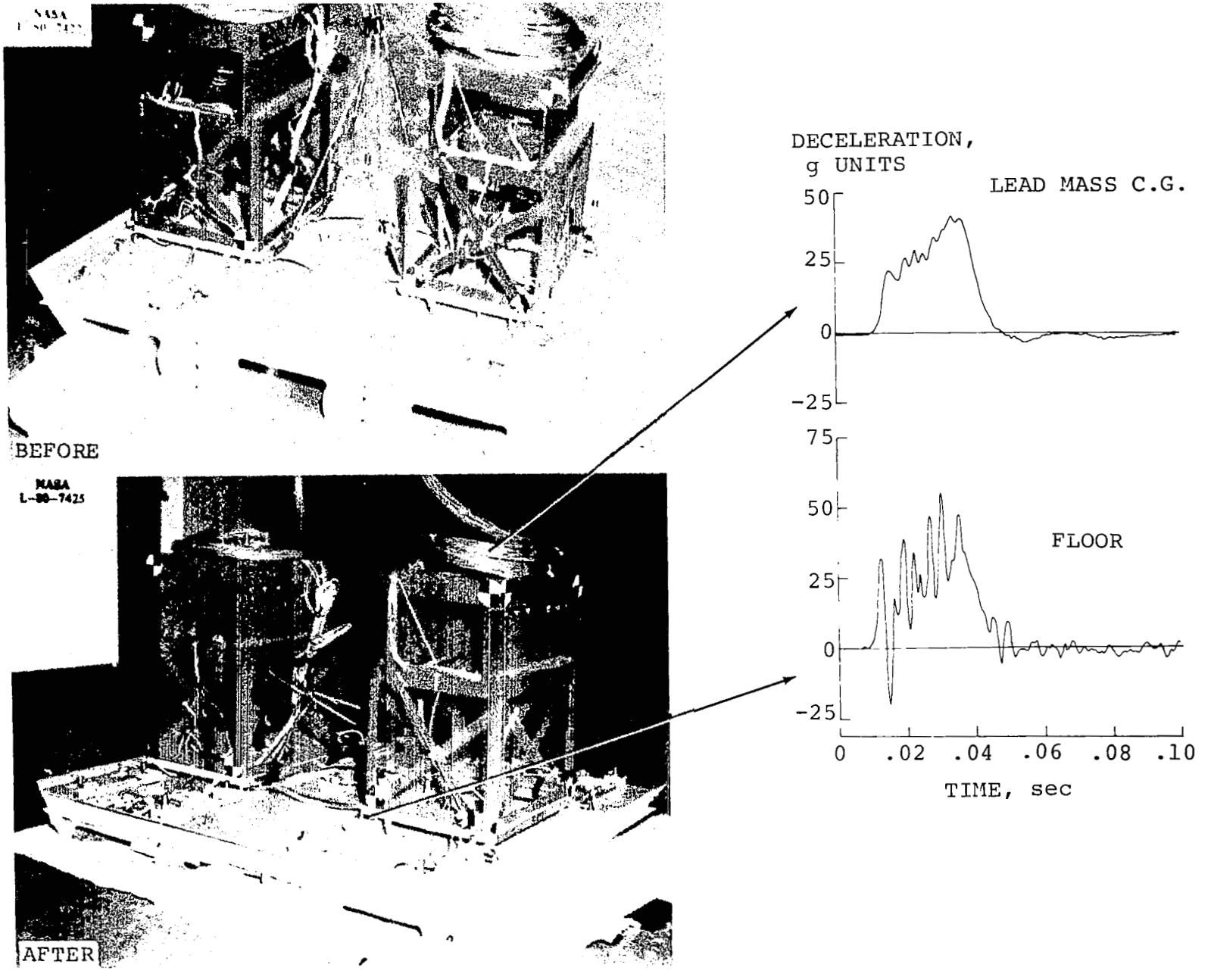

Figure 33. Dynamic test results for corrugated web concept.

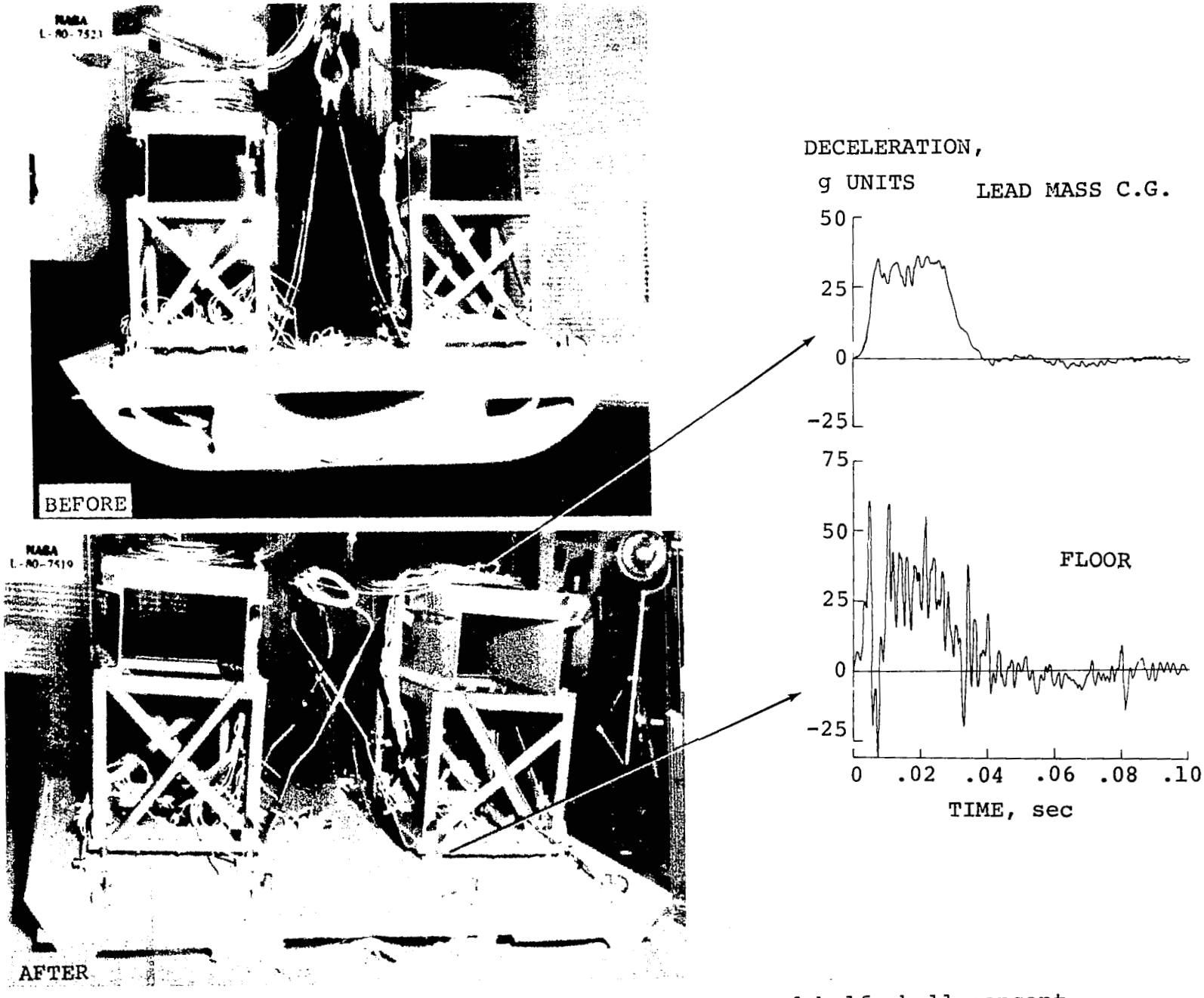

Figure 34. Dynamic test results for corrugated half-shell concept.

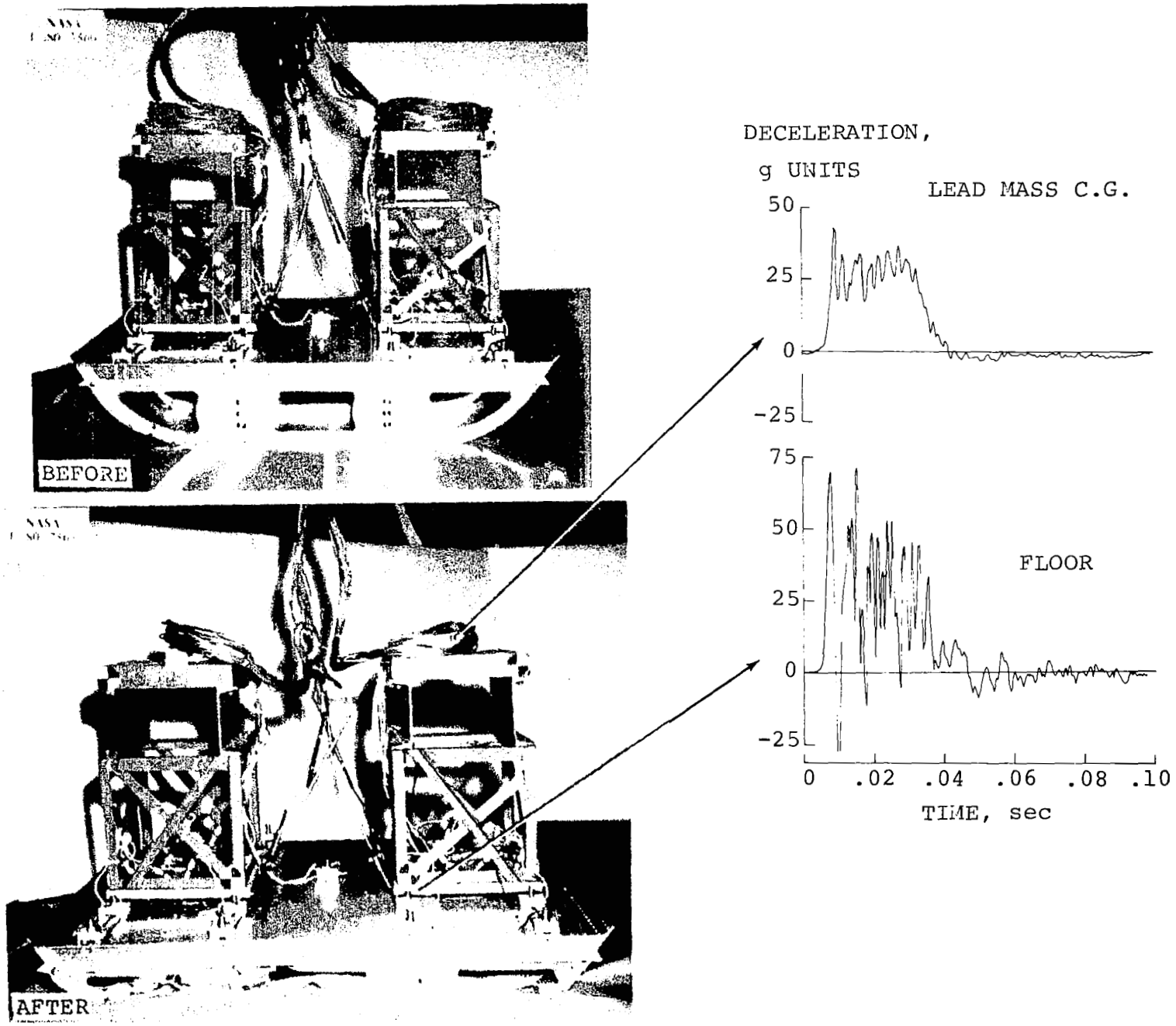

Figure 35. Dynamic test results for notched-corner "mini-mod" concept.

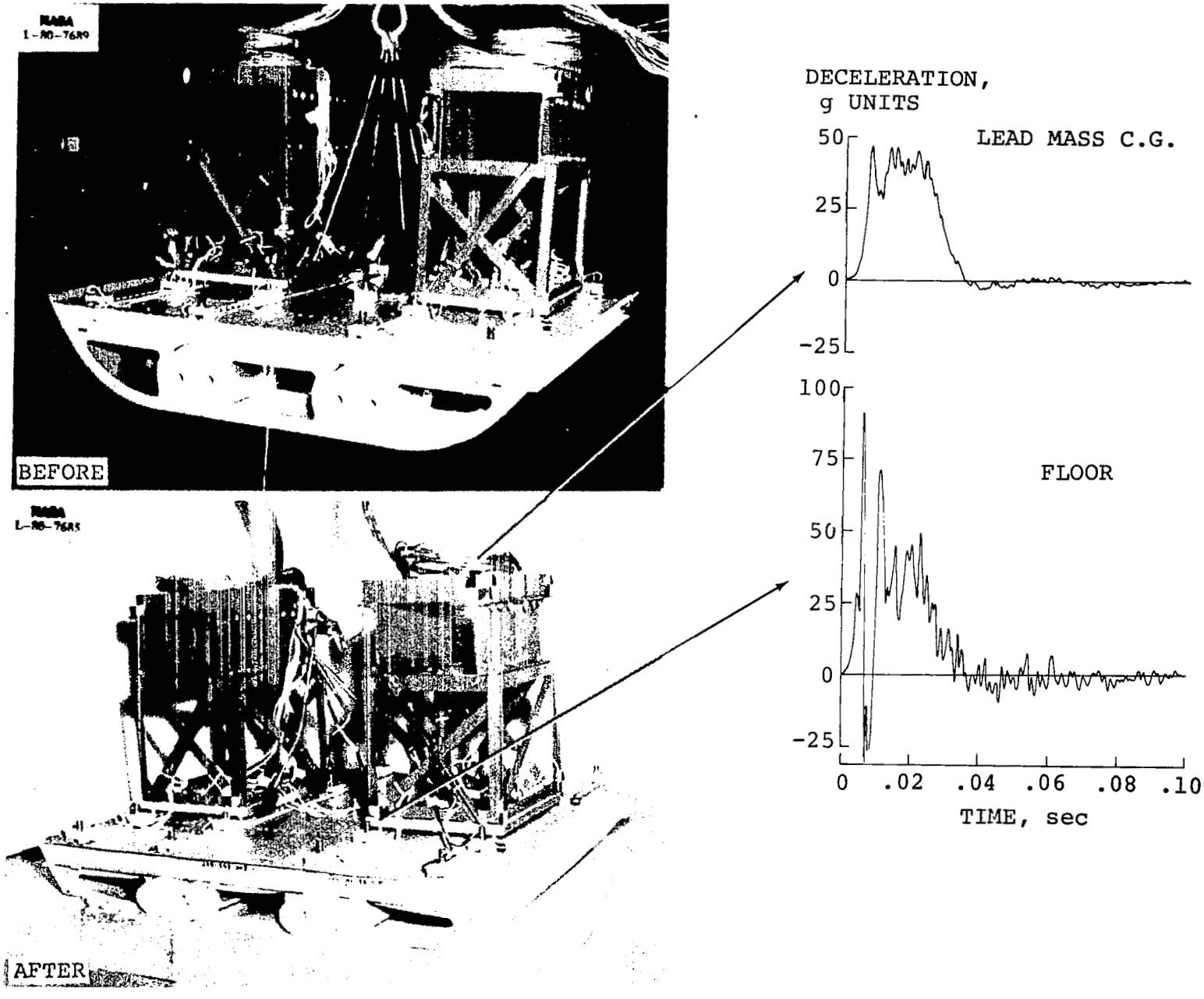

Figure 36. Dynamic test results for foam-filled cylinder concept.

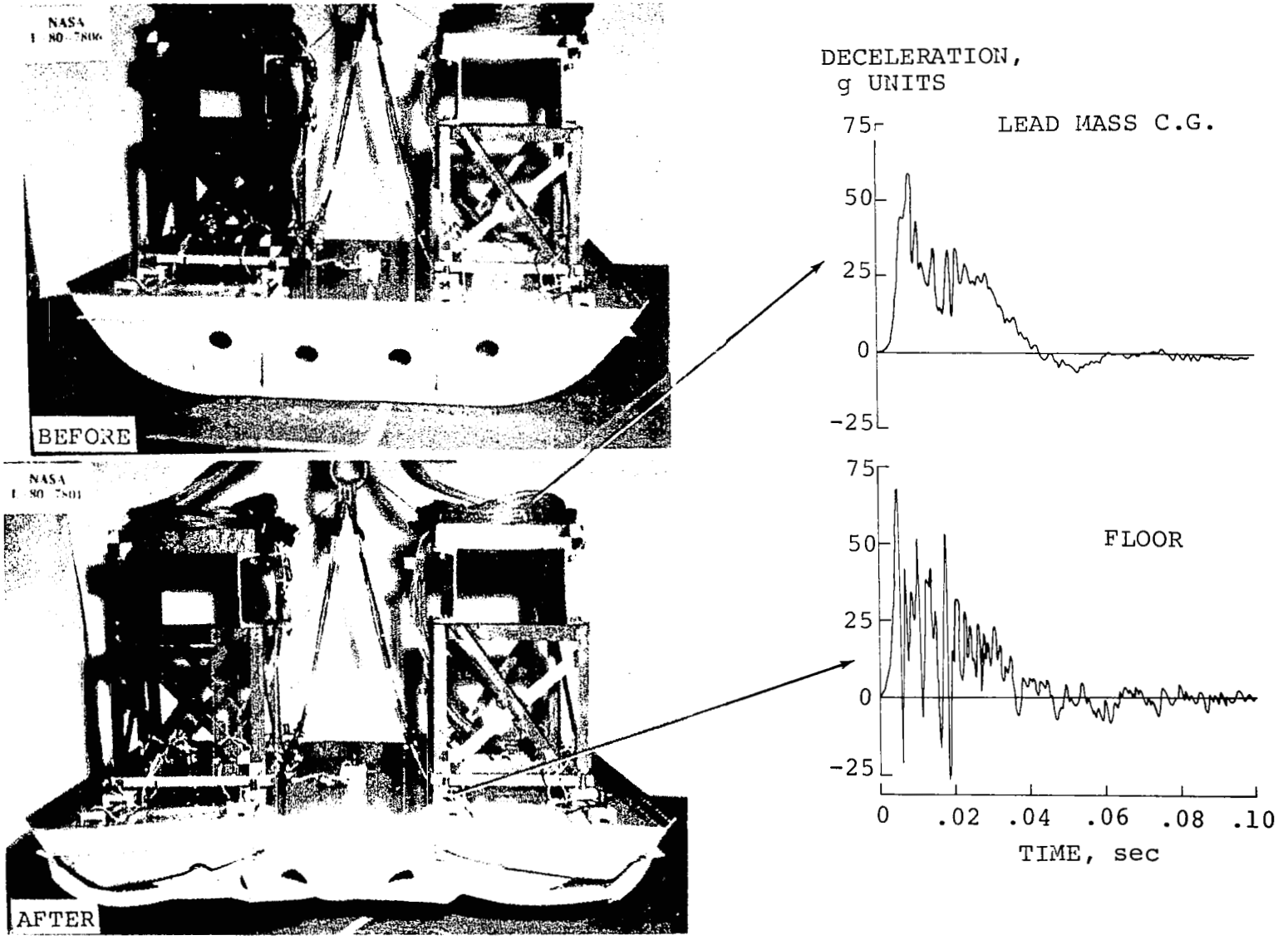

Figure 37. Dynamic test results for canted bulkhead concept.

Figure 33 presents the response for the corrugated beams - notched corners subfloor. Deceleration for the corner of the loading platform on the floor shows high frequency, local floor vibrations at approximately 350 Hz superimposed on the underlying pulse, however, similar shape, magnitude and duration to that of the c.g response are evident. Only minor oscillations are evident on the deceleration of the c.g. High inherent damping of the lead minimized the higher frequency vibrations. Duration of the basic deceleration pulse was approximately .04 seconds.

As may be noted in Figs. 26 and 33, the upper floor structure of the corrugated beams notched-corner subfloor was undeformed in both the static and dynamic tests. A comparison of the c.g. deceleration with the static load-deflection data shows the same basic shape for the dynamic response as that noted for the static data. Consequently, the static load-deflection response was very similar to the dynamic behavior of the subfloor. For example, deceleration rapidly reached approximately 20 g's and gradually increased to a peak of approximately 39 g's exhibiting the same character as the static load with stroke.

The behavior of the corrugated half-shell subfloor to impact loads is illustrated in Fig. 34. The deceleration on the floor at the corner of the loading platform shows basically the same load pulse as the c.g mass; however, a higher frequency local vibration of the floor around 600 Hz occurred on the pulse in this case. Deceleration of the lead mass c.g was around 30 g's throughout the approximately .04 seconds collapse time of the corrugated half-shell crush zone. The relatively constant limit load provided by the corrugated half-shell is desirable to achieve the maximum energy dissipation with available stroke.

As may be noted in the static case in Fig. 27, a plastic hinge occurred in the middle of the upper floor structure after approximately 7.62 cm (3 inches) of crush which corresponds to a deflection in the dynamic case at about 0.015 seconds. In the dynamic case, the upper floor structure was essentially undeformed during the impact loading due to the resistance of the vertical inertia of the loading platform to a change in motion direction. Consequently, during the first 7.62 cm (3 inches) of deflection, the static load-deflection was a good representation of the dynamic behavior.

Figure 35 presents the dynamic response on the notched corners concept to the crash loading. The floor response was essentially the same magnitude as that of the c.g except the superimposed floor vibrations on the basic pulse are predominantly around 600 Hz. Deceleration of the lead mass c.g. was fairly constant at about 25 g's during the .04 second pulse duration but somewhat higher amplitude vibrations than experienced on the previous c.g. decelerations are evident in this case at about 350 Hz.

In the static test of this section, plastic hinges formed in the upper floor at the lateral locations of the notched corners (Fig. 28) just prior to 2.54 cm (1 inch) of crushing. In the dynamic case however, the floor structure remained undeformed as shown in Fig. 35. Although the static load-deflection data had an initial high load peak followed by a gradual reduction in load, the dynamic response did not reflect as pronounced a variation but was generally more constant in amplitude which, as previously noted, is a desirable behavior. This behavior again may be attributed to the absence of any plastic hinge formation in the dynamic test.

Dynamic response data for the foam-filled cylinders subfloor are presented in Fig. 36. A comparison of the magnitude of the floor deceleration with that of the c.g. indicates that the floor response, with superimposed 600 Hz floor vibrations, was slightly lower in magnitude than the c.g. pulse. As shown in the top right of the figure, the c.g. deceleration was a relatively constant approximately 40 g pulse of about .035-second duration. A low amplitude higher frequency vibration is evident on the c.g. response as was the case for the previous subfloors.

This static load-deflection data for the foam-filled cylinders in Fig. 29 indicates that at approximately 5.72 cm (2.25 inches) of crush, lateral bending of the upper floor occurred due to plastic hinge formation at the location of the foam-filled cylinders. As may be noted, however, in the dynamic test, the floor remained undeformed.

The dynamic responses for the canted bulkheads subfloor are presented in Fig. 37. The measured deceleration on the floor again shows the characteristic local floor vibration of approximately 600 Hz superimposed on a basic load pulse that appears to be slightly lower in magnitude than the lead mass c.g. response. Deceleration of the lead mass had an initial peak of above 40 g's or more followed by a relatively constant level around 25 g's. Lower amplitude vibrations are also evident on the c.g. response.

Although the lateral bulkheads in this subfloor concept were canted 30° from the vertical, the stiff longitudinal floor beams caused the formation of plastic hinges at the location of the longitudinal beams early in the static loading cycle (Fig. 30). Following this buckling of the upper floor, the load level under the reduced stiffness of the section was relatively constant with deflection. A comparison of this static behavior with the shape of the dynamic c.g. response shows good correlation as far as similarity in the trend of response.

Beyond .01 second, the reduced stiffness of the static data of the nonlinear crush zone (springs) underpredicts the magnitude of the dynamic response. Again this may be attributed to the

differences between the static subfloor behavior (Fig. 30), and the dynamic behavior illustrated in the "after" test photograph in Fig. 37. As may be noted in the latter photograph, the dynamic behavior of the canted bulkheads subfloor did show the initial stages of upper floor buckling (plastic hinges formation); however, the severity is much less than was the case in the static tests. Consequently, the loss in stiffness in the dynamic test was less following the initial peak load and the measured deceleration level was subsequently higher than the static data.

As was mentioned previously, the method of applying the static load at the seat mass location resulted in a lateral outboard load component that increased as the floor deformed. For the dynamic conditions, the seat mass load acted inboard as the floor deformed due to the inertial reaction (Fig. 38). This phenomenon also resulted in higher inboard seat loads relative to the outboard seat loads in the KRASH dynamic analysis which did not occur in the NASTRAN static analysis. Thus, static analysis and structural load deflection test may not accurately define the seat and floor loads or loading through the inboard energy-absorbing beam when compared to dynamic analysis and test. Notice again the large differences in deformation of the structural floor between static and dynamic test results. The floor is deformed considerably in the static tests, as shown in Figs. 27 through 30, yet there is no noticeable deformation found in the dynamic tests shown in Figs. 34 through 36 and with only minor deformation in Fig. 37. This illustrates clearly the differences in floor loading (also seat loading) that can occur between static and dynamic loading.

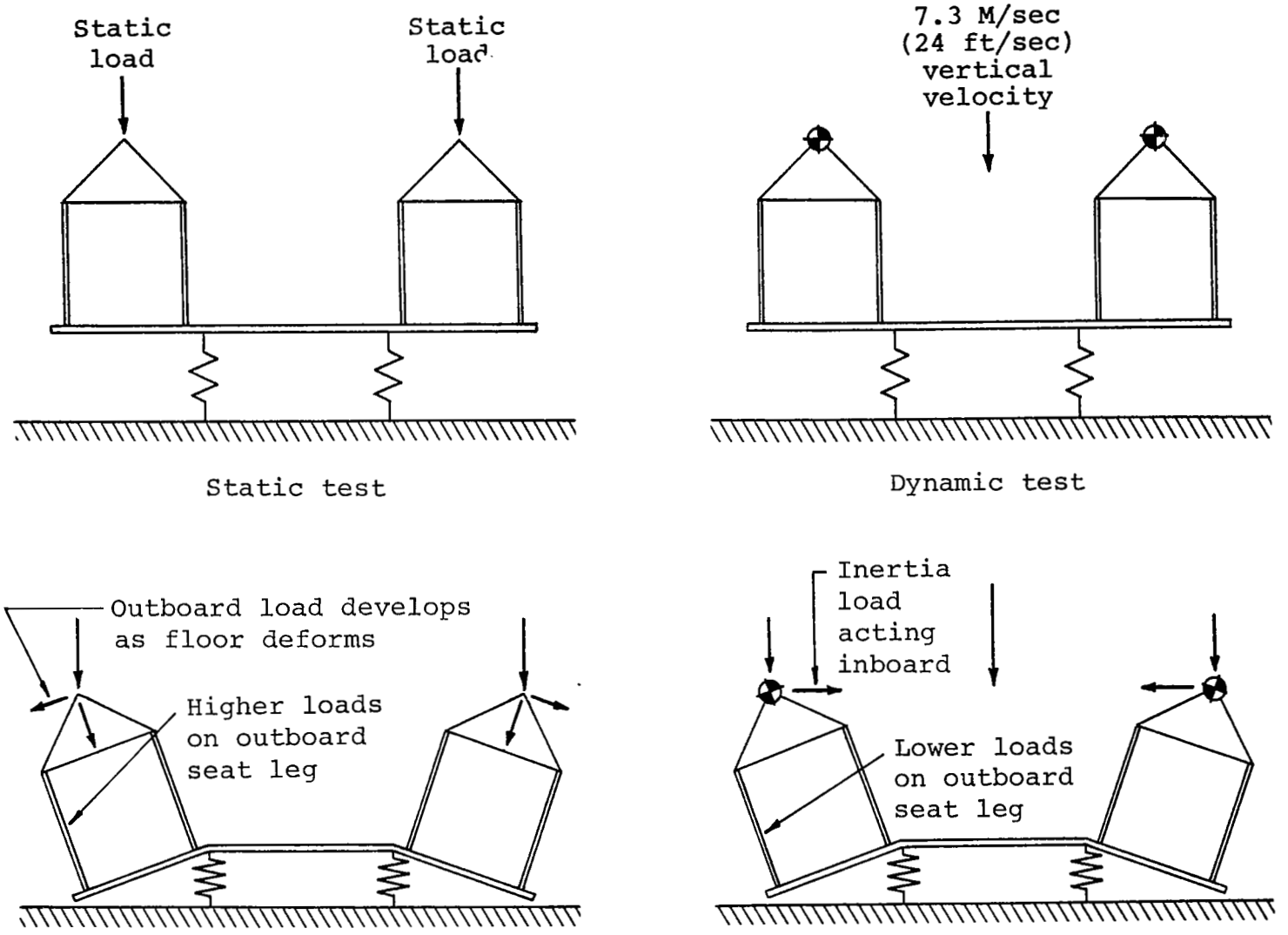

Figure 38. Comparison of static and dynamic loading.

5.5 ANALYTICAL CORRELATION

To incorporate crashworthy concepts into future aircraft designs, adequate analytical tools are needed to predict structure crash impact behavior. As described in Section 5.1, the initial design phase of the full-scale floor sections utilized the KRASH computer program to verify the structure adequacy for the NASA drop test conditions. Upon completion of the NASA static and dynamic testing of the floor sections, a brief test/analysis correlation was conducted to verify the reliability of the KRASH program.

The corrugated web concept was selected for correlation because the NASA tests showed it to have excellent energy-absorbing characteristics. The KRASH math model from the design phase was modified to represent the test configuration (Fig. 18). A rigid mass representation replaced the elastic occupant and energy-attenuating seat model. The load-deflection data for the energy-absorbing subfloor structure was obtained from the NASA static test results. Because the external crushing springs in the KRASH program do not permit the load-deflection data to be input in sufficient detail, a nonlinear beam in series with a stiff linear spring replaced the math model springs (Fig. 39).

The KRASH analysis simulated the 7.32 m/sec (24 ft/sec) pure vertical velocity impact test condition. The time history acceleration response of the rigid mass occupant/seat was selected for correlation. Figure 40 illustrates the floor section before and after test and the time history results obtained from test and KRASH. The plot shows excellent agreement between test and analytical results. The agreement in the results depends heavily on how good the load-deflection data is that defines the crushing springs. In this case, the static test data was a good representation of the dynamic behavior of the crushable structure.

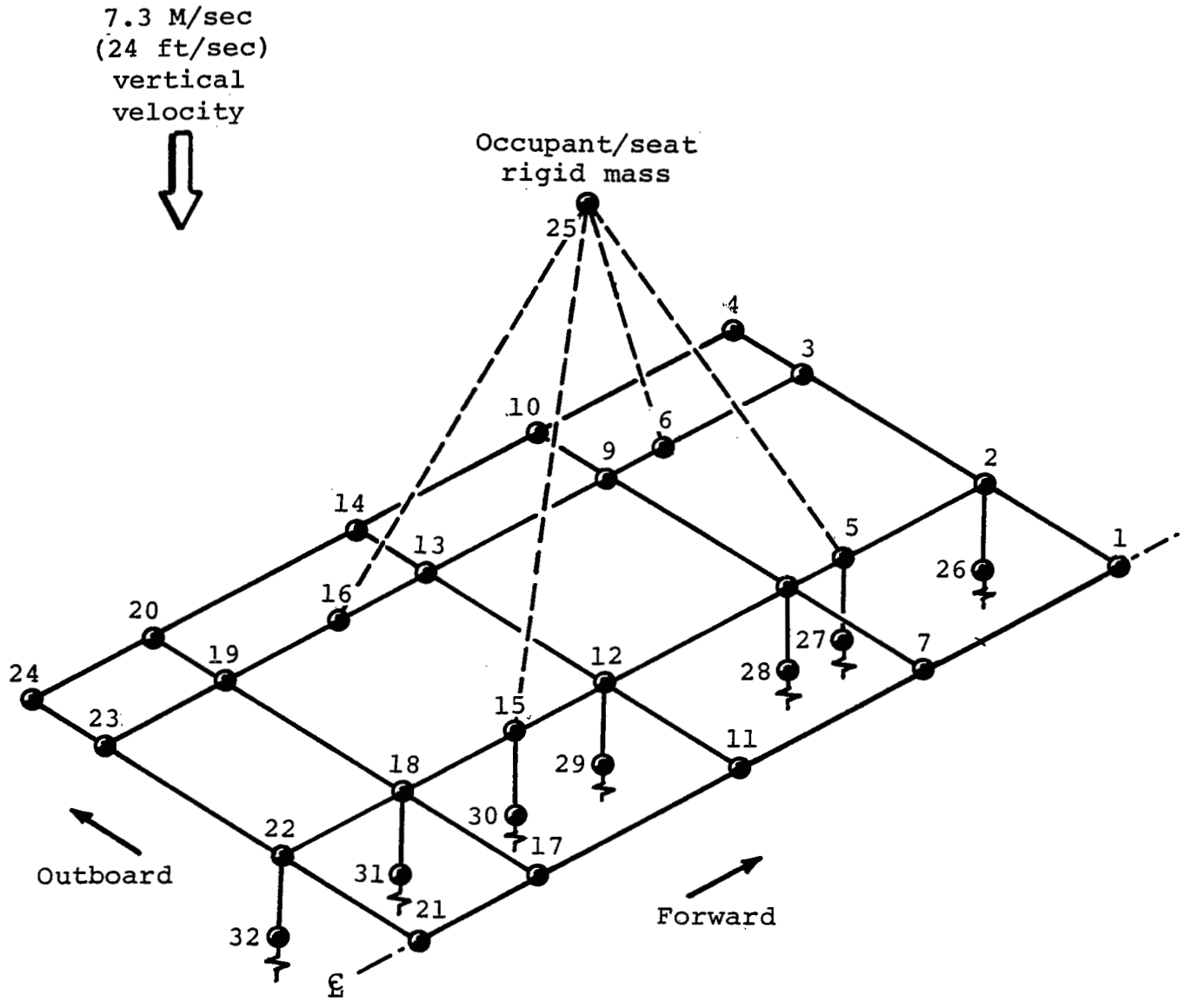

Figure 39. Revised KRASH math model of floor section with corrugated web concept.

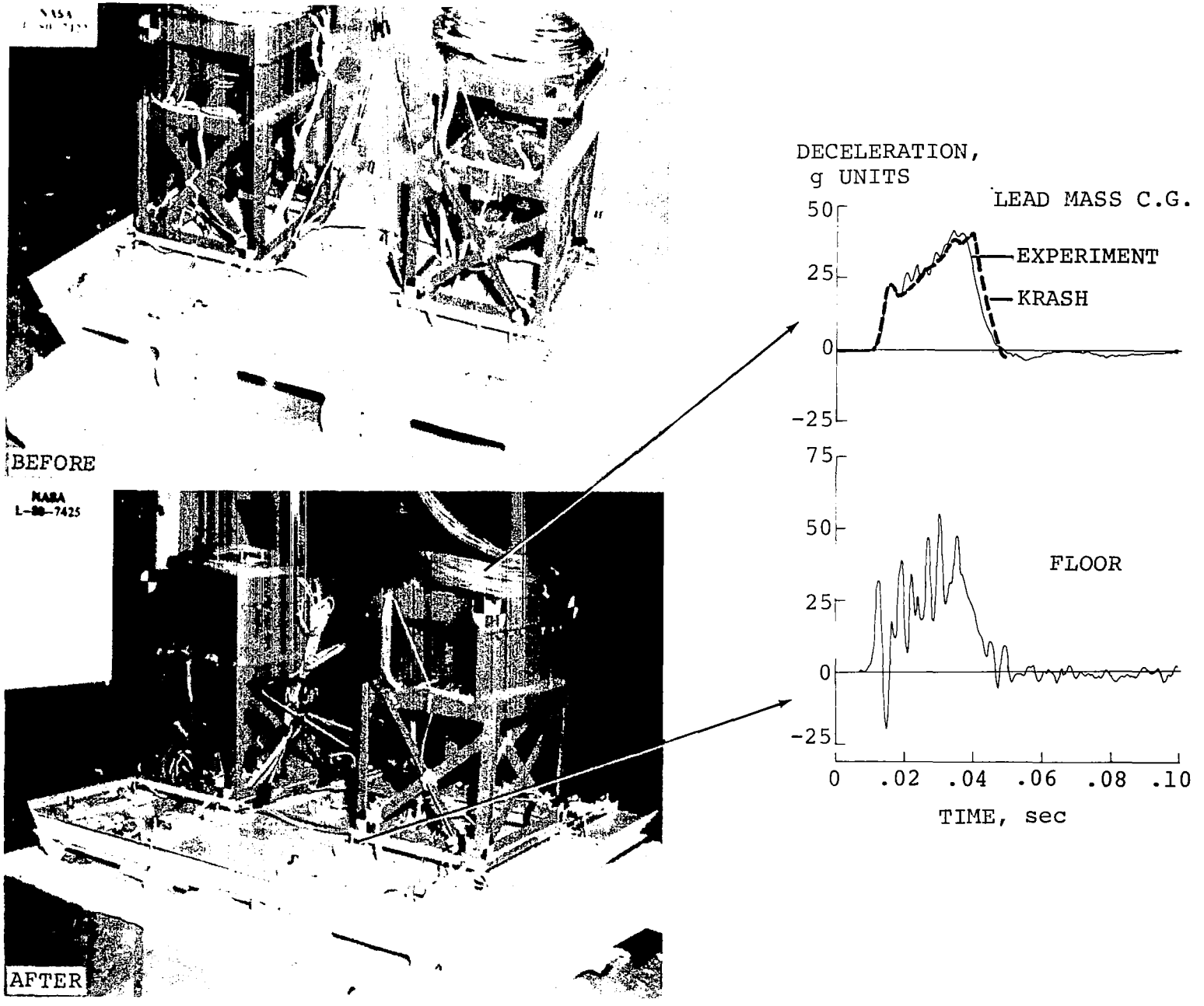

Figure 40. Comparison of test and KRASH results for 73 M/sec (24 ft./sec) vertical impact of floor section with corrugated web concept.

6. MODIFICATION OF FULL-SCALE AIRCRAFT STRUCTURE

6.1 FUSELAGE MODIFICATION

The third and final phase of the program entailed the structural modification of two twin-engine airplane fuselages with crashworthy subfloor structure concepts. Each of the five concepts used in the floor section design, fabrication, and testing phase was evaluated to determine the two most suitable concepts for incorporation in the fuselages. The primary factors considered in the evaluation of the concepts were crashworthiness capability, weight, and construction cost.

Of the two minimum modification concepts, the notched-corner design was selected over the canted bulkhead design because it exhibited better load-deflection and energy absorption characteristics in the dynamic tests. Also, the notched-corner concept was a slightly lighter weight design (see Section 5.2).

Of the more unconventional concepts, the corrugated web with notched-corners concept was judged superior to the corrugated half-shell and foam-filled cylinder concepts even though all three exhibited excellent load-deflection and energy absorption characteristics in the dynamic tests. The foam-filled cylinder concept was eliminated from consideration because it had a large amount of foam in the structure and carried an undesirable weight penalty. The corrugated half-shell concept was lightweight, but it was more costly to incorporate into the fuselage. The corrugated web with notched-corners design employed conventional construction and had the lightest weight of the three concepts.

On each of the airplanes, the fuselage subfloor structure from the main wing carry-through spar at FS 140 to aft of the rear cabin door at FS 244 was replaced with crashworthy subfloor structure. The modified area is illustrated in Fig. 41. Of the existing structure, the upper floor panel was left in place. The keel beams, bulkheads, stringers, and lower contour skin were removed, and the corrugated-web or notched-corner concepts installed. The crashworthy subfloor structure was designed so that the lower skin contour was maintained, including the skin gage. Seat tracks were installed on the upper floor panel to provide seat attachment capability for future crash testing. Figures 42 and 43 illustrate details of the construction of the corrugated web and notched-corners subfloor structures, respectively. The engineering drawings used for the fuselage modification work are included in Appendix E.

Photographic documentation of the actual modification work is presented in Fig. 44. The picture sequence shows (a) exterior views of the two original aircraft, (b) an interior view of the original floor structure, (c) a fuselage in the support cradle

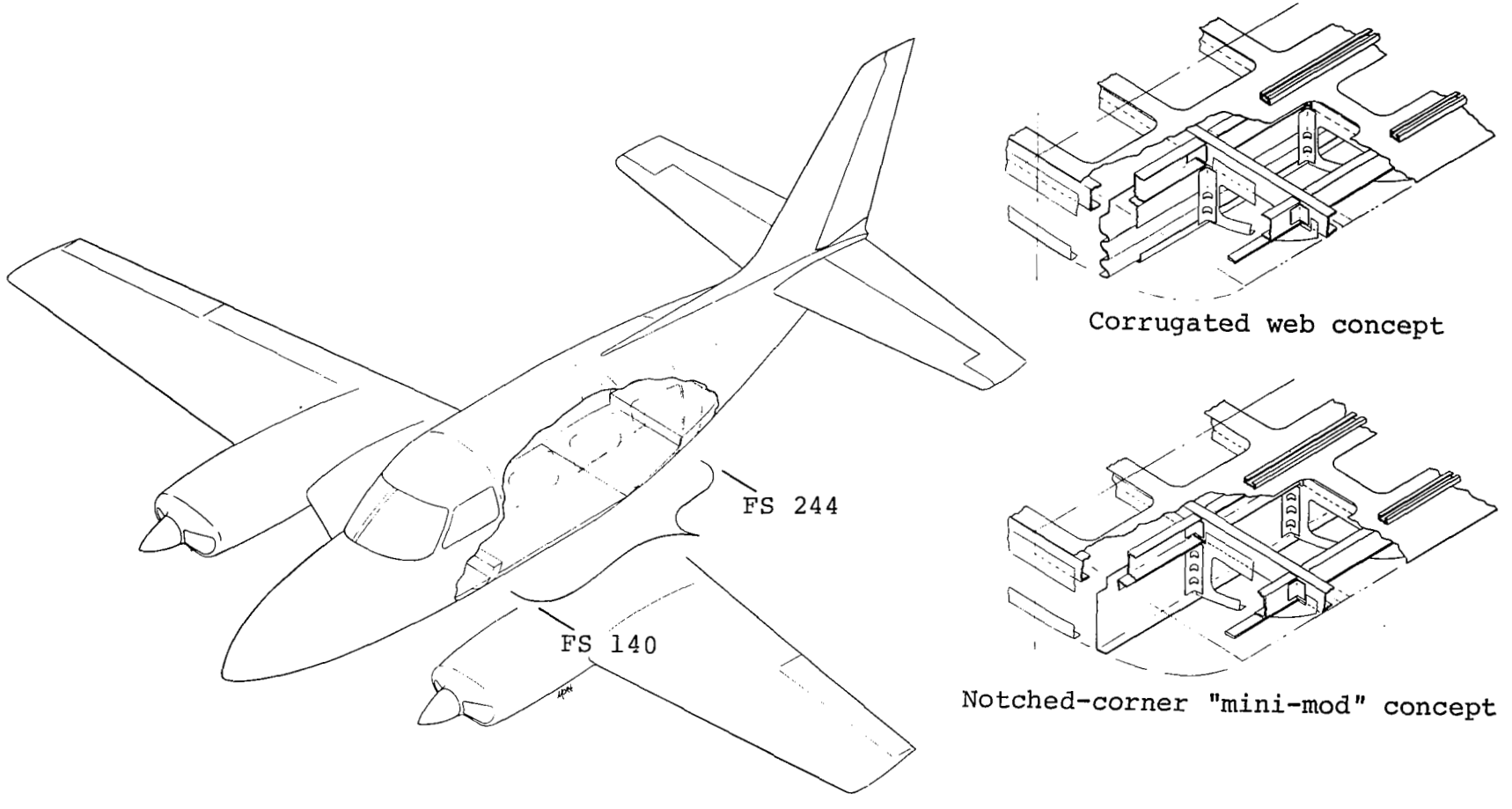

Figure 41. Fuselage modification schematic.

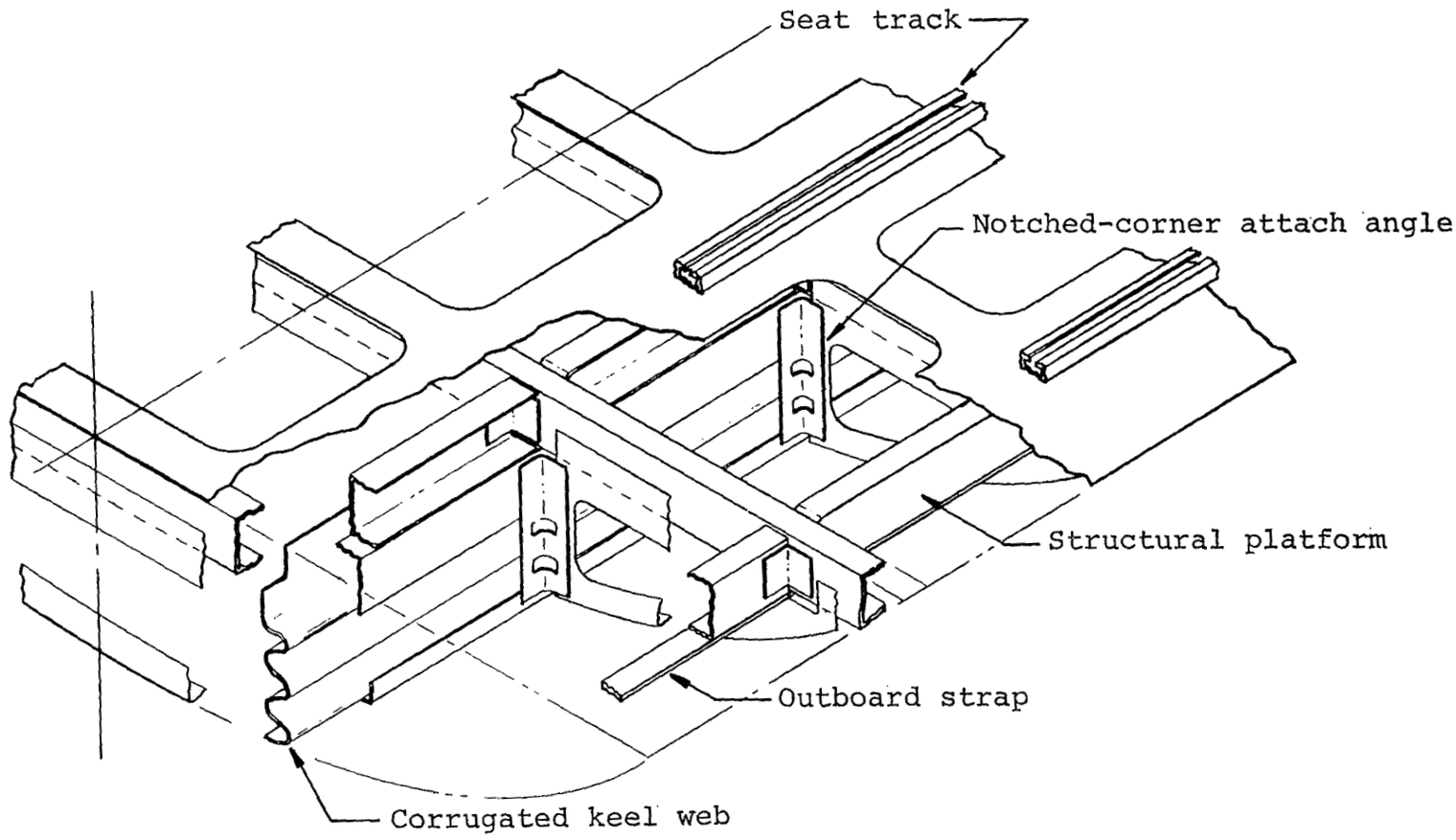

Figure 42. Fuselage modification detail of corrugated web concept.

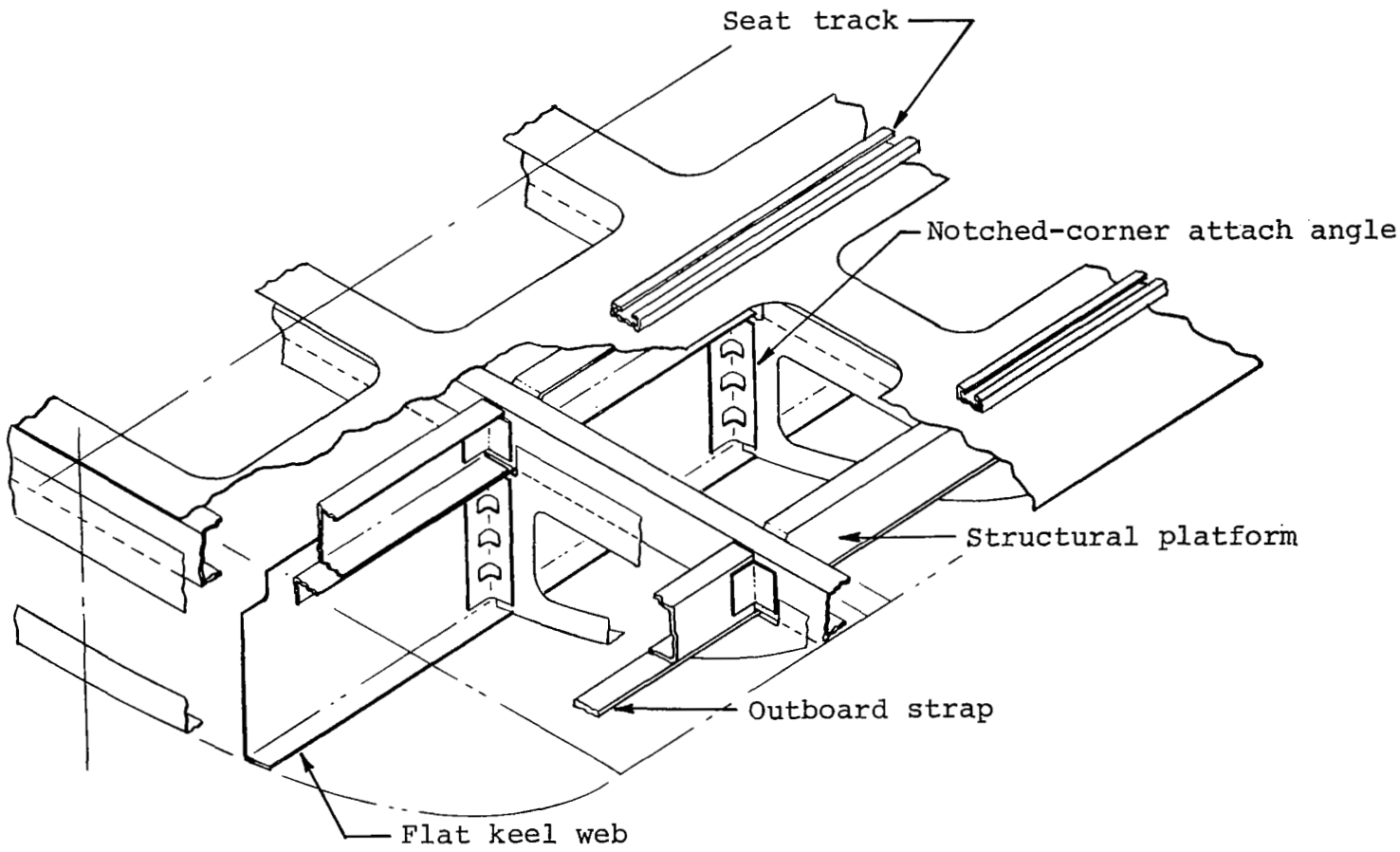

Figure 43. Fuselage modification detail of notched-corners concept.

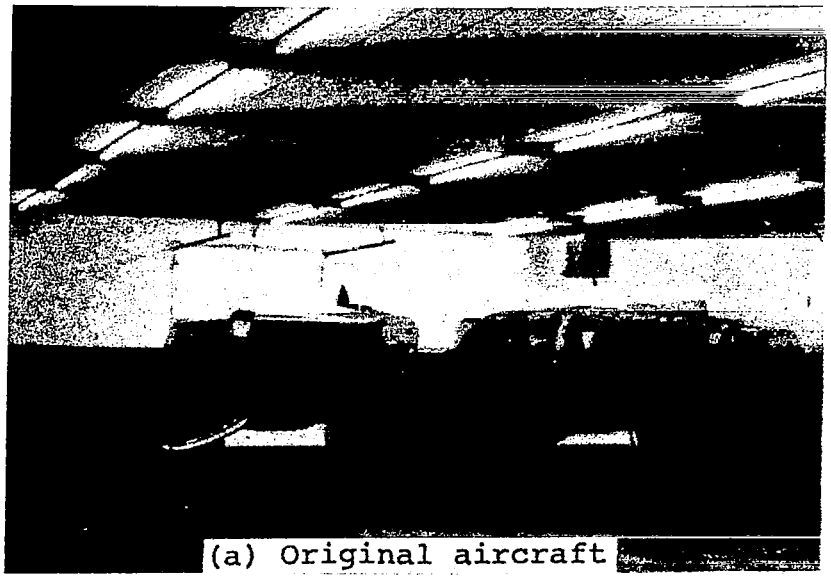

(a) Original aircraft

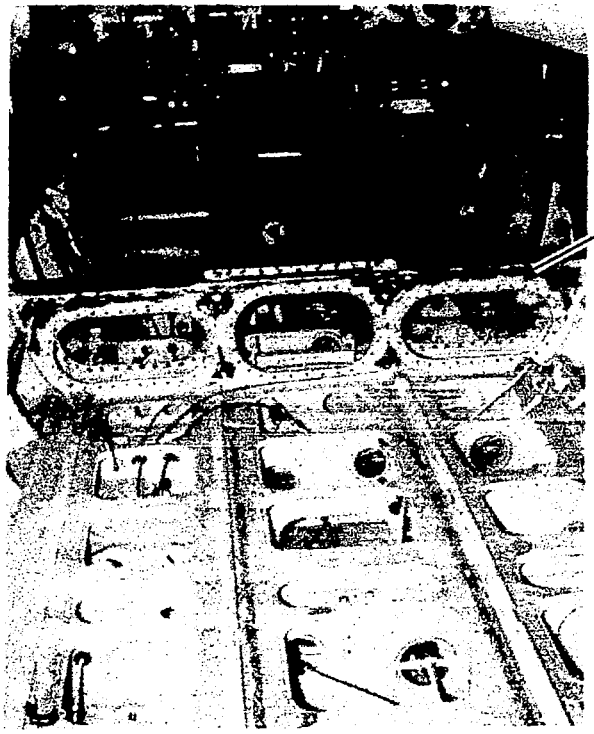

(b) Interior view showing floor with panels removed

Figure 44. Fuselage modification work sequence.

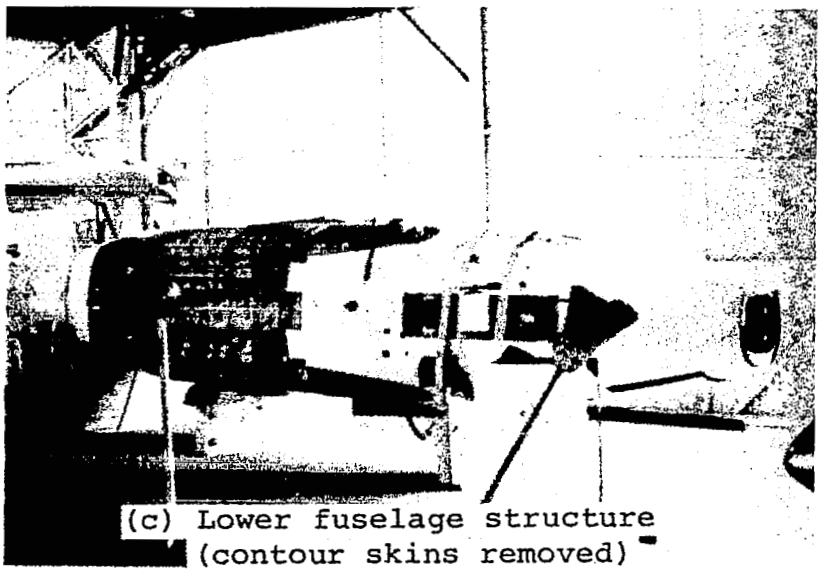

(c) Lower fuselage structure (contour skins removed)

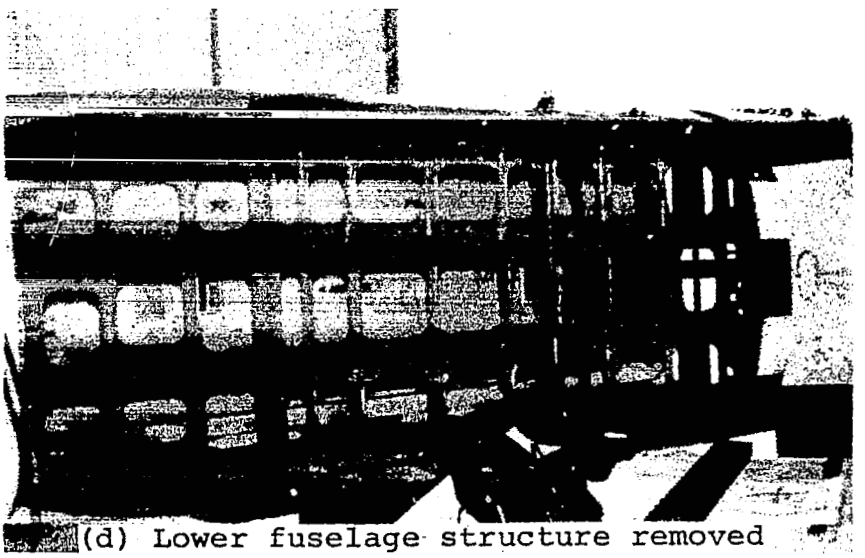

(d) Lower fuselage structure removed

Figure 44 (continued). Fuselage modification work sequence.

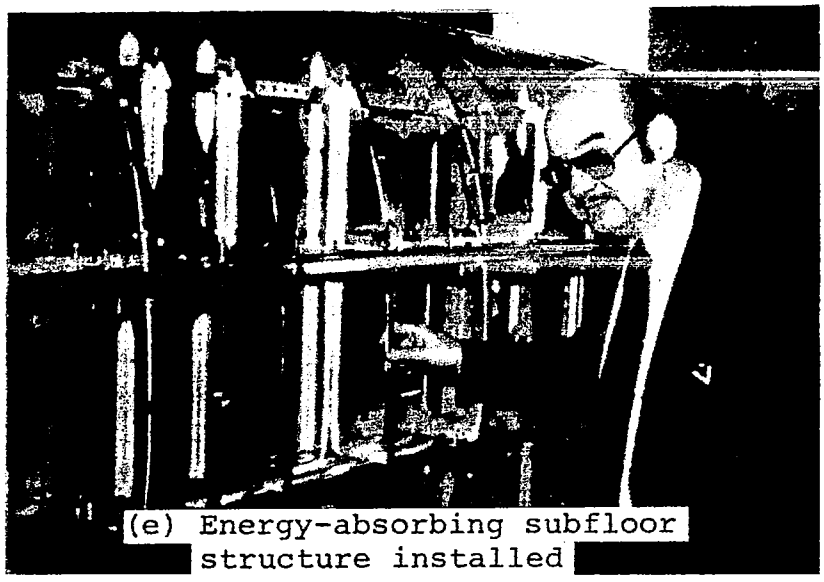

(e) Energy-absorbing subfloor structure installed

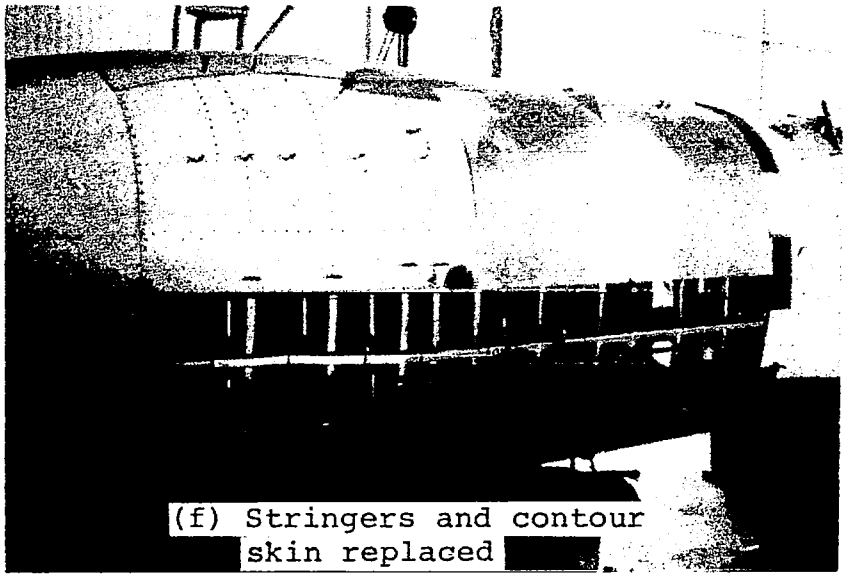

(f) Stringers and contour skin replaced

Figure 44 (continued). Fuselage modification work sequence.

with lower contour skins removed, (d) the original subfloor structure removed, (e) the corrugated web subfloor concept structure installed, and (f) the stringers and lower contour skin during installation. Detail photographs of the structural floor and crashworthy subfloor concepts during the fuselage modification work are shown in Figs. 45 and 46, respectively.

Both the corrugated-web and notched-corner crashworthy subfloor structures were designed for a twin-engine airplane with a non-pressurized cabin. As a result, the typical material thickness used in the subfloor structure was 0.0635 cm (0.025-in). However, for the same airplane with a pressurized cabin, the material thickness requirements are typically of 0.0813 cm (0.032-in) to 0.1016 cm (0.040-in). However, with the structural floor beefup underneath the floor, the lighter gauge webs may be adequate for a pressurized cabin.

A pressurized cabin airplane was used as a basis for assessing the weight penalty associated with incorporating the crashworthy subfloor structure. Modification of the airplane with the notched-corner design increased the original aircraft weight by approximately 6.8 kg (15 lb) while the corrugated-web design was approximately a 9.1 kg (20 lb) increase. For a 2724 kg (6000 lb) airplane, the weight increases were .25 percent of gross weight for the notched corner concept and .33 percent of gross weight for the corrugated web concept.

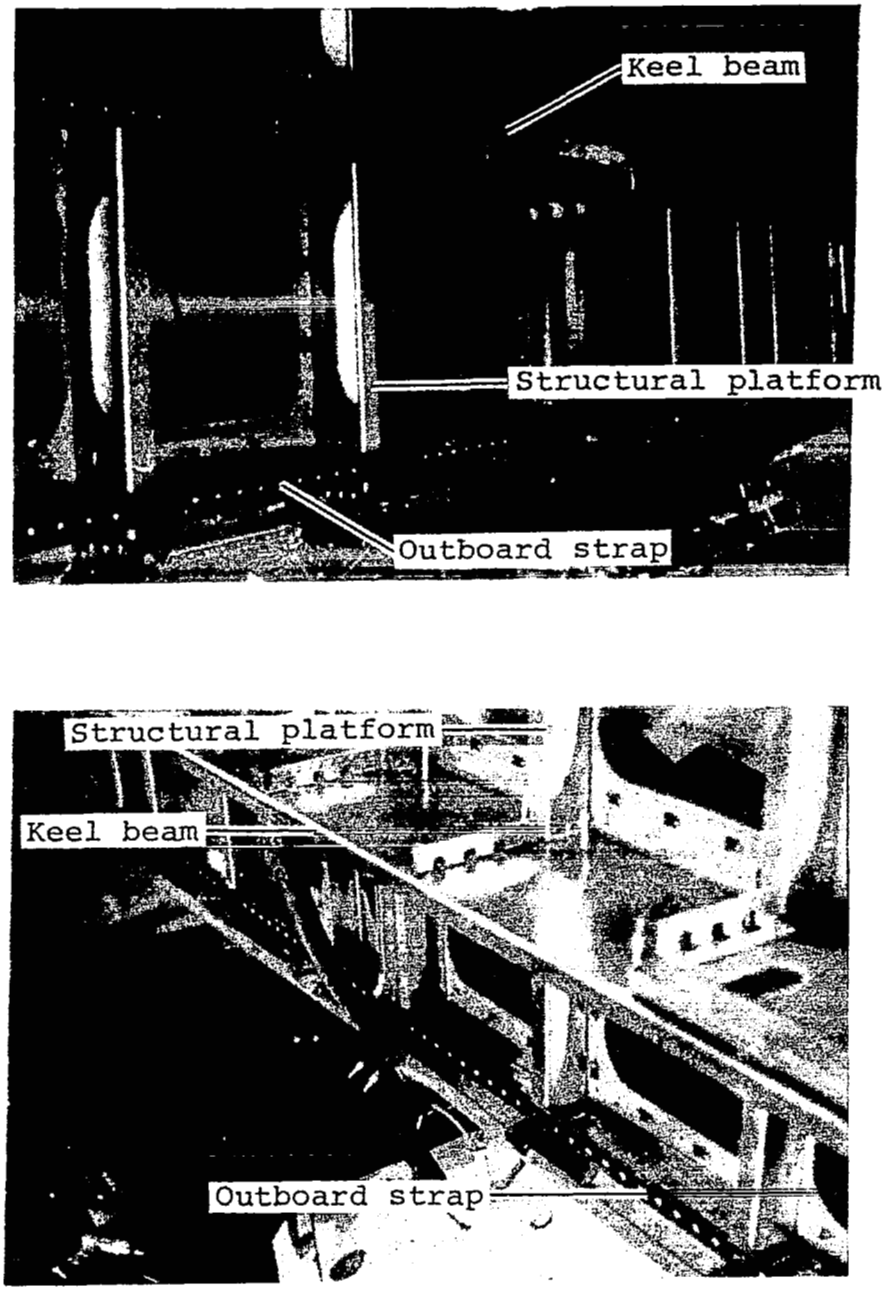

Figure 45. Structural floor in fuselage modification work.

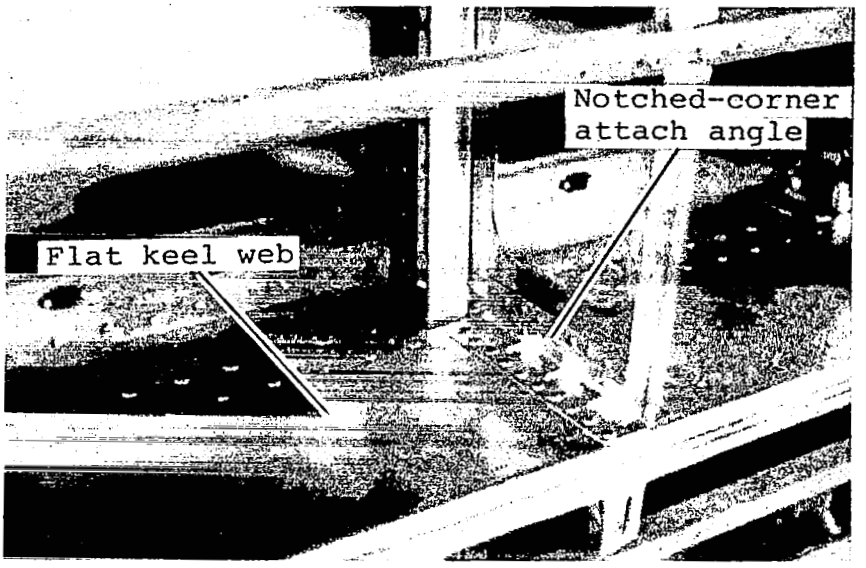

(a) Notched-corners "mini-mod" concept.

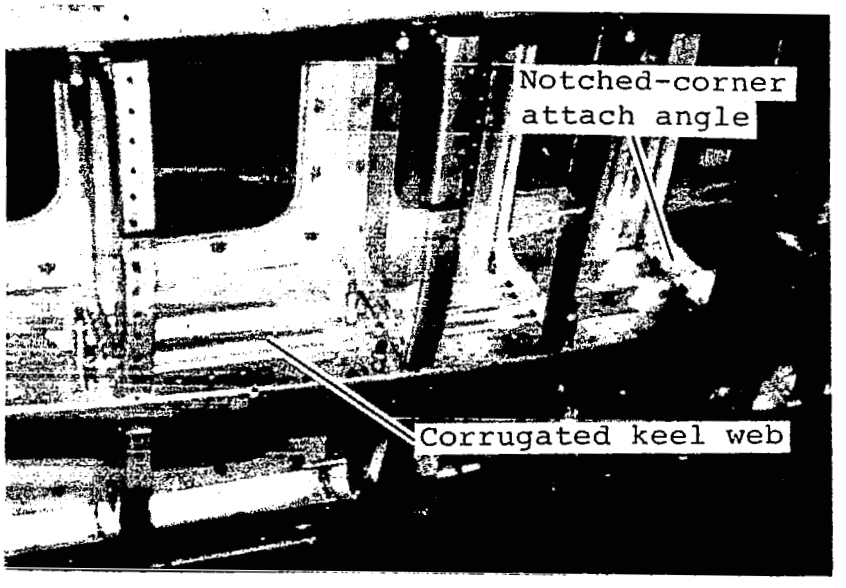

(b) Corrugated web with notched-corners concept

Figure 46. Crashworthy subfloor concepts in fuselage modification work.

6.2 KRASH ANALYSIS

A KRASH analysis was conducted to evaluate the crash impact performance of the twin-engine airplane with a crashworthy subfloor structure. To be consistent with the previous floor section test and analysis correlation work, the airplane configured with the corrugated-web concept was selected for the analytical investigation.

A KRASH math model of a twin-engine low-wing airplane was used based on the work done by Wittlin in Ref. 7. The model was developed specifically for FAA-sponsored correlation work using results from the full-scale airframe crash tests conducted at NASA-Langley Research Center in 1977.

Because the airplane is symmetrical about the centerline, only a half model was required to represent the structure. The original math model is shown in Fig. 47. It was comprised of 39 mass points, 4 massless mode points, 85 beam elements, and 13 external crushing springs.

The math model was updated to reflect the actual fuselage structural modifications for the incorporation of the corrugated-web subfloor concept. Extra mass points and beam elements were added to model the bulkhead at FS 244. The crushing springs at FS 137, FS 174, and FS 210 that represented the original lower fuselage structure were removed. From the floor section static test results, load-deflection data per length of structure was obtained to determine the distribution of crushing load between FS 140 and FS 244. At each bulkhead, a vertically aligned nonlinear beam element in series with a short stiff linear crushing spring was added to represent the crushing characteristics of the crashworthy subfloor structure.

To make the math model more representative of an actual airplane crash test article, three energy-attenuating seats and occupants were added in the cabin area. The simple seat/occupant models were comprised of three masses and three beams each. The seats were modeled to stroke at a constant 14.5g load based on the occupant weight.

Figure 48 illustrates the KRASH math model of the twin-engine low-wing airplane with the corrugated-web crashworthy subfloor structure. The figure also shows the special modeling techniques used for the lower fuselage crushable structure and the seat/occupant systems. Comprehensive documentation of the KRASH model is included in Appendix F.

From previous NASA full-scale airplane crash tests, a typical impact condition was selected for a KRASH analysis simulation. The aircraft had a 26.8 m/sec (60 mph) resultant velocity at

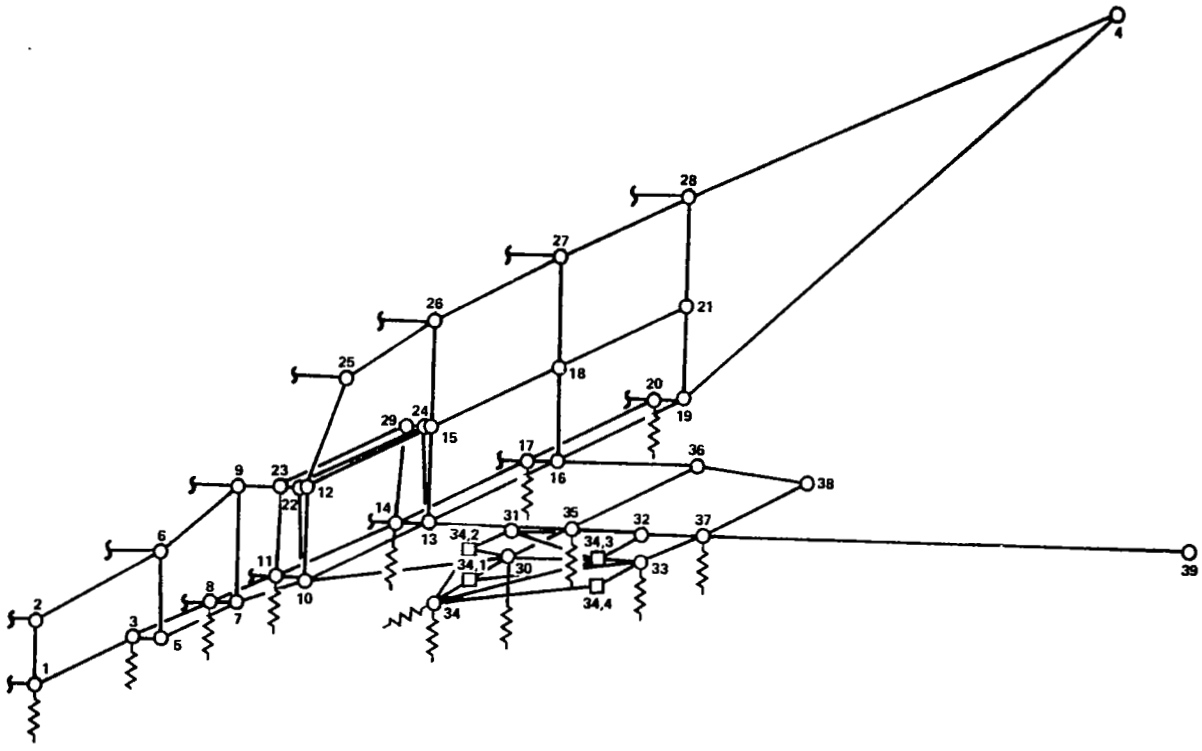

Figure 47. Baseline KRASH math model of low-wing twin-engine airplane.

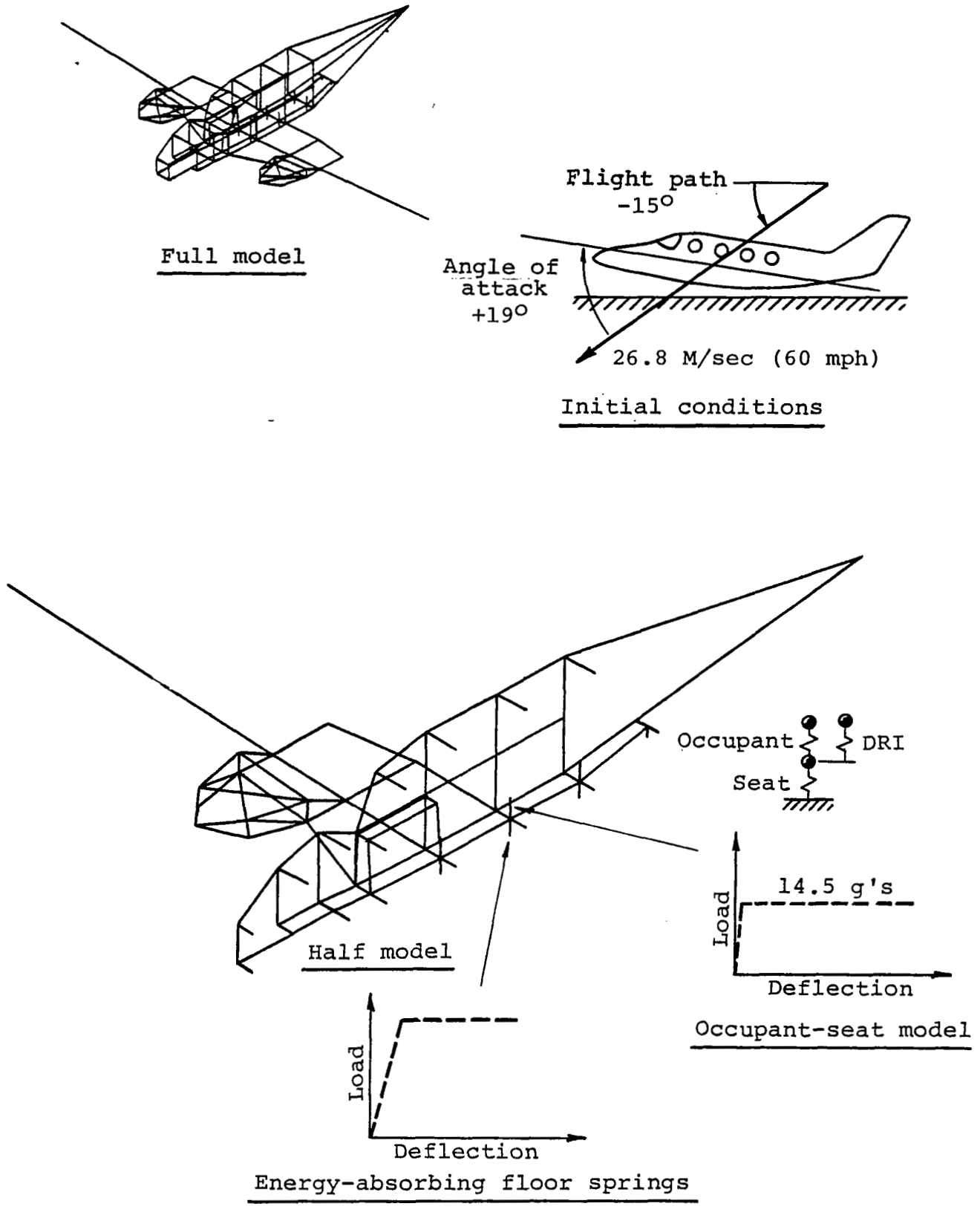

Figure 48. KRASH math model and impact condition for fourth test.

impact with a 15° nose-down flight path angle and a 19° nose-up angle of attack. The initial conditions input to KRASH were 25.9 m/sec (85.0 ft/sec) longitudinal velocity, 6.9 m/sec (22.8 ft/sec) vertical velocity, and 4° nose-up pitch attitude.

The analytical results showed that the simulated crash impact was survivable for the cabin occupants. The energy attenuating seats which were attached to the strong structural floor stroked between 7.4 cm (2.9 in.) and 8.9 cm (3.5 in.). The Dynamic Response Index (DRI) was less than 23 indicating no spinal injuries would have occurred for this particular impact.

7. CONCLUSIONS AND RECOMMENDATIONS

Five energy-absorbing lower fuselage structure concepts were developed for improving the crash protection of occupants and appear to be practical for incorporation into future metal airframes. Each of the concepts was incorporated into a floor test section that featured a seat-supporting structure floor or platform with an energy-absorbing crush zone underneath. The concepts were evaluated by static and dynamic testing at the NASA-Langley Research Center (Ref. 3). For most of the concepts, good results were obtained with control of loads to the structural floor, high energy absorption, and good structural integrity after impact. The lightest weight concepts were found to be those that efficiently utilized the existing structure for energy absorption rather than those that incorporated redundant, add-on materials such as foam.

Experimental static load-deflection data and dynamic deceleration response for five load-limiting subfloors indicate that the floor sections perform well throughout the loading cycle; that is, structural integrity and residual strength of the subfloors was maintained. The data also indicate that some of the sections were more effective in providing an essentially constant limit load with displacement than others. Further design iterations, however, could possibly alleviate the undesirable characteristics of the less effective sections.

The analysis and correlation with experimental results have shown the usefulness of statically determined crush data for dynamic analysis; however, the results also indicate that the analyst must exercise care and have some assurance that the static deformation behavior will approximate the dynamic deformation behavior. Also, the floor loading can be considerably different between static and dynamic tests or analyses.

With increasing emphasis on advanced composite materials for aircraft, concepts for composite airframe structures should also be investigated and evaluated relative to metal structure in the future.

APPENDIX A

DESIGN SUPPORT TEST DATA

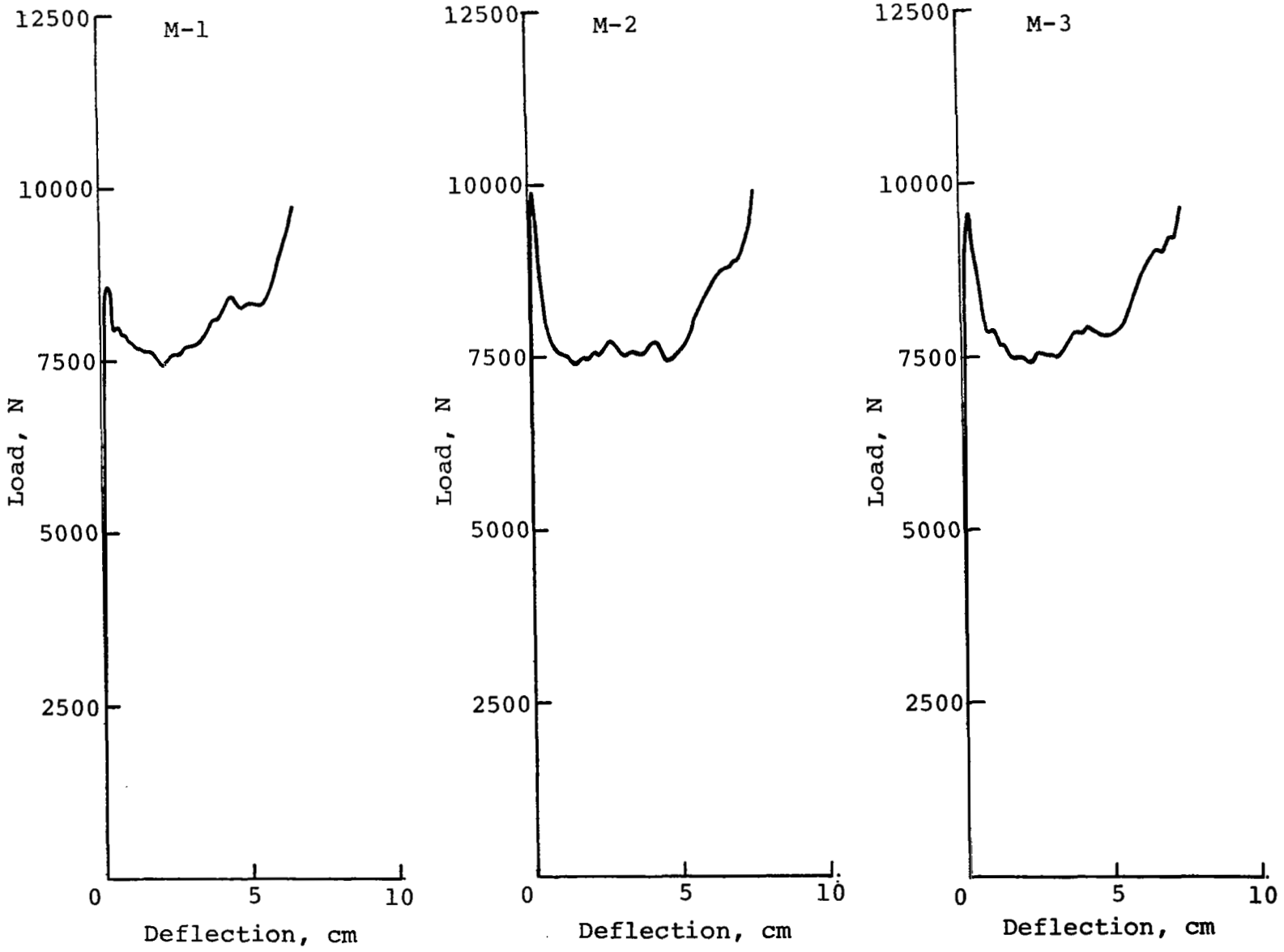

Figure A-1. Static test load-deflection data for formable keel beam with 0.9525 cm lower flange radius.

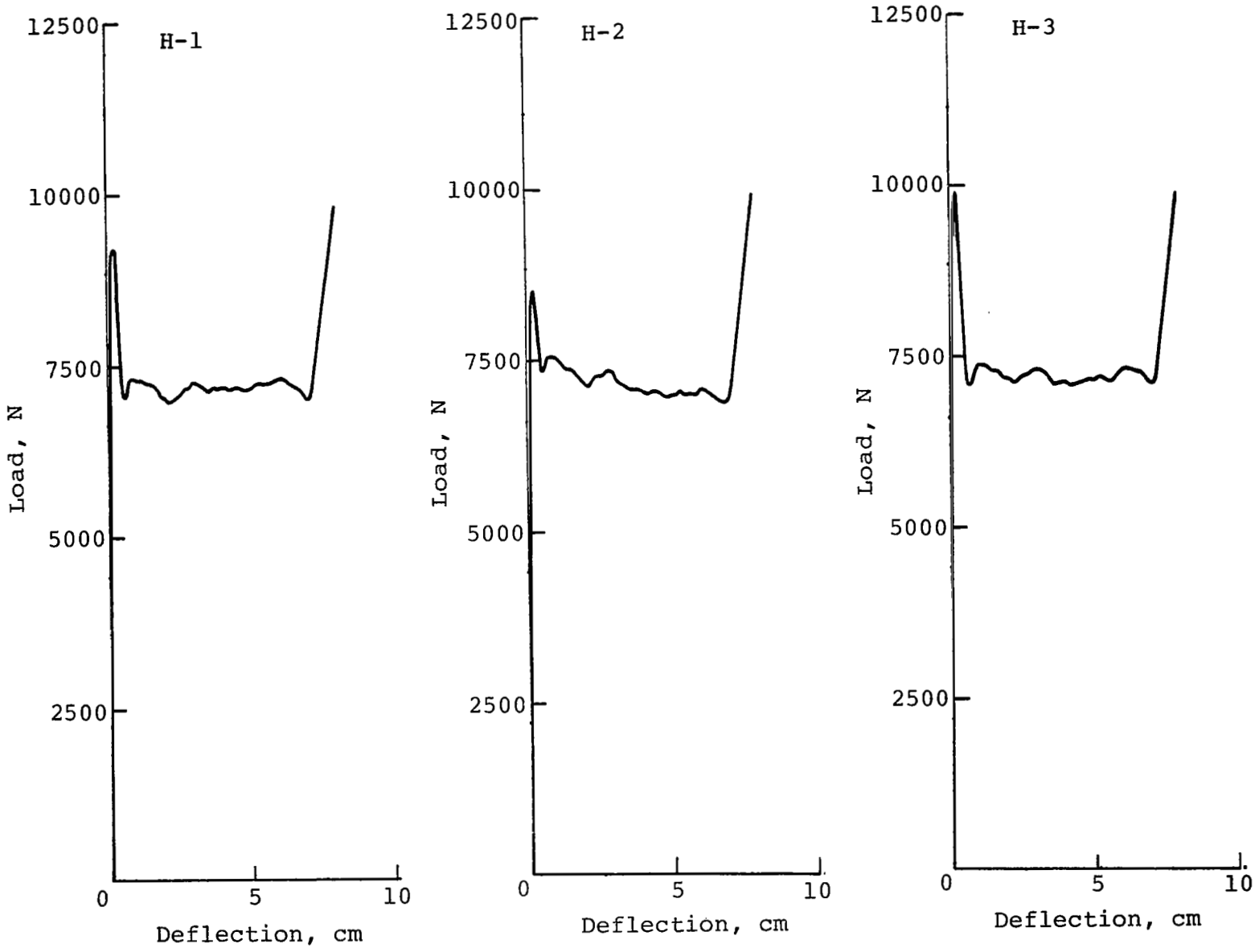

Figure A-2. Static test load-deflection data for formable keel beam with 1.27 cm lower flange radius.

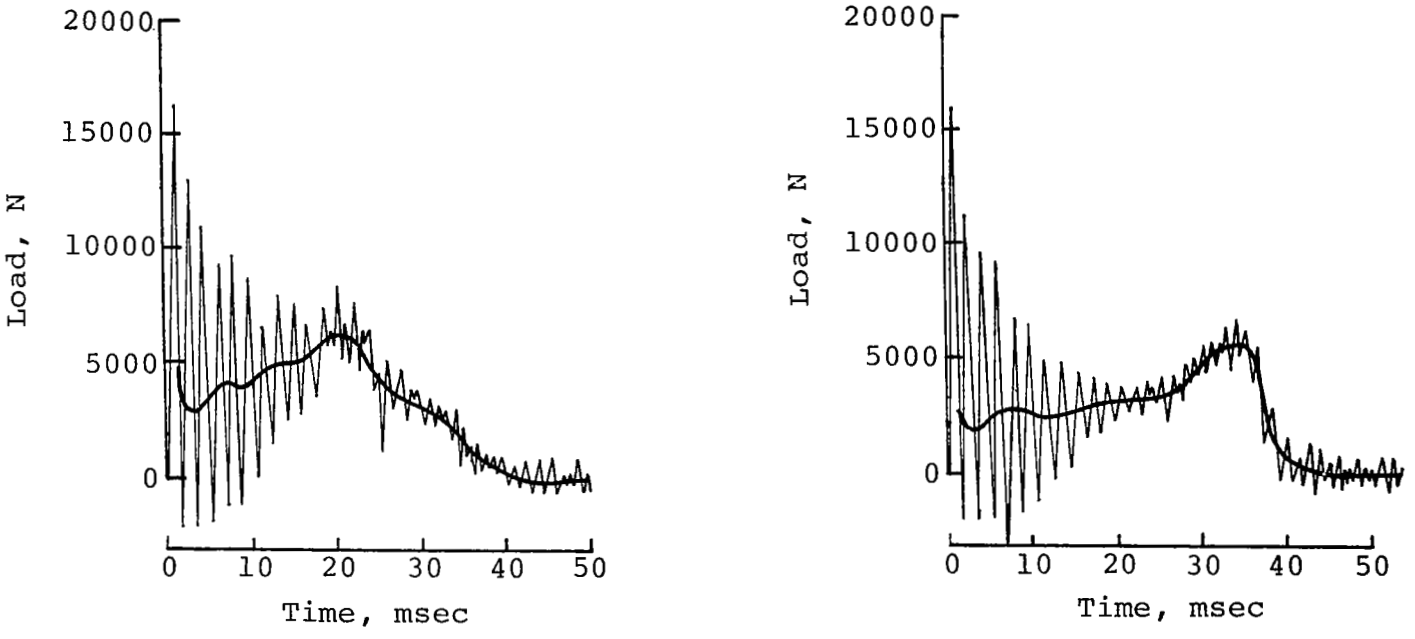

1.905 cm Formable beam
70-4 R=0.9525 cm

2.54 cm Formable beam
70-4 R=1.27 cm

Figure A-3. Dynamic test load versus time data for formable keel beams.

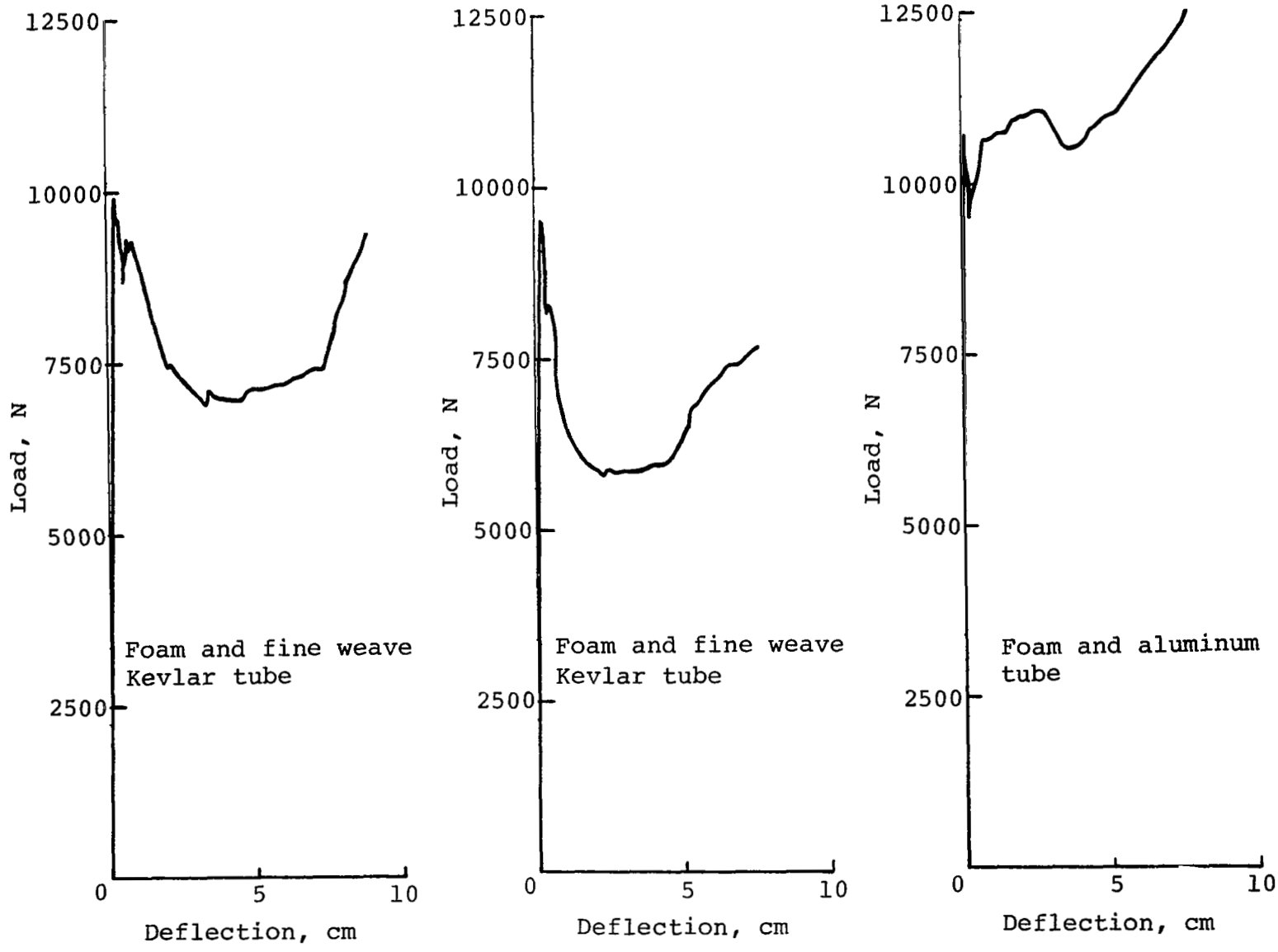

Figure A-4. Static test load-deflection data for foam with Kevlar and aluminum tubes.

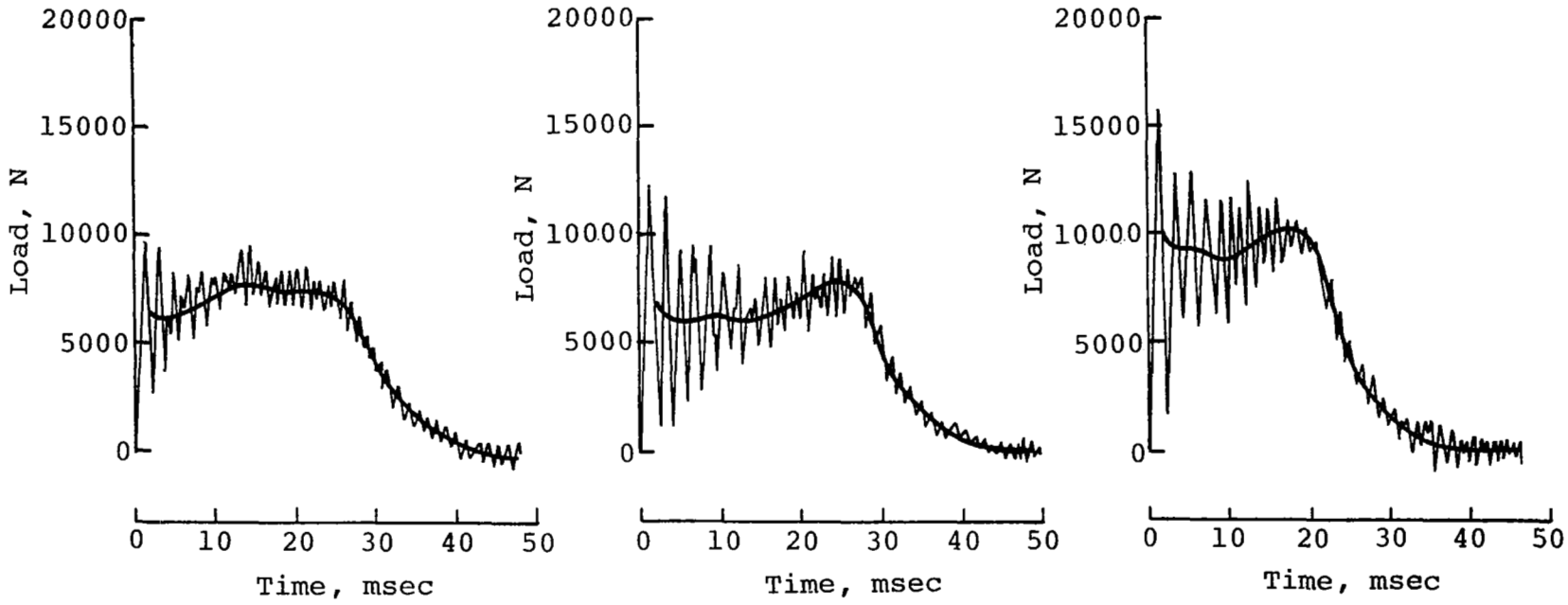

Foam and coarse weave Kevlar tube

70-9

Foam and close weave Kevlar tube

70-9

Foam and aluminum tube

70-9

Figure A-5. Dynamic test load versus time data for foam with Kevlar and aluminum tubes.

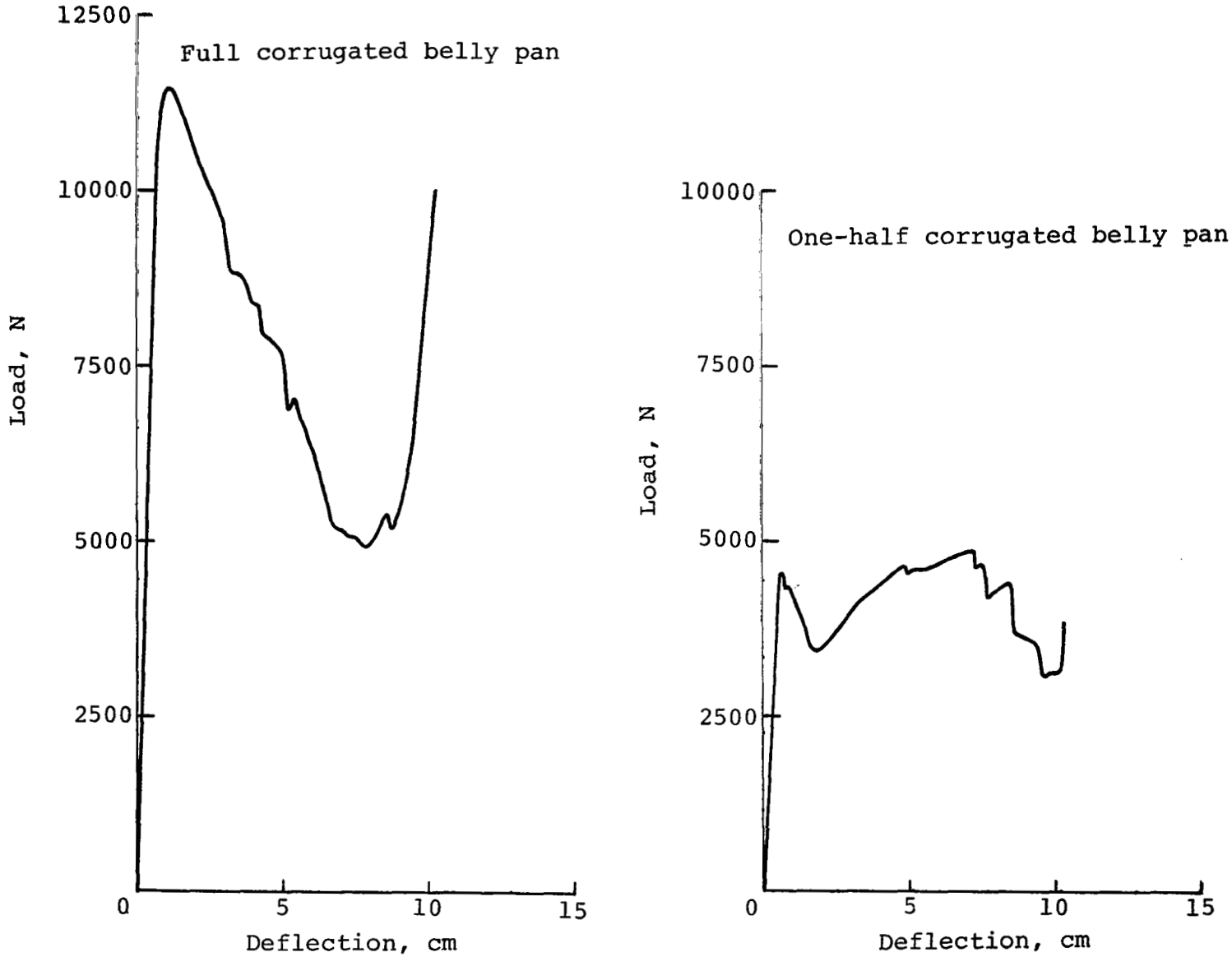

Figure A-6. Static test load-deflection data for corrugated belly pan.

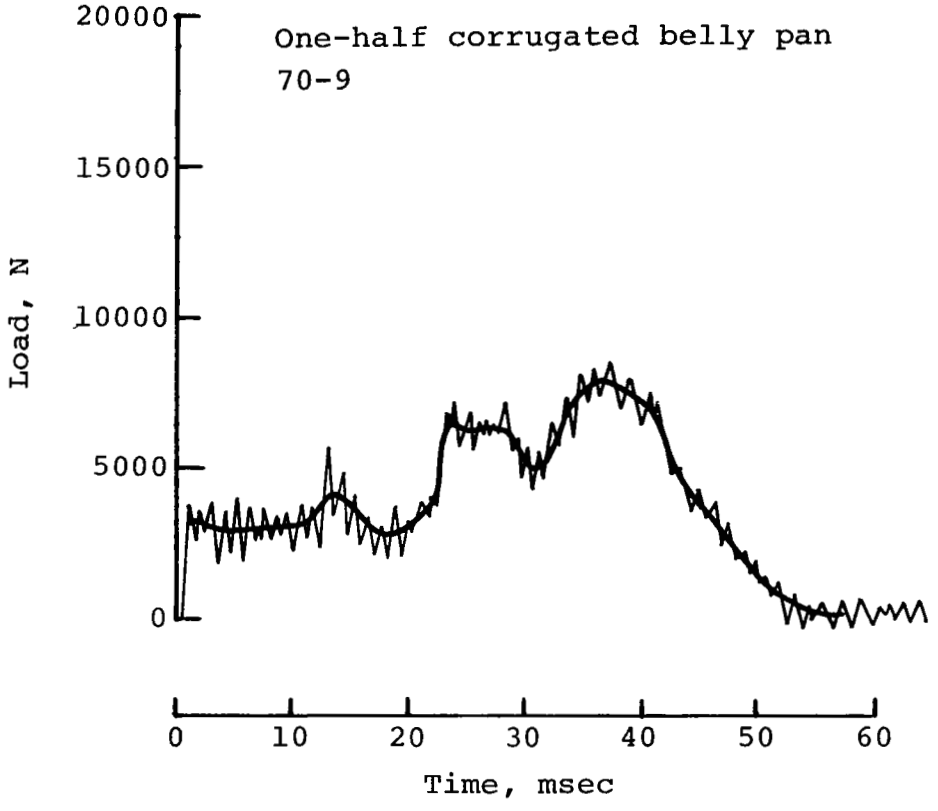

Figure A-7. Dynamic test load versus time data for corrugated belly pan.

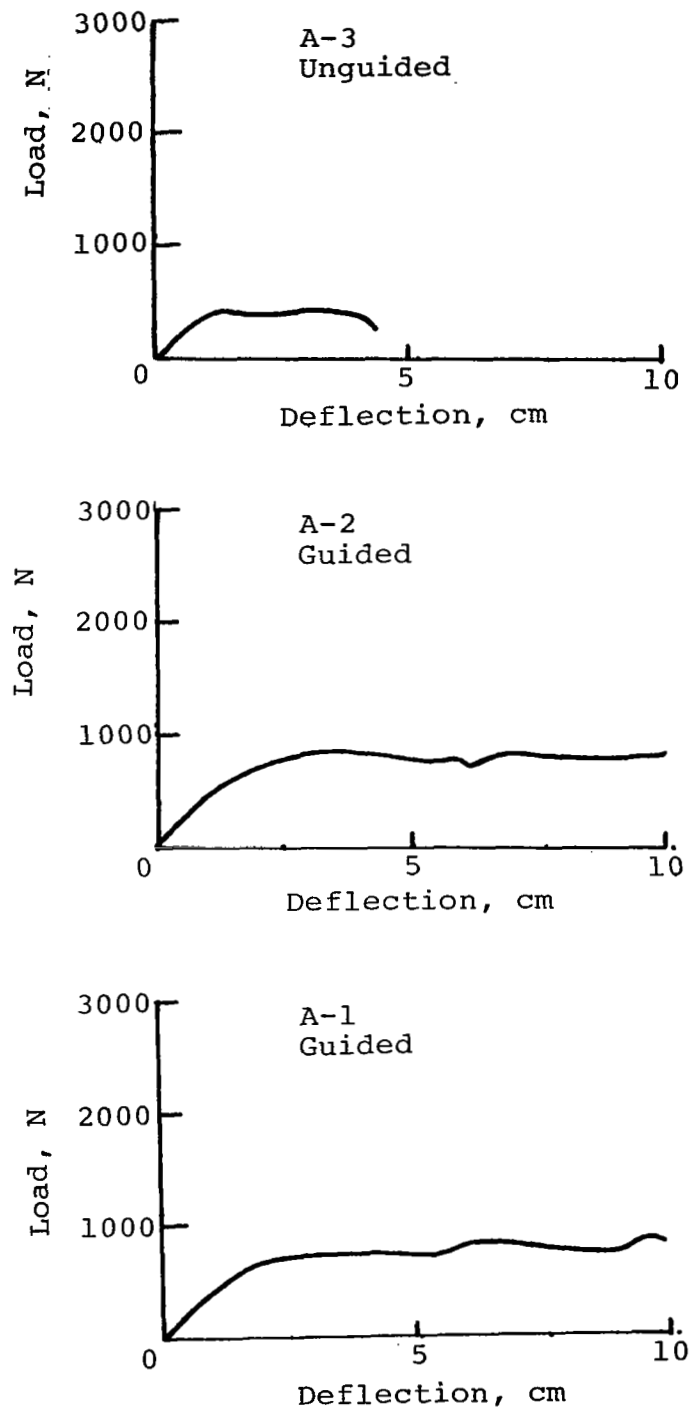

Figure A-8. Static test load-deflection data for 0.04064 cm corrugated web.

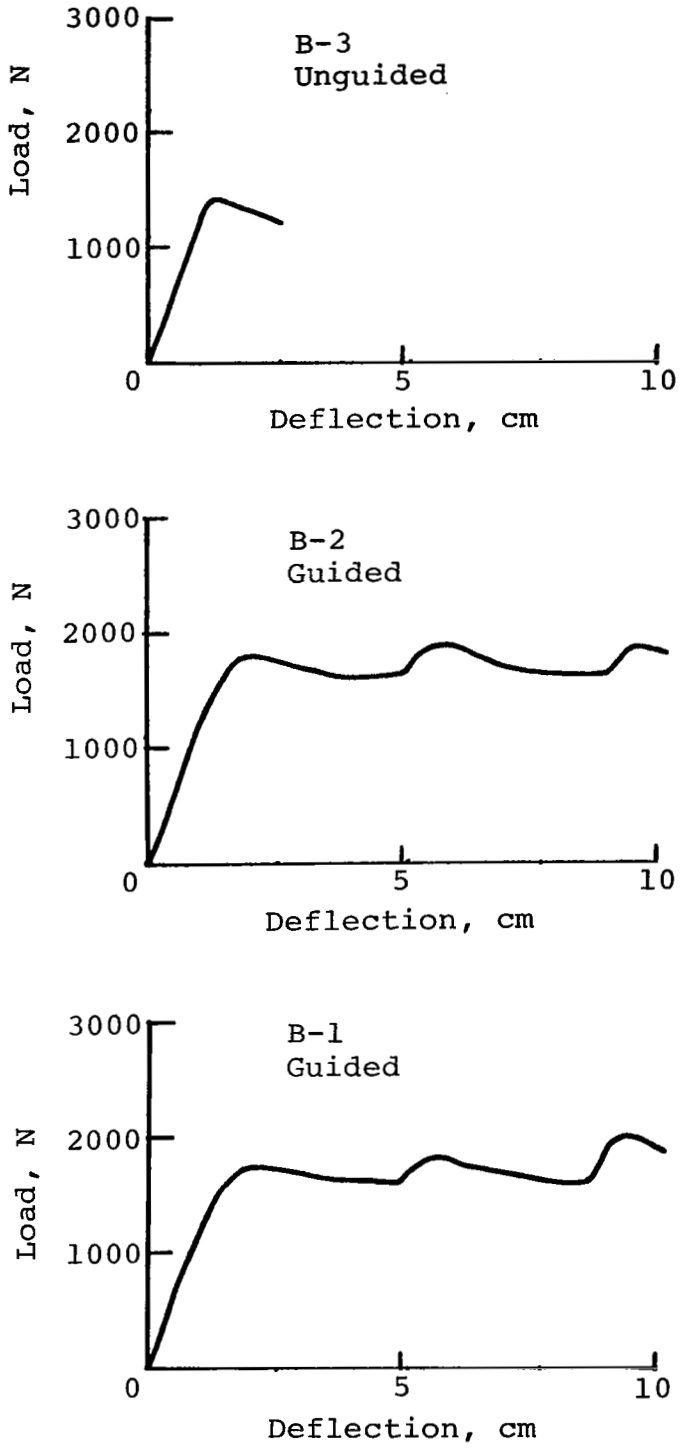

Figure A-9. Static test load-deflection data for 0.08128 cm corrugated web.

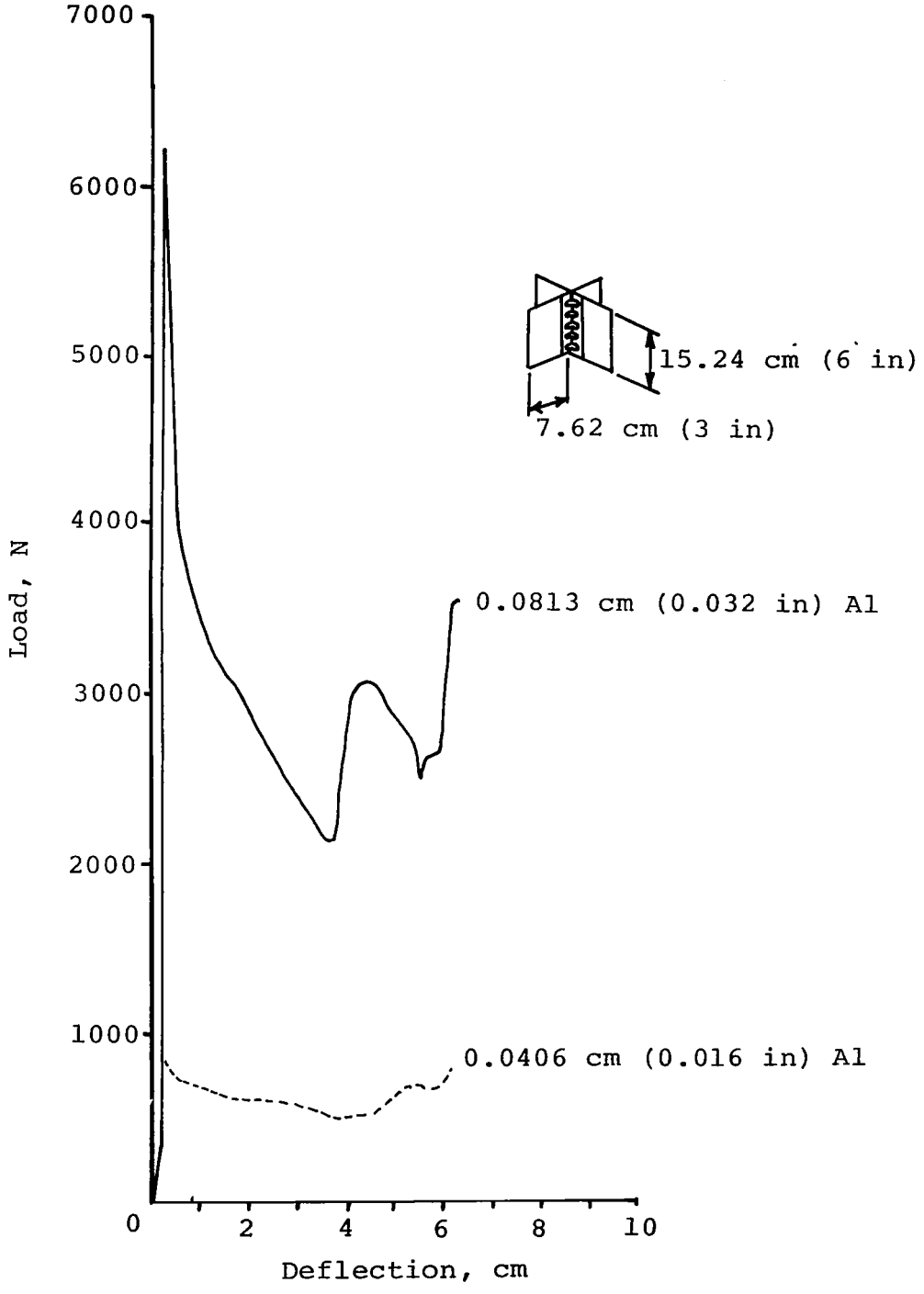

Figure A-10. Static test load-deflection data for cruciforms.

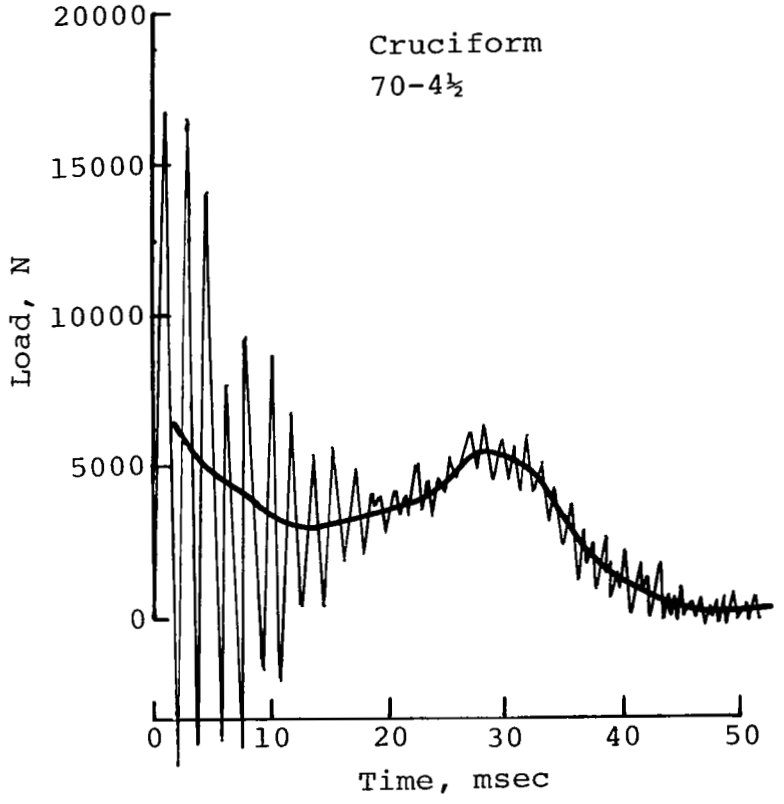

Figure A-11. Dynamic test load versus time data for 0.08128 cm cruciform.

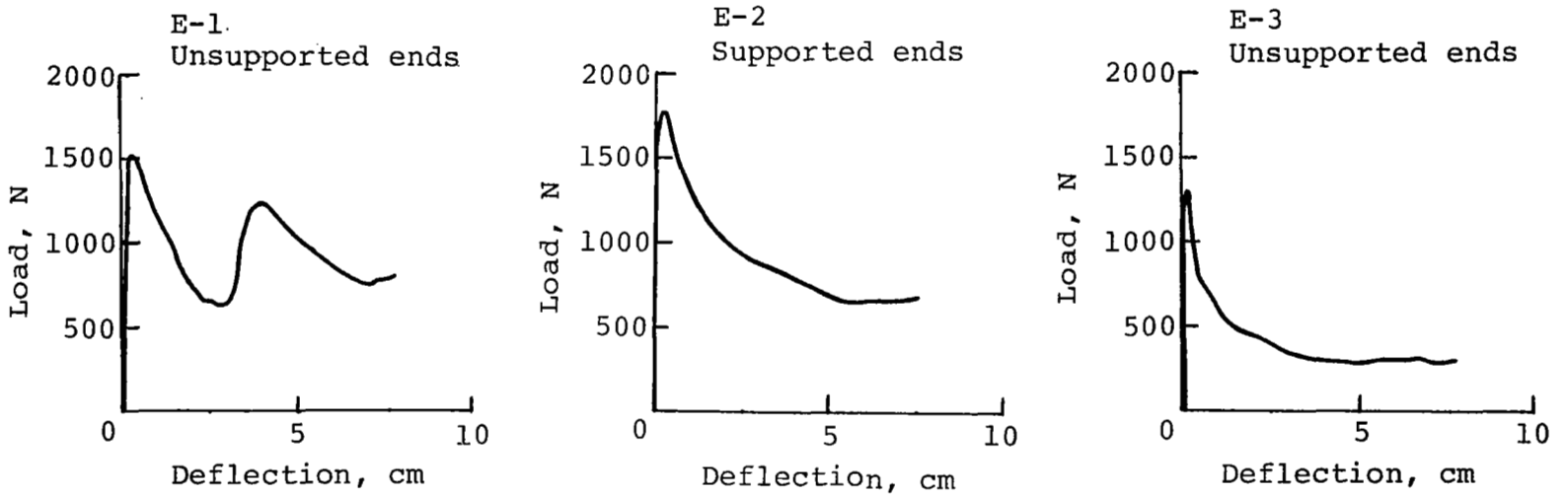

Figure A-12. Static test load-deflection data for 0.04064 cm boxes with notched-corners.

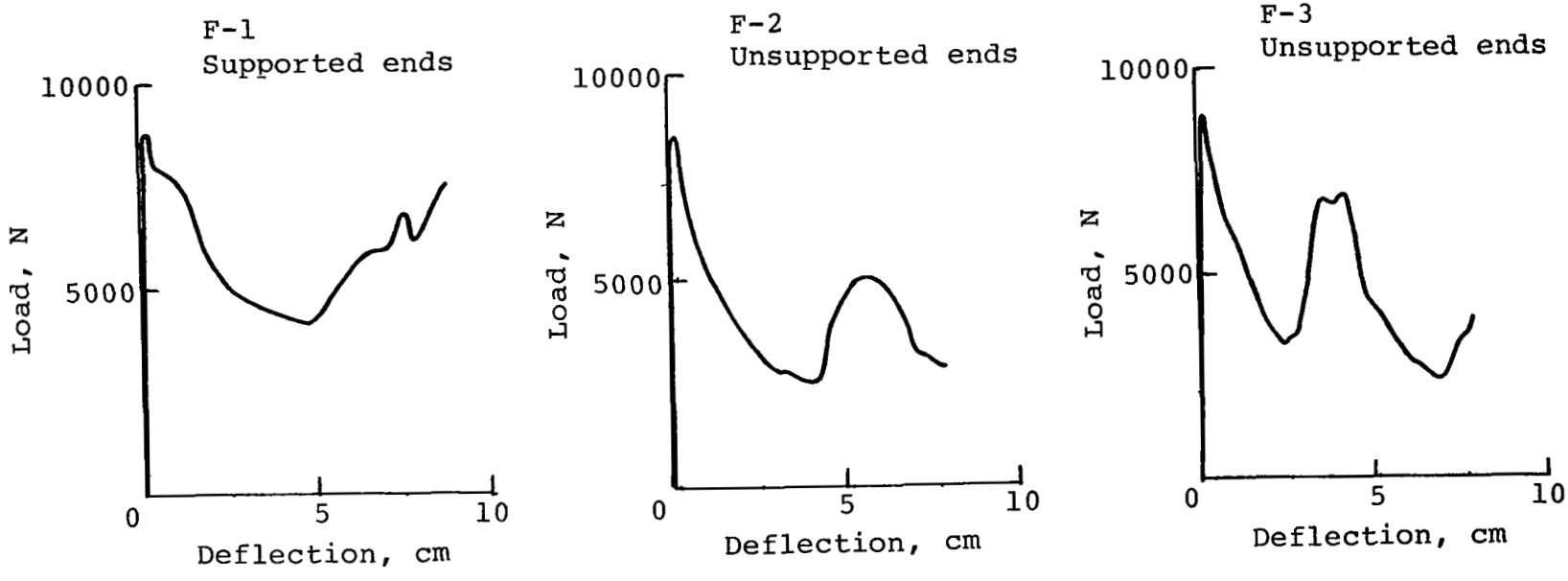

Figure A-13. Static test load-deflection data for 0.08128 cm boxes with notched-corners.

APPENDIX B

NASTRAN STATIC LOADS ANALYSIS

Derivation of external loads

General assumption

- Seat and man weighs 76.5kg (170 lb)
- Each forward seat leg carries the same compressive load at any instant as described in Reference 8
- Each aft seat leg carries the same tensile load at any instant as described in Reference 8
- Energy attenuator load is a constant 9323N (2096 lb) throughout the motion
- Lateral components are considered in the seat configuration by designing for an impact with a 30° yawed attitude (see page 17 of Reference 8)

Source of analysis method

Reference 8.

External Loads derivation

The loads were derived in a manner similar to that described in Reference 8. Seat geometries were constructed for four specific times after impact for both the longitudinal and the 30° nose down impact cases (see Fig. B-1). The occupant cg motions, occupant load factors, and seat structural member axial loads were calculated from the seat geometries and the assumed constant attenuator load (see Figs. B-2 to B-4). The member loads were then used to obtain floor reactions. The analysis is outlined below and the results summarized in Table B-I. From this table it is apparent that case 4 (30° nose down impact) and case 3a (longitudinal impact) are the critical load conditions.

TABLE B-I. SUMMARY OF EXTERNAL REACTIONS

30° Nose Down Impact (Ultimate Loads)

Seat Position	Seat: Forward Leg		Seat: Aft Leg		CG Vertical Displacement mm (in)
	Ha Horizontal Reaction N (lb)	Va Vertical Reaction N (lb)	Hj Horizontal Reaction N (lb)	Vj Vertical Reaction N (lb)	
1	-899 (-202)	6330 (1423)	-1330 (-299)	-2473 (-556)	0.0 (0.0)
2	778 (175)	6681 (1500)	-2949 (-663)	-2927 (-658)	61.214 (2.41)
3	3754 844	7215 (1622)	-6041 (-1358)	-3256 (-732)	140.716 (5.54)
4	16285 (3661)	9964 (2240)	-19585 (-4403)	-4253 (-956)	231.394 (9.11)

Longitudinal Impact (Ultimate Loads)

Seat Position	Seat: Forward Leg		Seat: Aft Leg		CG Vertical Displacement mm (in)
	Ha Horizontal Reaction N (lb)	Va Vertical Reaction N (lb)	Hj Horizontal Reaction N (lb)	Vj Vertical Reaction N (lb)	
1	-765 (-172)	6530 (1468)	-3510 (-789)	-6530 (-1468)	0.0 (0.0)
2	2131 (479)	7905 (1777)	-7971 (-1792)	-7905 (-1777)	85.852 (3.38)
3	10573 (2377)	10911 (2453)	-20239 (-4550)	-10911 (-2453)	148.082 (5.83)
3a	34972 (7862)	19777 (4446)	-54833 (-12327)	-19777 (-4446)	160.528 (6.32)

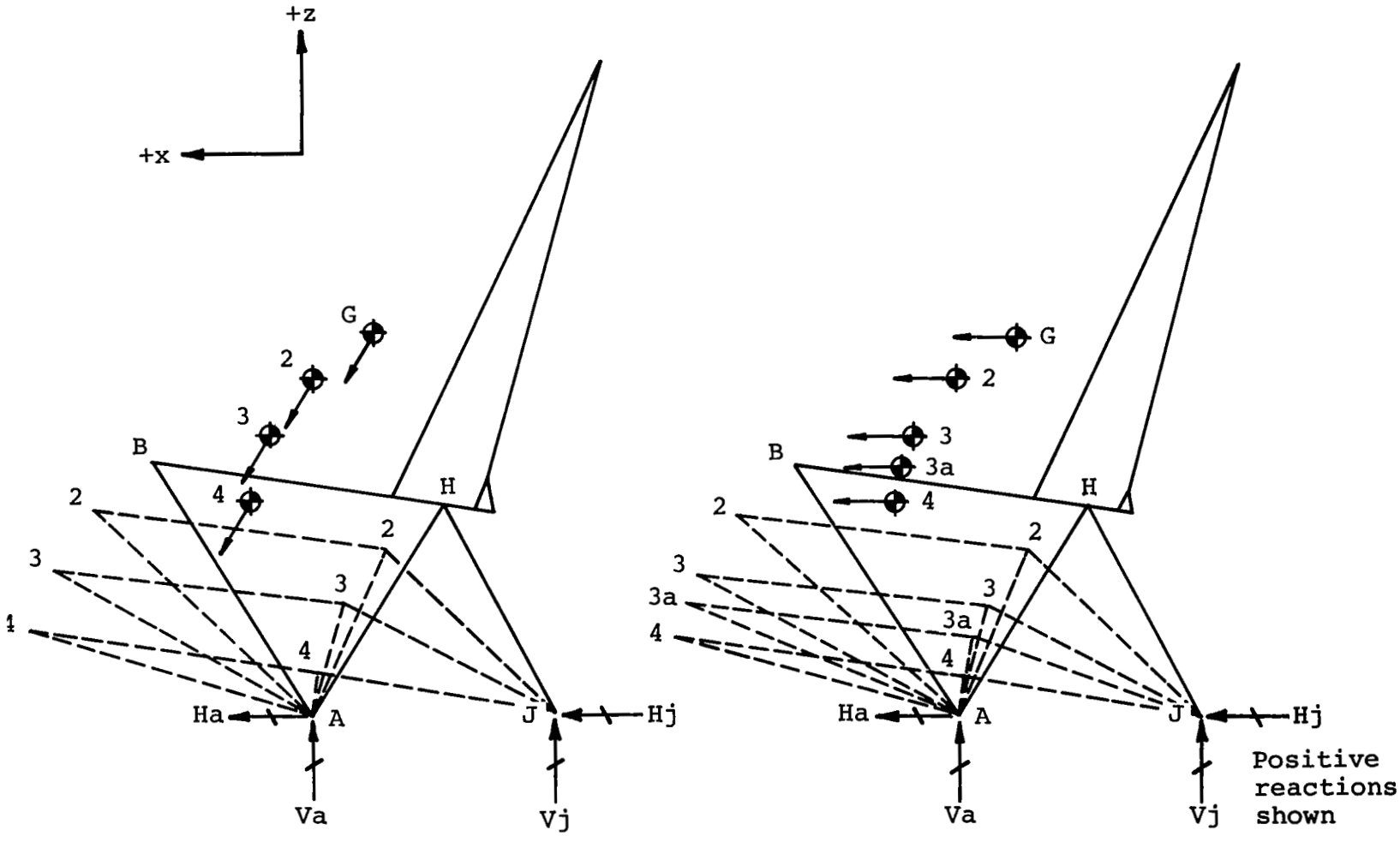

Figure B-1. NASA general aviation floor-mounted passenger seat.

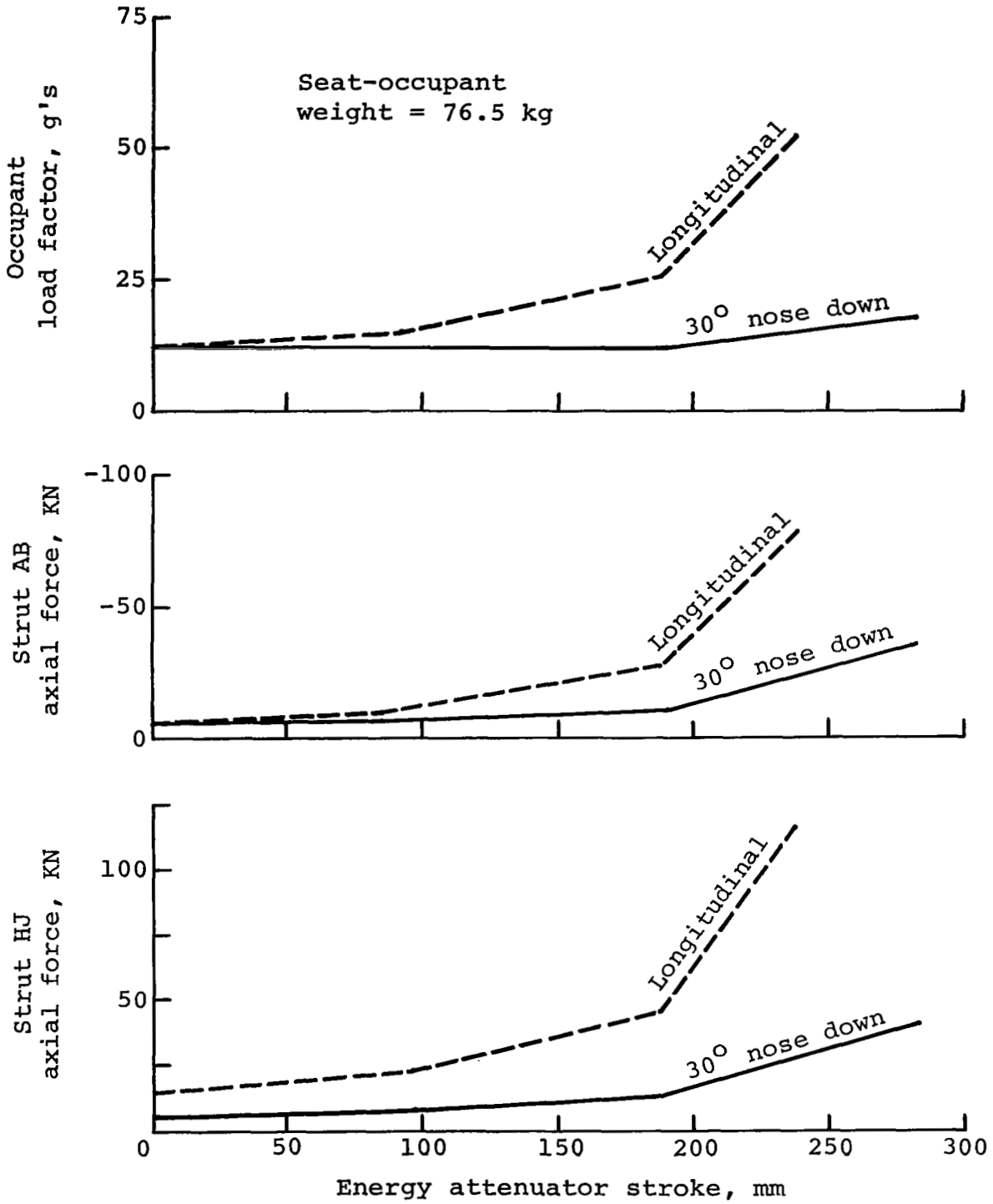

Figure B-2. Seat strut axial force and occupant load factor versus energy attenuator stroke.

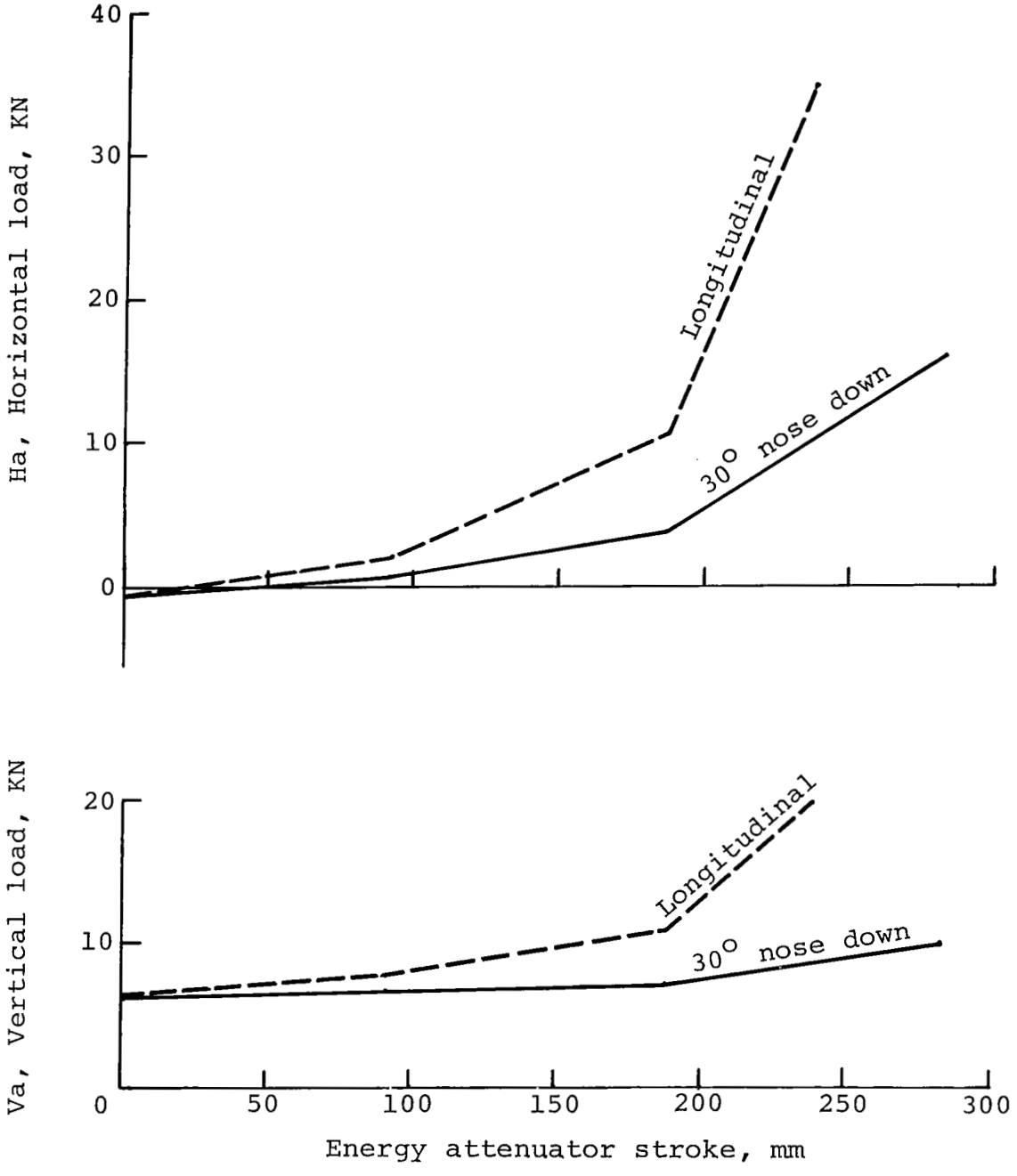

Figure B-3. Floor reaction loads at forward seat mount versus energy attenuator stroke.

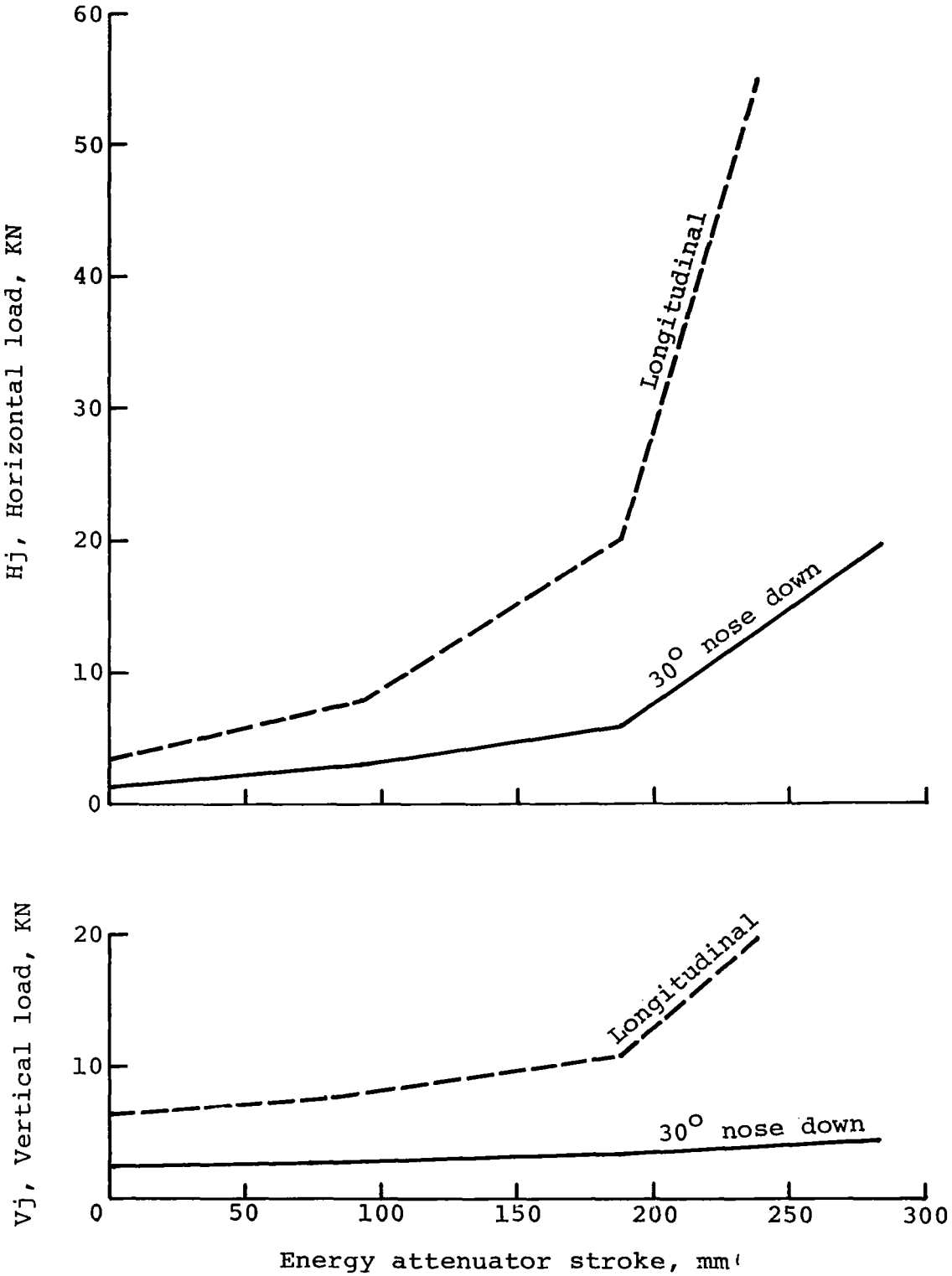

Figure B-4. Floor reaction loads at aft seat mount versus energy attenuator stroke.

30° nose down impact case

Seat motion during impact:

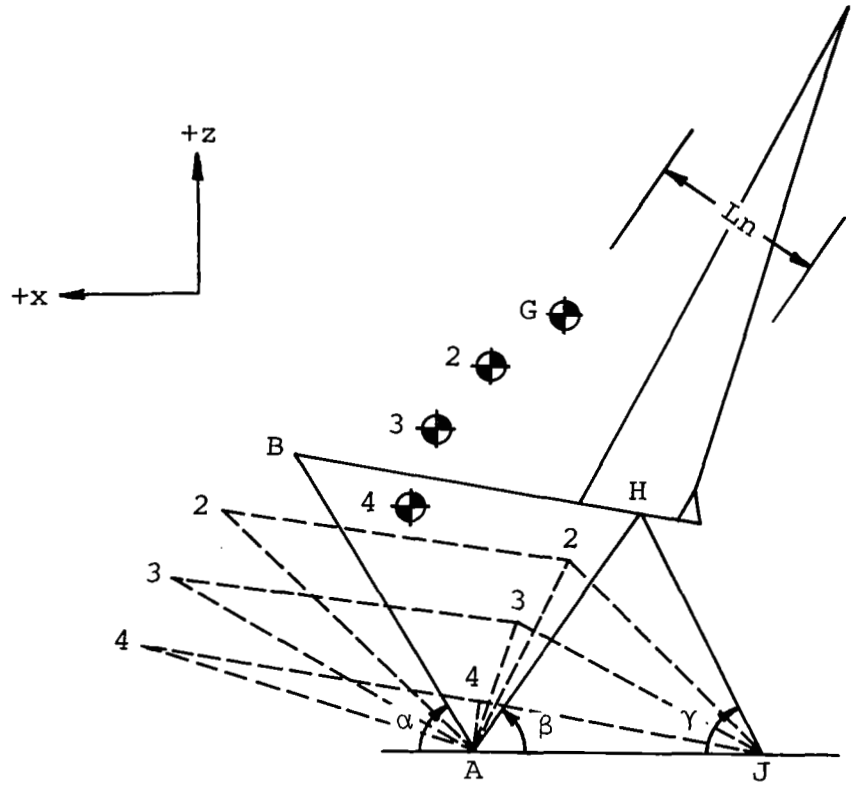

Seat Position	α, deg	β, deg	γ, deg	Ln, mm (in.)
1	56.65	58.23	61.75	195.83 (7.71)
2	42.27	66.30	44.77	237.74 (9.36)
3	28.43	73.69	28.32	250.95 (9.88)
4	17.42	78.84	12.25	227.33 (8.95)

Load Calculations:

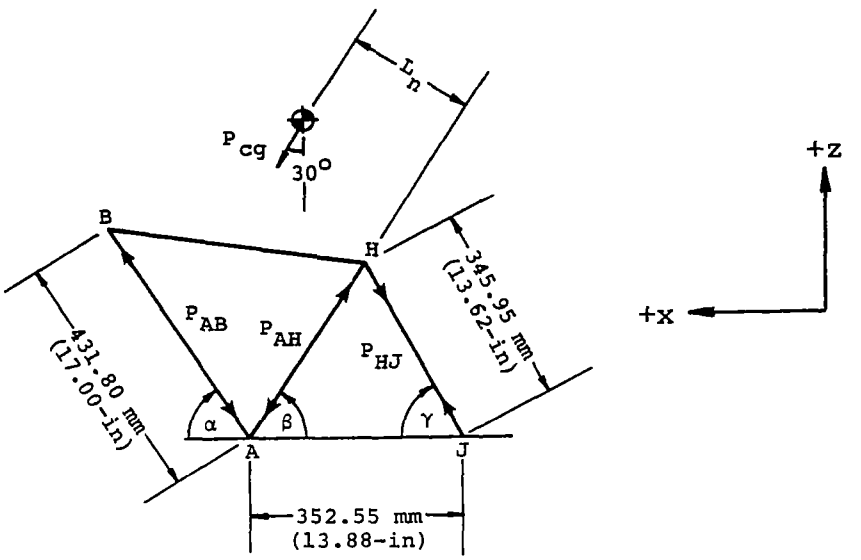

Initial length of member AH = 358.40 mm (14.11 in.)

Constant compressive load in member AH throughout the motion = 9323N (2096 lb)

From $\Sigma F_V = 0$, $\Sigma F_H = 0$, and $\Sigma M_A = 0$, the internal loads P_{AB} and P_{HJ} and the external load P_{CG} can be determined as follows:

$$\begin{bmatrix} -\sin\alpha & \sin\gamma & \cos 30° \\ \cos\alpha & -\cos\gamma & \sin 30° \\ 0 & 352.55\sin\gamma & -L_n \end{bmatrix} \begin{bmatrix} P_{AB} \\ P_{HJ} \\ P_{CG} \end{bmatrix} = \begin{bmatrix} 9323\sin\beta \\ 9323\cos\beta \\ 0 \end{bmatrix}$$

The occupant cg load factors are calculated as follows:

$$G_{occ} = \frac{P_{CG}}{756}$$

The vertical motion of the occupant cg is calculated using the following equation:

$$h_{CG} = 345.95 \sin \gamma + 233.68$$

The displacement of the occupant cg from its original position is given by the following expression:

$$\Delta v_{CG} = h_{CG_o} - h_{CG_i}$$

where i = 2, 3, 4, (seat positions)

The seat reactions which are the input loads to the floor are given by the following relations:

$$H_A = P_{AB} \cos \alpha - 9323 \cos \beta$$

$$V_A = P_{AB} \sin \alpha + 9323 \sin \beta$$

$$H_J = P_{HJ} \cos \gamma$$

$$V_J = P_{HJ} \sin \gamma$$

These floor loads for each seat position have been summarized in Table B-I.

Longitudinal impact case

The seat positions are identical to the 30° nose down impact case except that position 4 (rebound under longitudinal impact loads) is replaced by position 3a where

α = 22.92°

β = 76.84°

γ = 19.83°

h_{CG} = 351.03 mm (13.82 in.)

From $\Sigma F_V = 0$, $\Sigma F_H = 0$ and $\Sigma M_A = 0$, the internal strut loads and the external occupant cg forces can be determined as follows:

$$\begin{bmatrix} -\sin\alpha & \sin\gamma & 0 \\ \cos\alpha & -\cos\gamma & 1 \\ 0 & 352.55\sin\gamma & -h_{CG} \end{bmatrix} \begin{bmatrix} P_{AB} \\ P_{HJ} \\ P_{CG} \end{bmatrix} = \begin{bmatrix} 9323\sin\beta \\ 9323\cos\beta \\ 0 \end{bmatrix}$$

The occupant cg load factor is computed as follows:

$$G_{occ} = \frac{P_{CG}}{756}$$

The relationship between seat position and stroke of the energy attenuating member AH is given by the following equation:

$$L_{AH} = 345.95 \frac{\sin\gamma}{\sin\beta}$$

Following is a summary of the seat positions:

Seat Position	L_{AH}, mm (in.)	Stroke, mm (in.)
1	358.39 (14.11)	0
2	266.19 (10.48)	92.20 (3.63)
3	170.94 (6.73)	187.45 (7.38)
3a	120.40 (4.74)	237.99 (9.37)
4	74.93 (2.95)	283.46 (11.16)

Similar to the 30° nose down impact case discussed before, the occupant cg horizontal motions, seat member loads, and seat reactions are calculated for the longitudinal impact case. The results have been summarized in Table B-I.

Internal loads derivation

Using a half model, a NASTRAN static analysis was performed with load cases representing each impact condition (30° nose down and longitudinal). Two seats and occupants were included in the model

at locations either in the forward, middle, or aft floor section. The NASTRAN model is illustrated in Fig. B-5.

The external load input to the NASTRAN floor section model was at four discrete points: two each located along BL 19.25 and BL 8.25.

For the analysis the cabin was assumed unpressurized.

The critical internal load distribution from the NASTRAN analysis was at the aft seat location, forward leg (BL 19.25, FS 167.12). The floor at this location experienced a downward load of 19777N (4446 lb) and an aftward load of 34972N (7862 lb).

Loads

Summarized below are the NASTRAN calculated internal loads for the longitudinal impact case 3a with two passengers in aft-mounted seats. The applied external loads are those for the forward seat leg and seat position 3a as shown in Table B-I.

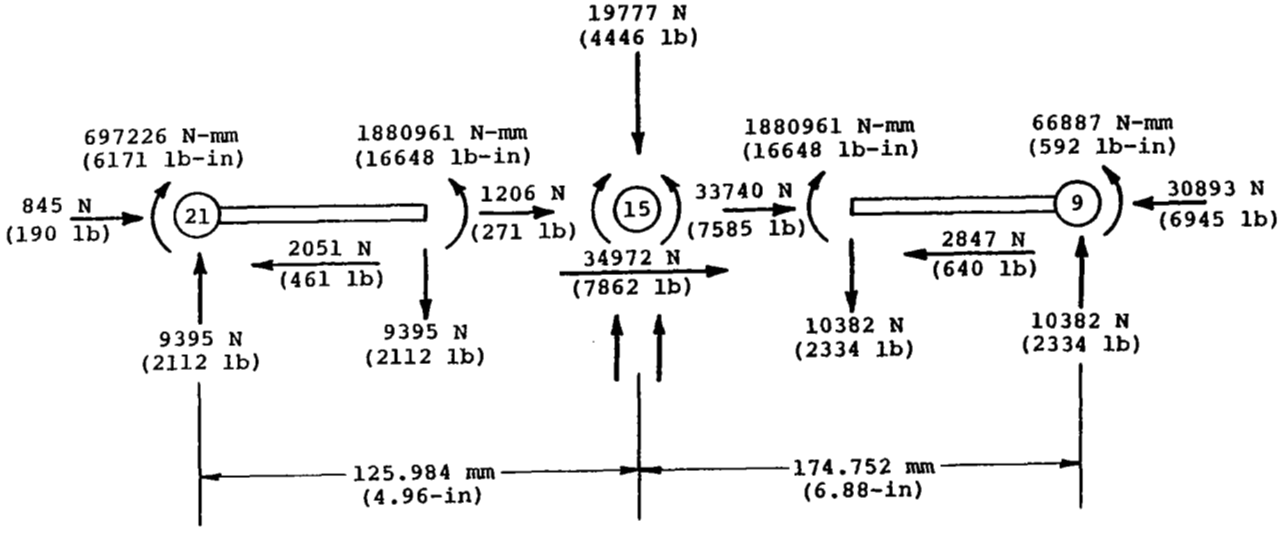

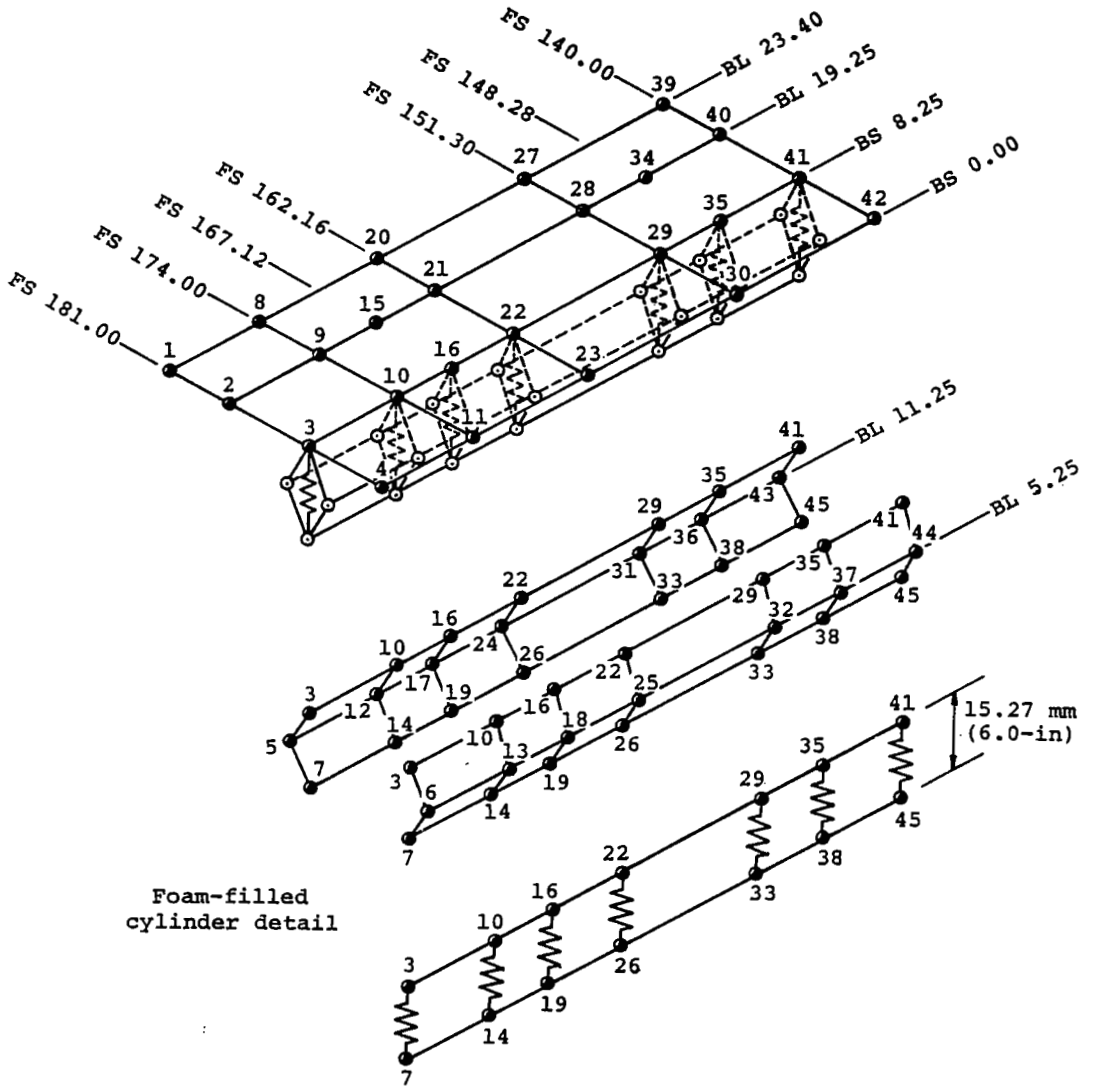

Figure B-5. NASTRAN model of crashworthy floor section with foam-filled cylinders concept.

Material properties

The material properties for various components of the floor section structure are presented below.

Seat track: 7075-T6 QQ-A-200/15 extrusion

(Reference 9, pp 3-259)

f_{TU} = 469 MPa (68 KSI)

f_{TY} = 393 MPa (57 KSI)

f_{CY} = 421 MPa (61 KSI)

E = 71.706 GPa (10.4 x 10^6 psi)

Channels and skin: 2024-T3 QQ-A-250/4 sheet

(Reference 9, pp 3-63)

f_{TU} = 434 MPa (63 KSI)

f_{TY} = 290 MPa (42 KSI)

f_{CY} = 269 MPa (39 KSI)

E = 72.395 GPa (10.5 x 10^6 psi)

Doubler: 2024-T3 QQ-A-250/4 sheet

(Reference 9, pp 3-63)

f_{TU} = 441 MPa (64 KSI)

f_{TY} = 290 MPa (42 KSI)

f_{CY} = 269 MPa (39 KSI)

E = 72.395 GPa (10.5 x 10^6 psi)

Section properties

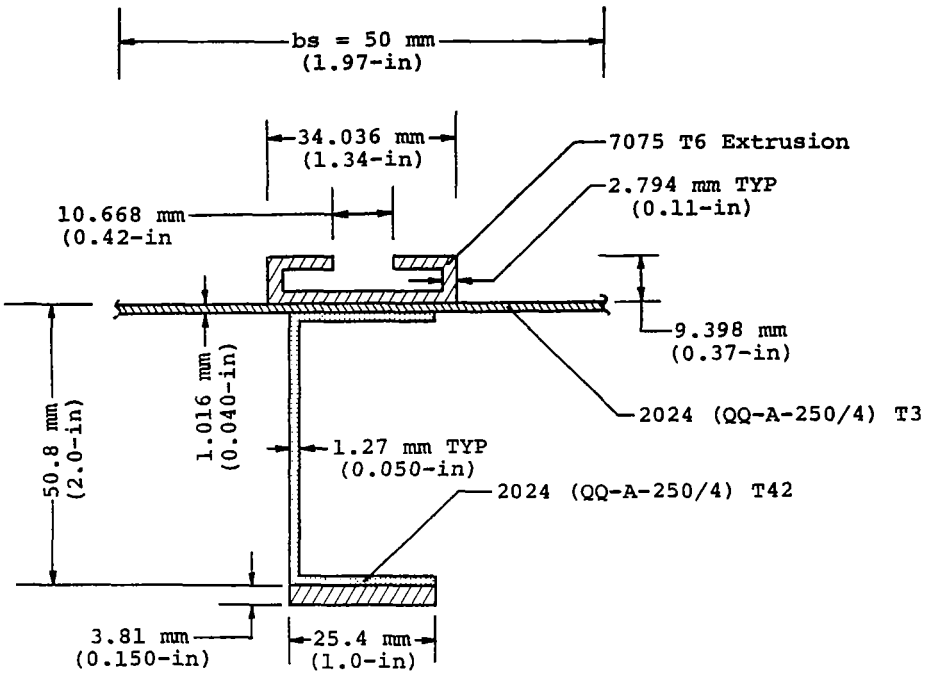

The effective width of skin is found as follows:

$$b_s = 1.7t\sqrt{\frac{E}{f_{cc}}} \qquad \text{(Reference 10, pp C7.11)}$$

The allowable crippling strength, f_{cc}, of a flange with one edge free is found as follows:

$$\frac{b}{t} = \frac{25.4 - \frac{1.27}{2}}{1.27} = 19.5$$

$$\text{so, } f_{cc} = (.031)\sqrt{(290)(72395)}$$

$$= 142 \text{ MPa } (20.596 \text{ KSI})$$

$$\text{SO, } b_s = (1.7)(1.27)\sqrt{72395/142}$$
$$= 50 \text{ mm } (1.97 \text{ in})$$

The cross-sectional area is 455 mm^2 (0.705 in^2) and the area moment of inertia for vertical bending about the section centroid is 290200 mm^4 (0.697 in^4).

Stresses

The bending stresses at the top and bottom flanges are calculated as follows:

- Top flange (compression)

$$f_b = \frac{Mz}{I_y} = \frac{(1880961)(26.214)}{(290200)}$$

$$= 170 \text{ MPa } (24.657 \text{ KSI})$$

- Bottom flange (tension)

$$f_b = \frac{Mc}{I_y} = \frac{(1880961)(38.81)}{(290200)}$$

$$= 252 \text{ MPa } (36.550 \text{ KSI})$$

The compressive axial stress in the section is computed as follows:

$$f_x = \frac{P}{A} = \frac{33740}{455}$$

$$= 74 \text{ MPa } (10.733 \text{ KSI})$$

Summing the bending and axial stresses yields the following maximum stresses:

- Top flange (compression)

$$f_{max} = 170 + 74$$
$$= 244 \text{ MPa } (35.39 \text{ KSI})$$

- Bottom flange (tension)

$$f_{max} = 252 - 74$$
$$= 178 \text{ MPa } (25.817 \text{ KSI})$$

The equivalent stress distribution is shown below.

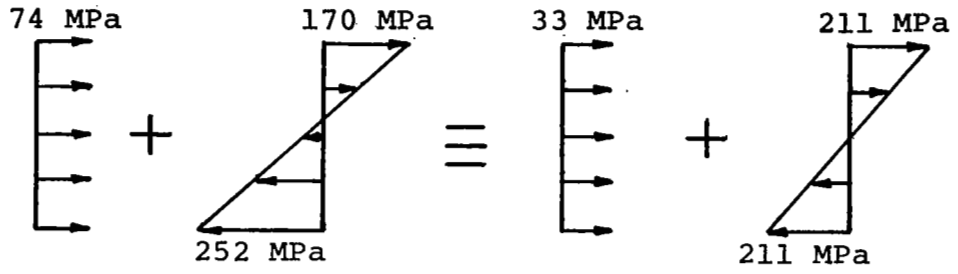

Therefore, the margin of safety at the bottom flange is determined as follows:

$$R_b = \frac{211}{434} = .4862 \text{ ultimate}$$

$$R_c = \frac{33}{142} = .2324 \text{ ultimate}$$

$$M.S._{ult} = \frac{1}{R_b + R_c} - 1$$

$$= \underline{0.39}$$

APPENDIX C

KRASH FLOOR SECTION MODEL LISTING

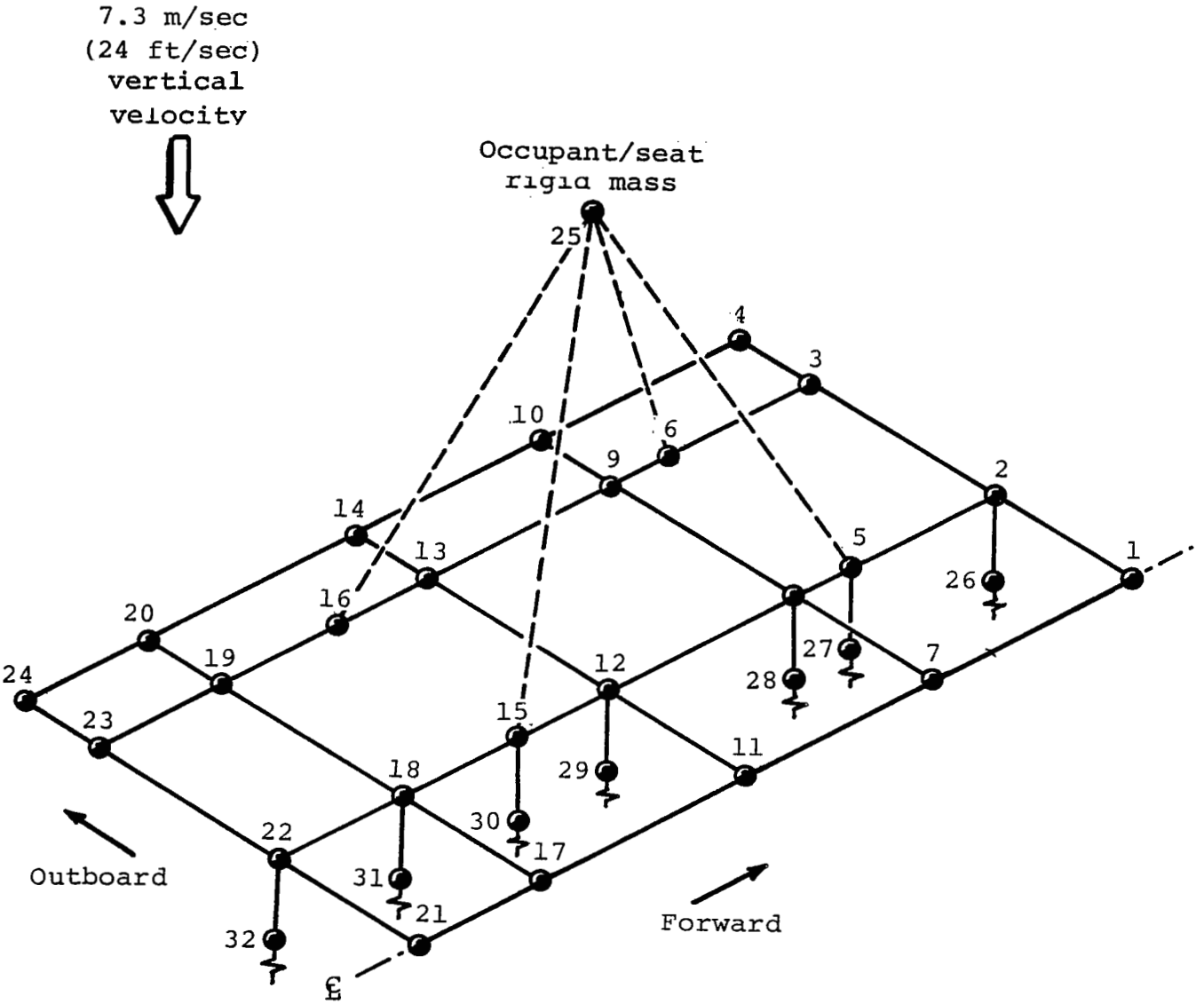

Figure C-1. KRASH math model of floor section with corrugated web concept.

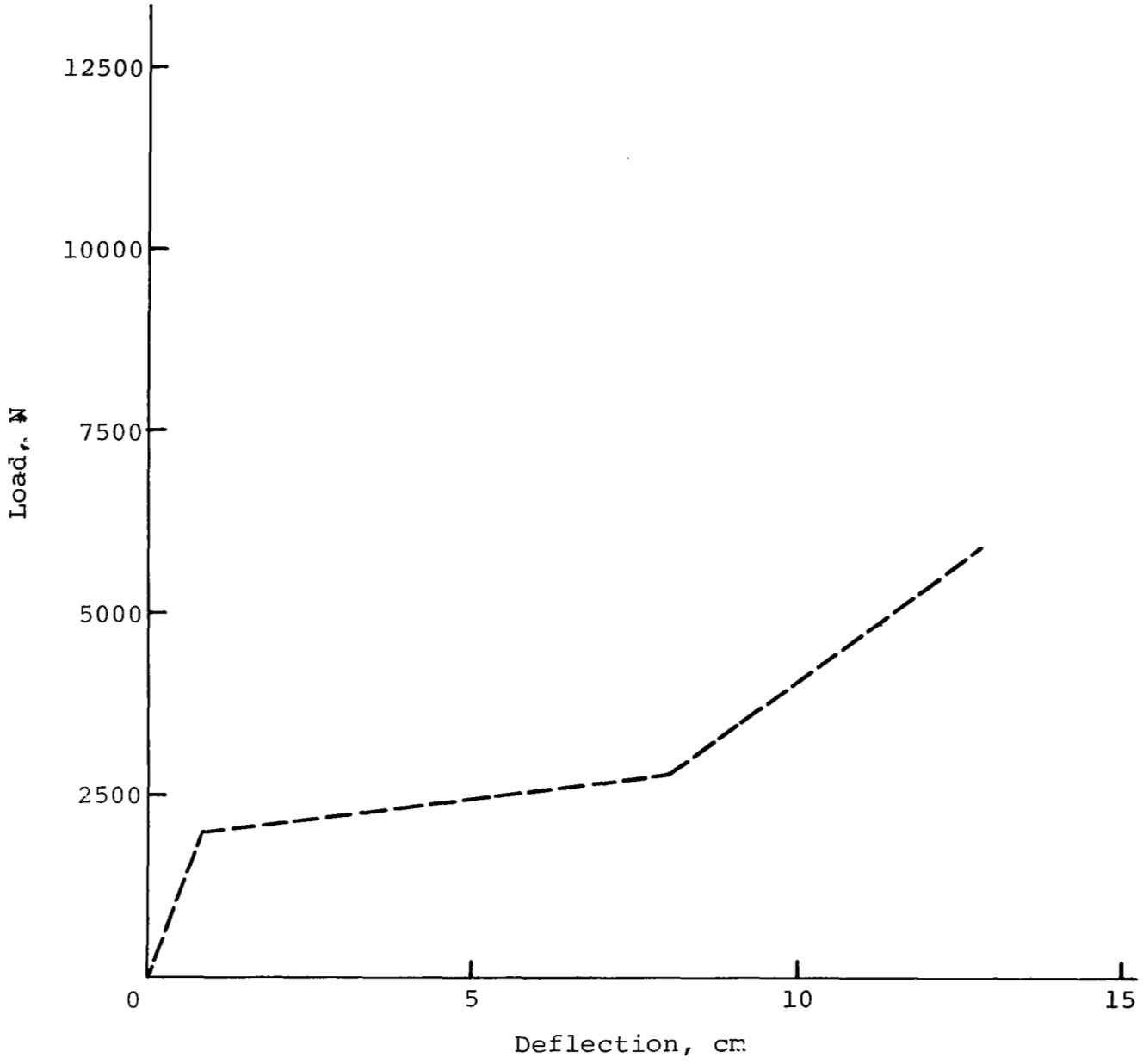

Figure C-2. Load-deflection parameters for nonlinear beam 2-26 at STA 140.00.

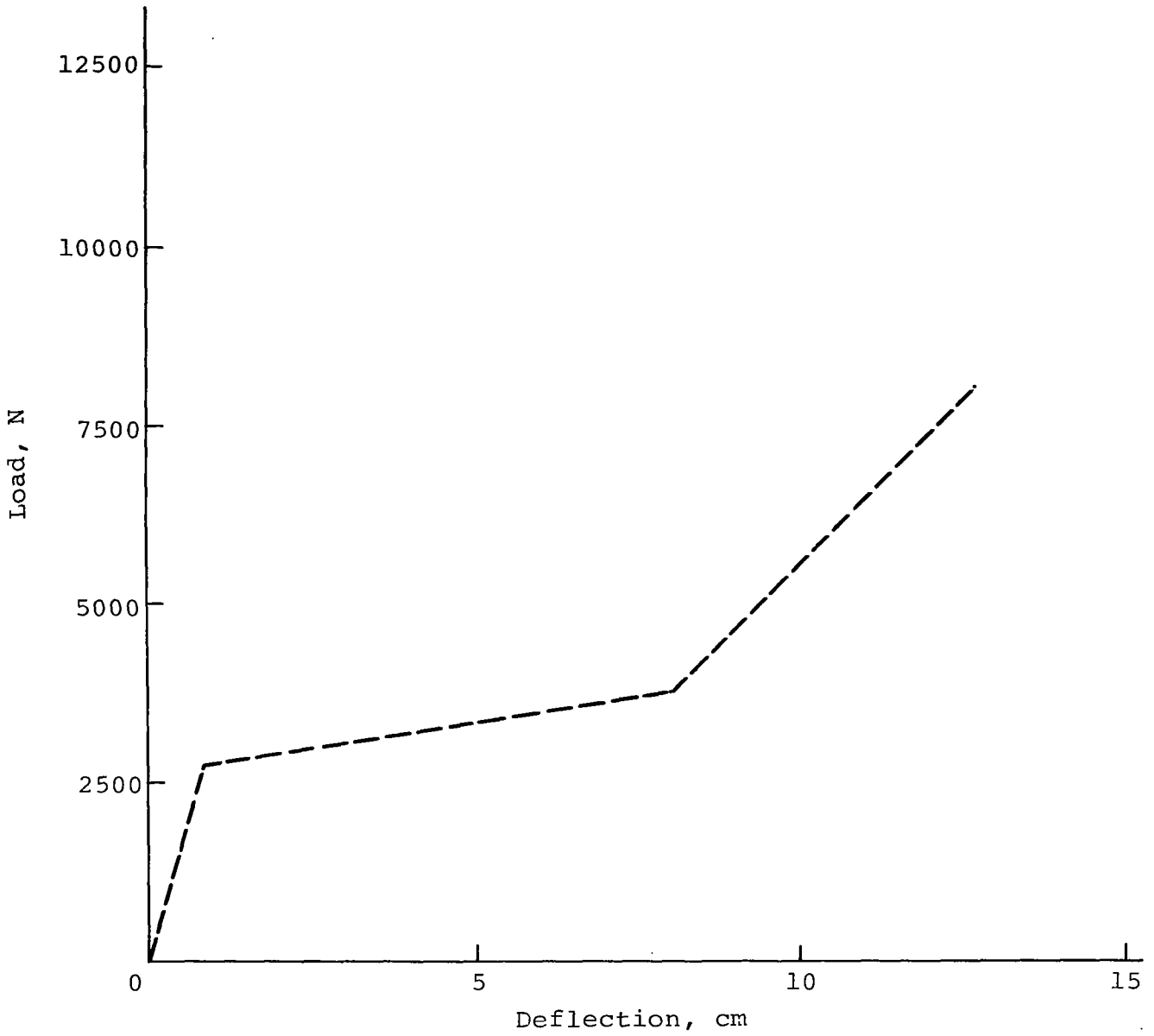

Figure C-3. Load-deflection parameters for nonlinear beam 5-27 at STA 148.28.

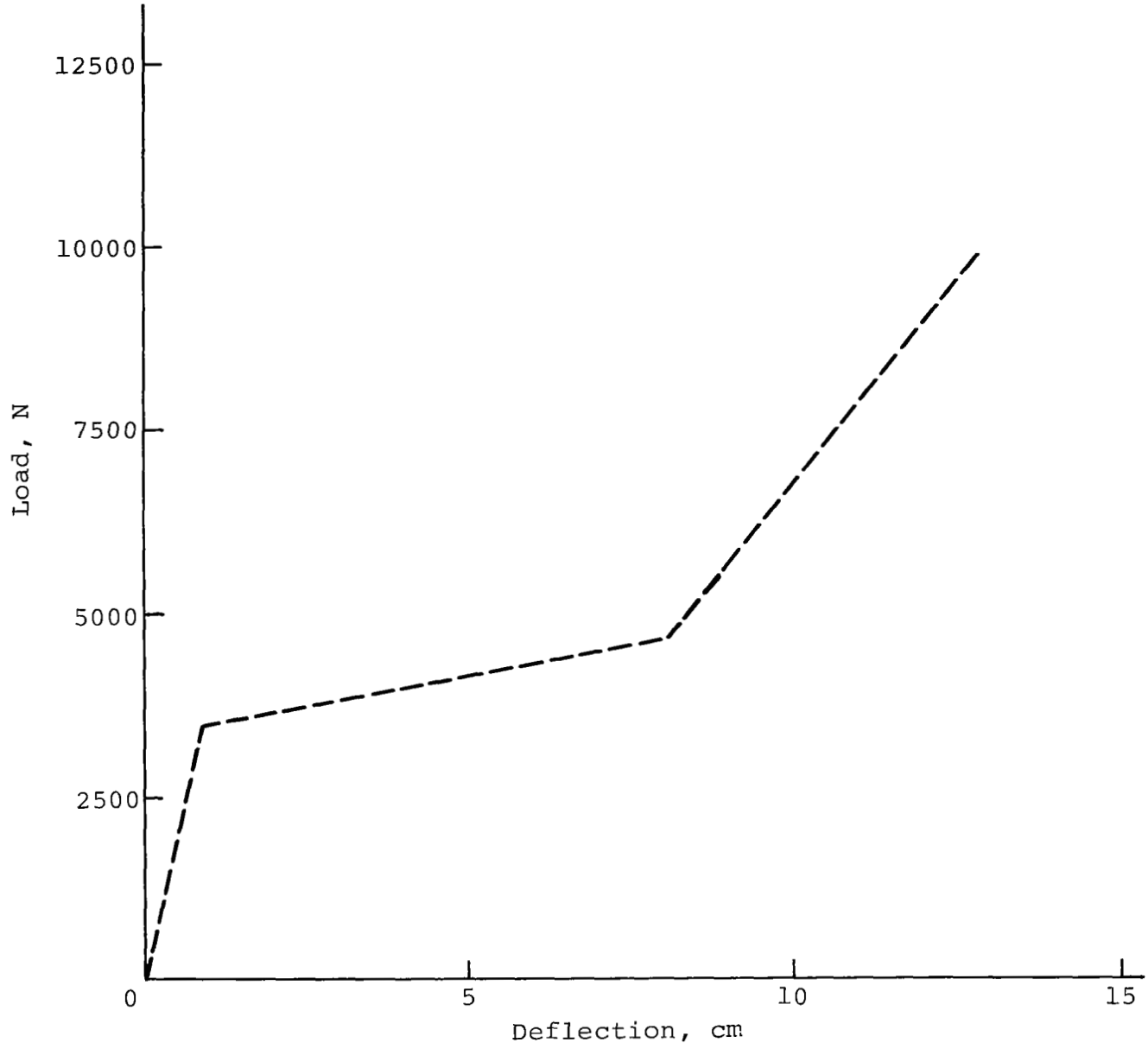

Figure C-4. Load-deflection parameters for nonlinear beam 8-28 at STA 151.30.

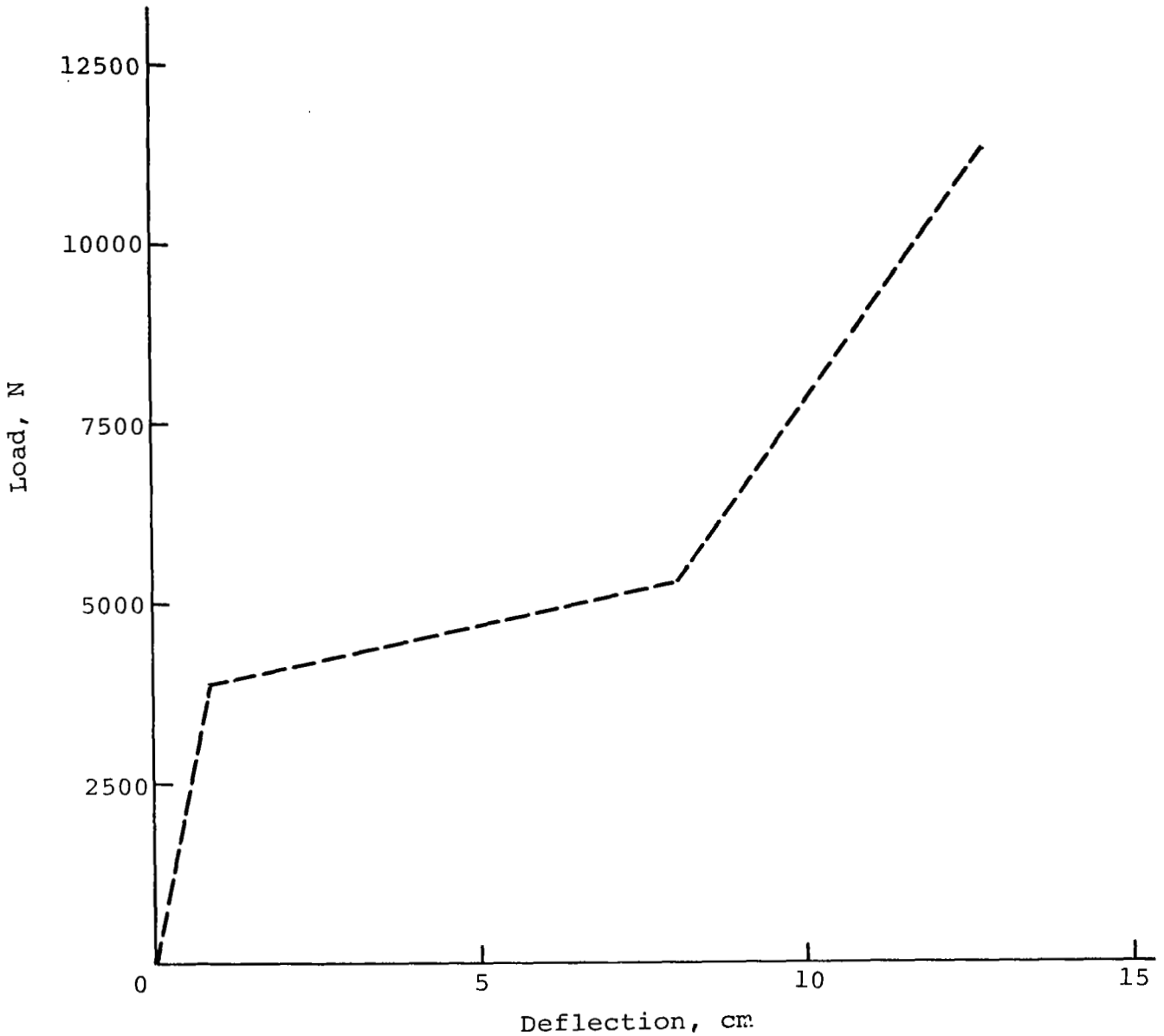

Figure C-5. Load-deflection parameters for nonlinear beam 12-29 at STA 162.16.

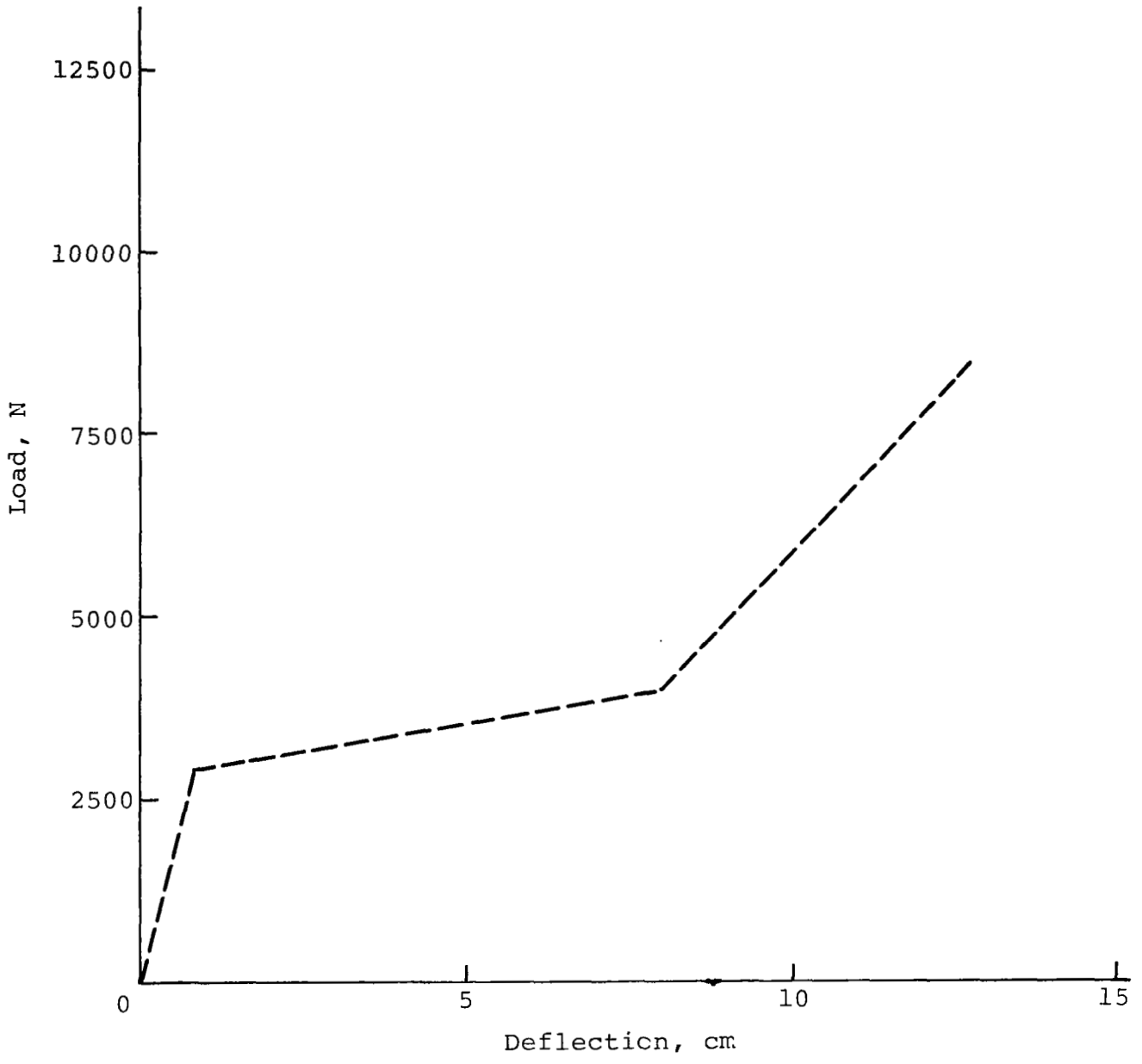

Figure C-6. Load-deflection parameters for nonlinear beam 15-30 at STA 167.12.

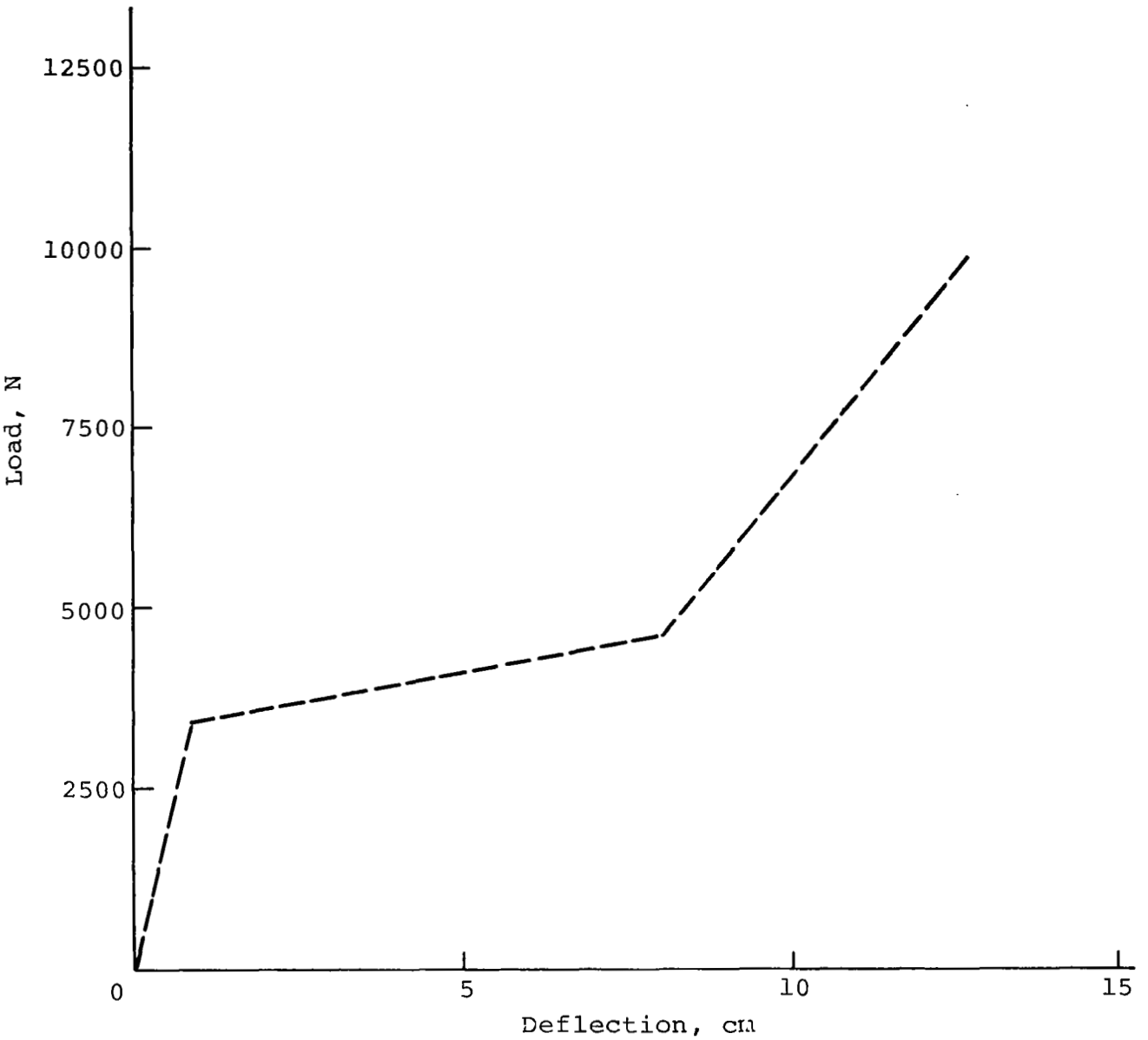

Figure C-7. Load-deflection parameters for nonlinear beam 18-31 at STA 174.00.

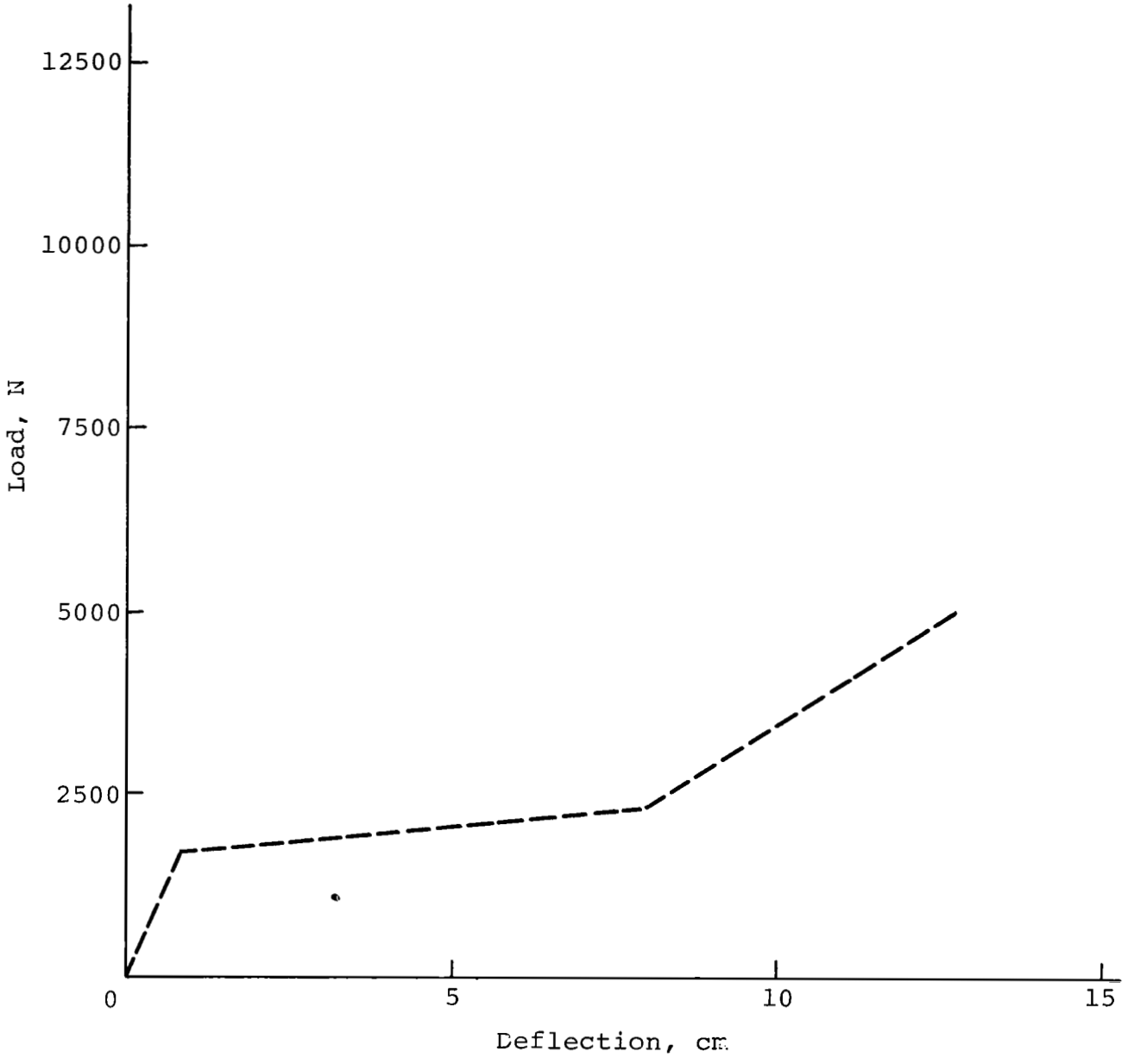

Figure C-8. Load-deflection parameters for nonlinear beam 22-32 at STA 181.00.

```
'EN16334.FLOORK8.DATA'
     $
     $
     $      NASA METAL FLOOR SECTION WITH CORRUGATED WEB ENERGY ABSORBING
     $      SUBFLOOR CONCEPT
     $
     $           -  24 FT/SEC VERTICAL IMPACT VELOCITY
     $           -  COMBINATION NONLINEAR BEAMS AND EXTERNAL
     $              CRUSHING SPRINGS TO ACCURATELY RESPRESENT
     $              STATIC TEST LOAD-DEFLECTION DATA
     $           -  RIGID OCCUPANT/SEAT MASS AT MID LOCATION
     $
     $
     $
     NASA AIRPLANE FLOOR SECTION W/MID RIGID SEAT AND OCCUPANT - HALF MODEL
     CORRUGATED WEB ENERGY ABSORBERS - 24 FPS VERTICAL IMPACT - 09/14/81
     123456789012345678901234567890123456789012345678901234567890123456789012
        32    7   46    7    0    0    0    0    0    0    0    0    2    0
         0    0    0    0    0    0    0327503275032750    0    0

     FLR                 1         20         40         60
           1000  0.000001      0.060        0.0        0.0        1.0

         1    1    1    1    1    0    1    0    1
        32    0   46   46    0    7    0    0    0    0
             0.0        0.0      288.0
             0.0        0.0        0.0
             0.0        0.0        0.0        0.0        0.0        0.0
           0.543     140.00       0.00        0.0        1.0        1.0        1.0
           0.584     140.00       8.25        0.0        1.0        1.0        1.0
           0.686     140.00      19.25        0.0        1.0        1.0        1.0
           0.414     140.00      23.40        0.0        1.0        1.0        1.0
           0.381     148.28       8.25        0.0        1.0        1.0        1.0
           0.282     148.28      19.25        0.0        1.0        1.0        1.0
           0.927     151.30       0.00        0.0        1.0        1.0        1.0
           0.903     151.30       8.25        0.0        1.0        1.0        1.0
           1.032     151.30      19.25        0.0        1.0        1.0        1.0
```

	0.741	151.30	23.40	0.0	1.0	1.0	1.0
	0.946	162.16	0.00	0.0	1.0	1.0	1.0
	0.975	162.16	8.25	0.0	1.0	1.0	1.0
	1.090	162.16	19.25	0.0	1.0	1.0	1.0
	0.758	162.16	23.40	0.0	1.0	1.0	1.0
	0.400	167.12	8.25	0.0	1.0	1.0	1.0
	0.296	167.12	19.25	0.0	1.0	1.0	1.0
	0.809	174.00	0.00	0.0	1.0	1.0	1.0
	0.863	174.00	8.25	0.0	1.0	1.0	1.0
	0.969	174.00	19.25	0.0	1.0	1.0	1.0
	0.641	174.00	23.40	0.0	1.0	1.0	1.0
	0.391	181.00	0.00	0.0	1.0	1.0	1.0
	0.488	181.00	8.25	0.0	1.0	1.0	1.0
	0.573	181.00	19.25	0.0	1.0	1.0	1.0
	0.284	181.00	23.40	0.0	1.0	1.0	1.0
	214.307	158.50	13.75	20.73	1.800E+2	1.800E+2	1.800E+2
	0.584	140.00	8.25	-5.0	1.0	1.0	1.0
	0.381	148.28	8.25	-5.0	1.0	1.0	1.0
	0.903	151.30	8.25	-5.0	1.0	1.0	1.0
	0.975	162.16	8.25	-5.0	1.0	1.0	1.0
	0.400	167.12	8.25	-5.0	1.0	1.0	1.0
	0.863	174.00	8.25	-5.0	1.0	1.0	1.0
	0.488	181.00	8.25	-5.0	1.0	1.0	1.0
0 26	3	1.00	0.0	141372.0	0.0	0.0	
0 27	3	1.00	0.0	192920.0	0.0	0.0	
0 28	3	1.00	0.0	236978.0	0.0	0.0	
0 29	3	1.00	0.0	270102.0	0.0	0.0	
0 30	3	1.00	0.0	202146.0	0.0	0.0	
0 31	3	1.00	0.0	236978.0	0.0	0.0	
0 32	3	1.00	0.0	119518.0	0.0	0.0	
	0.10000	0.10001	1.00000	1.00001	14137.2	141372.0	0.0
	0.10000	0.10001	1.00000	1.00001	19292.0	192920.0	0.0
	0.10000	0.10001	1.00000	1.00001	23697.8	236978.0	0.0
	0.10000	0.10001	1.00000	1.00001	27010.2	270102.0	0.0
	0.10000	0.10001	1.00000	1.00001	20214.6	202146.0	0.0
	0.10000	0.10001	1.00000	1.00001	23697.8	236978.0	0.0
	0.10000	0.10001	1.00000	1.00001	11951.8	119518.0	0.0

```
0  1 0  7      0.50      0.005      0.467      0.05       0.0  1.0  1.016
0  7 0 11      0.50      0.005      0.467      0.05       0.0  1.0  1.016
0 11 0 17      0.50      0.005      0.467      0.05       0.0  1.0  1.016
0 17 0 21      0.50      0.005      0.467      0.05       0.0  1.0  1.016
0  2 0  5      0.50      0.005      0.467      0.05       0.0  1.0  1.016
0  5 0  8      0.50      0.005      0.467      0.05       0.0  1.0  1.016
0  8 0 12      0.50      0.005      0.467      0.05       0.0  1.0  1.016
0 12 0 15      0.50      0.005      0.467      0.05       0.0  1.0  1.016
0 15 0 18      0.50      0.005      0.467      0.05       0.0  1.0  1.016
0 18 0 22      0.50      0.005      0.467      0.05       0.0  1.0  1.016
0  3 0  6      0.50      0.005      0.467      0.05       0.0  1.0  1.016
0  6 0  9      0.50      0.005      0.467      0.05       0.0  1.0  1.016
0  9 0 13      0.50      0.005      0.467      0.05       0.0  1.0  1.016
0 13 0 16      0.50      0.005      0.467      0.05       0.0  1.0  1.016
0 16 0 19      0.50      0.005      0.467      0.05       0.0  1.0  1.016
0 19 0 23      0.50      0.005      0.467      0.05       0.0  1.0  1.016
0  4 0 10      0.50      0.005      0.467      0.05       0.0  1.0  1.016
0 10 0 14      0.50      0.005      0.467      0.05       0.0  1.0  1.016
0 14 0 20      0.50      0.005      0.467      0.05       0.0  1.0  1.016
0 20 0 24      0.50      0.005      0.467      0.05       0.0  1.0  1.016
0  1 0  2      0.35      0.002      0.193      0.02       0.0  1.0  1.016
0  2 0  3      0.35      0.002      0.193      0.02       0.0  1.0  1.016
0  3 0  4      0.35      0.002      0.193      0.02       0.0  1.0  1.016
0  7 0  8      0.35      0.002      0.193      0.02       0.0  1.0  1.016
0  8 0  9      0.35      0.002      0.193      0.02       0.0  1.0  1.016
0  9 0 10      0.35      0.002      0.193      0.02       0.0  1.0  1.016
0 11 0 12      0.35      0.002      0.193      0.02       0.0  1.0  1.016
0 12 0 13      0.35      0.002      0.193      0.02       0.0  1.0  1.016
0 13 0 14      0.35      0.002      0.193      0.02       0.0  1.0  1.016
0 17 0 18      0.35      0.002      0.193      0.02       0.0  1.0  1.016
0 18 0 19      0.35      0.002      0.193      0.02       0.0  1.0  1.016
0 19 0 20      0.35      0.002      0.193      0.02       0.0  1.0  1.016
0 21 0 22      0.35      0.002      0.193      0.02       0.0  1.0  1.016
0 22 0 23      0.35      0.002      0.193      0.02       0.0  1.0  1.016
0 23 0 24      0.35      0.002      0.193      0.02       0.0  1.0  1.016
0  8 0 25      1.00      0.000      0.000      0.000      0.0  1.0  1.017
0  9 0 25      1.00      0.000      0.000      0.000      0.0  1.0  1.017
```

```
0 15 0 25       1.00      0.000      0.000      0.000        0.0  1.0  1.017
0 16 0 25       1.00      0.000      0.000      0.000        0.0  1.0  1.017
0  2 0 26 .00070686       0.005      0.467       0.05        0.0  1.0  1.016
0  5 0 27 .00096460       0.005      0.467       0.05        0.0  1.0  1.016
0  8 0 28 .00118489       0.005      0.467       0.05        0.0  1.0  1.016
0 12 0 29 .00135051       0.005      0.467       0.05        0.0  1.0  1.016
0 15 0 30 .00101073       0.005      0.467       0.05        0.0  1.0  1.016
0 18 0 31 .00118489       0.005      0.467       0.05        0.0  1.0  1.016
0 22 0 32 .00059759       0.005      0.467       0.05        0.0  1.0  1.016
  16          10.0E06   3.83E06   35000.0    34000.0    17000.0
  17          10.3E06   3.90E06   47000.0    39000.0    22000.0
      0.04
0  2 0 26     1    10      0.150      5.000
0  5 0 27     1    10      0.150      5.000
0  8 0 28     1    10      0.150      5.000
0 12 0 29     1    10      0.150      5.000
0 15 0 30     1    10      0.150      5.000
0 18 0 31     1    10      0.150      5.000
0 22 0 32     1    10      0.150      5.000
0.0         1.00000
0.150000    1.00000
0.325000    1.00000
0.325001    0.04172
2.000000    0.04172
3.150000    0.04172
3.150001    0.26891
4.000000    0.26891
4.500000    0.26891
5.000000    0.26891
0.0         1.00000
0.150000    1.00000
0.325000    1.00000
0.325001    0.04172
2.000000    0.04172
3.150000    0.04172
3.150001    0.26891
4.000000    0.26891
```

```
4.500000  0.26891
5.000000  0.26891
0.0       1.00000
0.150000  1.00000
0.325000  1.00000
0.325001  0.04172
2.000000  0.04172
3.150000  0.04172
3.150001  0.26891
4.000000  0.26891
4.500000  0.26891
5.000000  0.26891
0.0       1.00000
0.150000  1.00000
0.325000  1.00000
0.325001  0.04172
2.000000  0.04172
3.150000  0.04172
3.150001  0.26891
4.000000  0.26891
4.500000  0.26891
5.000000  0.26891
0.0       1.00000
0.150000  1.00000
0.325000  1.00000
0.325001  0.04172
2.000000  0.04172
3.150000  0.04172
3.150001  0.26891
4.000000  0.26891
4.500000  0.26891
5.000000  0.26891
0.0       1.00000
0.150000  1.00000
0.325000  1.00000
0.325001  0.04172
2.000000  0.04172
```

```
3.150000   0.04172
3.150001   0.26891
4.000000   0.26891
4.500000   0.26891
5.000000   0.26891
0.0        1.00000
0.150000   1.00000
0.325000   1.00000
0.325001   0.04172
2.000000   0.04172
3.150000   0.04172
3.150001   0.26891
4.000000   0.26891
4.500000   0.26891
5.000000   0.26891
```

1	1	1	1	1	1	1	0	1	0
2	1	1	1	1	1	1	0	1	0
3	1	1	1	1	1	1	0	1	0
4	1	1	1	1	1	1	0	1	0
5	1	1	1	1	1	1	0	1	0
6	1	1	1	1	1	1	0	1	0
7	1	1	1	1	1	1	0	1	0
8	1	1	1	1	1	1	0	1	0
9	1	1	1	1	1	1	0	1	0
10	1	1	1	1	1	1	0	1	0
11	1	1	1	1	1	1	0	1	0
12	1	1	1	1	1	1	0	1	0
13	1	1	1	1	1	1	0	1	0
14	1	1	1	1	1	1	0	1	0
15	1	1	1	1	1	1	0	1	0
16	1	1	1	1	1	1	0	1	0
17	1	1	1	1	1	1	0	1	0
18	1	1	1	1	1	1	0	1	0
19	1	1	1	1	1	1	0	1	0
20	1	1	1	1	1	1	0	1	0
21	1	1	1	1	1	1	0	1	0
22	1	1	1	1	1	1	0	1	0

23	1	1	1	1	1	1	0	1	0
24	1	1	1	1	1	1	0	1	0
25	1	1	1	1	1	1	0	1	0
26	1	1	1	1	1	1	0	1	0
27	1	1	1	1	1	1	0	1	0
28	1	1	1	1	1	1	0	1	0
29	1	1	1	1	1	1	0	1	0
30	1	1	1	1	1	1	0	1	0
31	1	1	1	1	1	1	0	1	0
32	1	1	1	1	1	1	0	1	0
1	1	1	1						
2	1	1	1						
3	1	1	1						
4	1	1	1						
5	1	1	1						
6	1	1	1						
7	1	1	1						
8	1	1	1						
9	1	1	1						
10	1	1	1						
11	1	1	1						
12	1	1	1						
13	1	1	1						
14	1	1	1						
15	1	1	1						
16	1	1	1						
17	1	1	1						
18	1	1	1						
19	1	1	1						
20	1	1	1						
21	1	1	1						
22	1	1	1						
23	1	1	1						
24	1	1	1						
25	1	1	1						
26	1	1	1						
27	1	1	1						

28	1	1	1
29	1	1	1
30	1	1	1
31	1	1	1
32	1	1	1
33	1	1	1
34	1	1	1
35	1	1	1
36	1	1	1
37	1	1	1
38	1	1	1
39	1	1	1
40	1	1	1
41	1	1	1
42	1	1	1
43	1	1	1
44	1	1	1
45	1	1	1
46	1	1	1
1	1	0	0
2	1	0	0
3	1	0	0
4	1	0	0
5	1	0	0
6	1	0	0
7	1	0	0
8	1	0	0
9	1	0	0
10	1	0	0
11	1	0	0
12	1	0	0
13	1	0	0
14	1	0	0
15	1	0	0
16	1	0	0
17	1	0	0
18	1	0	0

```
     19     1     0     0
     20     1     0     0
     21     1     0     0
     22     1     0     0
     23     1     0     0
     24     1     0     0
     25     1     0     0
     26     1     0     0
     27     1     0     0
     28     1     0     0
     29     1     0     0
     30     1     0     0
     31     1     0     0
     32     1     0     0
     33     1     0     0
     34     1     0     0
     35     1     0     0
     36     1     0     0
     37     1     0     0
     38     1     0     0
     39     1     0     0
     40     1     0     0
     41     1     0     0
     42     1     0     0
     43     1     0     0
     44     1     0     0
     45     1     0     0
     46     1     0     0
     26     0     1     1
     27     0     1     1
     28     0     1     1
     29     0     1     1
     30     0     1     1
     31     0     1     1
     32     0     1     1
END
```

APPENDIX D

CRASHWORTHY FLOOR SECTIONS DESIGN DRAWINGS

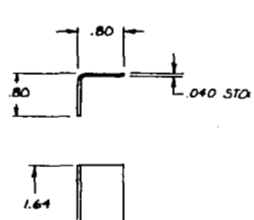

DETAIL -131 CLIP
.16 BR
SCALE 1/1

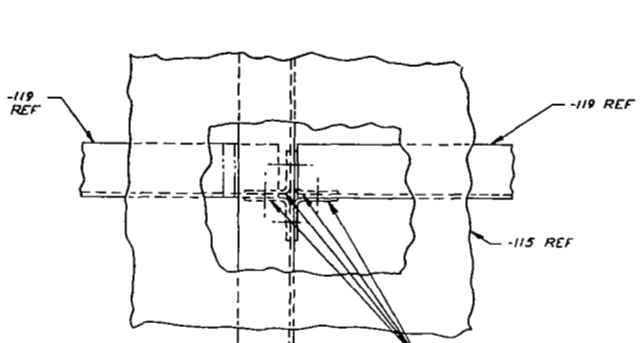

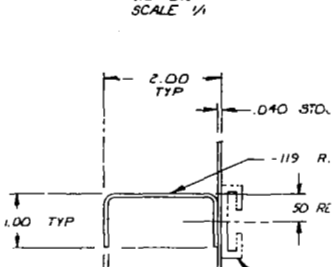

SCALE 1/1

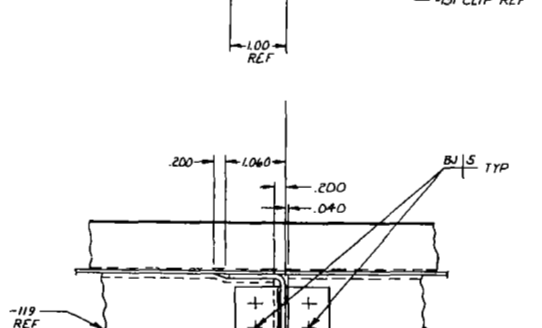

VIEW A
SCALE 1/1

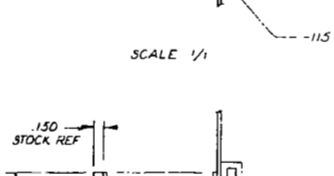

SCALE 1/1

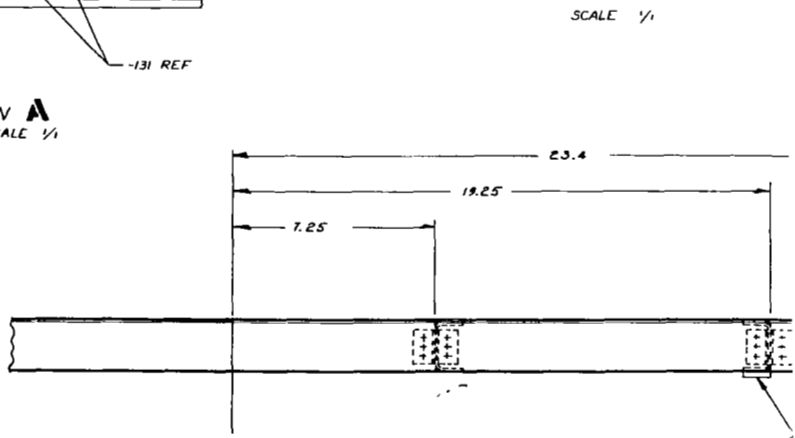

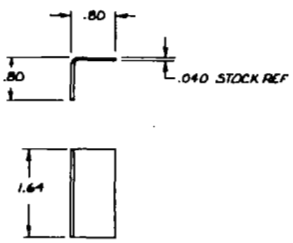

DETAIL -131 CLIP
.16 BR
SCALE 1/1

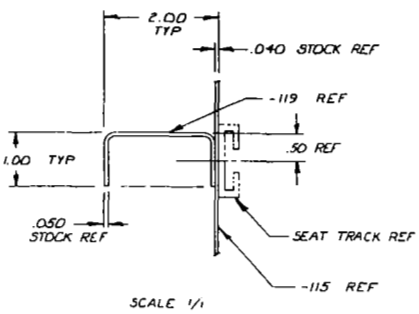

SCALE 1/1

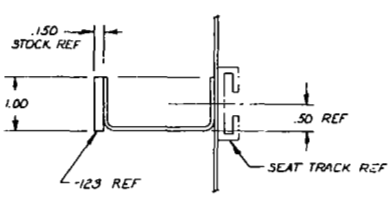

SCALE 1/1

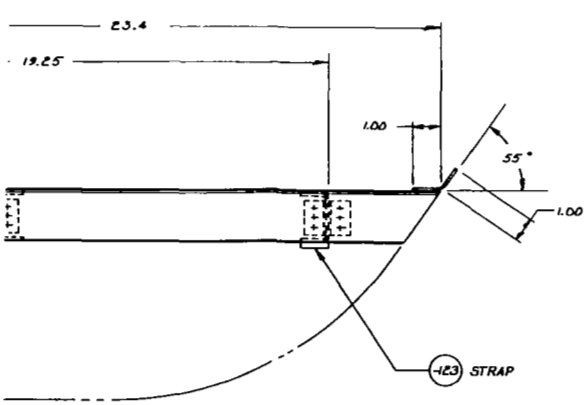

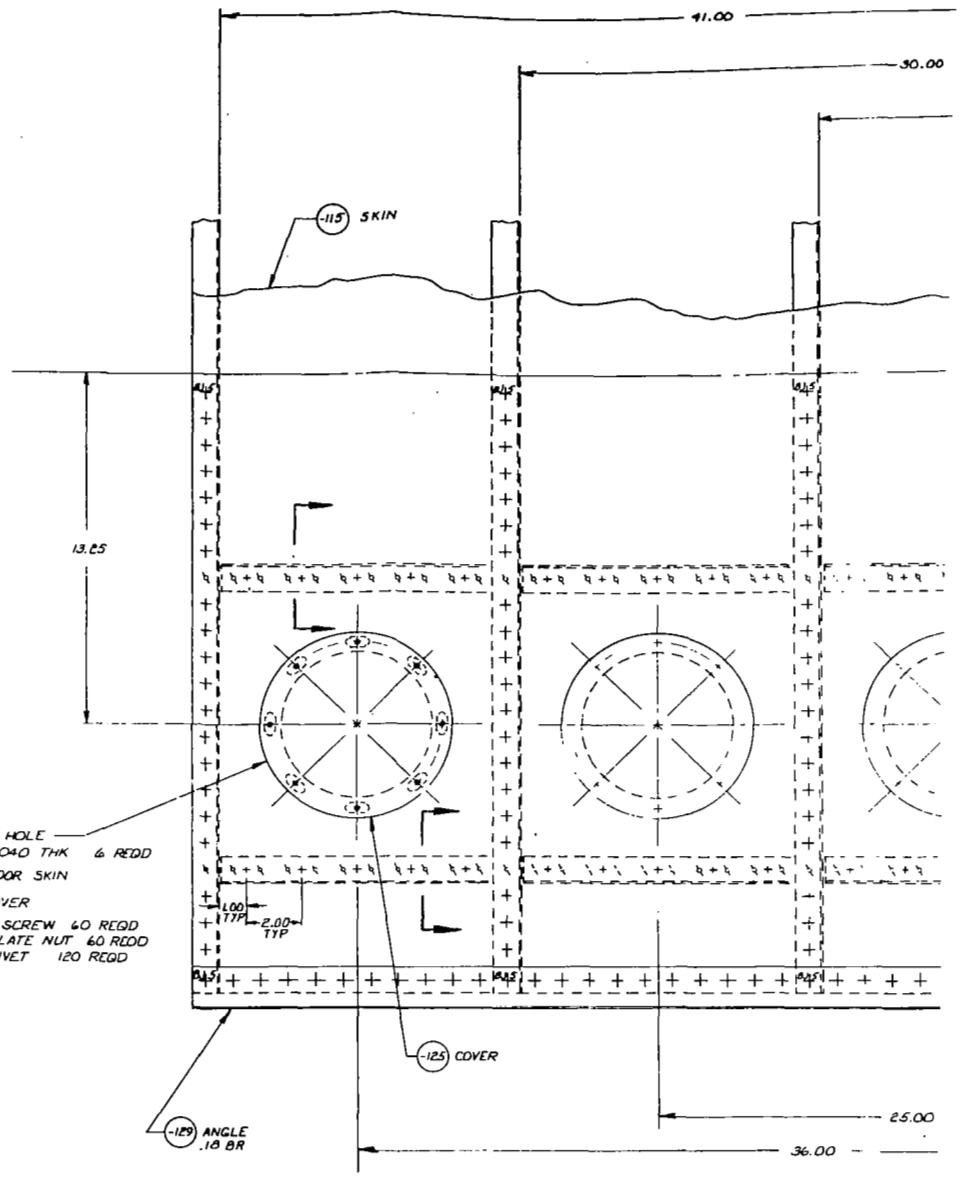

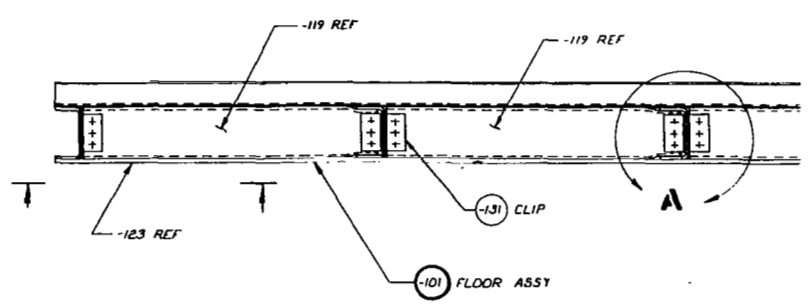

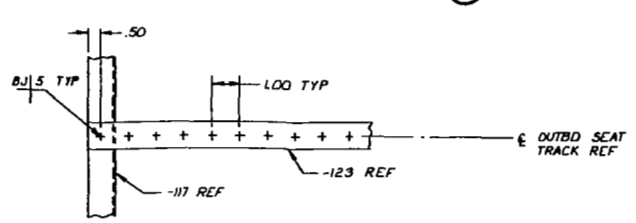

REV	DESCRIPTION	DATE	APPROVED
A	REDESIGNED & REDRAWN	8-9-79	

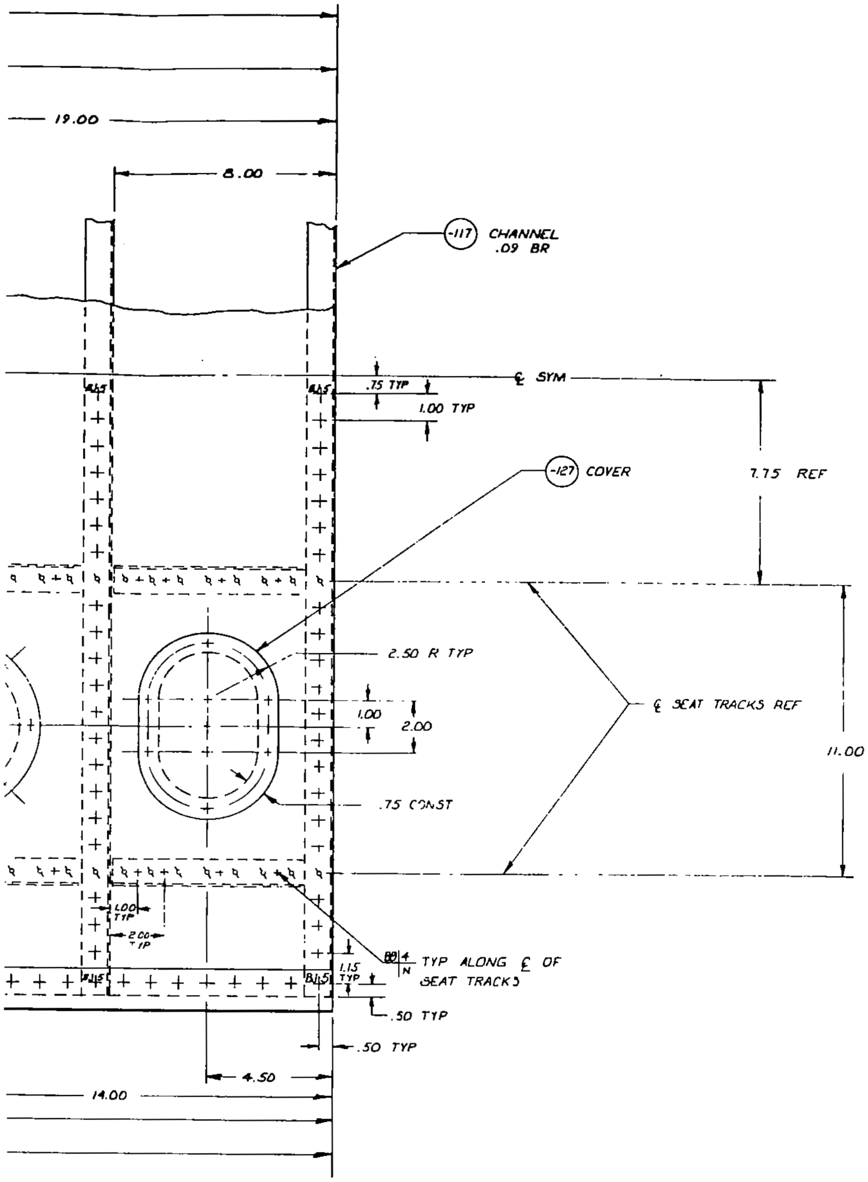

NOTES:

1. ʮ DENOTES LOCATION FOR SEAT TRACK INSTALLATION FASTENERS. THESE HOLES SHALL BE MATCH DRILLED TO THE SEAT TRACK WHEN SEAT TRACK IS INSTALLED BY NASA

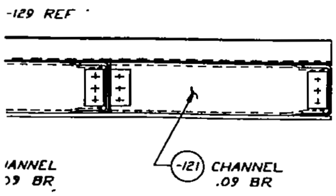

QTY	PART OR IDENTIFYING NO.	NOMENCLATURE OR DESCRIPTION	STOCK SIZE / MATERIAL / MATERIAL SPEC			
60	MS35207-263	SCREW				
60	MS 21059L3	PLATE NUT				
AR	MS 20470AD5	RIVET				
AR	MS 20426AD4	RIVET				
AR	MS 20426AD3	RIVET				
64	299-353-002-131	CLIP	.040×2.0×2.0 2024 AL ALY QQ-A-250/4 TEMP-T3	T3	K	XPD-1
2	-129	ANGLE	.080×2.5×42.0 2024 AL ALY QQ-A-250/4 TEMP-T3	T3		
2	-127	COVER	.040×5.0×7.0 2024 AL ALY QQ-A-250/4 TEMP-T3	T3		
6	-125	COVER	.040×7.0×7.0 2024 AL ALY QQ-A-250/4 TEMP-T3	T3		
2	-123	STRAP	.150×1.0×42.0 2024 AL ALY QQ-A-250/4 TEMP-T3	T3		
4	-121	CHANNEL	.050×4.5×8.0 2024 AL ALY QQ-A-250/4 TEMP-O	T42		
12	-119	CHANNEL	.050×4.6×11.0 2024 AL ALY QQ-A-250/4 TEMP-O	T42		
5	-117	CHANNEL	.050×4.5×42.0 2024 AL ALY QQ-A-250/4 TEMP-O	T42		
1	299-353-002-115	SKIN	.040×42.0×42.0 2024 AL ALY QQ-A-250/4 TEMP-T3	T3	K	XPD-1
-101	299-353-002-101	FLOOR ASSY				

PARTS LIST

-101		TEST
DASH NO.	NEXT ASSY	USED ON
APPLICATION		

UNLESS OTHERWISE SPECIFIED:
1. MARK PER BPS 4030
2. BREAK ALL SHARP EDGES .015 X 45 OR .015 R
3. TORQUE PER BPS 4018
4. SAFETY PER BPS 4043
5. DIMENSIONAL LIMITS APPLY AFTER PLATING

APPLICABLE DOCUMENTS:
ABBREVIATIONS PER MIL STD 12
DIMENSIONING AND TOLERANCING PER ANSI Y14.5 1973
ELECTRICAL SYMBOLS PER ANSI Y32.2
ELECTRICAL REF DESIGNATIONS PER ANSI Y32.16

LAST DATUM LTR USED
HEAT TREAT: BPS 4139
UNLESS OTHERWISE SPECIFIED DIMENSIONS ARE IN INCHES
SURFACE ROUGHNESS PER ANSI B46.1
✓ MACHINED SURFACES EXCEPT AS NOTED

CONTRACT NUMBER: NAS1-14890
DRAWN: 8-9-79

Bell Helicopter TEXTRON
Division of Textron Inc.

TITLE: FLOOR ASSY - TEST SPECIMEN, CRASHWORTHY STRUCTURE

CODE IDENT NO: 97499
DWG NO: 299-353-002
SCALE: 1/2 & NOTED
SHEET 1 OF 1

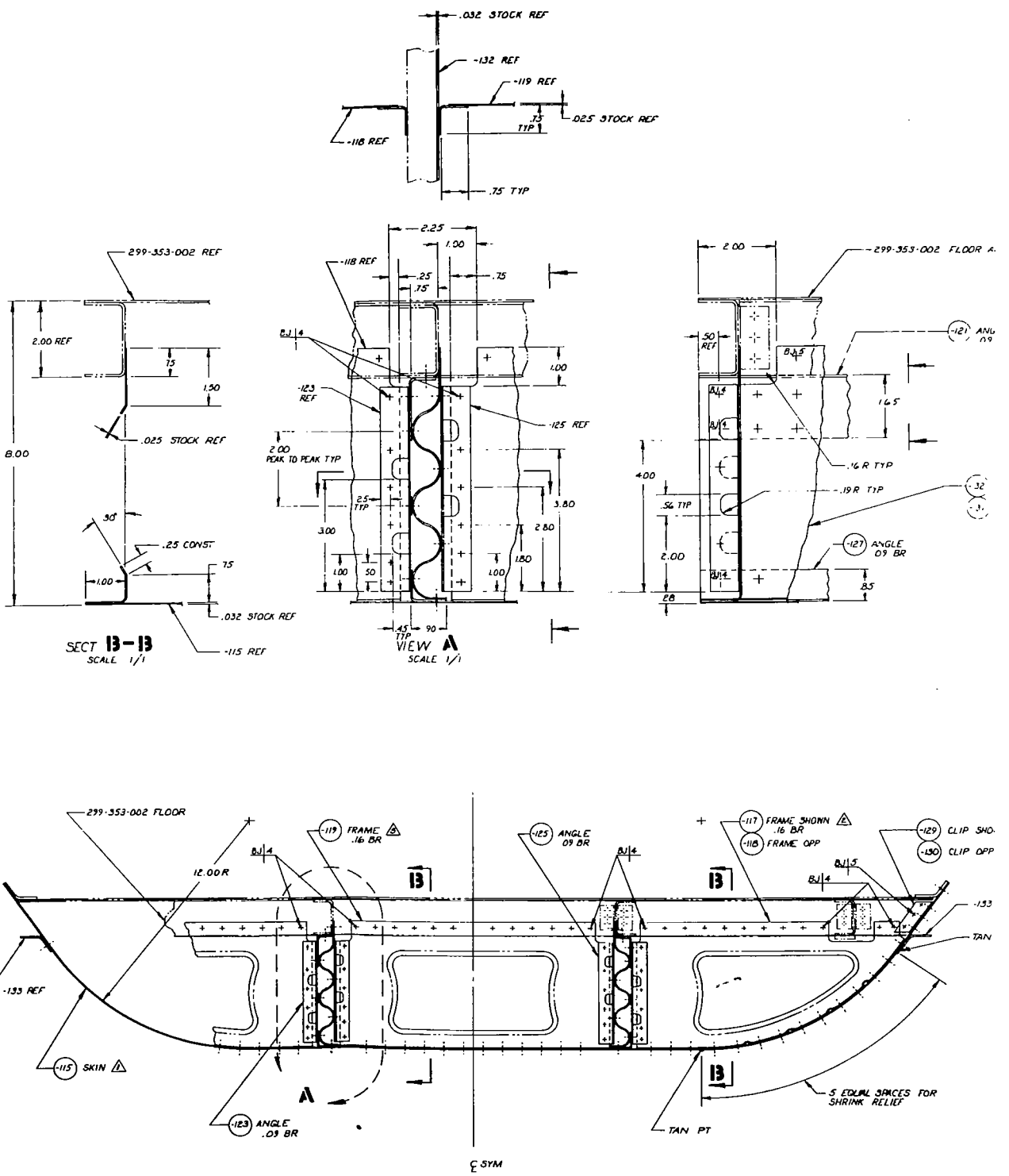
.032 STOCK REF
-132 REF
-119 REF
.75 TYP
.025 STOCK REF
-118 REF
.75 TYP
299-353-002 REF
2.00 REF
.75
1.50
.025 STOCK REF
8.00
90°
.25 CONST.
.75
1.00
.032 STOCK REF
-115 REF
SECT B-B
SCALE 1/1
2.25
1.00
-118 REF
.25
.75
.75
BJ 4
1.00
-123 REF
-125 REF
2.00 PEAK TO PEAK TYP
2.5 TYP
3.80
2.80
1.80
.300
1.00
.50
1.00
.45 TYP
90
VIEW A
SCALE 1/1
2.00
299-353-002 FLOOR A
-121 ANG
.09
.50 REF
BJ 5
BJ 4
1.65
BJ 4
.16 R TYP
4.00
.19 R TYP
.56 TYP
-127 ANGLE .09 BR
2.00
BJ 4
.28
.85
299-353-002 FLOOR
12.00 R
-119 FRAME .16 BR
BJ 4
B
-125 ANGLE .09 BR
BJ 4
B
-117 FRAME SHOWN
.16 BR
-118 FRAME OPP
BJ 5
BJ 4
-129 CLIP SHO
-130 CLIP OPP
-193
TAN
-193 REF
-115 SKIN
A
B
5 EQUAL SPACES FOR SHRINK RELIEF
-123 ANGLE .09 BR
TAN PT
℄ SYM

12 STOCK REF

-132 REF

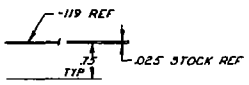

.75 TYP

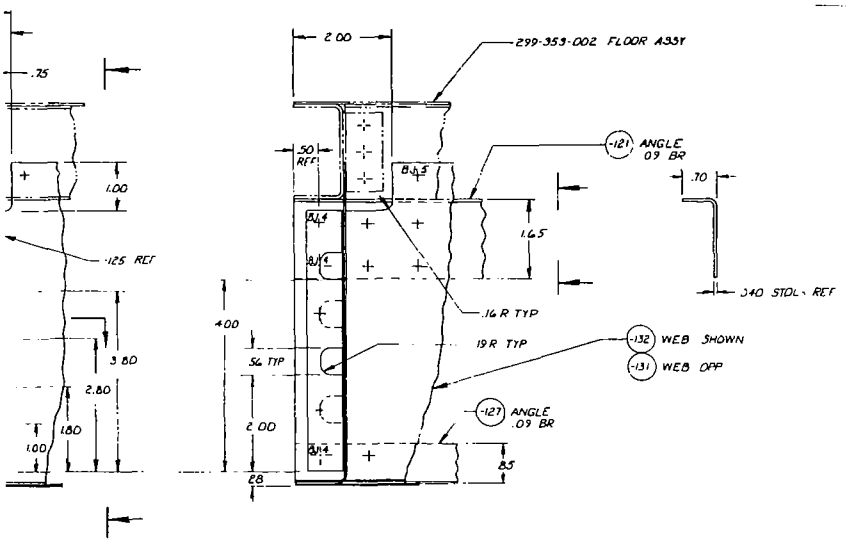

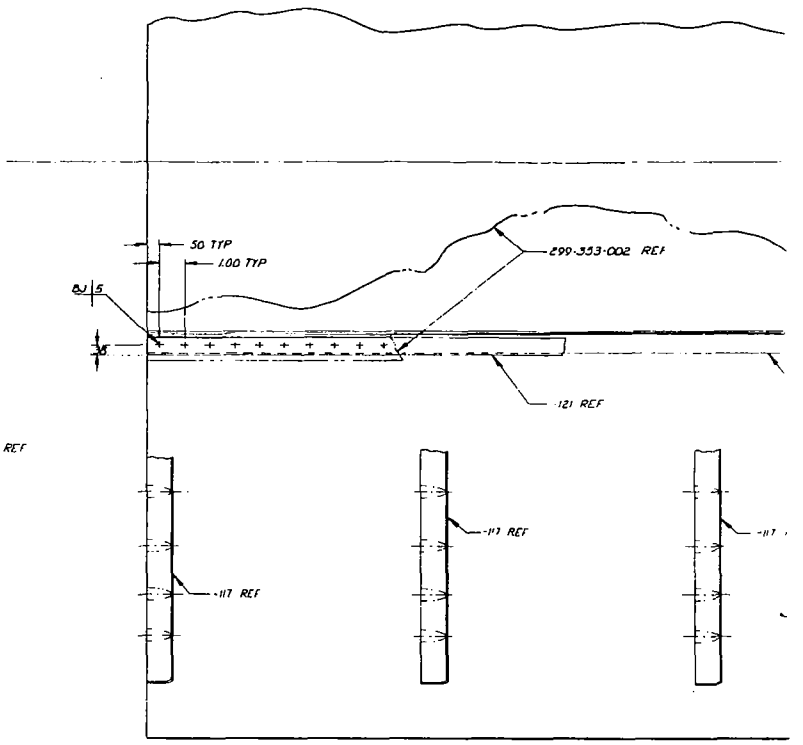

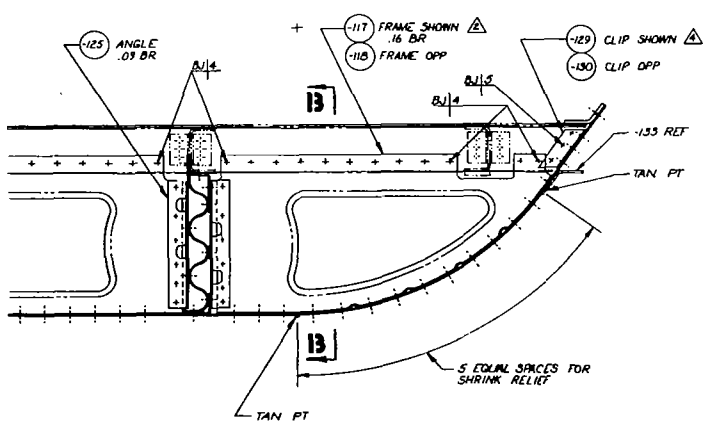

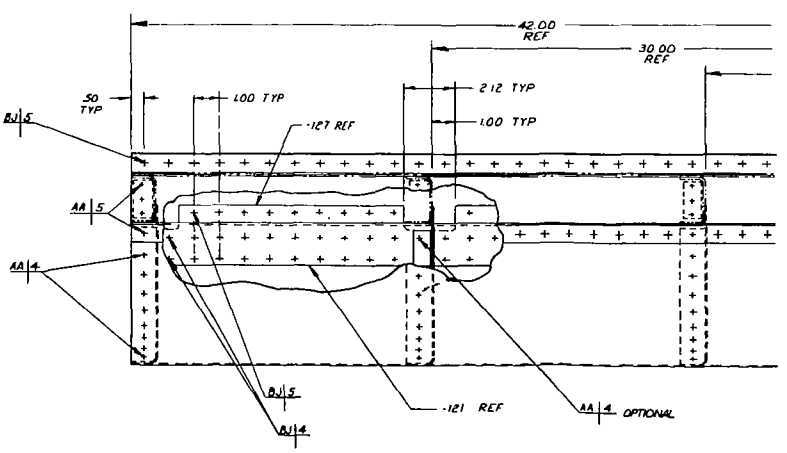

SYM

REV	DESCRIPTION	DATE	APPROVED

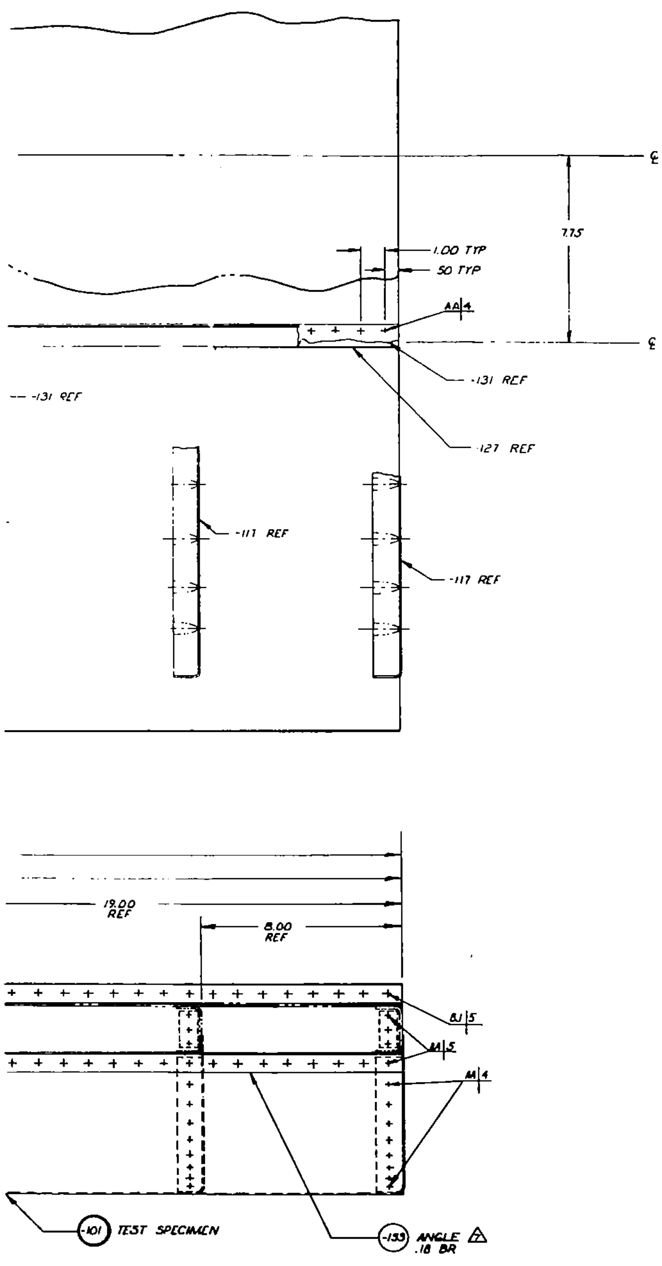

NOTES:

1. -115 SKIN IS THE SAME AS 299-353-003-115 SKIN EXCEPT FOR FASTENER LOCATIONS
2. -117/-118 FRAMES ARE THE SAME AS 299-353-003-117/-118 FRAMES EXCEPT AS SHOWN IN VIEW A
3. -119 FRAME IS THE SAME AS 299-353-003-119 FRAME EXCEPT AS SHOWN IN VIEW A
4. -129/-130 CLIP IS THE SAME AS 299-353-003-129/-130 [illegible]
5. FINISH CODE PER 299-099-031. APPLY ONE COAT OF ACRYLIC LACQUER TO EXTERIOR SURFACE OF -115 SKIN GLOSS WHITE PER MIL-L-81352 COLOR NUMBER 17038 PER FED. STD 595 A APPLY ONE COAT OF ACRYLIC LACQUER TO EXTERIOR SURFACE OF FLOOR MATTE GREY PER MIL-L-81352 COLOR NUMBER 36231 PER FED STD 595 A
6. MS20470AD4 RIVETS MAY BE USED IN LIEU OF MS20600AD4 RIVETS
7. -133 ANGLE IS THE SAME AS 299-353-002-129 ANGLE

QTY	PART OR IDENTIFYING NO.	CODE IDENT NO.	NOMENCLATURE OR DESCRIPTION	STOCK SIZE	MATERIAL	MATERIAL SPEC			
1	299-353-002-101		FLOOR ASSY						
AR	MS20600AD5		RIVET		STD				
AR	MS20600AD4		RIVET		STD				
AR	MS20470AD5		RIVET		STD				
AR	MS20470AD4		RIVET		STD				
2	299-353-004-133		ANGLE	.050×2.5×42.0	2024 AL ALY	QQ-A-250/4 TEMP-T3	T3	K	XPD-1
1	-132		WEB	.032×10.0×42.0	2024 AL ALY	QQ-A-250/4 TEMP-T3	T3	K	XPD-1
1	-131		WEB	.032×10.0×42.0					
5	-130		CLIP	.032×2.0×2.5					
5	-129		CLIP	.032×2.0×2.5					
2	-127		ANGLE	.032×2.0×42.0					
10	-125		ANGLE	.032×2.0×6.0					
10	-123		ANGLE	.032×2.0×6.0					
2	-121		ANGLE	.040×2.5×42.0					
5	-119		FRAME	.025×8.0×15.0					
5	-118		FRAME	.025×8.0×15.0					
5	-117		FRAME	.025×8.0×15.0					
1	299-353-004-115		SKIN	.032×42×56.0	2024 AL ALY	QQ-A-250/4 TEMP-T3	T3	K	XPD-1
	299-353-004-101		TEST SPECIMEN						
-101									

PARTS LIST WO 602D EWA 699 BR1.01

-101	TEST
DASH NO.	NEXT ASSY / USED ON — APPLICATION

CONTRACT NUMBER NAS1-14890

Bell Helicopter TEXTRON

TITLE: TEST SPECIMEN - CORRUGATED BEAM, CRASHWORTHY STRUCTURE

CODE IDENT NO. 97499

DWG NO. 299-353-004

SCALE 1/2 & NOTED SHEET 1 OF 1

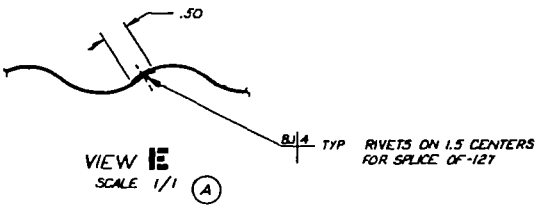

VIEW **E**
SCALE 1/1 (A)

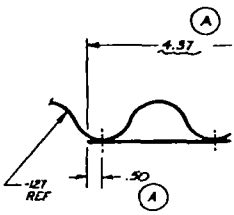

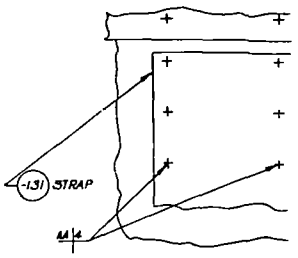

VIEW **D**
SCALE 1/1

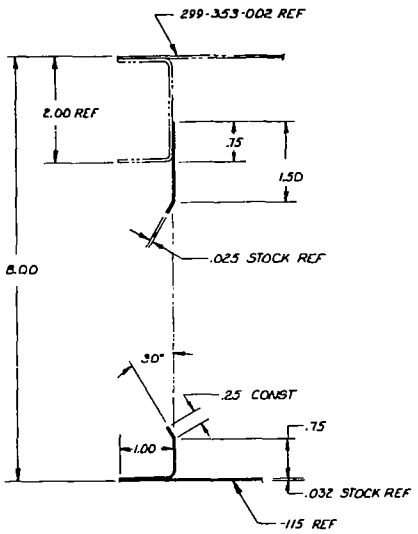

SECT **A-A**
SCALE 1/1

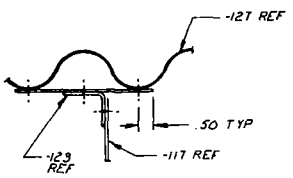

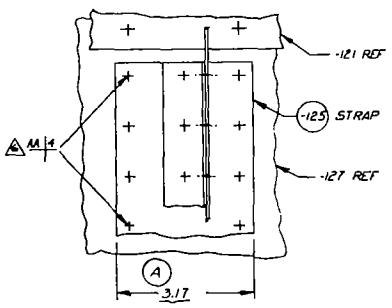

VIEW **C**
SCALE 1/1

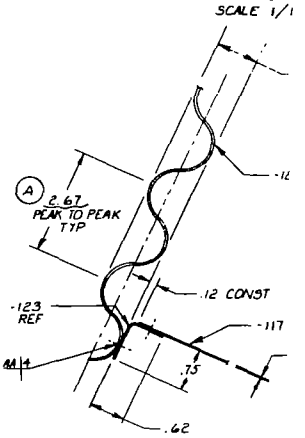

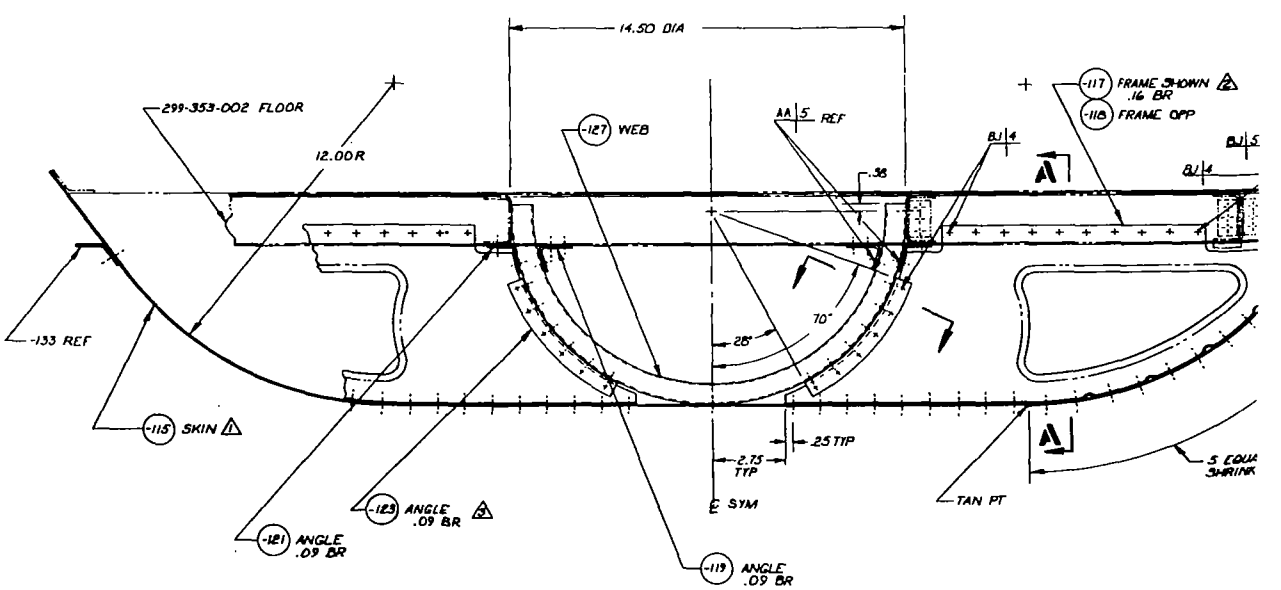

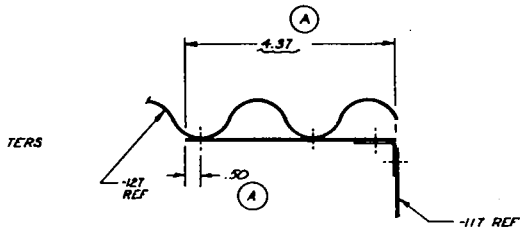
A
4.37
TERS
-127 REF
.50
A
-117 REF

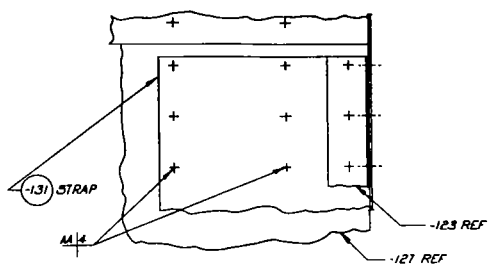
-131 STRAP
AA 4
-123 REF
-127 REF

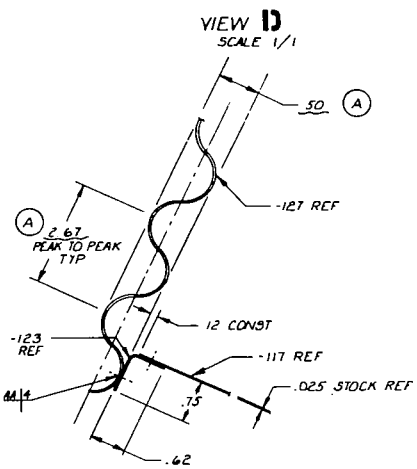
VIEW D
SCALE 1/1
.50
A
-127 REF
A
2.67
PEAK TO PEAK
TYP
.12 CONST
-123 REF
-117 REF
.025 STOCK REF
.75
.62

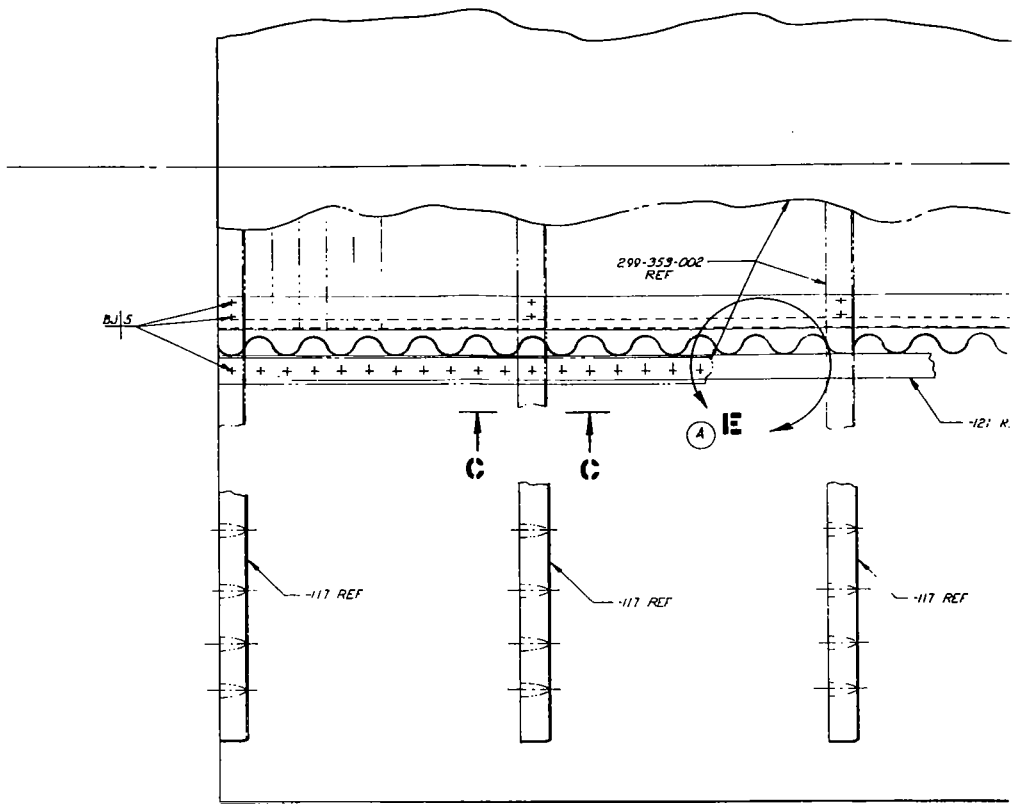
299-359-002
REF
BJ 5
A
E
C
C
-121 R
-117 REF
-117 REF
-117 REF

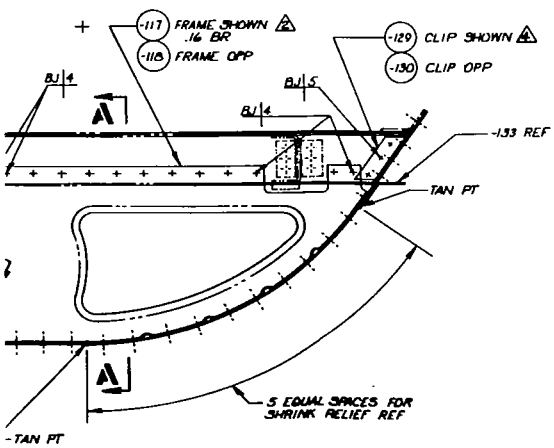
-117 FRAME SHOWN
.16 BR
-118 FRAME OPP
-120 CLIP SHOWN
-130 CLIP OPP
BJ 4
BJ 5
BJ 4
A
-133 REF
TAN PT
A
5 EQUAL SPACES FOR
SHRINK RELIEF REF
TAN PT

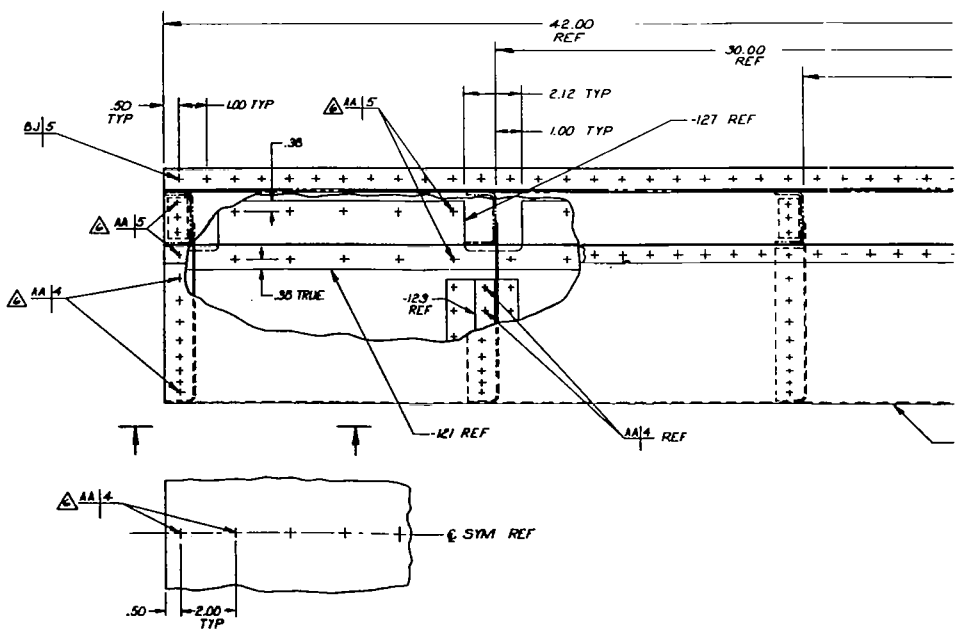
42.00
REF
30.00
REF
.50
TYP
1.00 TYP
2.12 TYP
1.00 TYP
BJ 5
AA 5
.38
-127 REF
AA 5
.38 TRUE
-129
REF
AA 4
-121 REF
AA 4 REF

AA 4
℄ SYM REF
.50
2.00
TYP

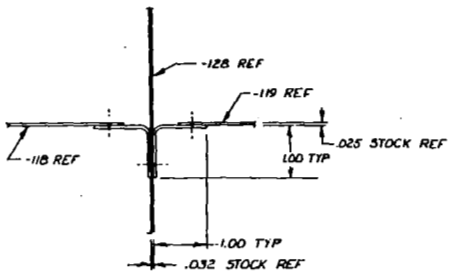
-128 REF
-119 REF
-118 REF
.025 STOCK REF
1.00 TYP
1.00 TYP
.032 STOCK REF

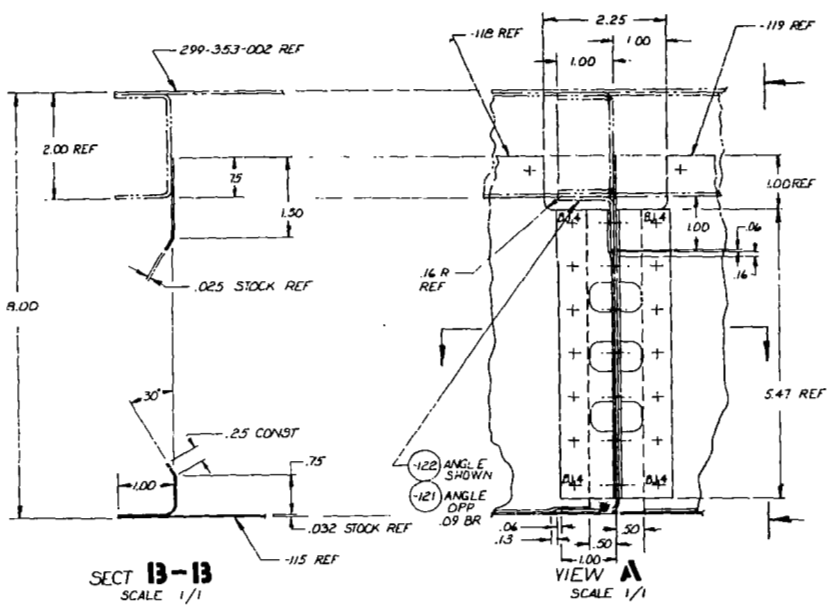
299-353-002 REF
2.00 REF
.75
1.50
.025 STOCK REF
8.00
30°
.25 CONST
.75
1.00
.032 STOCK REF
-115 REF
SECT B-B
SCALE 1/1
-118 REF
2.25
1.00
1.00
-119 REF
1.00 REF
.16 R REF
1.00
.06
.16
5.47 REF
-122 ANGLE SHOWN
-121 ANGLE OPP .09 BR
.06
.13
.50
.50
1.00
VIEW A
SCALE 1/1

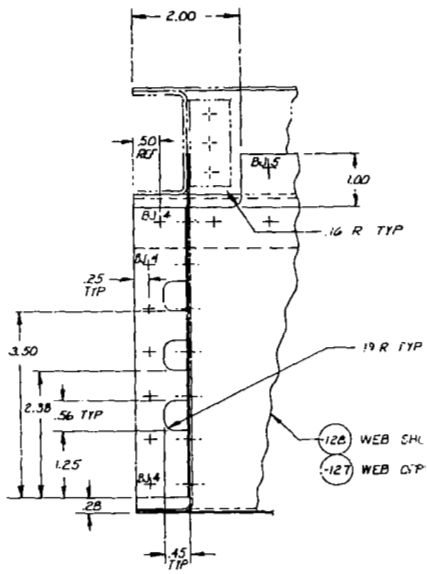
2.00
.50 REF
1.00
.16 R TYP
.25 TYP
3.50
.19 R TYP
2.38
.56 TYP
1.25
.28
.45 TYP
-128 WEB SHO
-127 WEB OPP

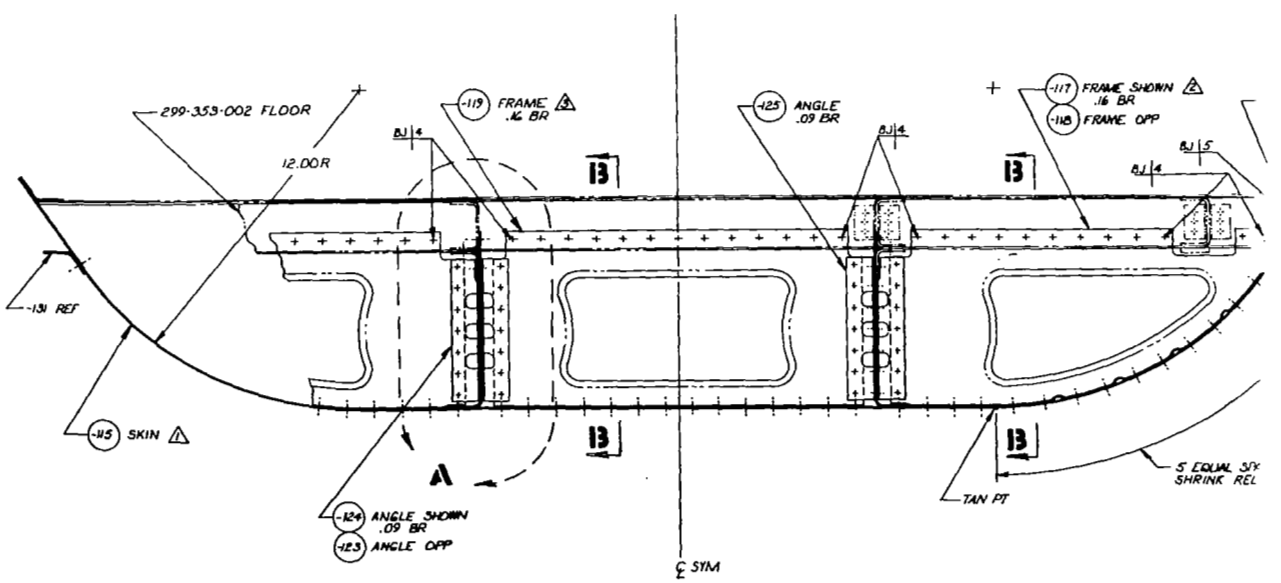
299-353-002 FLOOR
12.00 R
-119 FRAME .16 BR
-125 ANGLE .09 BR
-117 FRAME SHOWN .16 BR
-118 FRAME OPP
-131 REF
-115 SKIN
-124 ANGLE SHOWN .09 BR
-123 ANGLE OPP
TAN PT
5 EQUAL SPA
SHRINK REL
℄ SYM

NN

-129 C
-130 C

CES FOR
EF REF

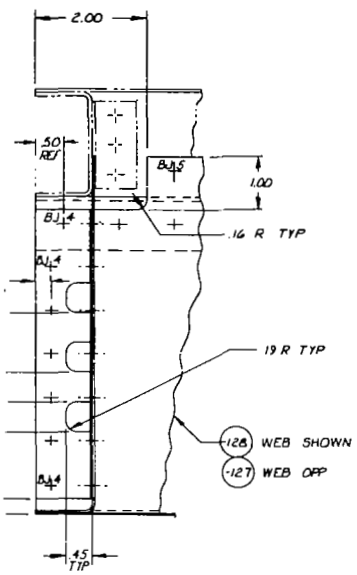
2.00
.50 REF
BJ 5
1.00
BJ 4
.16 R TYP
BJ 4
.19 R TYP
-128 WEB SHOWN
-127 WEB OPP
BJ 4
.45 TYP

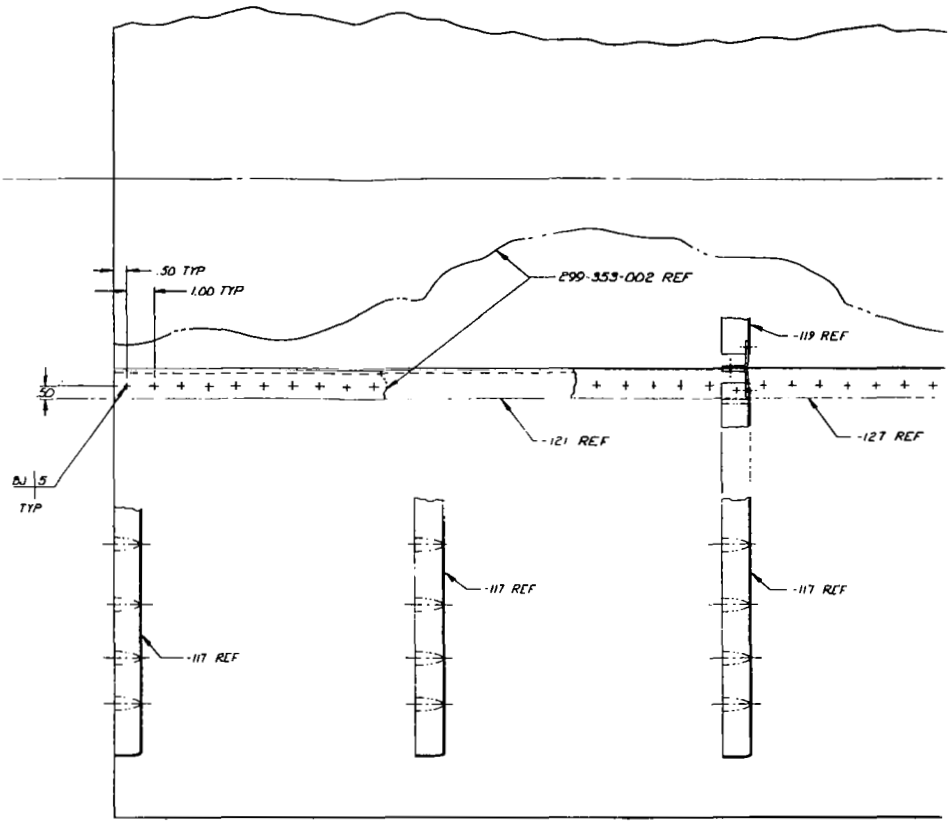
.50 TYP
1.00 TYP
299-353-002 REF
-119 REF
.50
-121 REF
-127 REF
BJ 5 TYP
-117 REF
-117 REF
-117 REF

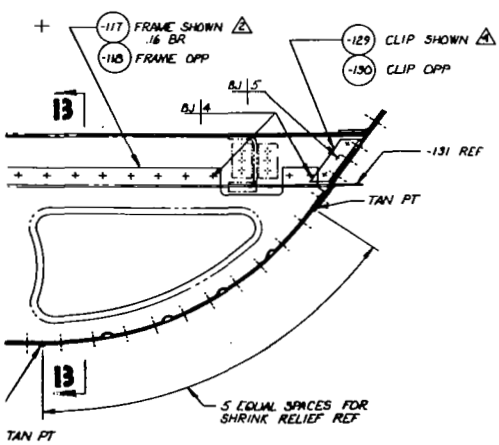
-117 FRAME SHOWN .16 BR
-118 FRAME OPP
-129 CLIP SHOWN
-130 CLIP OPP
BJ 5
BJ 4
13
-131 REF
TAN PT
13
5 EQUAL SPACES FOR SHRINK RELIEF REF
TAN PT

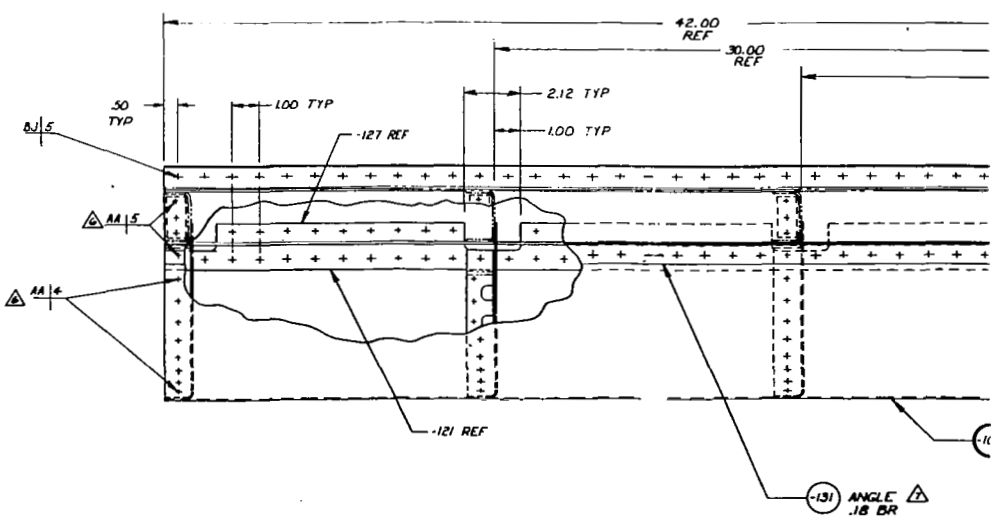
42.00 REF
30.00 REF
.50 TYP
1.00 TYP
2.12 TYP
1.00 TYP
BJ 5
-127 REF
AA 5
AA 4
-121 REF
-131 ANGLE .18 BR

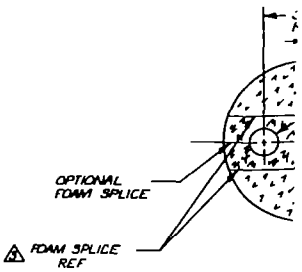

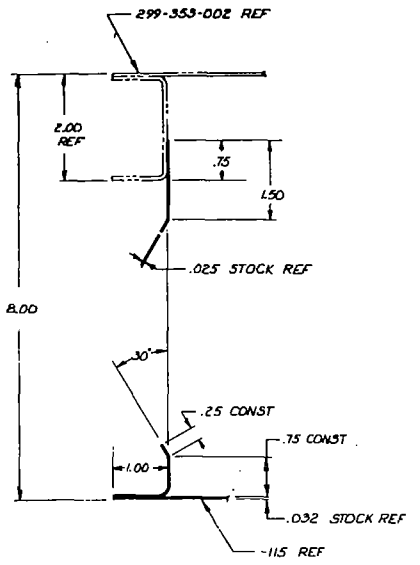

SECT **A-A**
SCALE 1/1

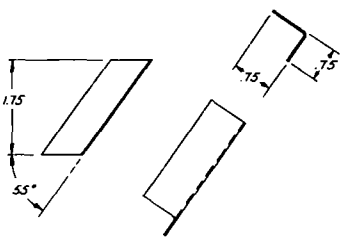

DETAIL -129 CLIP
SCALE 1/1
.12 BR

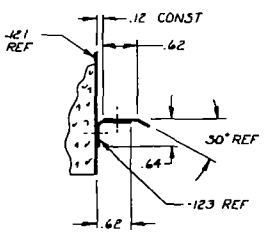

SECT **C-C**
SCALE 1/1

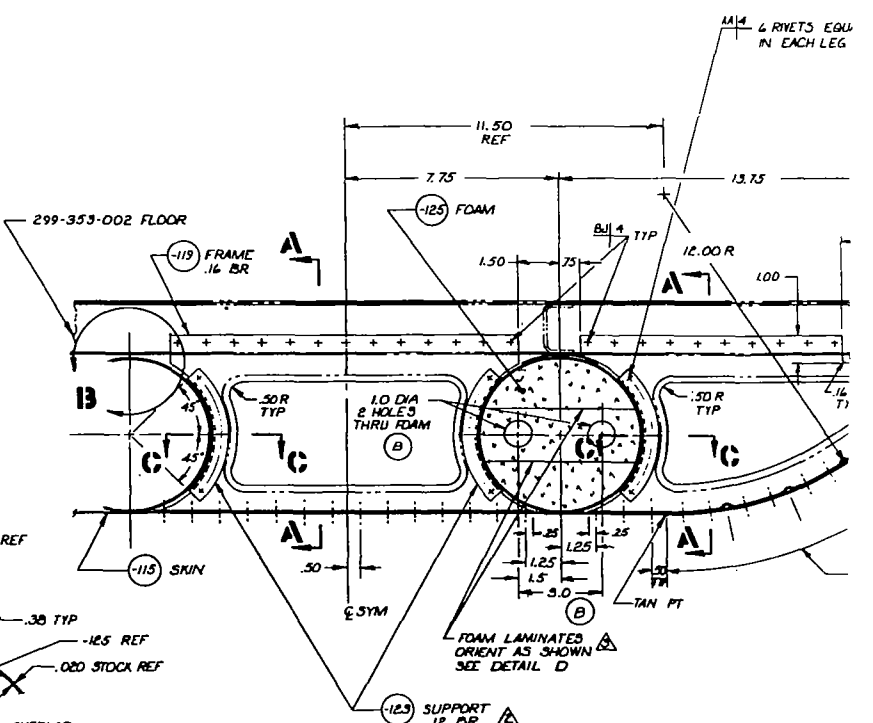

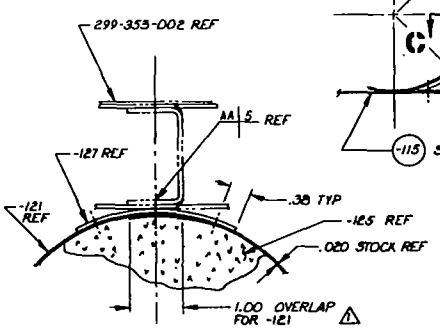

VIEW **B**
SCALE 1/1

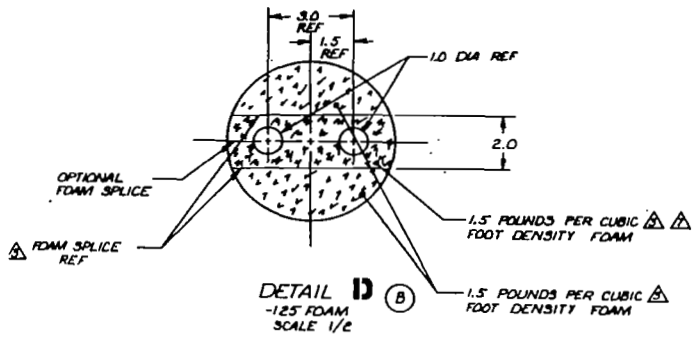

DETAIL D (8)
-125 FOAM
SCALE 1/2

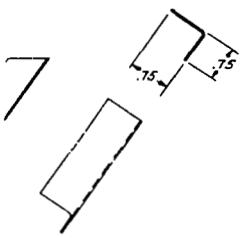

1/1 -129 CLIP
SCALE 1/1
.12 BR

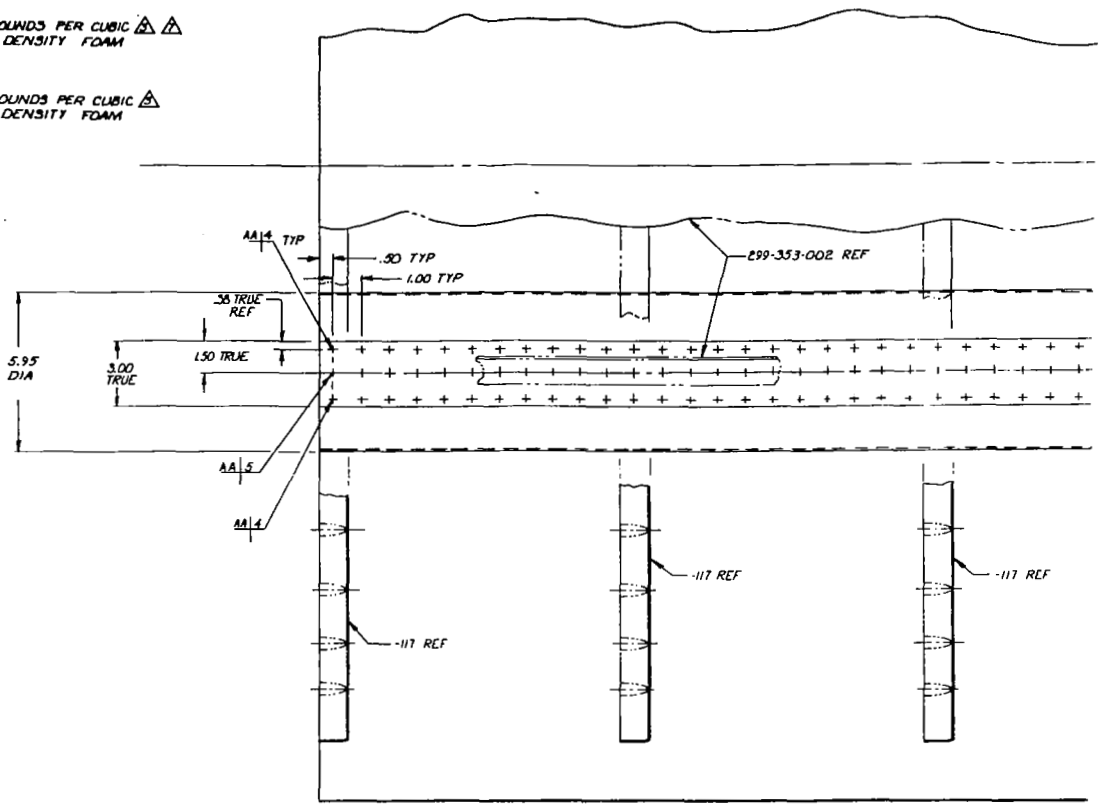

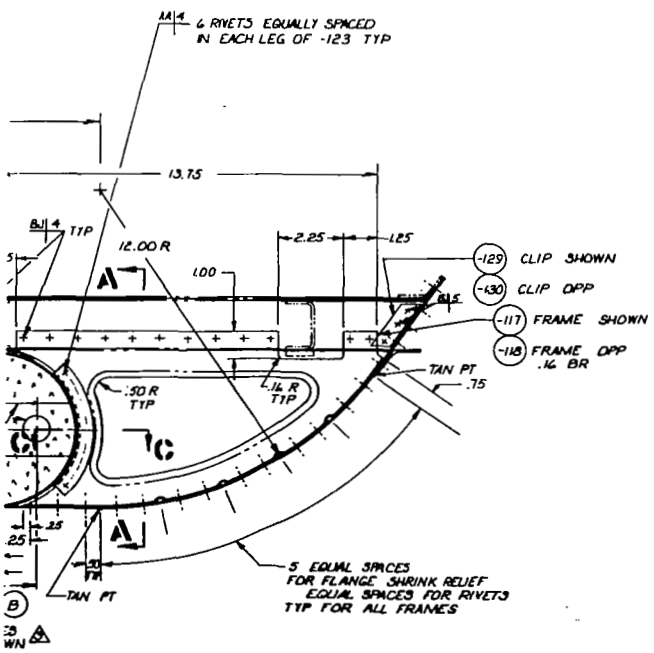

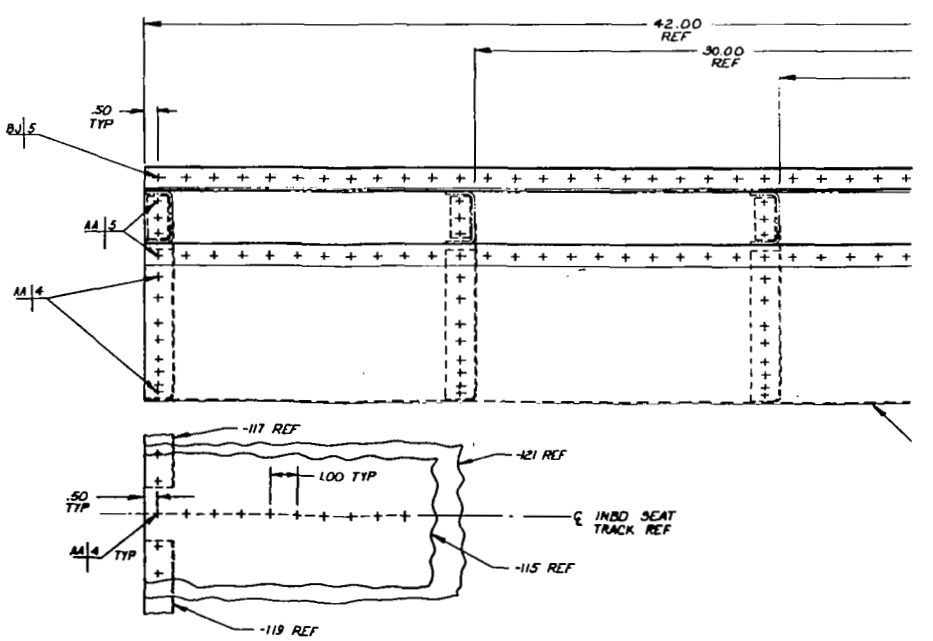

REV	DESCRIPTION	DATE	APPROVED
A	REDESIGNED (RE DRAWN)	8-17-79	
B	ADDED DETAIL D AND NOTES 7 & 8		
	REMOVED TBD FROM P/L FOR -125	10-17-79	

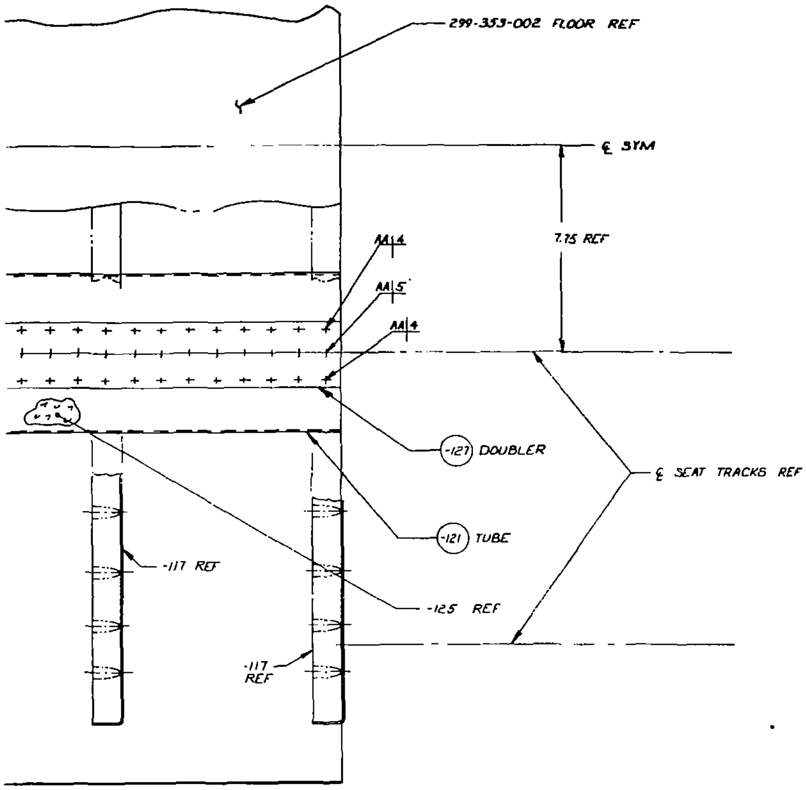

NOTES:

1. OVERLAP FOR -121 SHOWN AT TOP OF TUBE OVERLAP MAY BE PLACED AT BOTTOM OF TUBE FOR EASE OF FABRICATION
2. FLANGE OF -123 MAY BE SLOTTED BETWEEN RIVETS FOR STRETCH RELIEF
3. BOND FOAM BLOCKS TOGETHER TO FABRICATE FOAM CYLINDER AND BOND FOAM CYLINDER TO -121 TUBE USING ADHESIVE PER BPS 4403
4. FINISH CODE PER 299-099-031 APPLY ONE COAT OF ACRYLIC LACQUER TO EXTERIOR SURFACE OF -115 SKIN GLOSS WHITE PER MIL-L-81352 COLOR NUMBER 17038 PER FED STD 595A. APPLY ONE COAT OF ACRYLIC LACQUER TO EXTERIOR SURFACE OF FLOOR MATTE GREY PER MIL-L-81352 COLOR NUMBER 36231 PER FED STD 595 A
5. MS20470AD RIVETS MAY BE USED IN LIEU OF MS20600AD RIVETS
6. -131 ANGLE IS THE SAME AS 299-353-002-129 ANGLE
7. CENTER FOAM MAY BE FABRICATED IN ONE FOOT LENGTHS AND BONDED PER NOTE 3
8. (B) FOAM MATERIAL TO BE RIGID KLEGECELL FOAM OF 1.5 POUNDS PER CUBIC FOOT DENSITY AS SHOWN ON F/D. FOAM MATERIAL IS A PRODUCT OF AMERICAN KLEGECELL CORP 204 NORTH DOOLEY ST. GRAPEVINE TEXAS 76051 CODE IDENT 55606

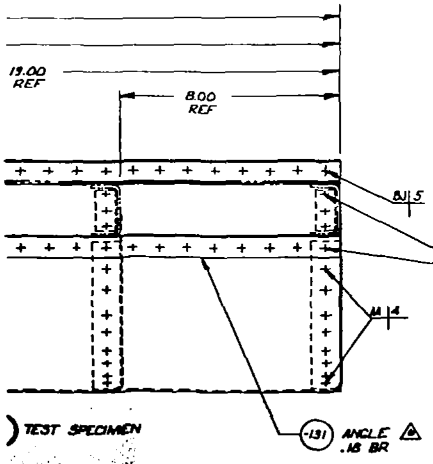

QTY REQD -101	PART OR IDENTIFYING NO.	CODE IDENT NO.	NOMENCLATURE OR DESCRIPTION	STOCK SIZE	MATERIAL	MATERIAL SPEC	TEMPER	FINISH CODE 299-099-031	ZONE
1	299-353-002-101		FLOOR ASSY						
AR			ADHESIVE	EA 9309 PER 299-947-125 TYPE I					
AR	MS20600AD5		RIVET						
AR	MS20600AD4		RIVET						
AR	MS20470AD5		RIVET						
AR	MS20470AD4		RIVET						
2	299-353-003-131		ANGLE	.050×2.5×42.0	2024 AL ALY	QQ-A-250/4 TEMP-T3	T3	K	XPD-1
5	299-353-003-130		CLIP	.032×2.0×2.5	2024 AL ALY	QQ-A-250/4 TEMP-T3	T3	K	XPD-1
5	-129		CLIP	.032×2.0×2.5	2024 AL ALY	QQ-A-250/4 TEMP-T3	T3		
2	-127		DOUBLER	.030×3.0×42.0	2024 AL ALY	QQ-A-250/4 TEMP-T3	T3	K	XPD-1
AR	-125		FOAM						
20	-123		SUPPORT	.025×2.0×6.0	2024 AL ALY	QQ-A-250/4 TEMP-T3	T3	K	XPD-1
2	-121		TUBE	.020×20.0×42.0	2024 AL ALY	QQ-A-250/4 TEMP-T3	T3		
5	-119		FRAME	.025×8.0×15.0	2024 AL ALY	QQ-A-250/4 TEMP-T3	T3		
5	-118		FRAME	.025×8.0×15.0	2024 AL ALY	QQ-A-250/4 TEMP-T3	T3		
5	-117		FRAME	.025×8.0×15.0	2024 AL ALY	QQ-A-250/4 TEMP-T3	T3		
1	299-353-003-115		SKIN	.032×42.0×56.0	2024 AL ALY	QQ-A-250/4 TEMP-T3	T3	K	XPD-1
	299-353-003-101		TEST SPECIMEN						

PARTS LIST WO 602D EWA 499 BR 1.01

CONTRACT NUMBER NAS1-14890

Bell Helicopter TEXTRON
Division of Textron Inc

TITLE: TEST SPECIMEN-TUBULAR, CRASHWORTHY STRUCTURE

CODE IDENT NO. 97499 DWG NO. 299-353-003

SCALE AS NOTED SHEET 1 OF 1

-101 TEST

131

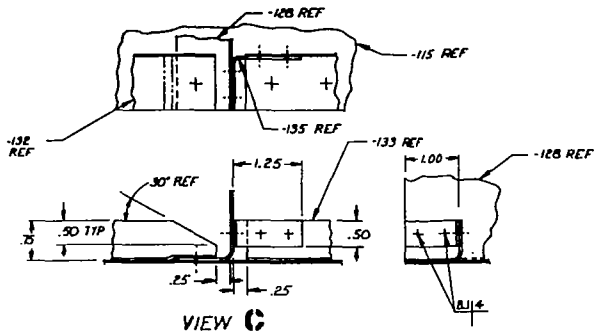

VIEW **C**
SCALE 1/1
STIFFENER DETAIL

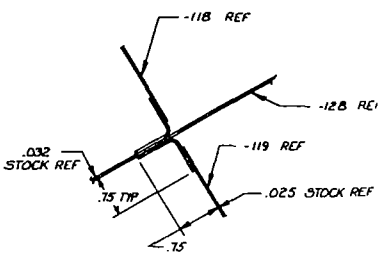

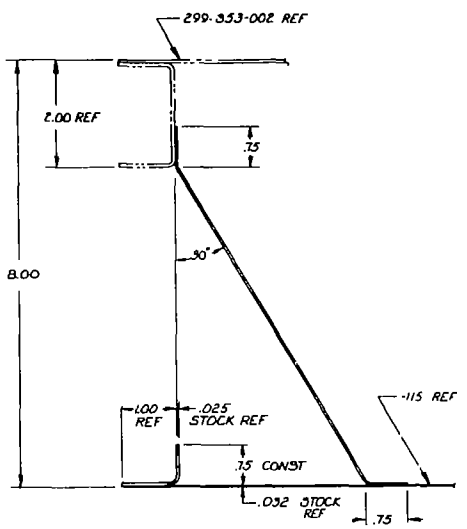

SECT **B-B**
SCALE 1/1

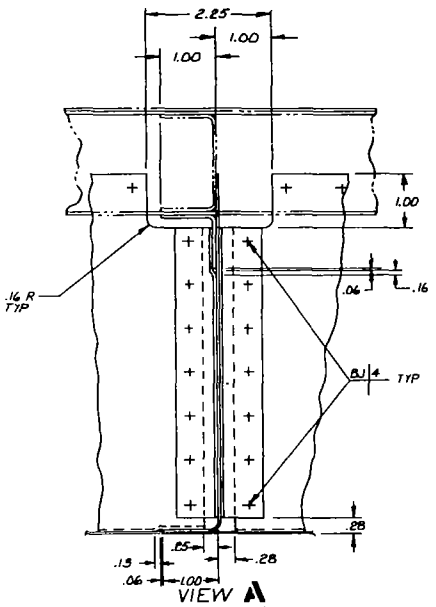

VIEW **A**
SCALE 1/1
STIFFENERS OMITTED
FOR CLARITY IN THIS VIEW

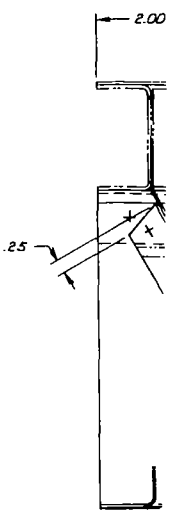

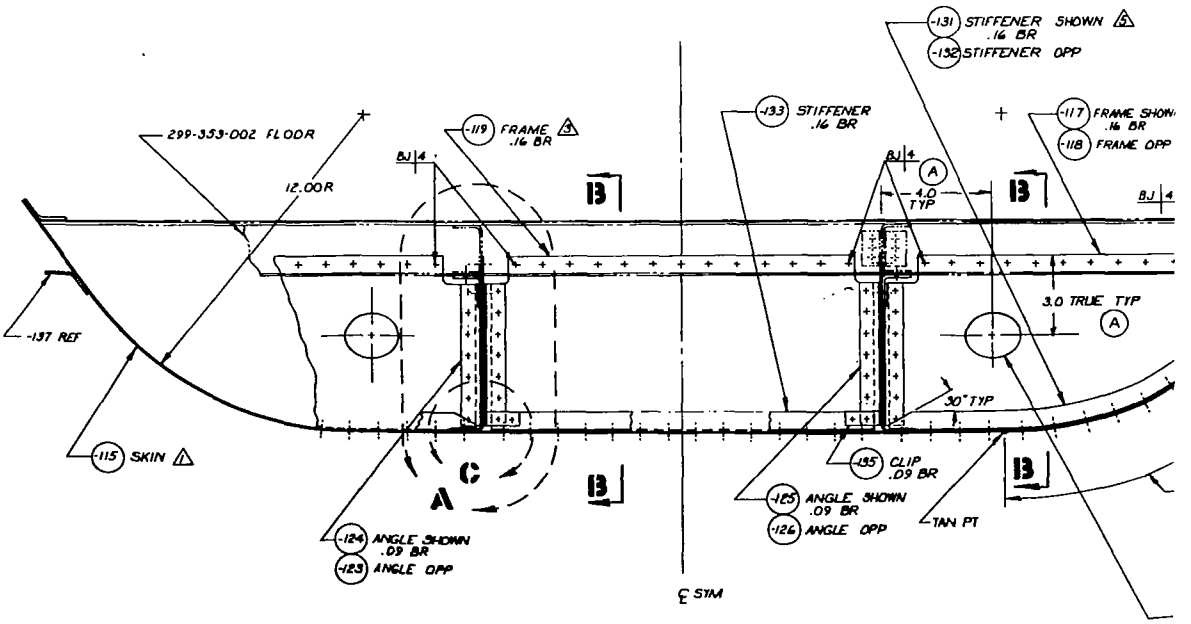

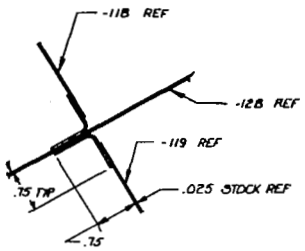
-118 REF
-128 REF
-119 REF
.025 STOCK REF
.75 TYP
.75

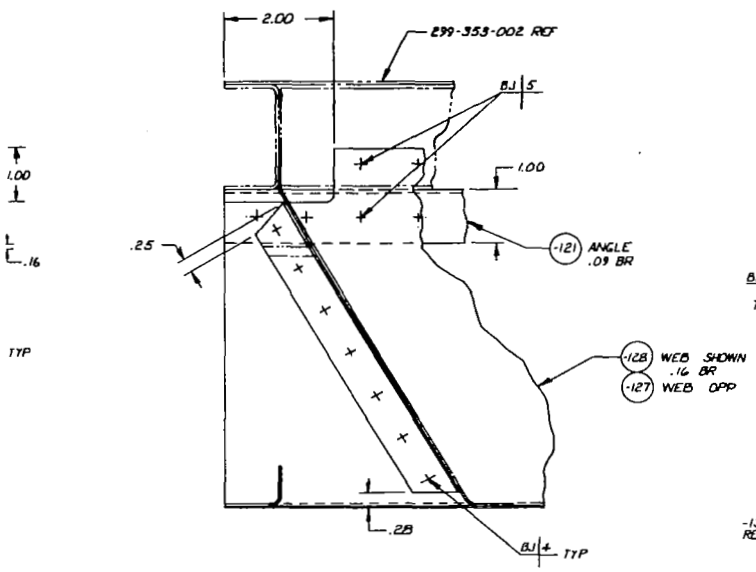
2.00
299-353-002 REF
BJ 5
1.00
1.00
.25
-121 ANGLE .09 BR
.16
TYP
-128 WEB SHOWN .16 BR
-127 WEB OPP
.28
BJ 4 TYP

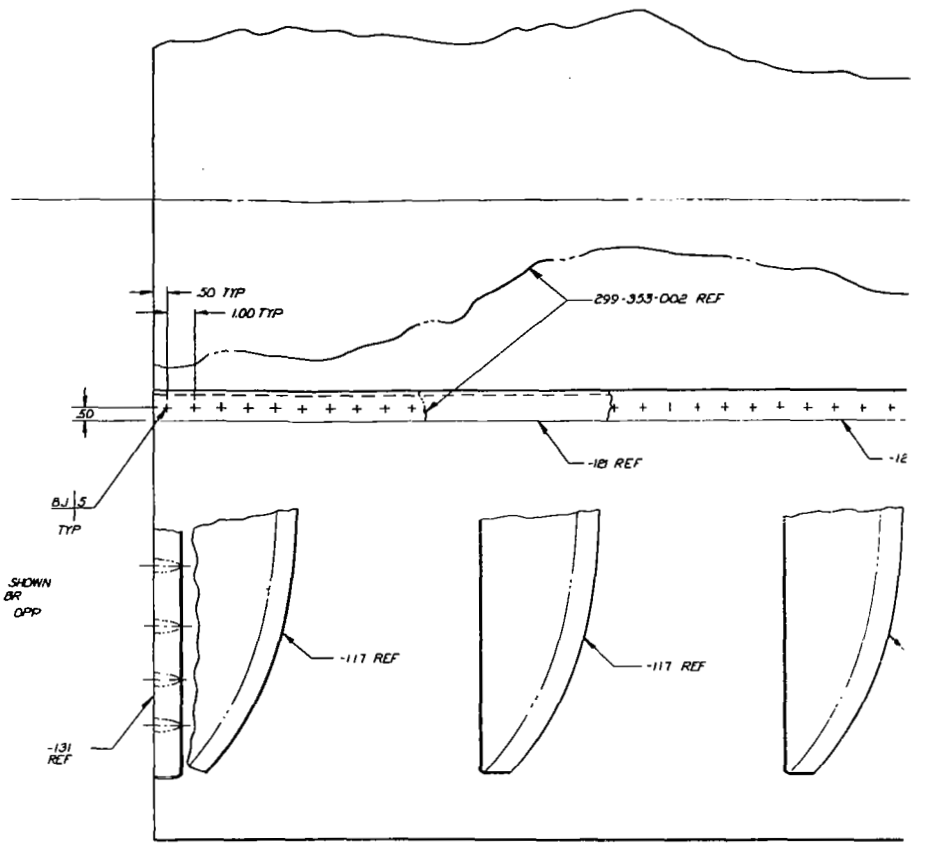
.50 TYP
1.00 TYP
299-353-002 REF
.50
-18 REF
-12
BJ 5
TYP
-117 REF
-117 REF
-131 REF

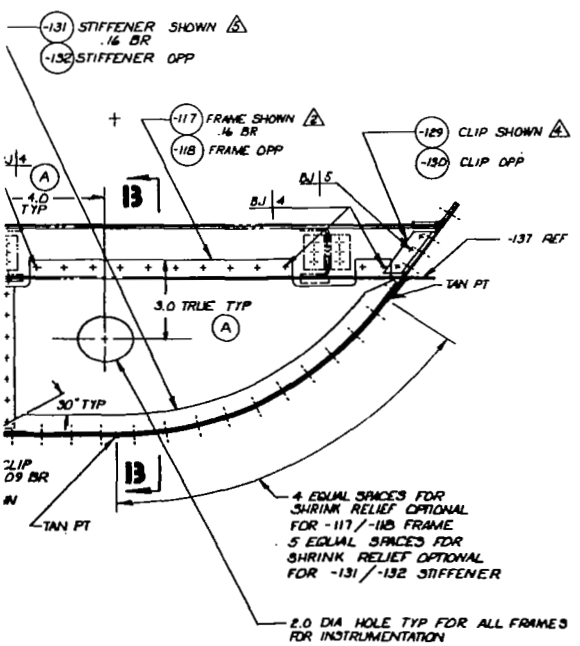
-131 STIFFENER SHOWN .16 BR
-132 STIFFENER OPP
-117 FRAME SHOWN .16 BR
-118 FRAME OPP
-129 CLIP SHOWN
-130 CLIP OPP
BJ 4
A
4.0 TYP
13
BJ 5
BJ 4
-137 REF
TAN PT
3.0 TRUE TYP
A
30° TYP
CLIP .09 BR IN
13
TAN PT
4 EQUAL SPACES FOR SHRINK RELIEF OPTIONAL FOR -117/-118 FRAME
5 EQUAL SPACES FOR SHRINK RELIEF OPTIONAL FOR -131/-132 STIFFENER
2.0 DIA HOLE TYP FOR ALL FRAMES FOR INSTRUMENTATION (A)

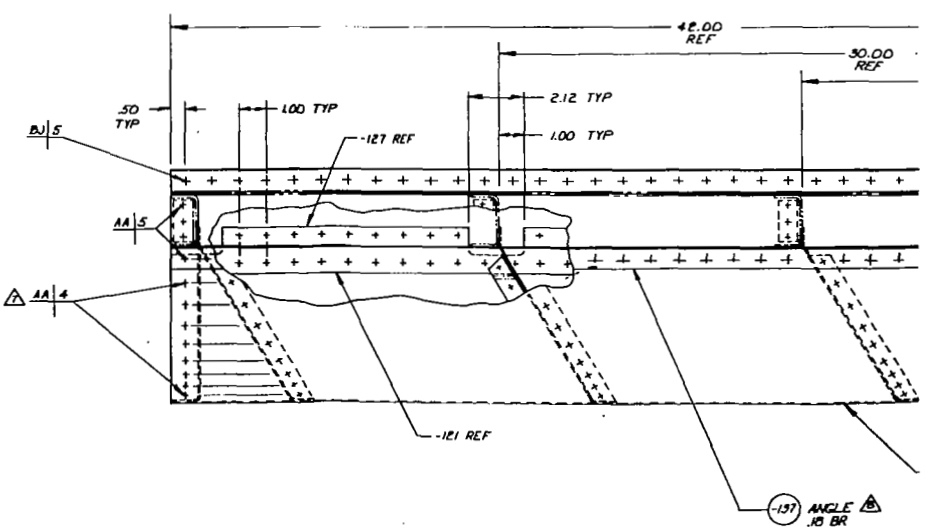
42.00 REF
30.00 REF
.50 TYP
1.00 TYP
2.12 TYP
1.00 TYP
BJ 5
-127 REF
AA 5
AA 4
-121 REF
-137 ANGLE .18 BR

REV	DESCRIPTION	DATE	APPROVED
A	ADDED .20 DIA HOLE TO -117/-118 FRAME FOR INSTRUMENTATION	10-3-79	

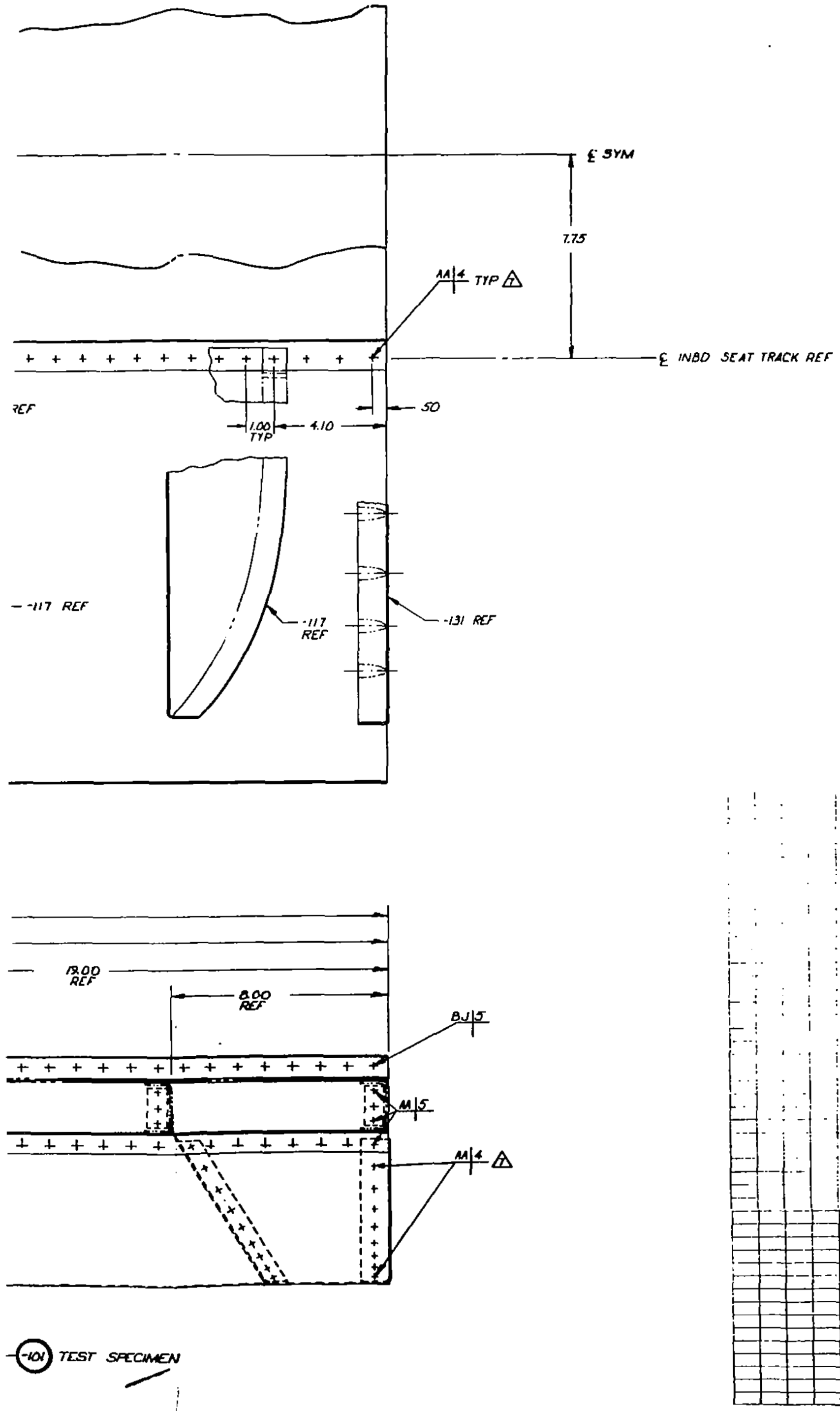

(-101) TEST SPECIMEN

NOTES:

1. -115 SKIN IS THE SAME AS 299-353-003-115 SKIN EXCEPT FOR FASTENER LOCATIONS
2. DIMENSIONS NOT SHOWN FOR -117/-118 FRAMES ARE THE SAME AS 299-353-003-117/-118 FRAMES
3. DIMENSIONS NOT SHOWN FOR -119 FRAME ARE THE SAME AS 299-353-003-119 FRAME
4. -129/-130 CLIP IS THE SAME AS 299-353-003-129/-130 CLIP
5. -131/-132 STIFFENER MAY BE MADE FROM 299-353-006 -117/-118 FRAMES RESPECTIVELY
6. FINISH CODE PER 299-099-031 APPLY ONE COAT OF ACRYLIC LACQUER TO EXTERIOR SURFACE OF -115 SKIN GLOSS WHITE PER MIL-L-81352 COLOR NUMBER 17038 PER FED STD 595A. APPLY ONE COAT OF ACRYLIC LACQUER TO EXTERIOR SURFACE OF FLOOR MATTE GREY PER MIL-L-81352 COLOR NUMBER 36231 PER FED STD 595A
7. MS20470AD4 RIVETS MAY BE USED IN LIEU OF MS20600AD4 RIVETS
8. -137 ANGLE IS THE SAME AS 299-353-002-129 ANGLE

QTY REQD -101	PART OR IDENTIFYING NO.	CODE IDENT NO.	NOMENCLATURE OR DESCRIPTION	STOCK SIZE	MATERIAL	MATERIAL SPEC		FINISH CODE	ZONE
	299-353-005-101		TEST SPECIMEN						
1	299-353-005-115		SKIN	.032×42.0×56.0	2024 AL ALY	QQ-A-250/4 TEMP T3	T3	K	XPD-1
4	-117		FRAME	.025×9.0×16.0					
4	-118		FRAME	.025×9.0×16.0					
4	-119		FRAME	.025×9.0×15.0					
2	-121		ANGLE	.040×2.5×42.0					
4	-123		ANGLE	.032×2.5×7.0					
4	-124		ANGLE	.032×2.5×7.0					
4	-125		ANGLE	.032×2.5×7.0					
4	-126		ANGLE	.032×2.5×7.0					
1	-127		WEB	.032×8.0×42.0					
1	-128		WEB	.032×8.0×42.0					
5	-129		CLIP	.032×2.0×2.5					
5	-130		CLIP	.032×2.0×2.5					
2	-131		STIFFENER	.025×8.0×16.0					
2	-132		STIFFENER	.025×8.0×16.0					
2	-133		STIFFENER	.025×2.5×15.0					
4	299-353-005-135		CLIP	.032×.50×2.5	2024 AL ALY	QQ-A-250/4 TEMP T3	T3	K	XPD-1
2	299-353-005-137		ANGLE	.050×2.5×42.0	2024 AL ALY	QQ-A-250/4 TEMP T3	T3	K	XPD-1
AR	MS20470AD4		RIVET		STD				
AR	MS20470AD5		RIVET		STD				
AR	MS20600AD4		RIVET		STD				
AR	MS20600AD5		RIVET		STD				
1	299-353-002-101		FLOOR ASSY						

PARTS LIST WO 602D EWA 699BR1.01

-101 TEST

CONTRACT NUMBER NAS1-14890

Bell Helicopter TEXTRON Division of Textron Inc.

TEST SPECIMEN CANTED BULKHEAD CRASHWORTHY STRUCTURE

CODE IDENT NO. 97499 DWG NO. 299-353-005

SCALE 1/2 & NOTED SHEET 1 OF 1

APPENDIX E

FUSELAGE MODIFICATION DESIGN DRAWINGS

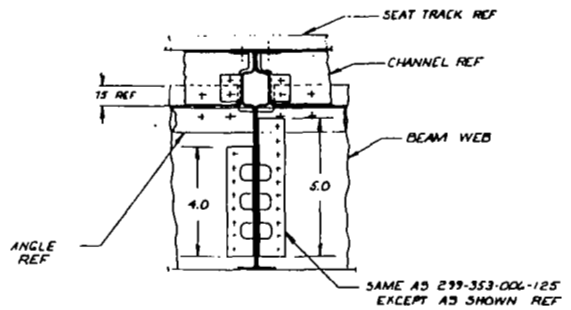

SECT D-D A/12
SCALE 1/2

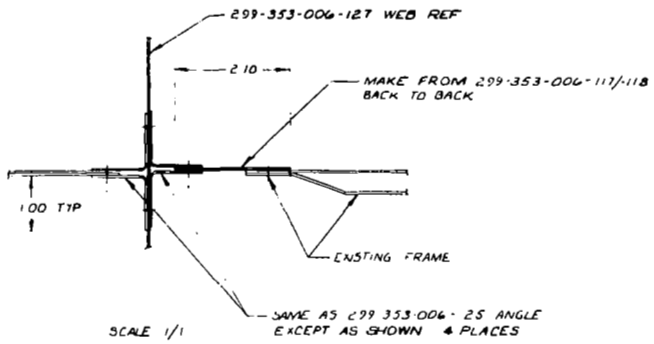

SCALE 1/1

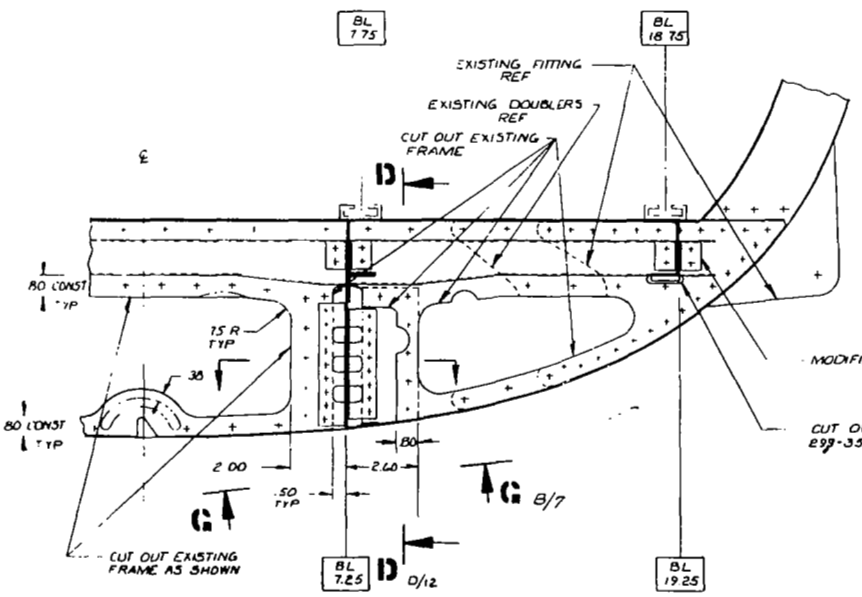

SECT C-C B/10
ROTATED 90° COUNTER CLOCKWISE
SCALE 1/2
(APPLIES TO FIRST SHIP)

11 10 9

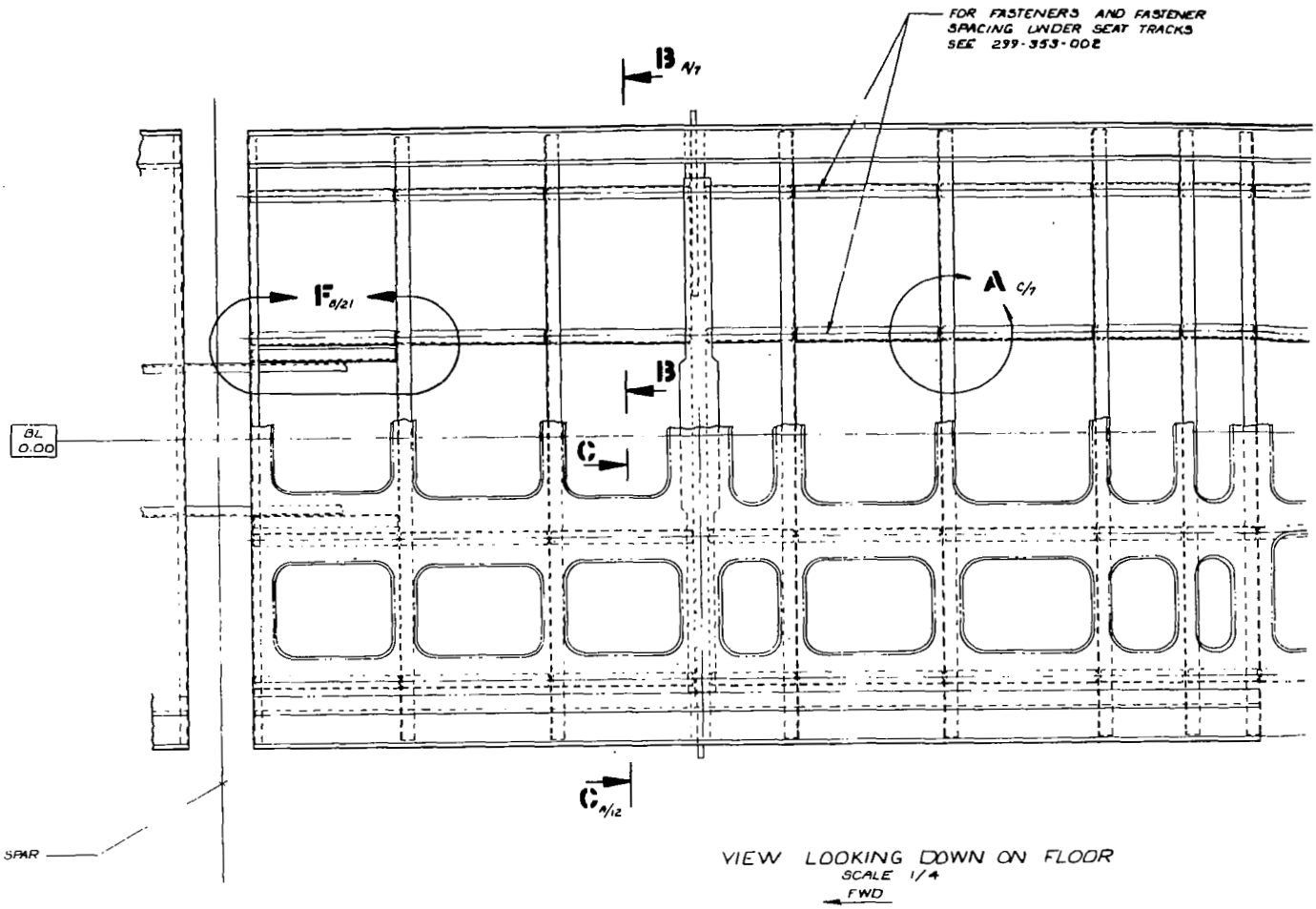

VIEW LOOKING DOWN ON FLOOR
SCALE 1/4
FWD

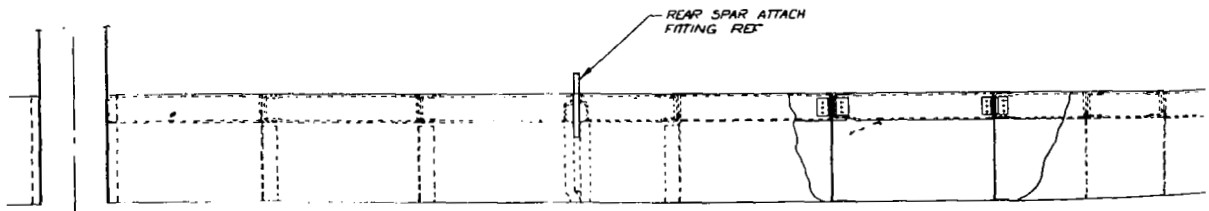

MODIFIED 299-353-002-131 CLIPS TYP

CUT OUT FOR 299-353-002-123 STRAP

DWG NO 299-353-010 REV SHEET 1

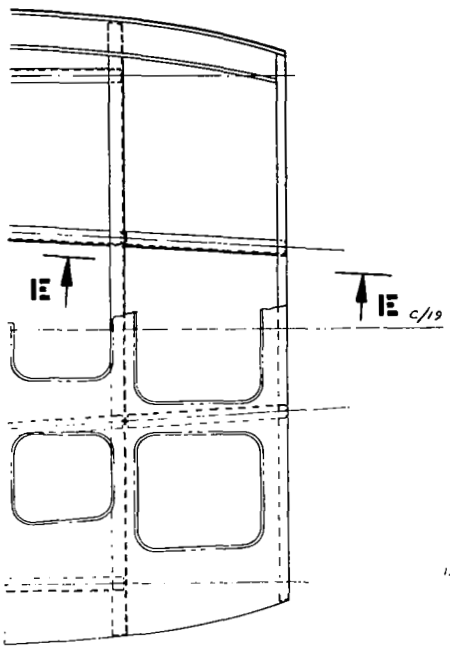

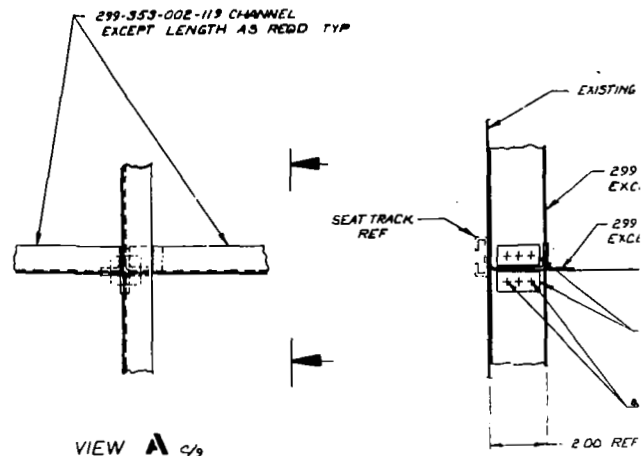

VIEW A C/9
SCALE 1/2
(TYPICAL BOTH SHIPS)

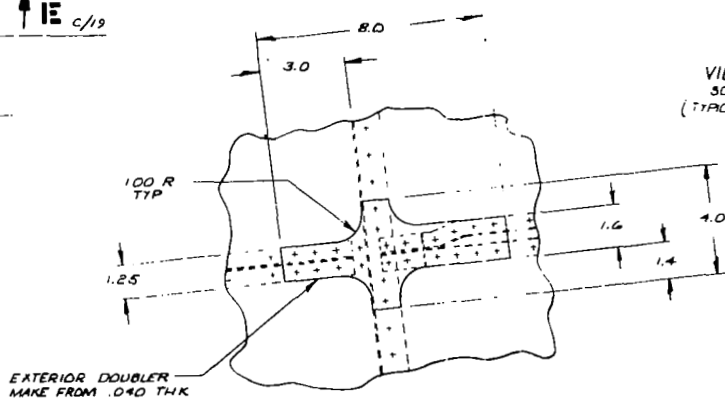

VIEW G A/2
SCALE 1/2
TYP FOR AFT SPAR FRAME ONLY

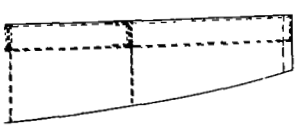

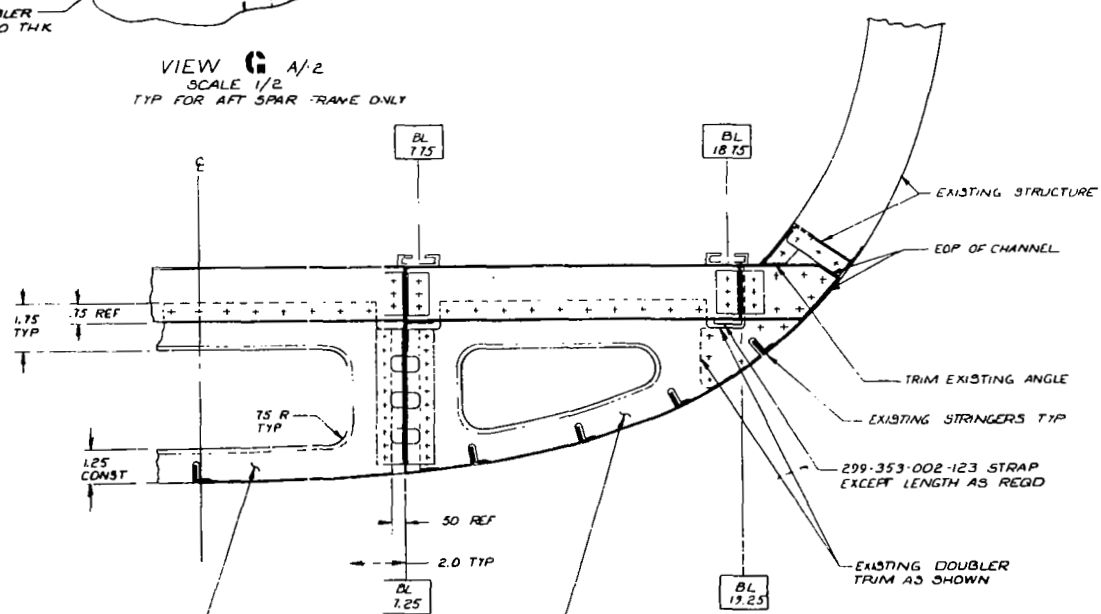

SECT B-B D/10
ROTATED 90° CLOCKWISE
SCALE 1/2
(APPLIES TO FIRST SHIP)

5 4

SKIN

)2-117 CHANNEL
'NGTH AS REQD TYP

)6-121 ANGLE
IGTH AS REQD

299-353-006-128 WEB
EXCEPT LENGTH AS REQD

153-002-131 CLIPS TYPICAL

REF

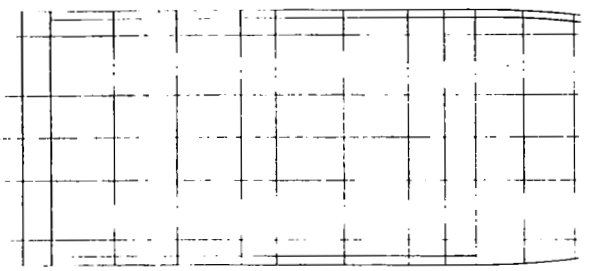

PLAN VIEW
ENERGY ABSORBING
STRUCTURE
SCALE 1/10

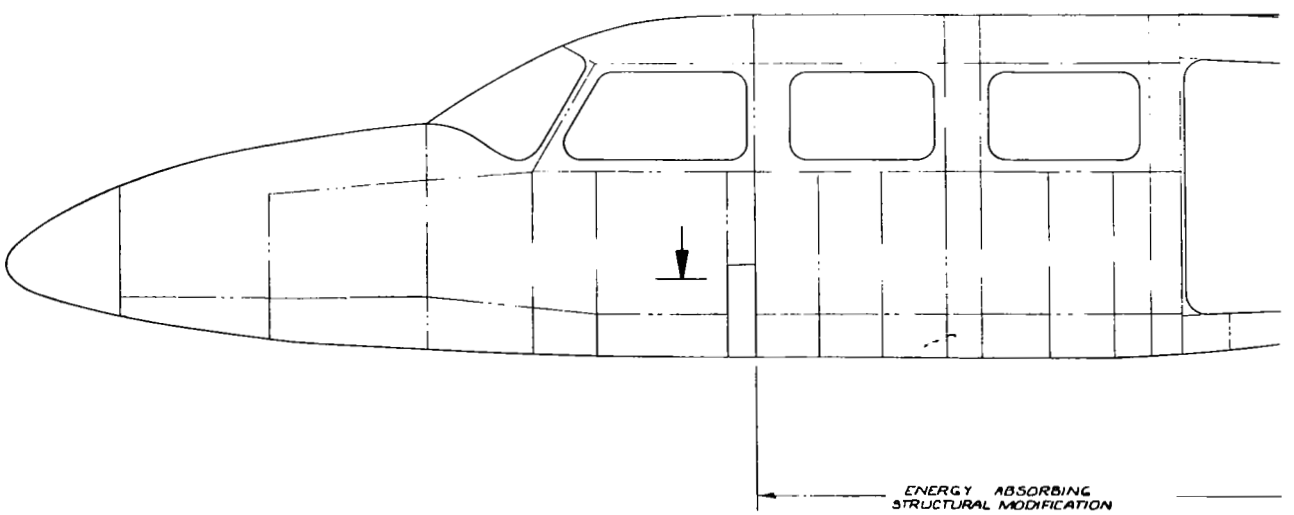

ENERGY ABSORBING
STRUCTURAL MODIFICATION

PROFILE VIEW
SCALE 1/10

DWG NO	REV	SHT
299-353-010		1

REV	DESCRIPTION	DATE	APPROVED

REVISIONS

REV	DESCRIPTION	DATE	APPROVED

REVISIONS

REV	DESCRIPTION	DATE	APPROVED

℄ SEAT TRACK

SEAT TRACK

℄ AIRCRAFT

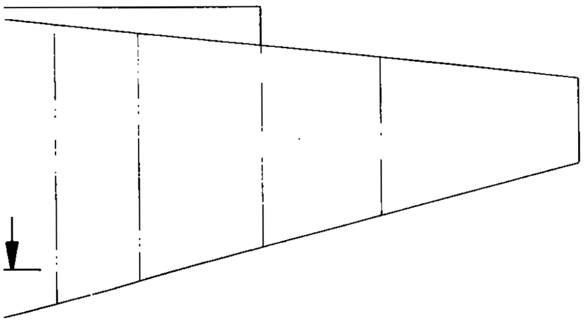

NOTES:

1. THIS DWG COVERS THE MODIFICATION OF TWO N. FUSELAGES THE FIRST IS MODIFIED TO REFLECT THE CONFIGURATION OF 299-353-002 STRUCTURAL FLOOR AND 299-353-006 NOTCHED CORNER SUB FLOOR STRUCTURE. THESE DWGS SHOULD BE REFERRED TO FOR MATERIAL AND DIMENSIONS THE SECOND IS MODIFIED TO REFLECT THE CONFIGURATION OF 299-353-002 STRUCTURAL FLOOR AND 299-353-004 CORRUGATED BEAM SUB FLOOR STRUCTURE THESE DWGS SHOULD BE REFERRED TO FOR MATERIAL AND DIMENSIONS
2. WHERE APPLICABLE TWO SECTION VIEWS ARE SHOWN TO NOTE THE DIFFERENCES IN SUB FLOOR STRUCTURE BETWEEN SHIP ONE AND SHIP TWO

DWG NO 299-353-010 REV SHEET 1

SOURCES QUALIFIED AND APPROVED BY BHT FOR STANDARDS AND MATERIALS ARE LISTED IN REPORT 299-099-900.

FOR APPROVED INTERCHANGEABLE EQUIVALENTS AND SUPERSEDED PARTS — SEE BHT STANDARD 170-001

UNLESS OTHERWISE SPECIFIED
1 MARK PER BPS 4000
2 BREAK ALL SHARP EDGES .015 X 45° OR .015 R
3 TORQUE PER BPS 4010
4 SAFETY PER BPS 4043
5 DIMENSIONAL LIMITS APPLY AFTER PLATING

APPLICABLE DOCUMENTS
ABBREVIATIONS PER MIL-STD-12
DIMENSIONING AND TOLERANCING PER ANSI Y14.5-1973
ELECTRICAL SYMBOLS PER ANSI Y32.2
ELECTRICAL REF DESIGNATIONS PER ANSI Y32.16

RIVET CODE PER NAS 523

INSTALL PER (EXCEPT AS NOTED)
1 ALL RIVETS EQUALLY SPACED BETWEEN END RIVETS UNLESS OTHERWISE SHOWN. QUANTITY AS SHOWN OR NOTED
2 EDGE DISTANCE UNIVERSAL HEAD - 2 TIMES SHANK DIA; COUNTERSUNK HEAD - 2 1/2 TIMES SHANK DIA UNLESS OTHERWISE SHOWN

LAST DATUM LTR USED
LAST SECTION LETTER USED

UNLESS OTHERWISE SPECIFIED DIMENSIONS ARE IN INCHES
TOLERANCES ON DECIMALS / ANGLES

SURFACE ROUGHNESS PER ANSI B46.1
✓ MACHINED SURFACES EXCEPT AS NOTED

CONTRACT NUMBER DAAK51-C-0037
DRAWN Mark Abrace 9/25/81
CHECKED
STRESS
WEIGHTS
GROUP ENGR
DES
MFG DESIGN
PROJECT
CUSTOMER

Bell Helicopter TEXTRON
Division of Textron Inc.

TITLE FUSELAGE STRUCTURAL MODIFICATION ENERGY ABSORBING

DWG SIZE J12 | CODE IDENT NO 97499 | DWG NO 299-353-010

SCALE NOTED | ISSUED | SHEET 1 OF 2

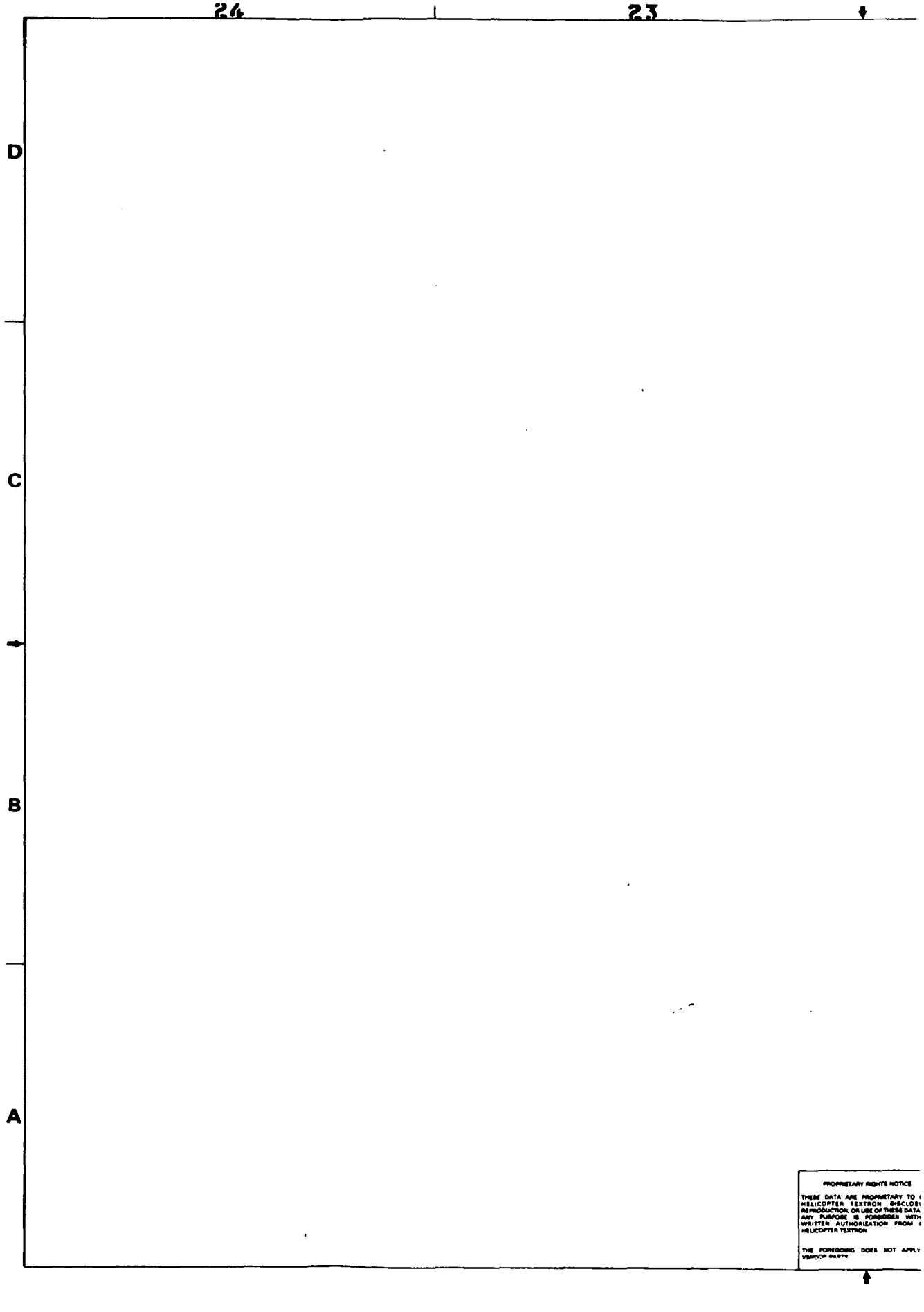

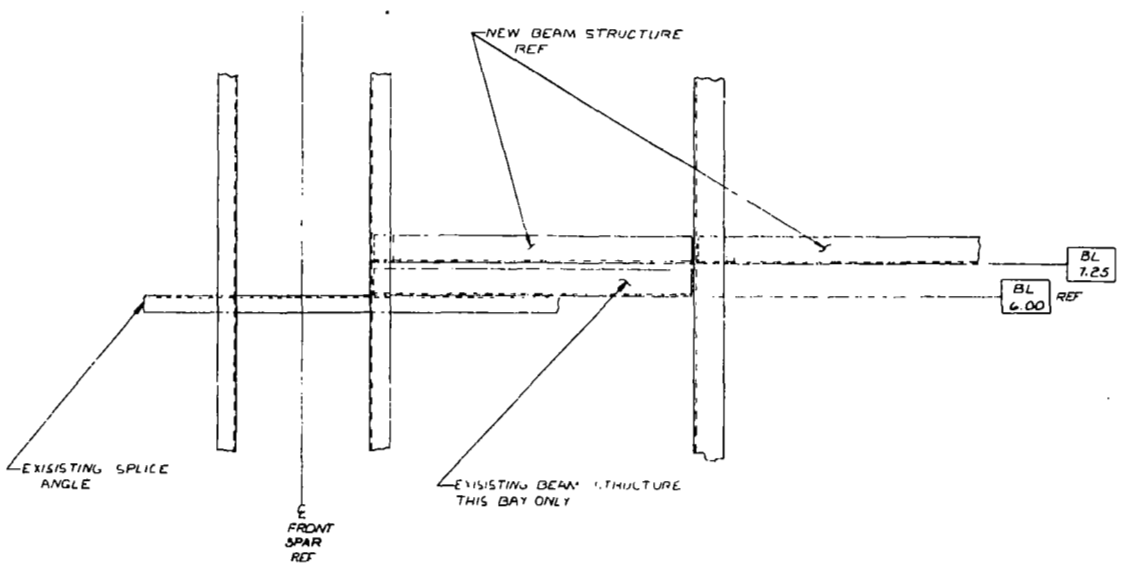

VIEW F 0/10
SCALE 1/2

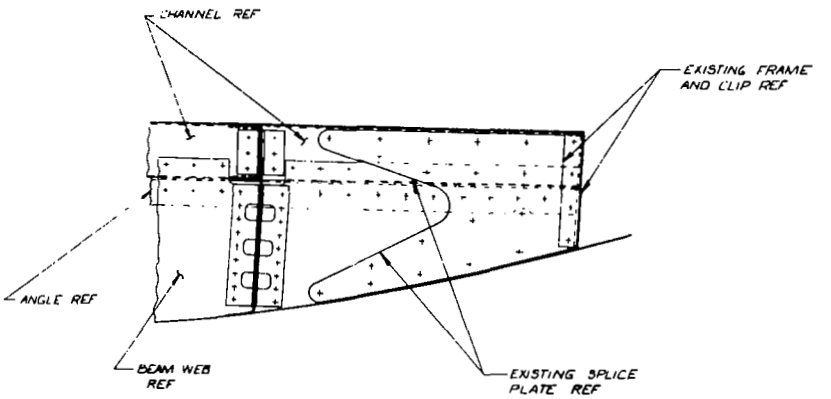

SECT E - E c/s
SCALE 1/2

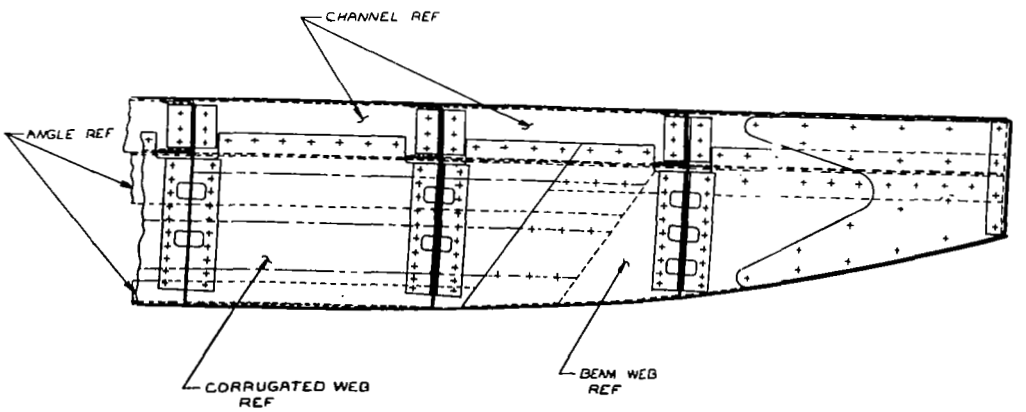

SECT E - E c/s
SCALE 1/2
SHIP TWO ONLY

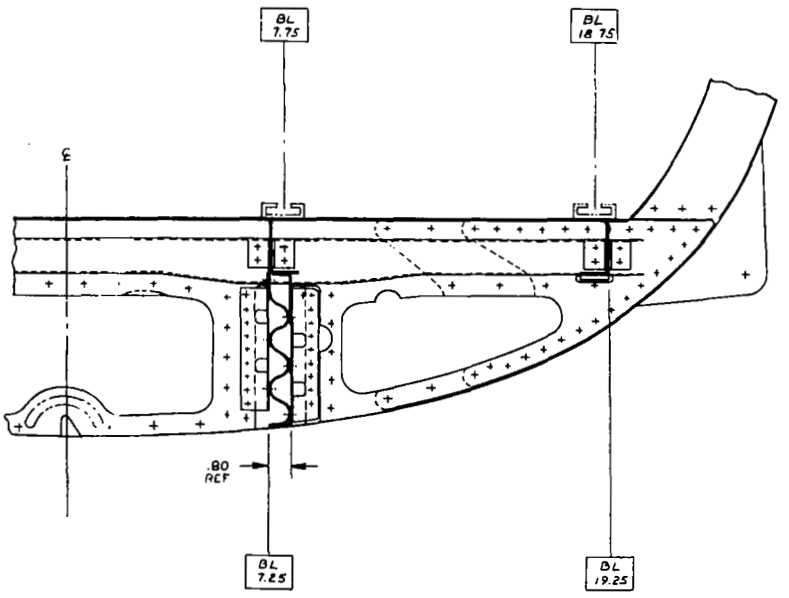

SECT C - C
ROTATED -90° COUNTER CLOCKWISE
SCALE 1/2
SHIP TWO ONLY

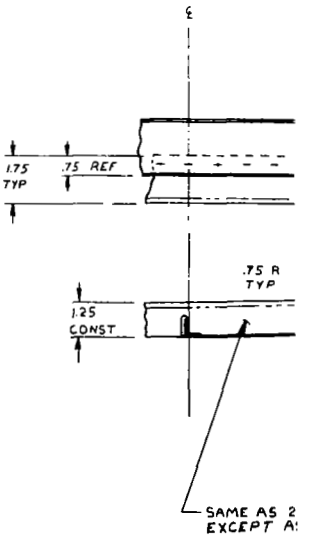

S
ROTATED
SH

REVISIONS				REVISIONS				REVISIONS			
REV	DESCRIPTION	DATE	APPROVED	REV	DESCRIPTION	DATE	APPROVED	REV	DESCRIPTION	DATE	APPROVED

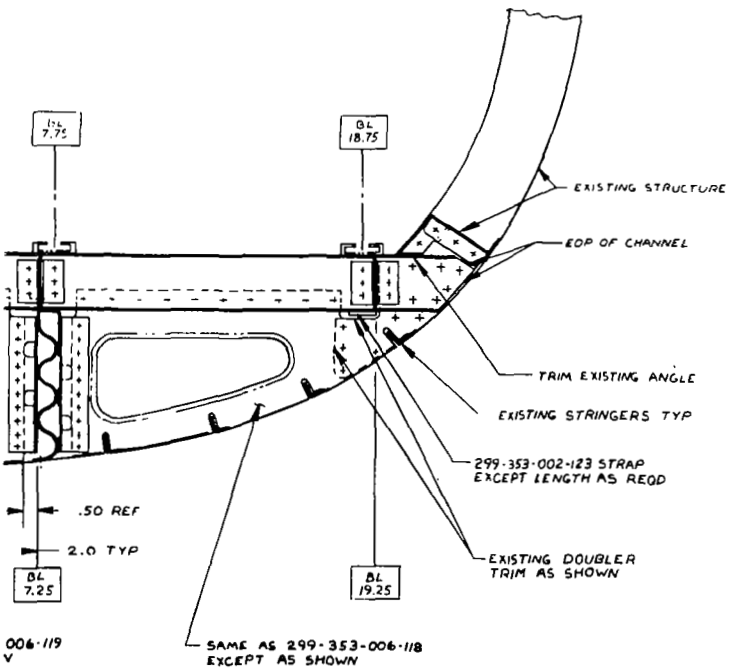

13-13
VTER CLOCKWISE
1/2
ONLY

DASH NO	NEXT ASSY APPLICATION	USED ON	DASH NO.	NEXT ASSY APPLICATION	USED ON

RIVET CODE PER MAS 823

BASIC CODE	INSTALL PER (EXCEPT AS NOTED)
1	
2	
3	
4	
5	
6	
7	
8	

LAST DATUM LTR USED

LAST SECTION
LETTER USED

TOLERANCES ON
DECIMALS ANGLES
XXX ± .010
XX ± .03 ± 1/2°
X ± 1

SURFACE ROUGHNESS PER ANSI B46.1
✓ MACHINED SURFACES
EXCEPT AS NOTED

DRAWN	Hoel
CHECKED	
STRESS	
WEIGHTS	
GROUP ENGR	
DER	
MET ENGR	
PROJECT	
CUSTOMER	

Bell Helicopter TEXTRON
Division of Textron Inc.

TITLE
FUSELAGE STRUCTURAL MODIFICATION ENERGY ABSORBING

DWG SIZE	CODE IDENT NO	DWG NO
J12	97499	299-353-010

SCALE NOTED | ISSUED | SHEET 2 OF 2

299-353-010 REV 2

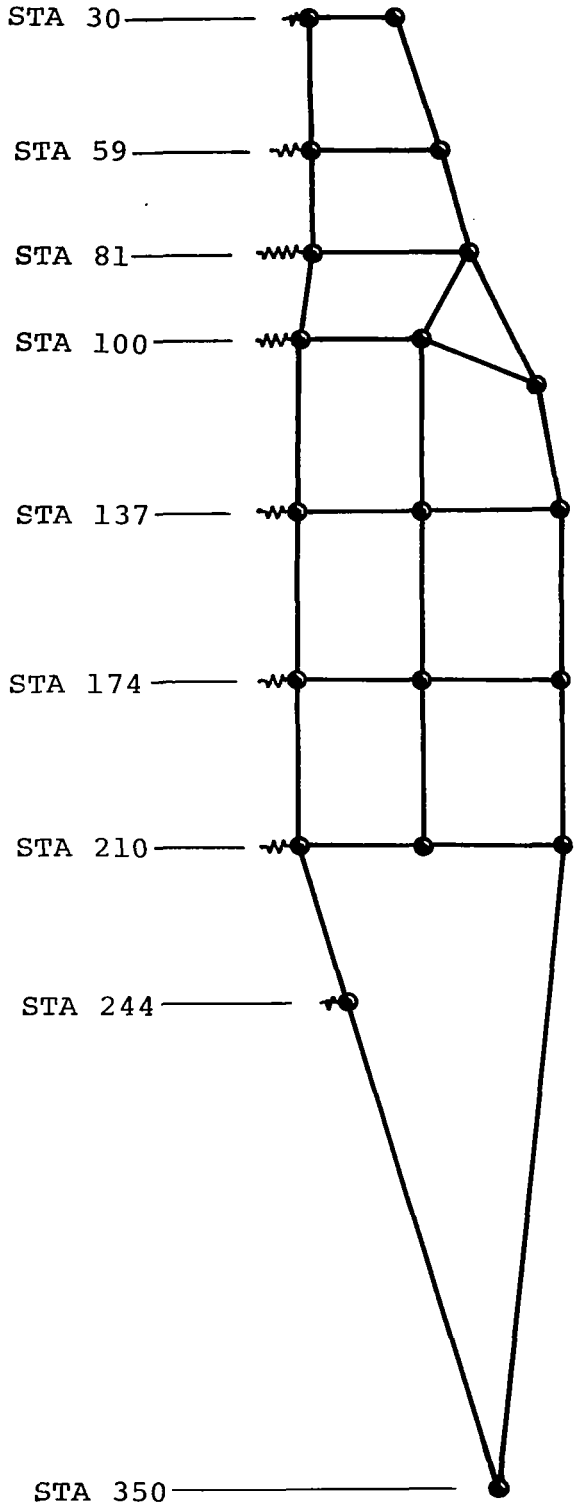

Figure F-1. Left side view of KRACH model.

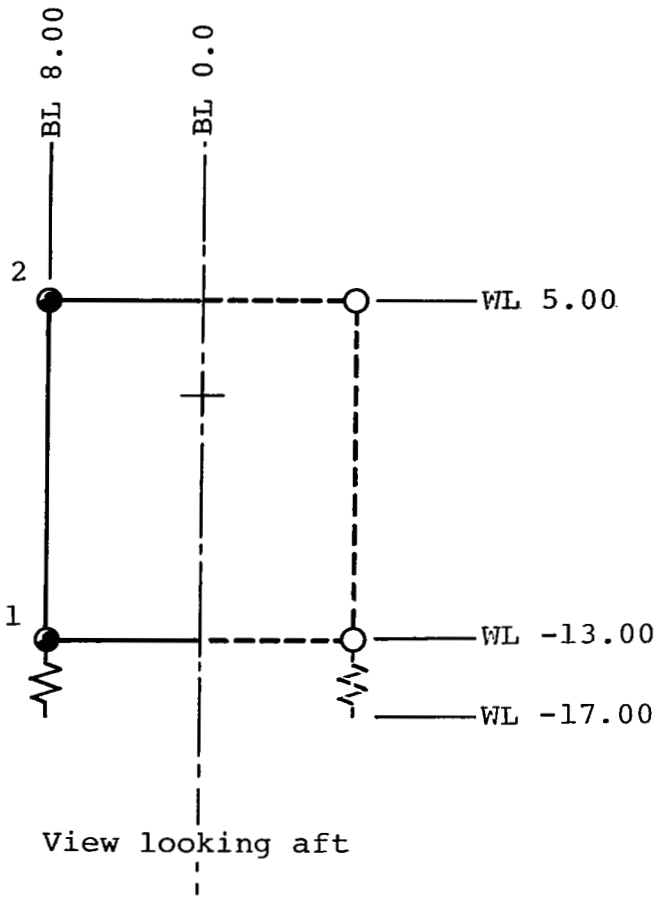

Figure F-2. Fuselage bulkhead model at STA 30.

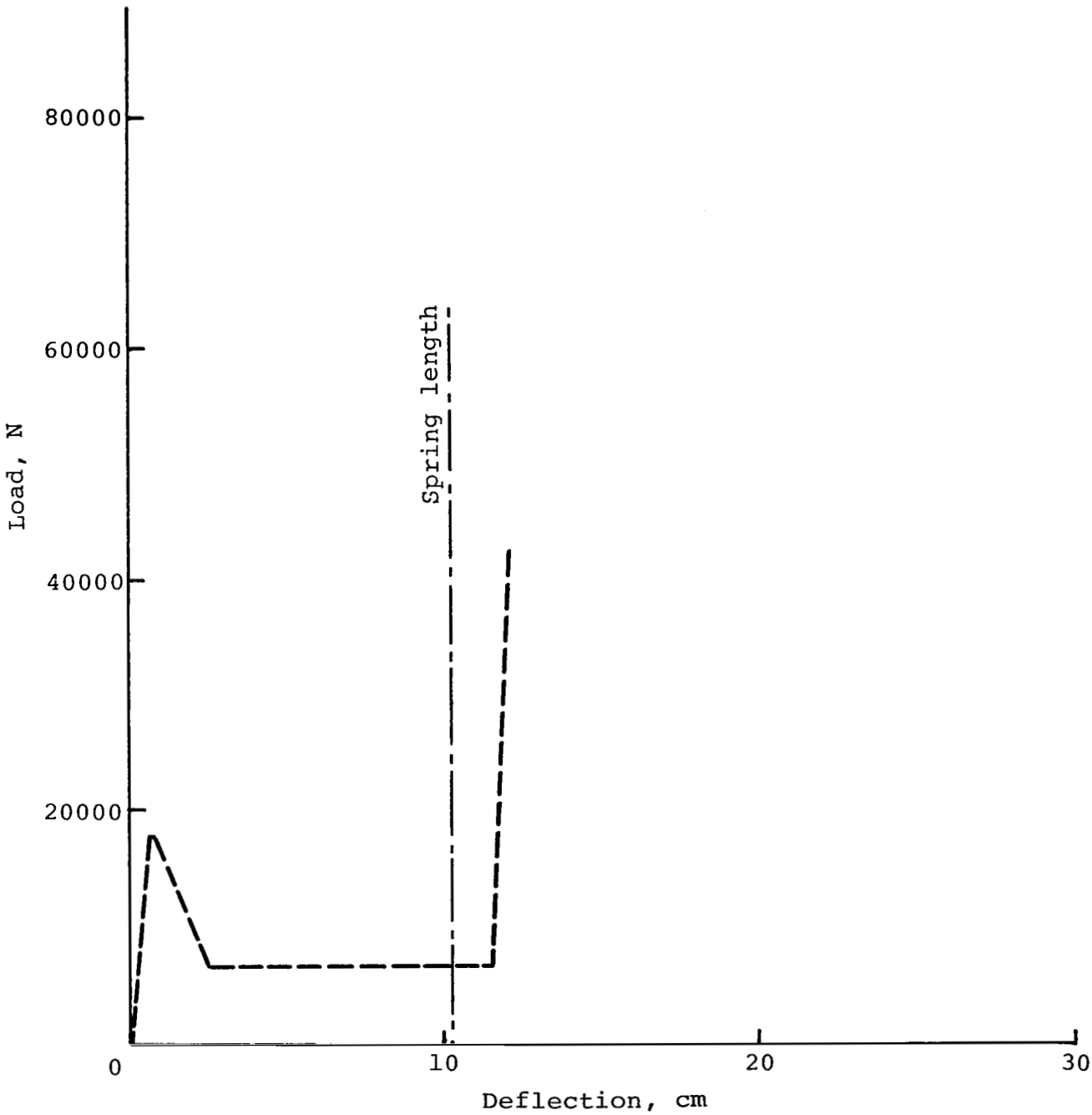

Figure F-3. Load-deflection parameters for crushing spring at STA 30, mass point 1.

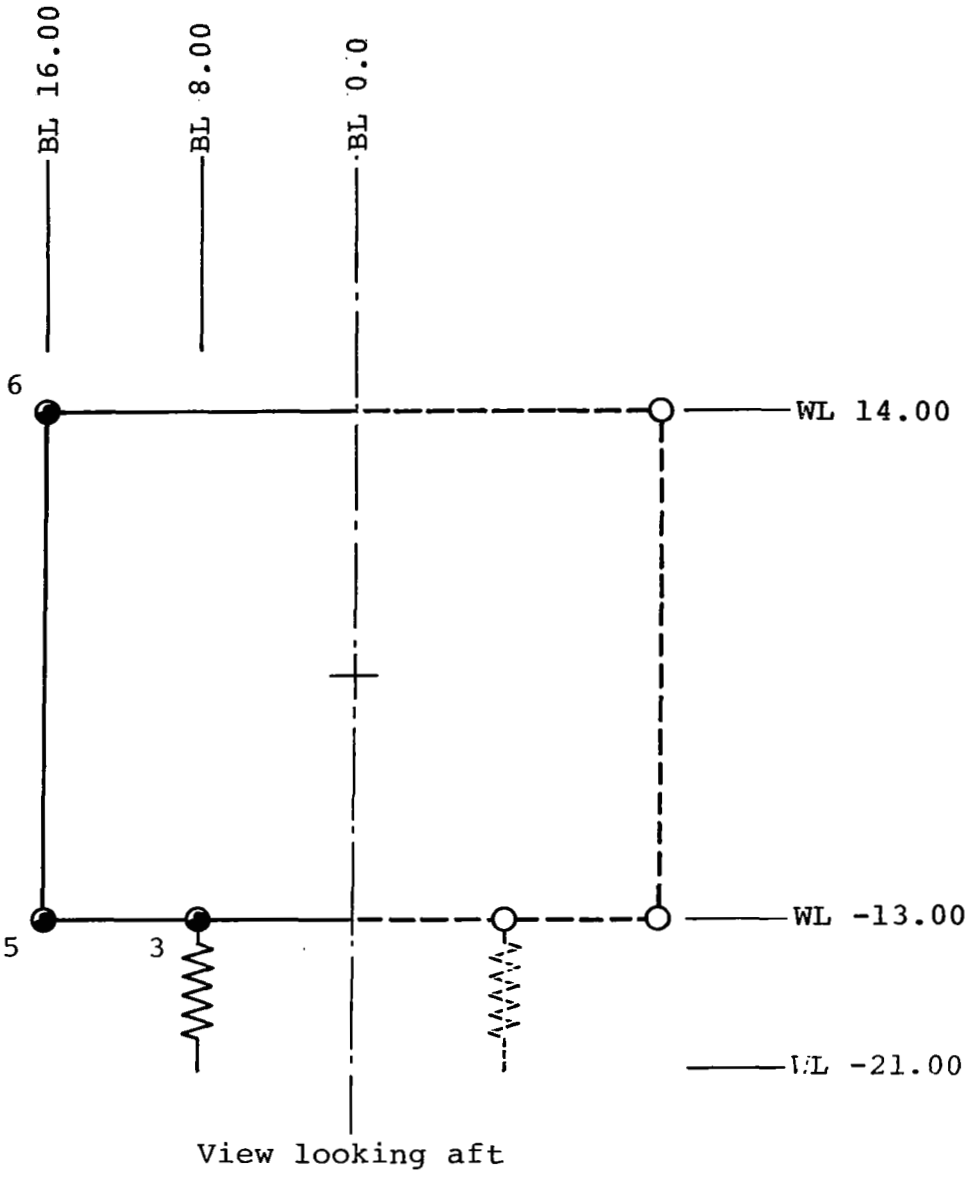

Figure F-4. Fuselage bulkhead model at STA 59.

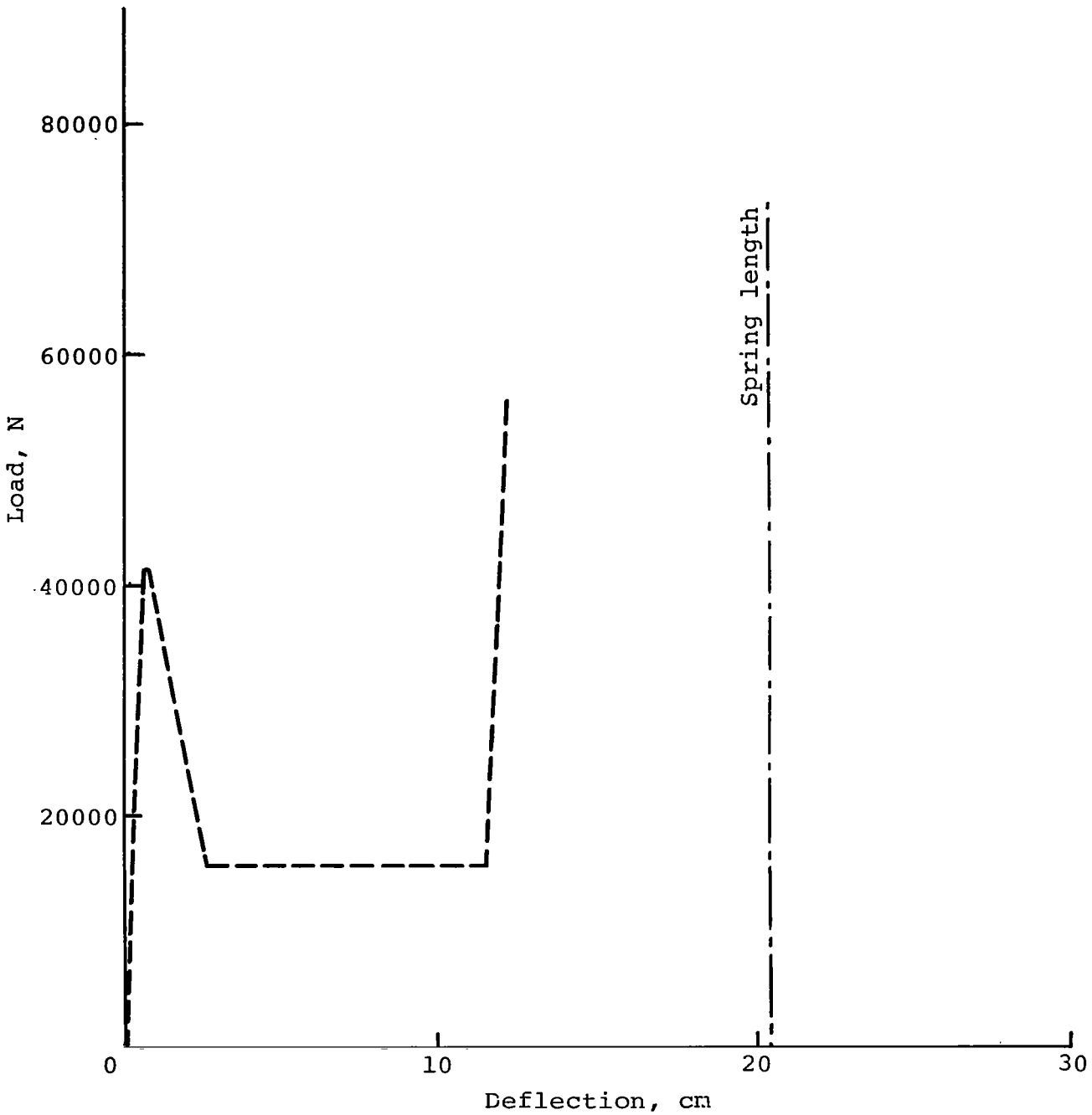

Figure F-5. Load-deflection parameters for crushing spring at STA 59, mass point 3.

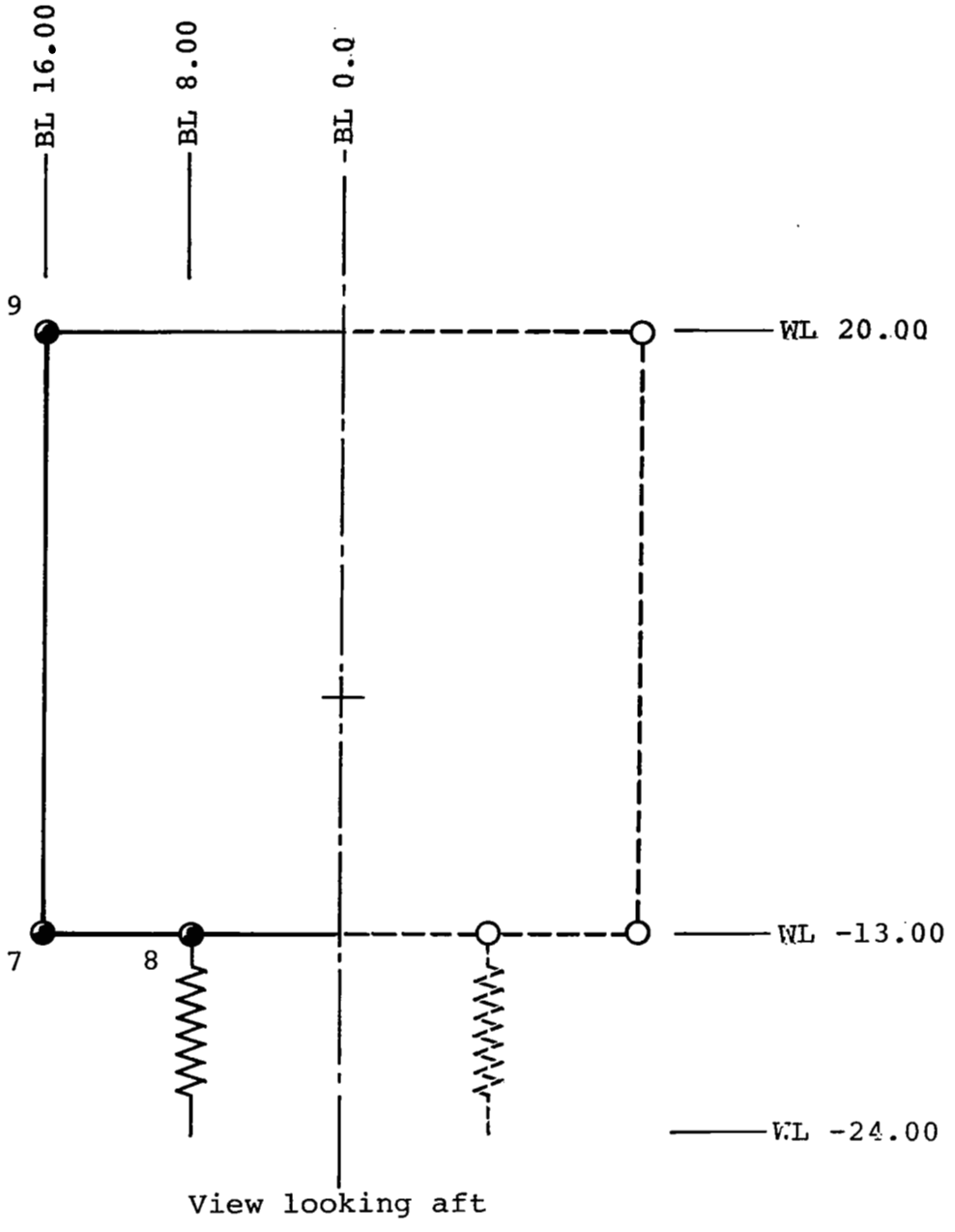

Figure F-6. Fuselage bulkhead model at STA 81.

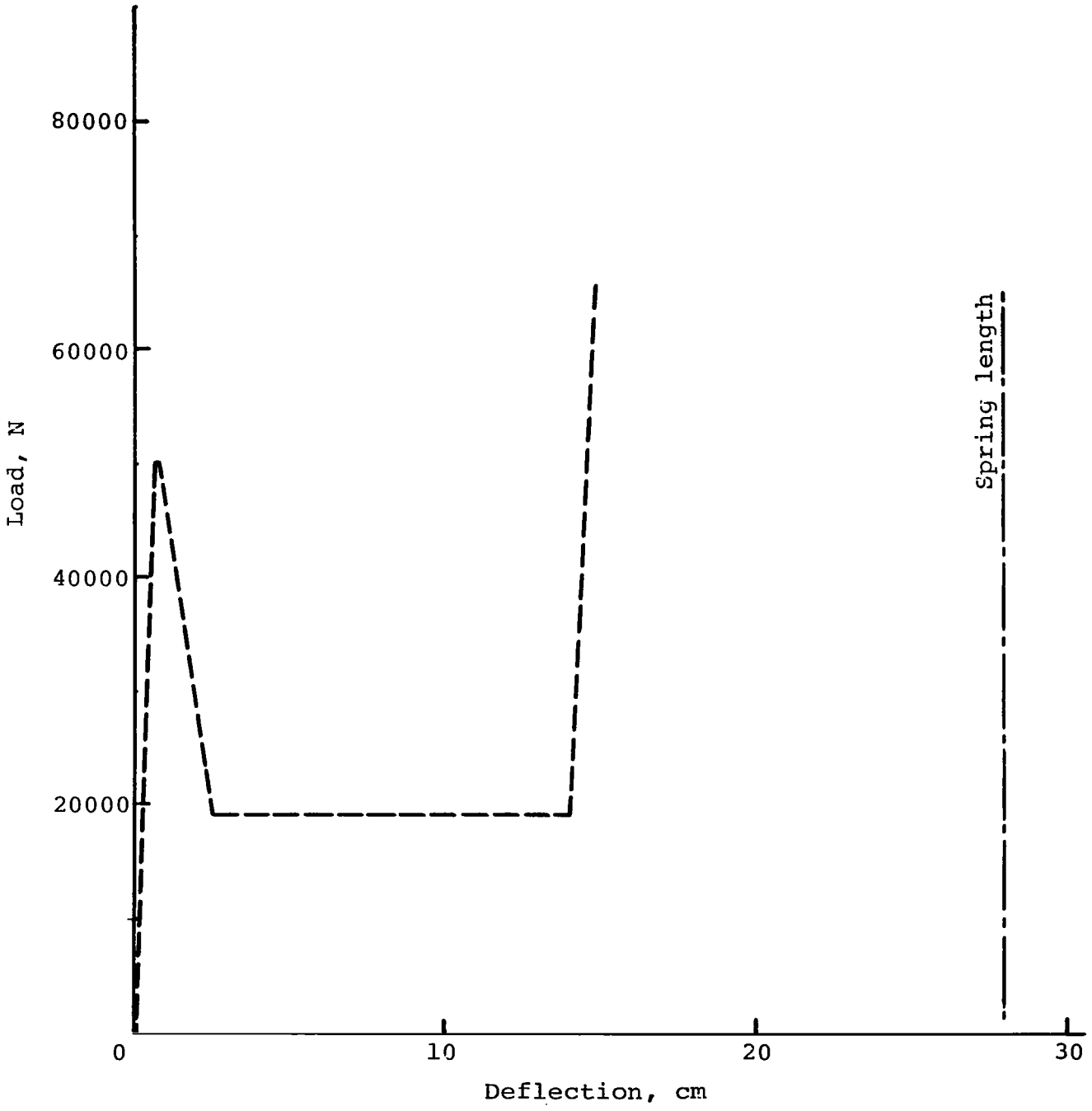

Figure F-7. Load-deflection parameters for crushing spring at STA 81, mass point 8.

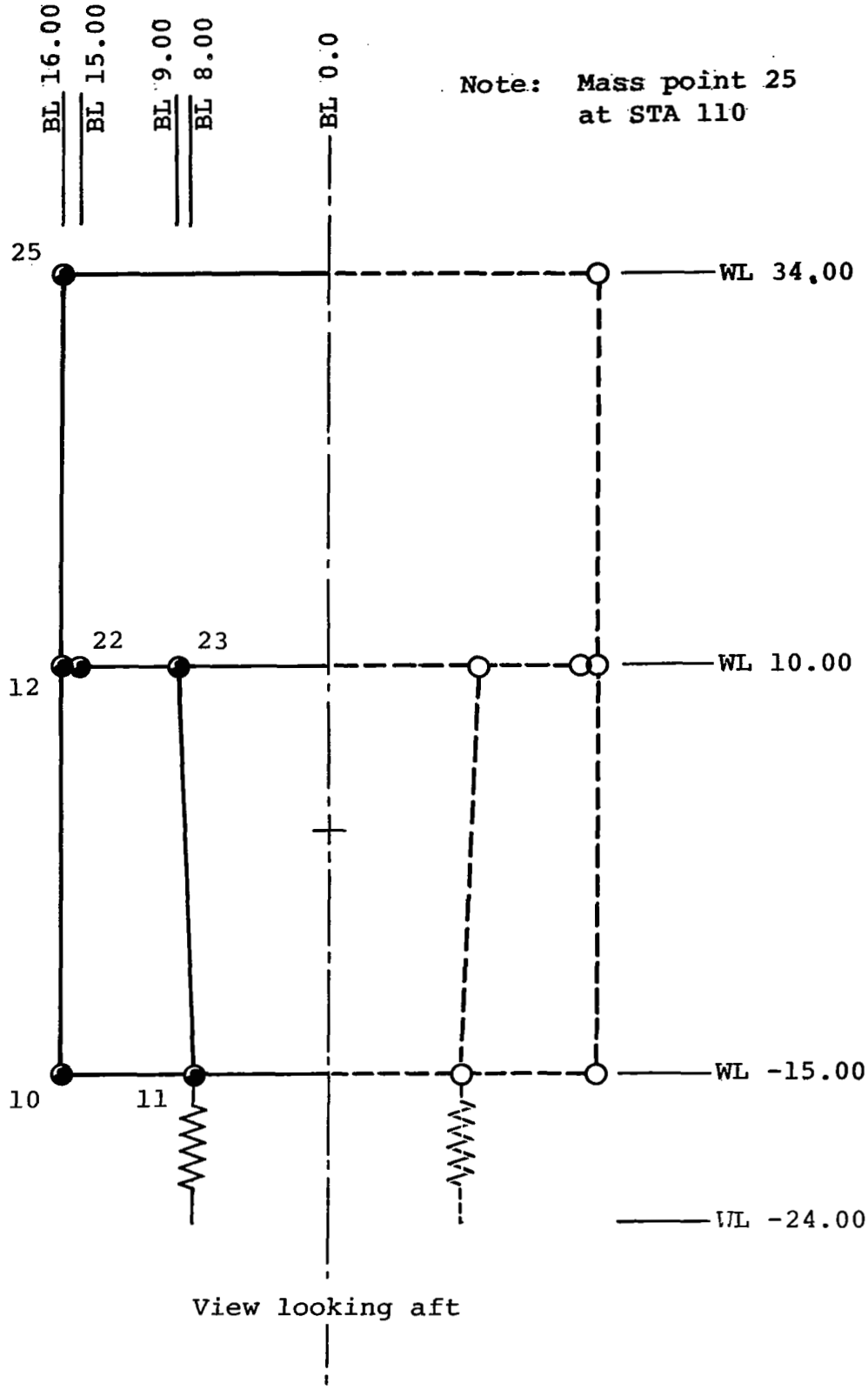

Figure F-8. Fuselage bulkhead model at STA 100.

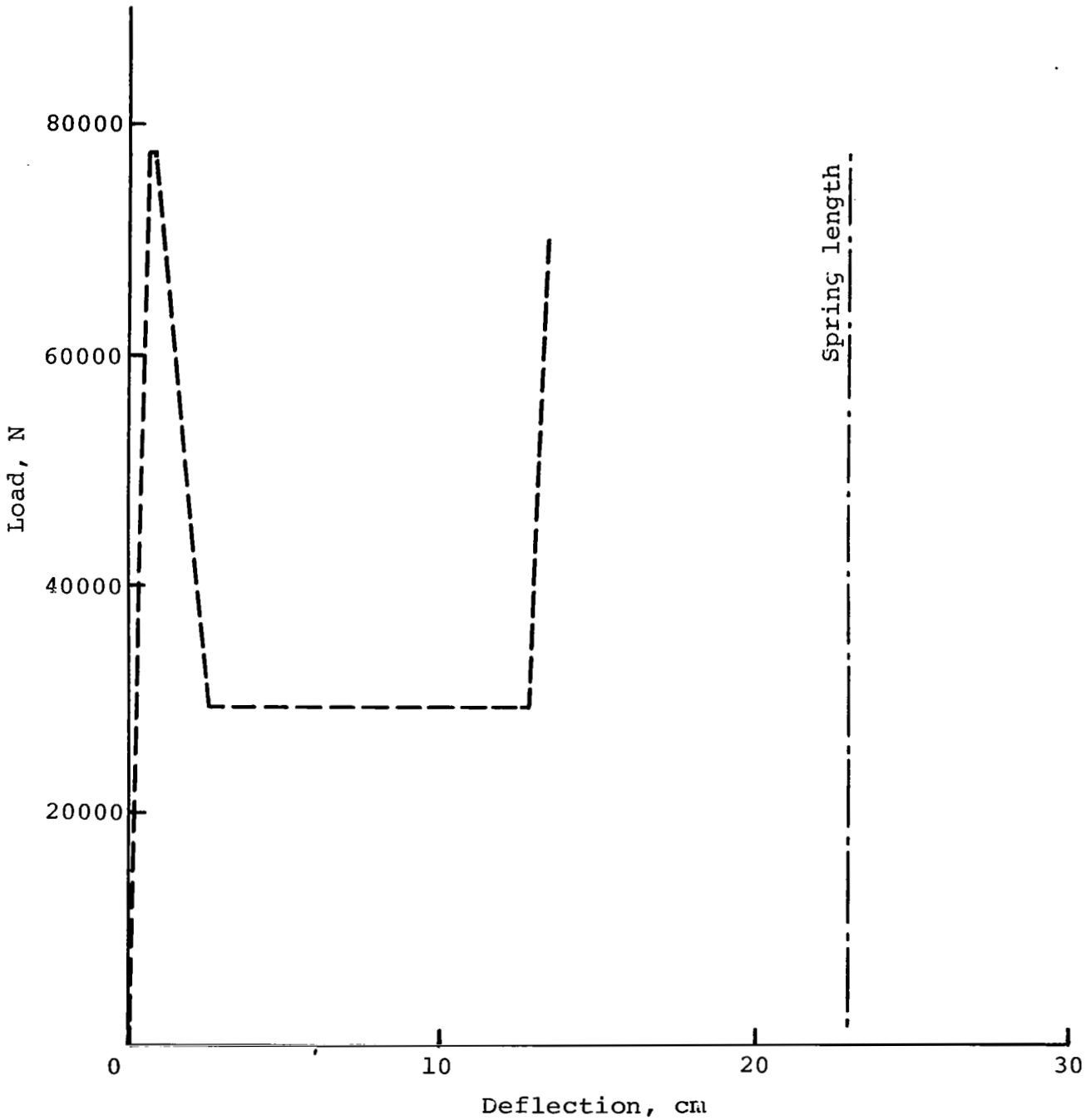

Figure F-9. Load-deflection parameters for crushing spring at STA 100, mass point 11.

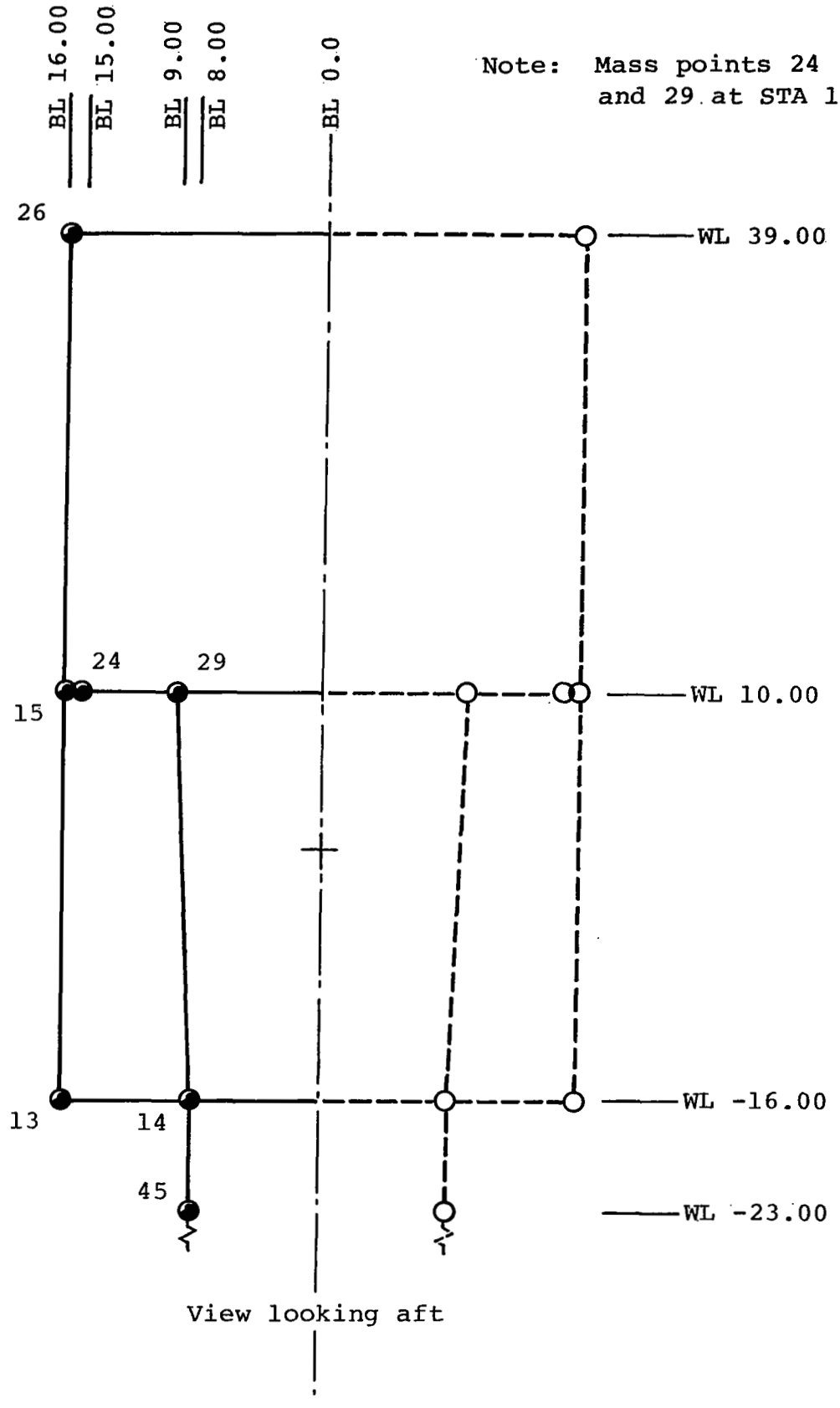

Figure F-10. Fuselage bulkhead model at STA 137.

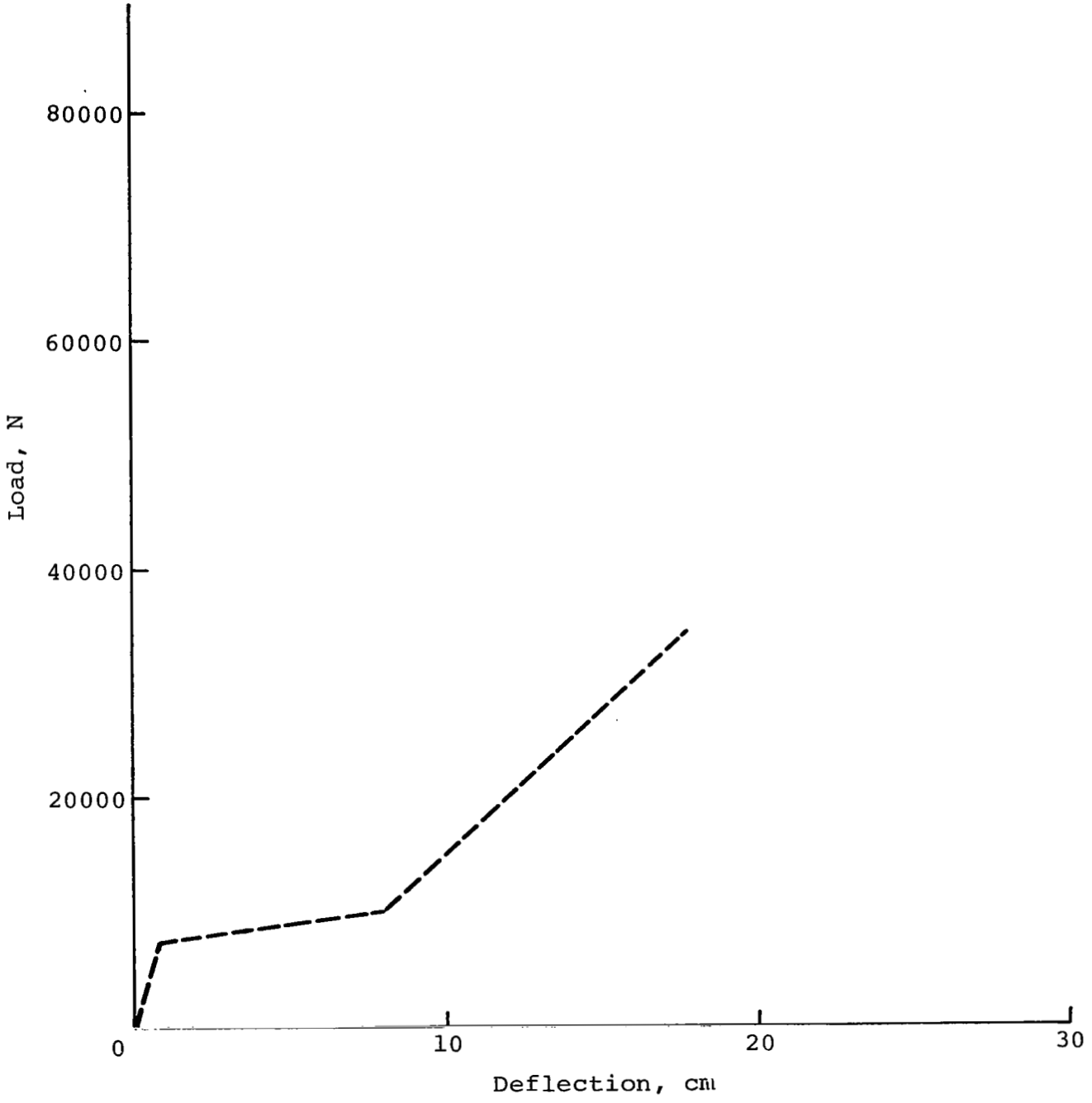

Figure F-11. Load-deflection parameters for nonlinear beam 14-45 at STA 137.

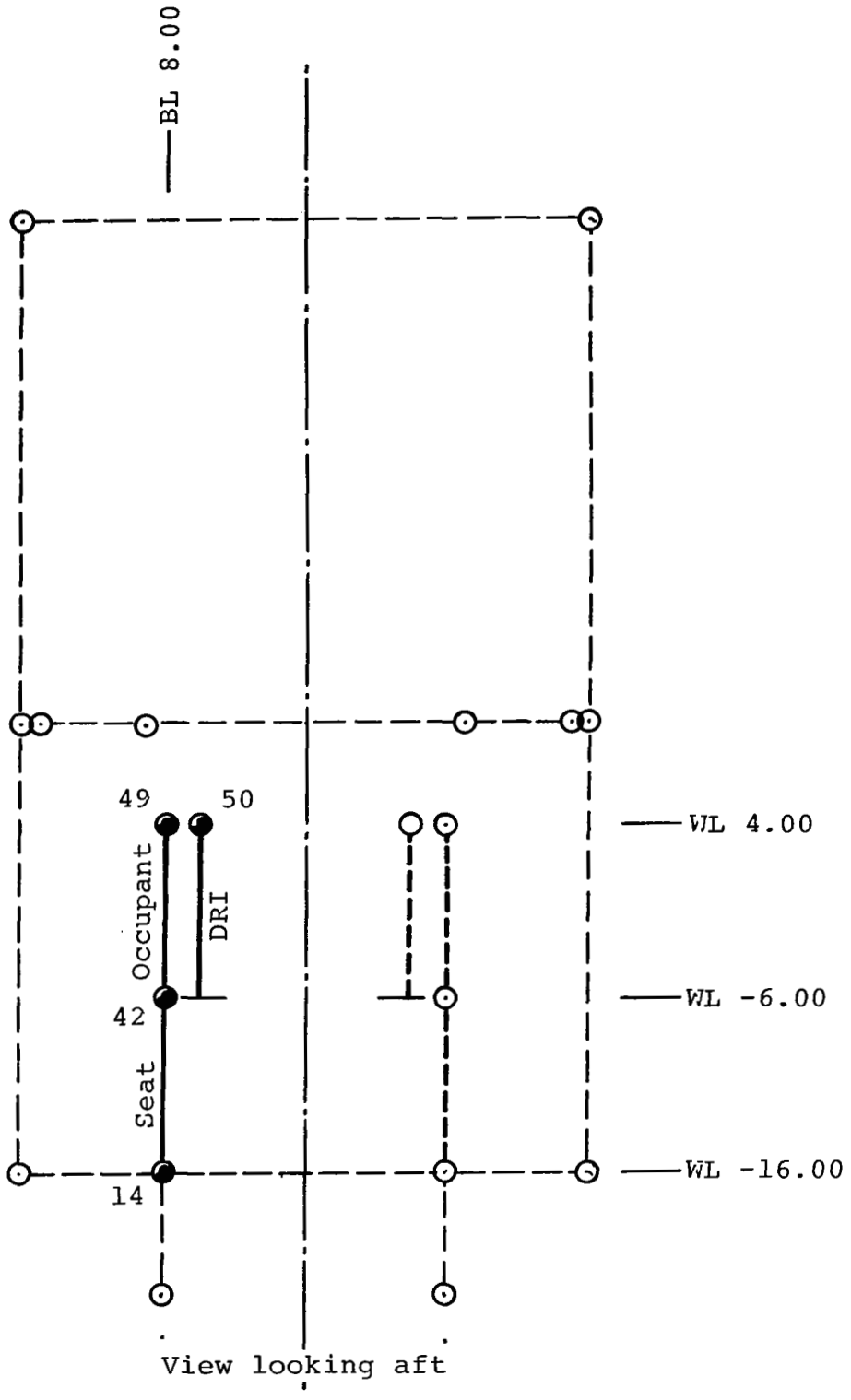

Figure F-12. Occupant-seat modeling at STA 137.

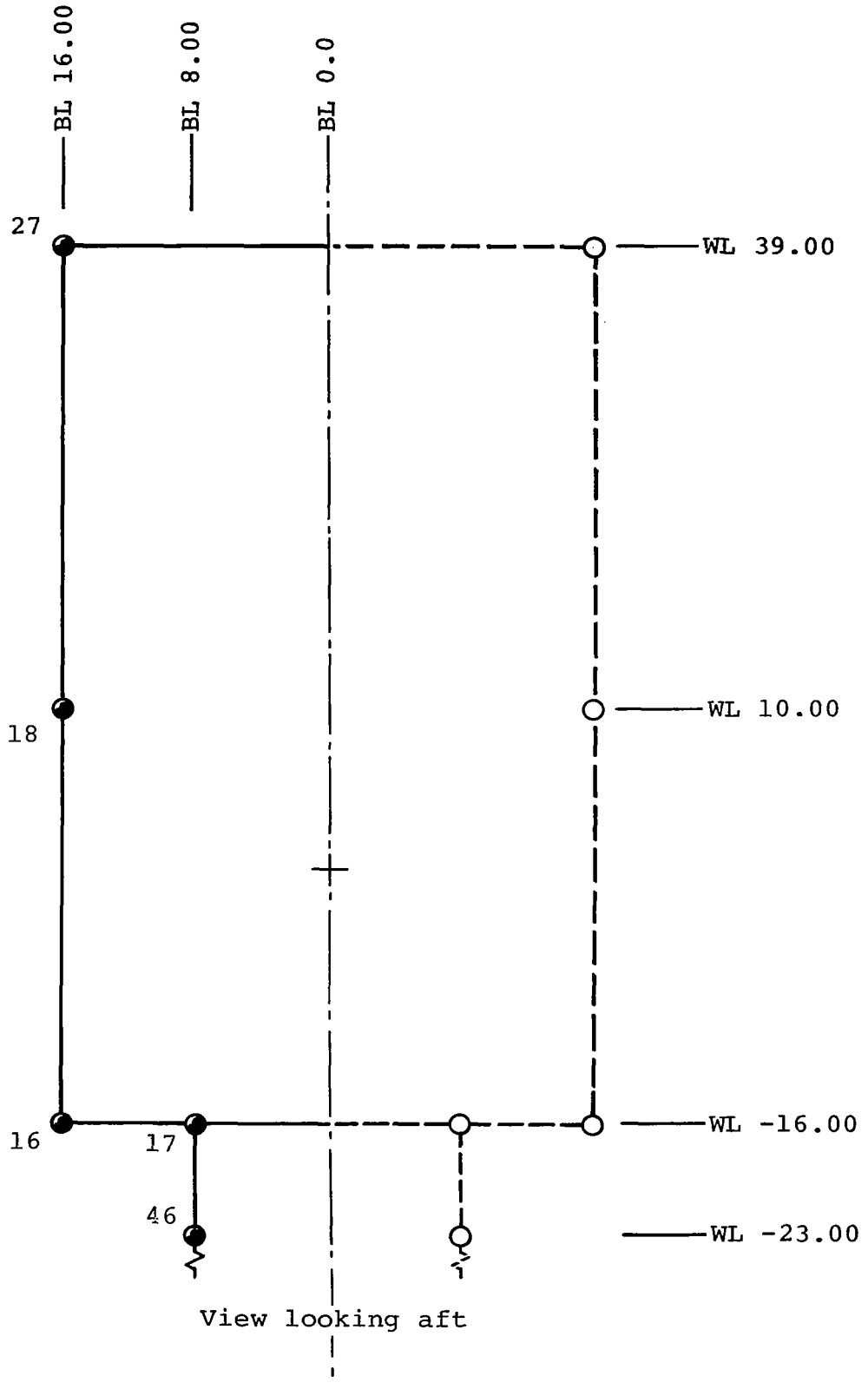

Figure F-13. Fuselage bulkhead model at STA 174.

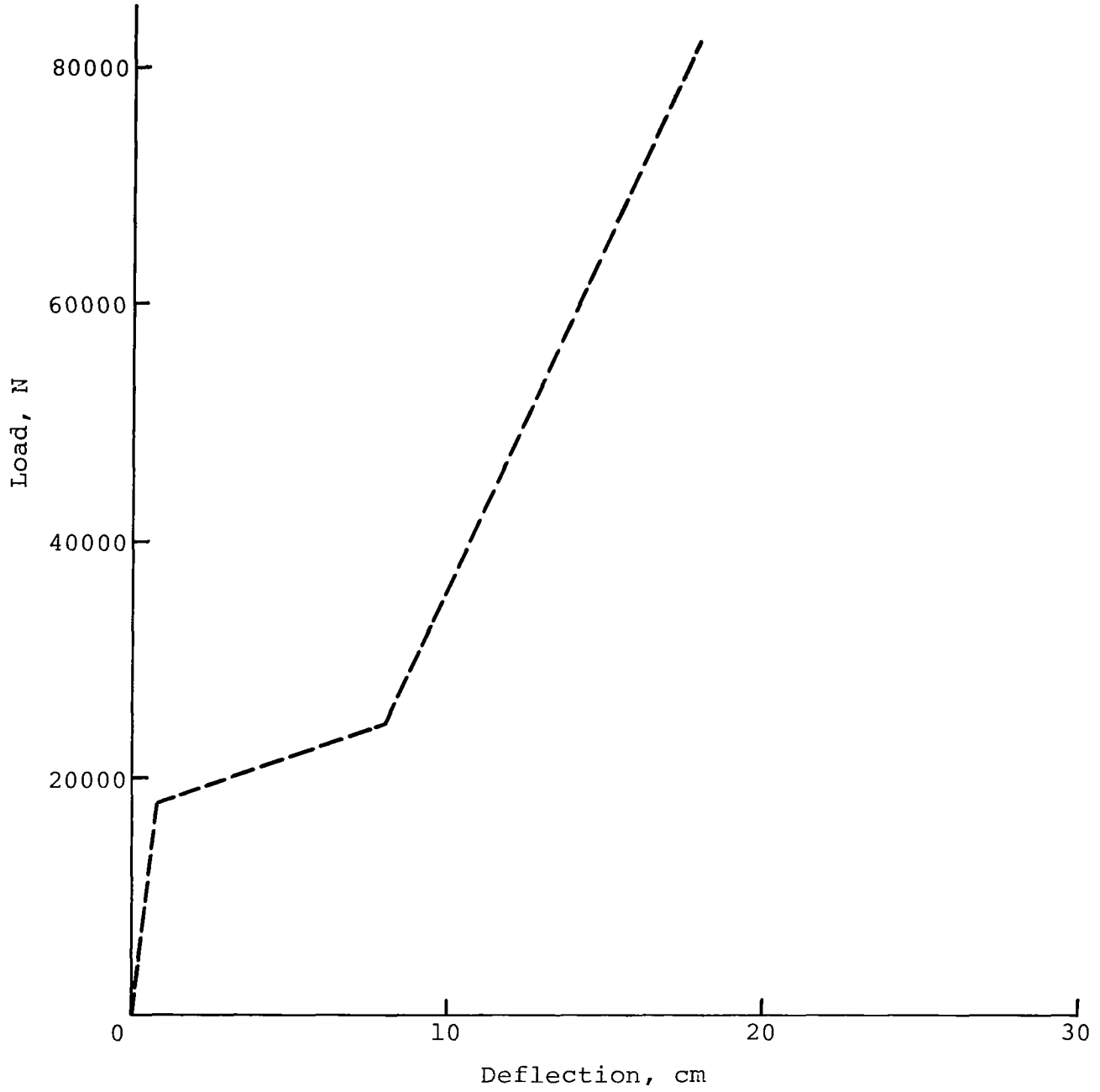

Figure F-14. Load-deflection parameters for nonlinear beam 17-46 at STA 174.

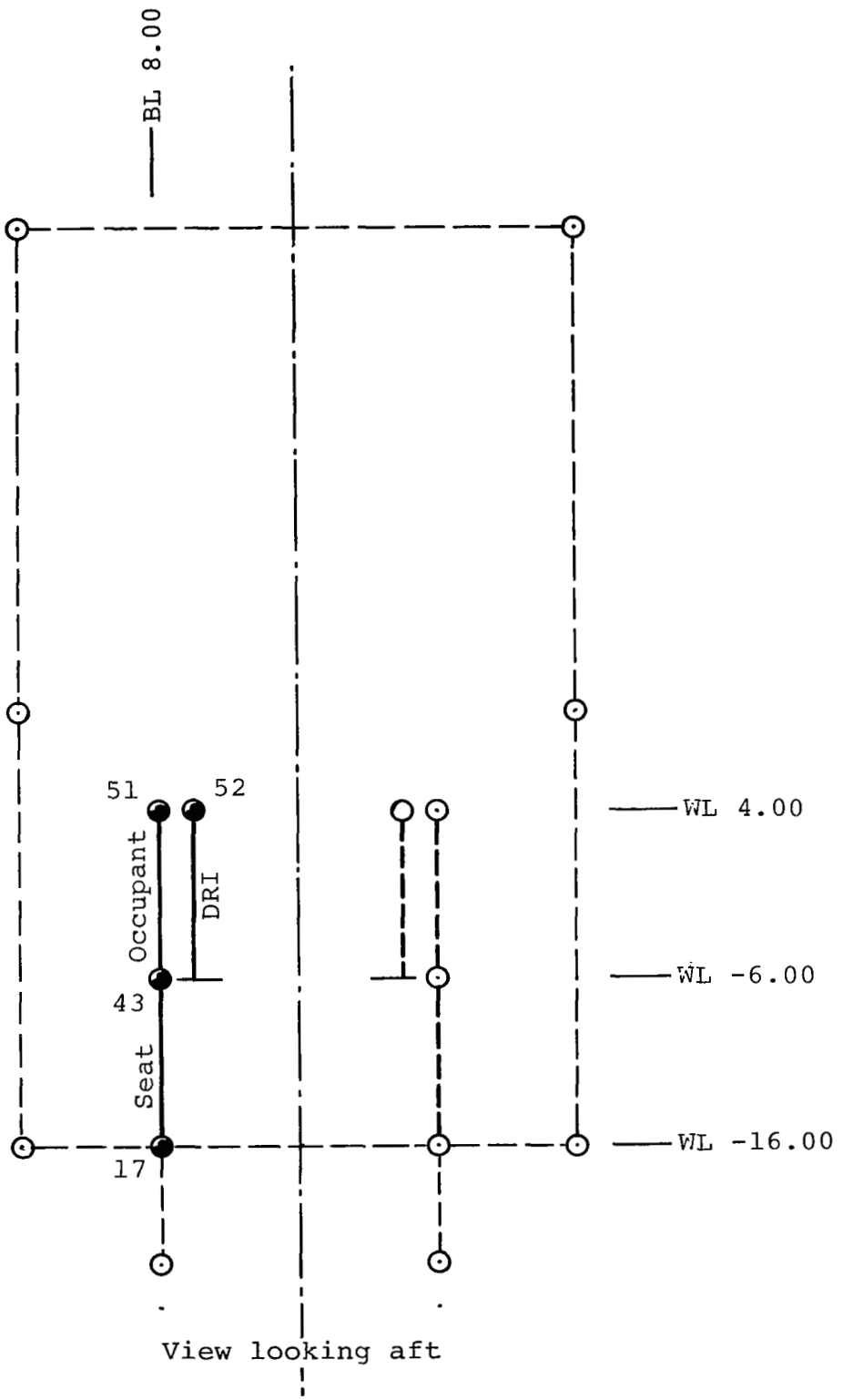

Figure F-15. Occupant seat modeling at STA 174.

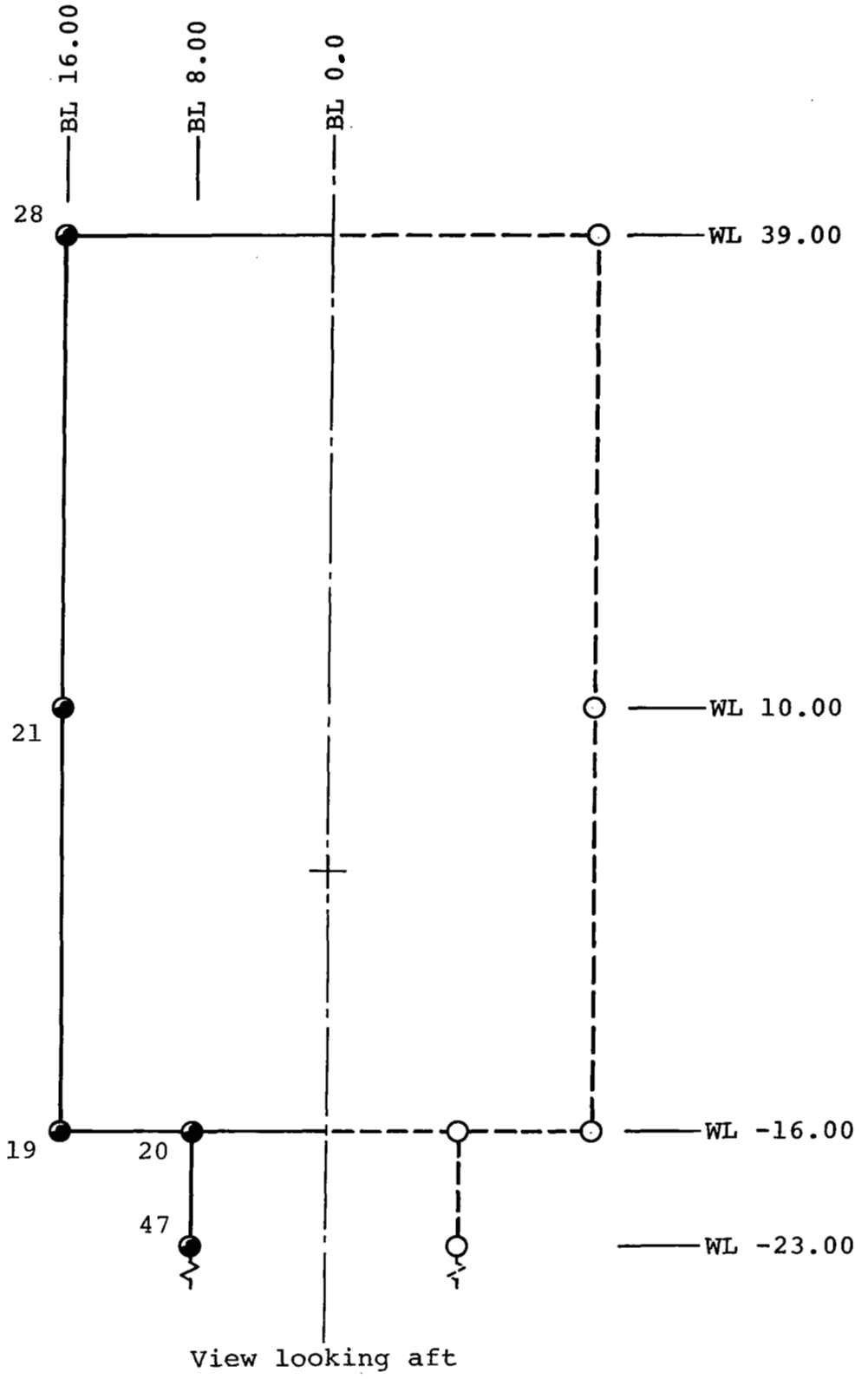

Figure F-16. Fuselage bulkhead model at STA 210.

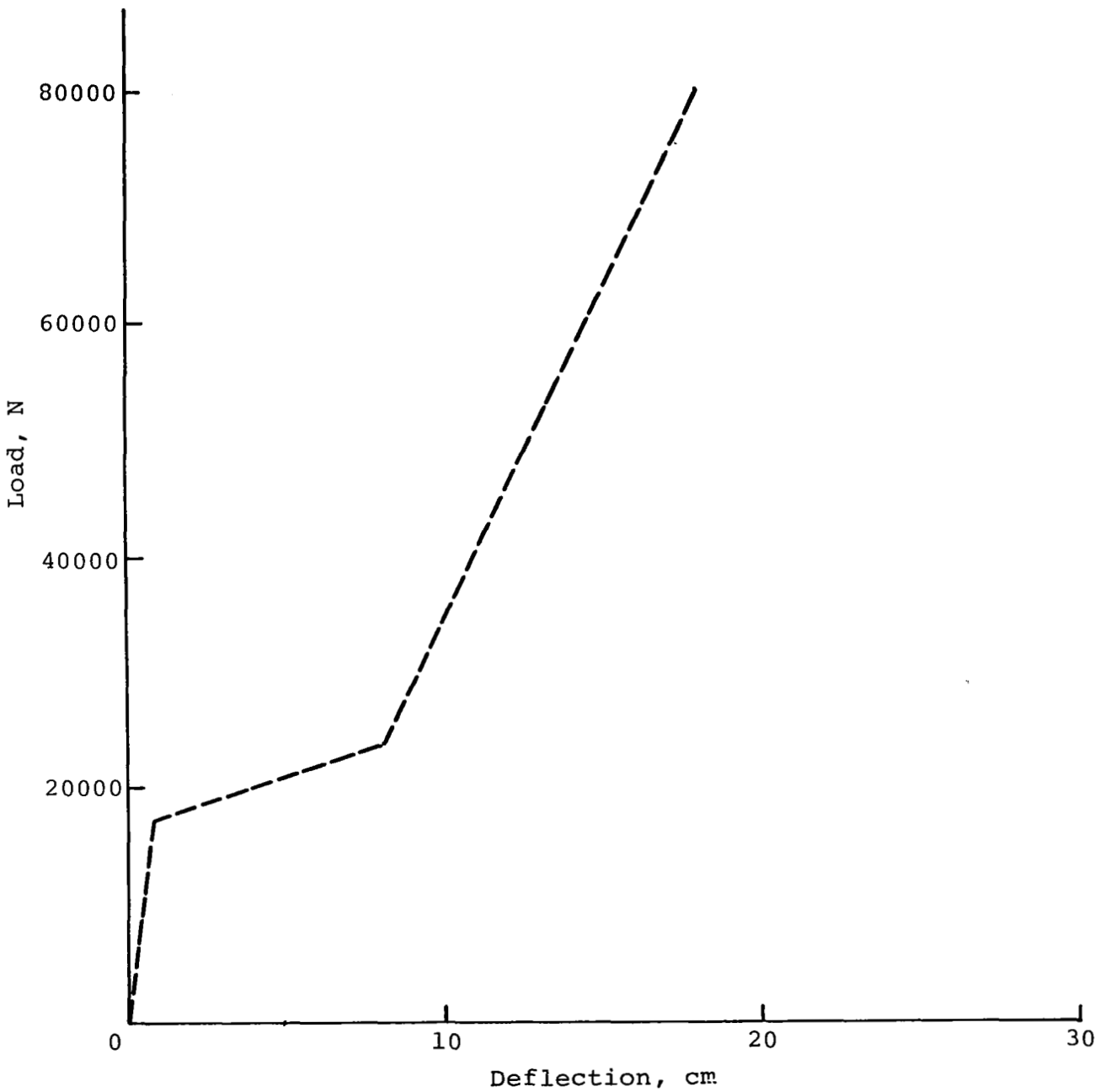

Figure F-17. Load-deflection parameters for nonlinear beam 20-47 at STA 210.

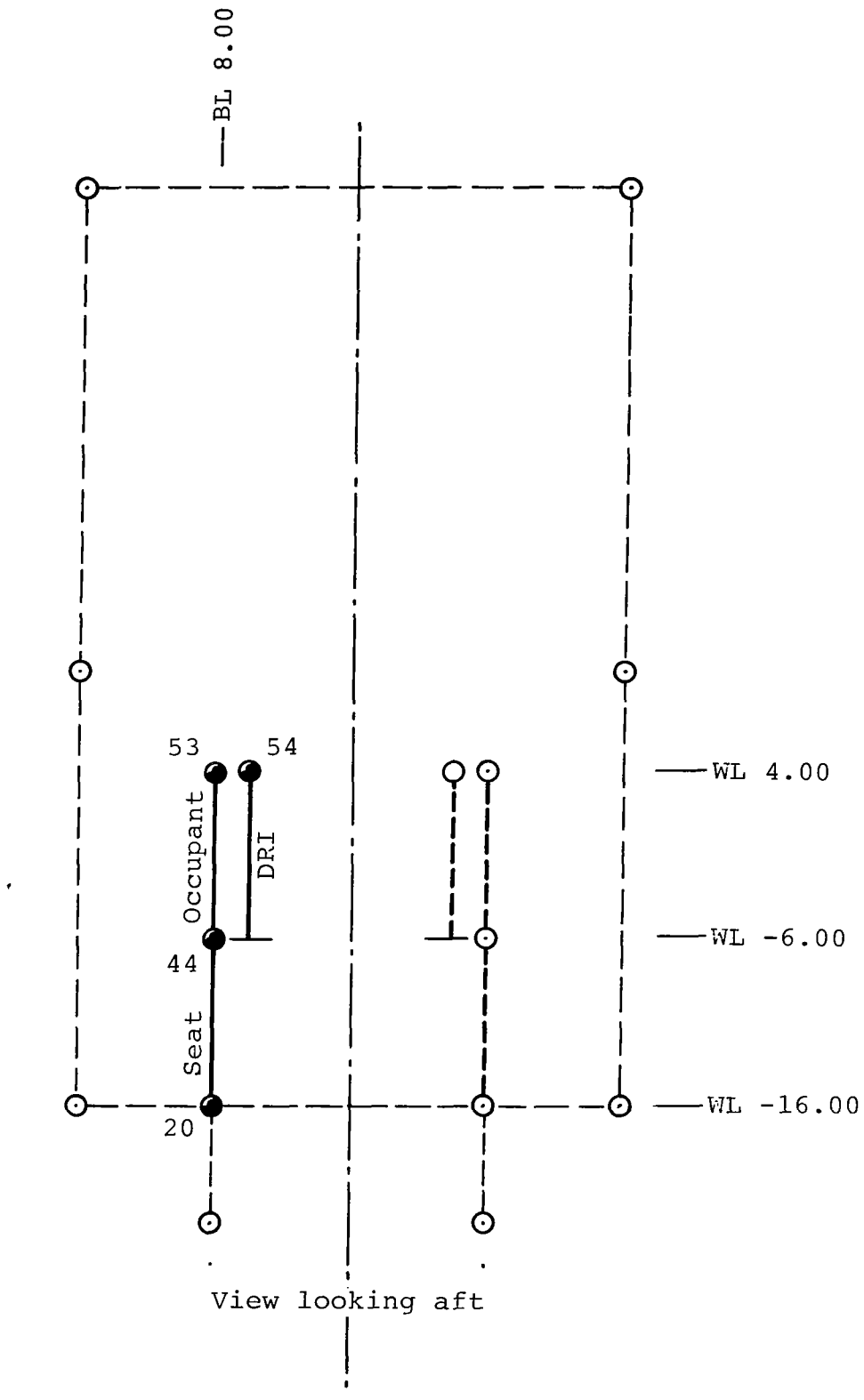

Figure F-18. Occupant seat modeling at STA 210.

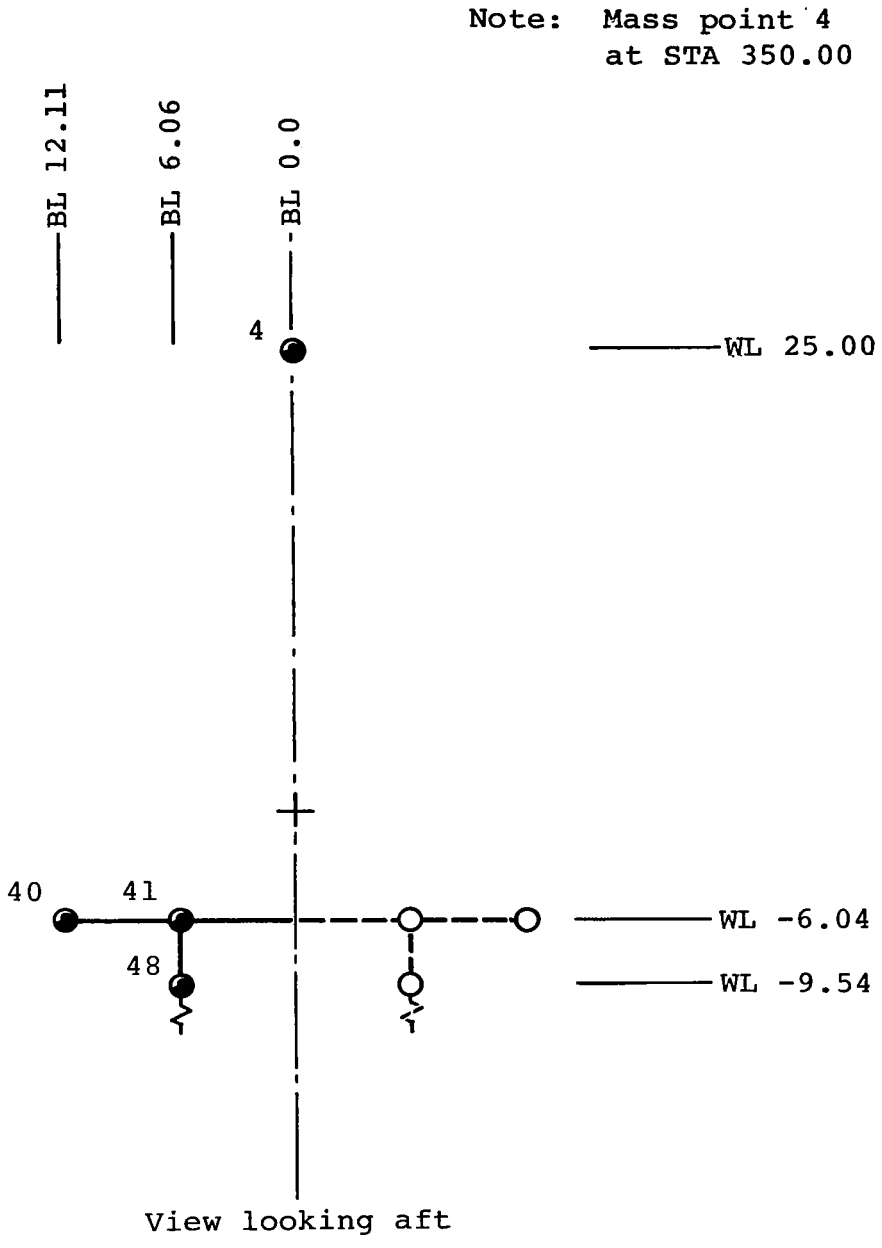

Figure F-19. Fuselage bulkhead model at STA 244.

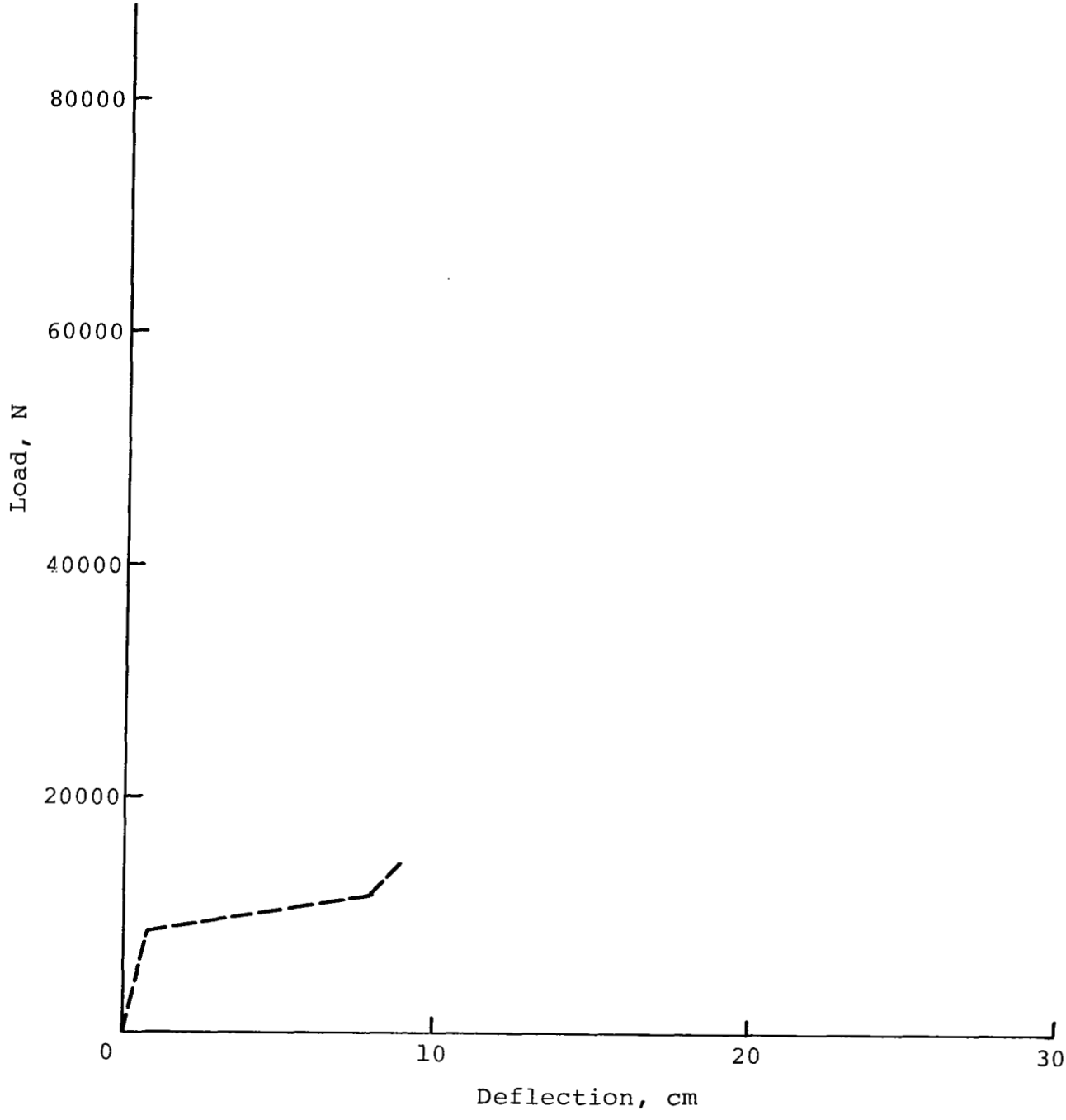

Figure F-20. Load-deflection parameters for nonlinear beam 41-48 at STA 244.

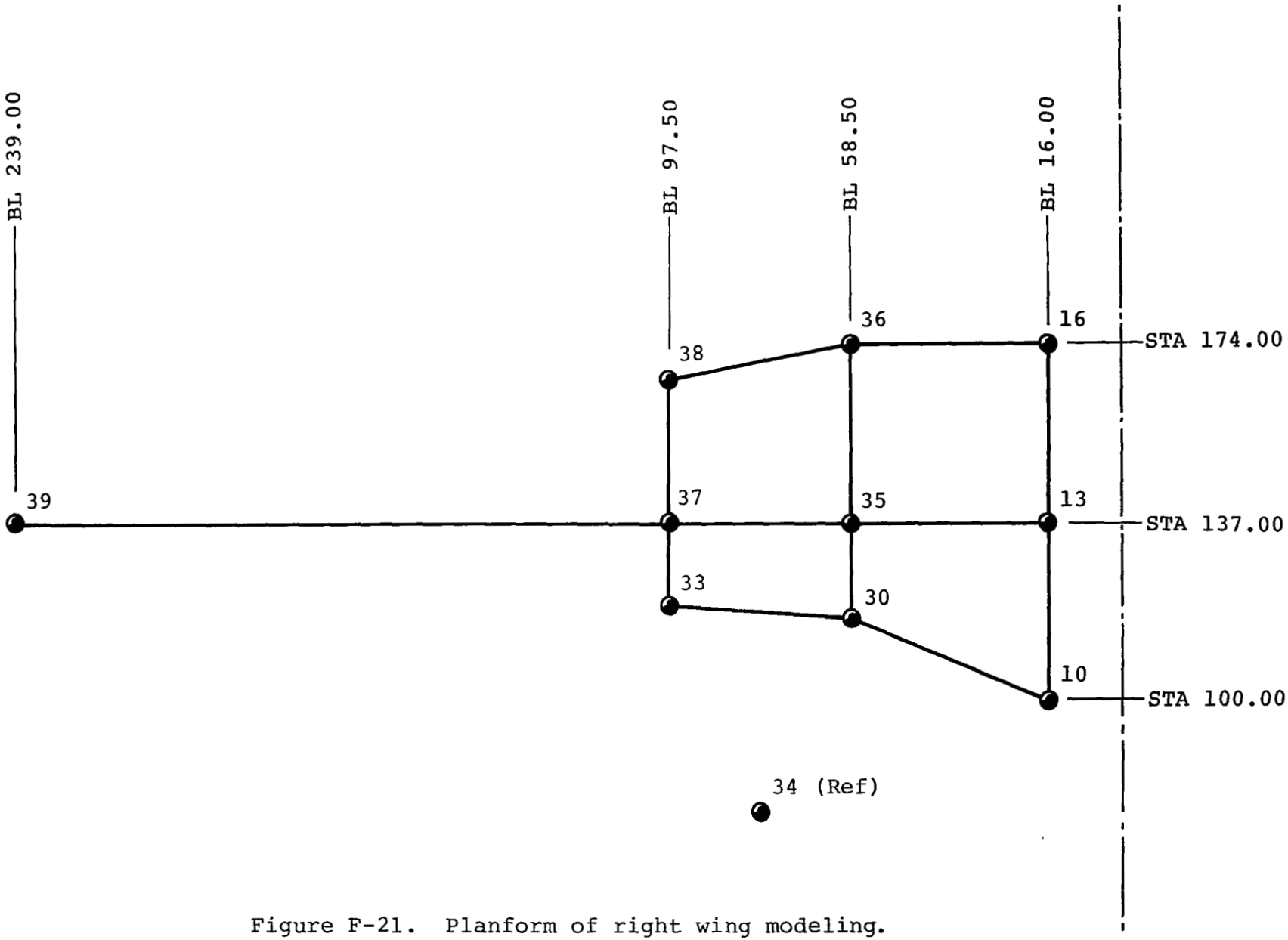

Figure F-21. Planform of right wing modeling.

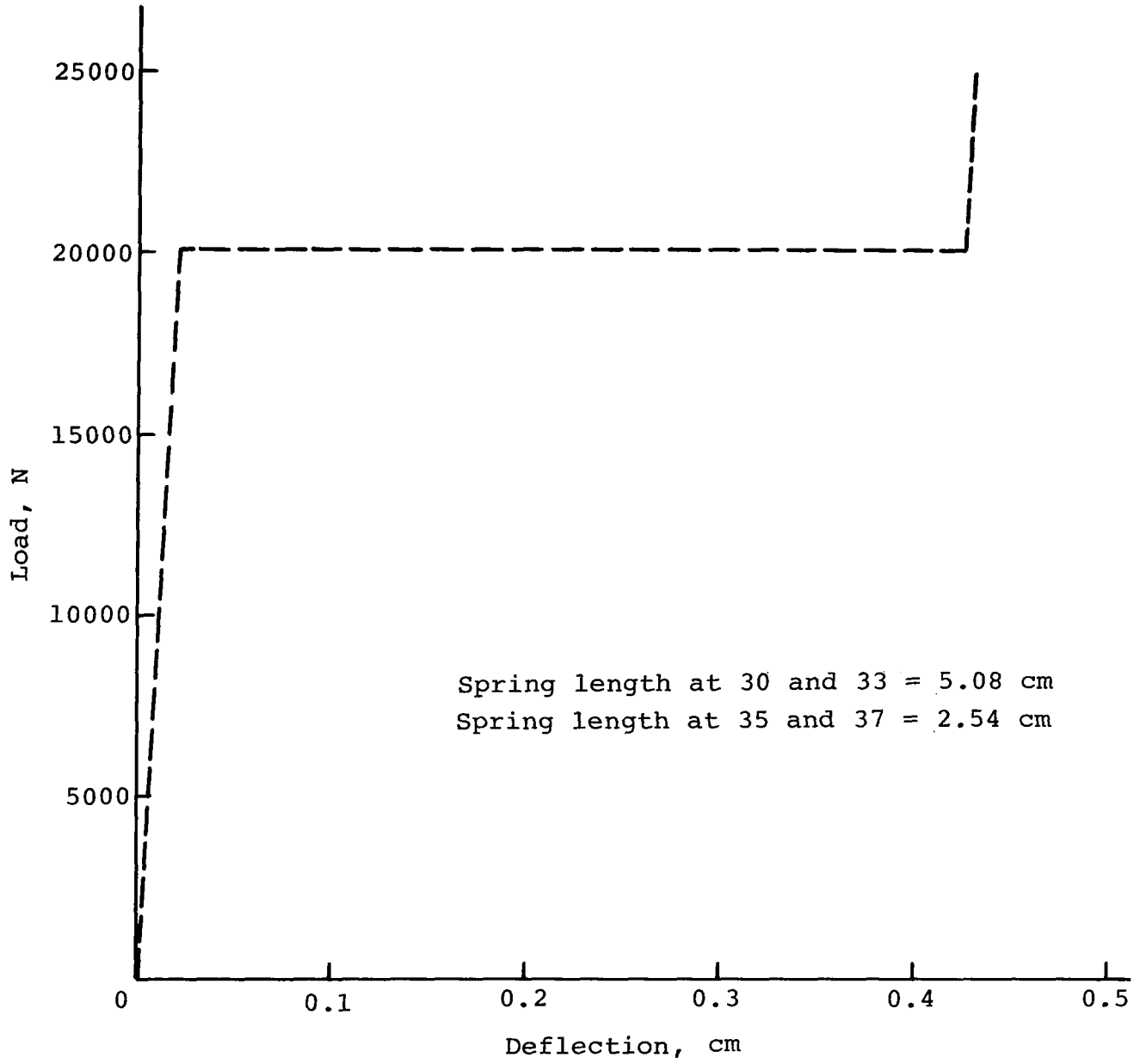

Figure F-22. Load deflection parameters for wing crushing springs at mass points 30, 33, 35, and 37.

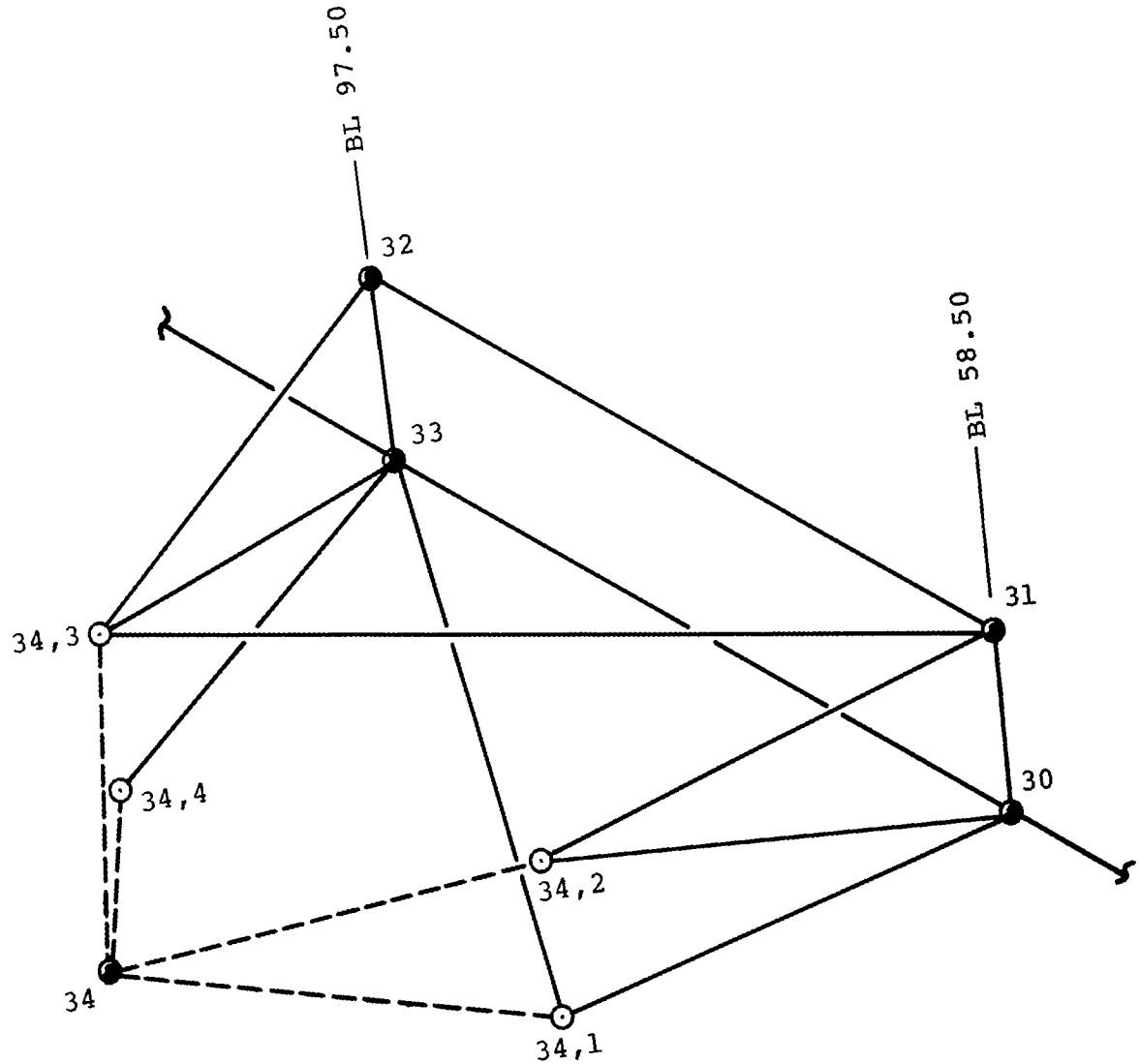

Engine and support structure modeling.

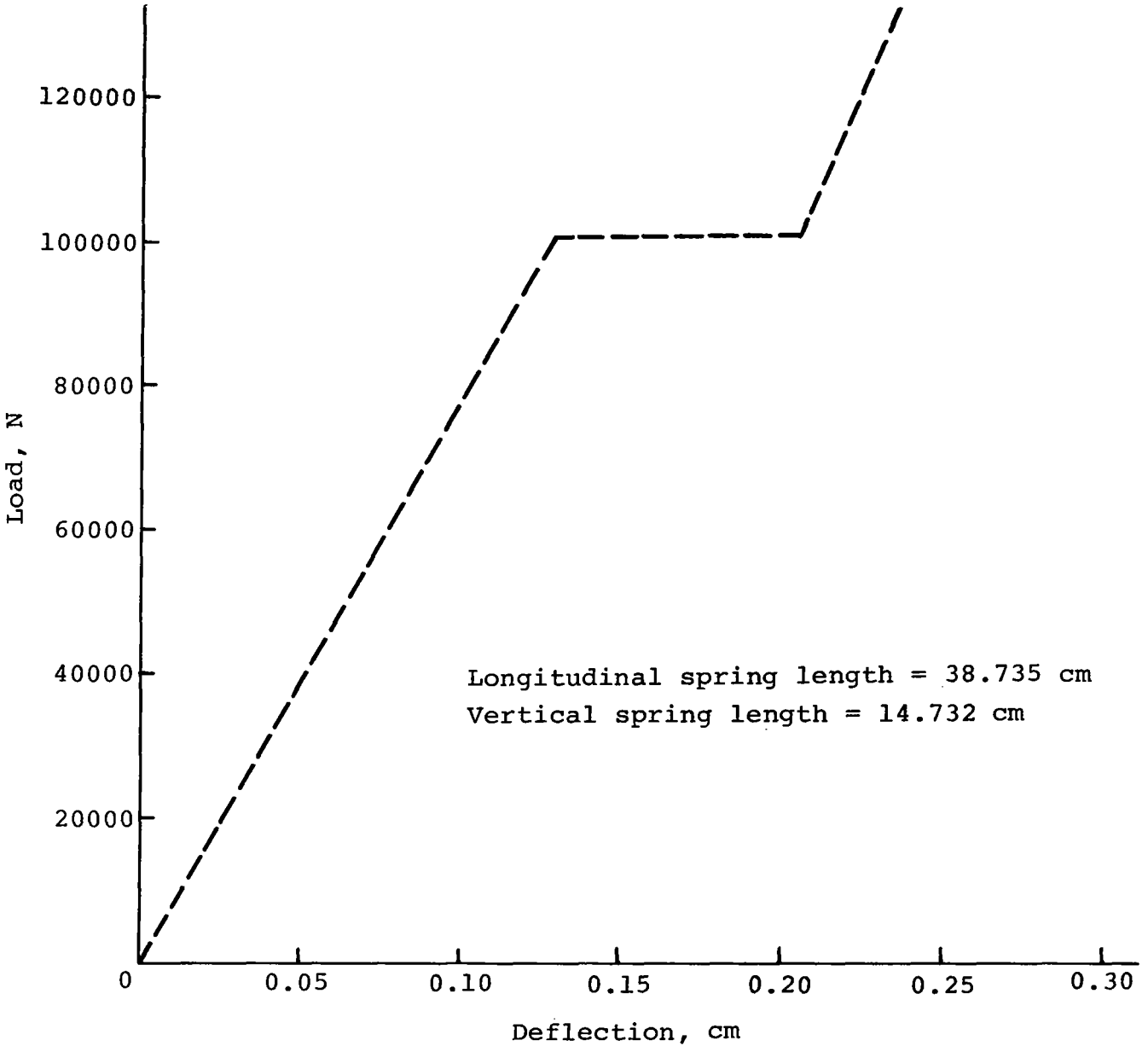

Figure F-24. Load-deflection parameters for engine cg crushing springs at mass point 34.

```
KRASH MODEL PER GIL WITTLIN - 60 MPH CRASH TEST #4
CORRUGATED WEB SUBFLOOR CONCEPT  - DKSN06 VERSION - 16 FEB 82
123456789012345678901234567890123456789012345678901234567890123456789012
   54   14  102   31    4    0    0    3    0    0    0    0    0   18
    0    0    0    0    0    0    032750327503275O    0    0

NAVA                 1          10          20          30          40
           1000  0.000001  0.040000        0.0         0.0         1.0

    1    1    1    1    1    0    0    0    1
   54    4  102  102    0   13    0    3    0    0
1020.01760       0.0 273.31296
       0.0       0.0       0.0
       0.0 0.0698132       0.0       0.0         0.0         0.0
   3.200     30.00     -8.00    -13.00       0.719     0.614     0.614
   3.100     30.00     -8.00      5.00       0.696     0.595     0.595
   6.000     59.00     -8.00    -13.00       0.405     0.965     0.933
 223.500    350.00      0.00     25.00     108.565  3390.802  3390.802
   6.000     59.00    -16.00    -13.00       0.251     0.965     0.778
   5.900     59.00    -16.00     14.00       0.583     0.949     1.102
   3.500     81.00    -16.00    -13.00       0.267     0.536     0.366
   3.600     81.00     -8.00    -13.00       0.336     0.551     0.438
   3.500     81.00    -16.00     20.00       0.521     0.536     0.620
  18.500    100.00    -16.00    -15.00       0.760     3.420     3.381
  12.000    100.00     -8.00    -15.00       0.632     2.218     2.332
  11.900    100.00    -16.00     10.00       1.930     2.685     3.130
  55.200    137.00    -16.00    -16.00      69.691    72.976     4.396
  25.100    137.00     -8.00    -16.00      34.846    35.852     1.553
  10.900    137.00    -16.00     10.00       1.393     1.640     0.322
 108.800    174.00    -16.00    -16.00     139.306   146.690     9.516
  52.550    174.00     -8.00    -16.00      69.513    72.719     4.237
  10.600    174.00    -16.00     10.00       1.355     1.595     0.313
  30.000    210.00    -16.00    -16.00       1.441    23.901    24.173
  15.000    210.00     -8.00    -16.00       0.759    11.950    12.124
  28.000    210.00    -16.00     10.00       3.578     4.213     0.827
  26.800    100.00    -15.00     10.00      15.700    15.700     0.035
```

26.700	100.00	-9.00	10.00	15.700	15.700	0.035
74.600	136.00	-15.00	10.00	43.970	43.970	0.098
5.900	110.00	-16.00	34.00	0.757	0.135	0.785
10.600	137.00	-16.00	39.00	1.493	3.533	4.568
10.400	174.00	-16.00	39.00	1.464	3.134	4.150
27.820	210.00	-16.00	39.00	3.917	22.222	24.938
74.600	136.00	-9.00	10.00	43.970	43.970	0.098
90.960	117.00	-58.50	-14.04	31.993	2.954	30.698
28.100	117.40	-58.50	-4.44	9.883	0.912	9.483
28.100	119.30	-97.50	-1.75	9.883	0.730	9.301
181.920	119.30	-97.50	-11.35	63.985	4.729	60.218
744.100	77.00	-78.00	-5.69	216.868	686.750	686.750
181.920	137.00	-58.50	-14.04	63.664	57.694	113.504
90.960	174.00	-58.50	-14.04	31.832	34.174	62.078
363.830	137.00	-97.50	-11.35	127.325	115.386	227.001
181.920	166.50	-97.50	-11.35	63.664	45.411	101.220
184.500	137.00	-239.00	-1.60	2372.848	113.321	2483.301
30.000	244.00	-12.11	-6.04	1.441	23.901	24.173
15.000	244.00	-6.06	-6.04	0.759	11.950	12.124
73.200	137.00	-8.00	-6.00	60.000	60.000	60.000
73.200	174.00	-8.00	-6.00	60.000	60.000	60.000
73.200	210.00	-8.00	-6.00	60.000	60.000	60.000
25.100	137.00	-8.00	-23.00	34.846	35.852	1.553
52.550	174.00	-8.00	-23.00	69.513	72.719	4.237
15.000	210.00	-8.00	-23.00	0.759	11.950	12.124
15.000	244.00	-6.06	-9.54	0.759	11.950	12.124
60.000	137.00	-8.00	4.00	60.000	60.000	60.000
60.000	174.00	-8.00	4.00	60.000	60.000	60.000
60.000	210.00	-8.00	4.00	60.000	60.000	60.000
60.000	137.00	-8.00	4.00	60.000	60.000	60.000
60.000	174.00	-8.00	4.00	60.000	60.000	60.000
60.000	210.00	-8.00	4.00	60.000	60.000	60.000
1	34	92.25	-64.74	-12.41		
2	34	92.25	-64.74	-4.01		
3	34	92.25	-91.27	-2.18		
4	34	92.25	-91.27	-10.58		
0 3	3	8.00	0.40	48000.0	0.0	0.0

```
0  8     3   11.00       0.40       40000.0       0.0        0.0
0 11     3    9.00       0.40       44000.0       0.0        0.0
0 45     3    1.00       0.40     1058536.5       0.0        0.0
0 46     3    1.00       0.40     2492682.8       0.0        0.0
0 47     3    1.00       0.40     2439004.8       0.0        0.0
0 48     3    1.00       0.40     1209736.5       0.0        0.0
0  1     3    4.00       0.40       33200.0       0.0        0.0
0 35     3    1.00       0.40      600000.0       0.0        0.0
0 37     3    1.00       0.40      600000.0       0.0        0.0
0 30     3    2.00       0.40      600000.0       0.0        0.0
0 33     3    2.00       0.40      600000.0       0.0        0.0
0 34     1   15.25       0.40      600000.0       0.0        0.0
0 34     3    5.80       0.40      600000.0       0.0        0.0
   0.25       0.30       1.00        4.50        9310.00    3500.0        0.0
   0.25       0.30       1.00        5.50       11300.00    4300.0        0.0
   0.25       0.30       1.00        5.00       17500.00    6600.0        0.0
   0.10       0.10001    1.00        1.00001    52926.83   529268.3       0.0
   0.10       0.10001    1.00        1.00001   124634.14  1246341.4       0.0
   0.10       0.10001    1.00        1.00001   121950.24  1219502.4       0.0
   0.10       0.10001    1.00        1.00001    60486.83   604868.3       0.0
   0.25       0.30       1.00        4.50        4050.00    1500.0        0.0
   0.01       0.02       0.03        0.20        4500.00    4500.0        0.0
   0.01       0.02       0.03        0.20        4500.00    4500.0        0.0
   0.01       0.02       0.03        0.20        4500.00    4500.0        0.0
   0.01       0.02       0.03        0.20        4500.00    4500.0        0.0
   0.05       0.06       0.07        0.08       22500.00   22500.0        0.0
   0.05       0.06       0.07        0.08       22500.00   22500.0        0.0
0  1 0  0   0.53529      0.0       1.220000    0.014138       0.0   0.0   0.0 4
0  2 0  0   0.26086      0.0       0.284860    0.009417       0.0   0.0   0.0 4
0  1 0  2   0.04967      0.0       0.004710    0.044960       0.0   0.0   0.0 4
0  3 0  5   0.34329      0.0       0.268870    0.010554       0.0   0.0   0.0 4
0  5 0  6   0.08563      0.0       0.003120    0.029280       0.0   0.0   0.0 4
0  8 0  0   0.37926      0.0       3.173400    0.007992       0.0   0.0   0.0 4
0  7 0  8   0.49369      0.0       3.263000    0.011510       0.0   0.0   0.0 4
0  7 0  9   0.39347      0.0       0.005910    1.758974       0.0   0.0   0.0 4
0  9 0  0   0.59974      0.0       7.233200    0.055420       0.0   0.0   0.0 4
0 11 0  0   0.58854      0.0       3.951800    0.008520       0.0   0.0   0.0 4
```

0	10	0	11	0.37926	0.0	3.173400	0.007992	0.0	0.0	0.0	4
0	10	0	12	0.23526	0.0	0.007101	0.197950	0.0	0.0	0.0	4
0	12	0	0	0.25126	0.0	10.186000	0.007250	0.0	0.0	0.0	4
0	1	0	3	0.83751	0.0	7.873200	9.146200	0.0	0.0	0.0	4
0	2	0	6	0.19686	0.0	0.472330	3.977220	0.0	0.0	0.0	4
0	3	0	8	2.00060	0.0	120.930000	2.322900	0.0	0.0	0.0	4
0	8	0	11	0.61568	0.0	4.182300	0.060520	0.0	0.0	0.0	4
0	5	0	7	0.14963	0.0	0.352290	1.181700	0.0	0.0	0.0	4
0	7	0	10	0.21645	0.0	8.161530	5.443600	0.0	0.0	0.0	4
0	6	0	9	0.31966	0.0	0.562840	16.589800	0.0	0.0	0.0	4
0	9	0	12	0.32870	0.0	2.213900	5.361600	0.0	0.0	0.0	4
0	6	0	0	0.08563	0.0	0.029280	0.003116	0.0	0.0	0.0	4
0	4	0	28	0.37630	0.0	12.357200	13.130450	0.0	0.0	0.0	4
0	4	0	40	0.41830	0.0	30.579700	16.329840	0.0	0.0	0.0	4
0	14	0	0	1.17710	0.0	7.903600	0.017040	0.0	0.0	0.0	4
0	13	0	14	0.96588	0.0	4.268800	0.016600	0.0	0.0	0.0	4
0	13	0	15	0.35289	0.0	0.010652	0.296920	0.0	0.0	0.0	4
0	17	0	0	1.62710	0.0	11.498000	11.026260	0.0	0.0	0.0	4
0	16	0	17	1.79640	0.0	7.873000	0.155560	0.0	0.0	0.0	4
0	16	0	18	1.38136	0.0	0.052729	0.908478	0.0	0.0	0.0	4
0	20	0	0	0.88281	0.0	5.927700	0.012780	0.0	0.0	0.0	4
0	19	0	20	0.72420	0.0	3.201600	0.012450	0.0	0.0	0.0	4
0	19	0	21	0.23526	0.0	7.123710	0.197950	0.0	0.0	0.0	4
0	11	0	14	0.76672	0.0	5.770140	14.621800	0.0	0.0	0.0	4
0	14	0	17	0.96766	0.0	5.761740	12.206400	0.0	0.0	0.0	4
0	17	0	20	0.41355	0.0	5.761740	12.206400	0.0	0.0	0.0	4
0	10	0	13	0.35258	0.0	0.023790	0.155300	0.0	0.0	0.0	4
0	13	0	16	0.35258	0.0	0.023790	0.155300	0.0	0.0	0.0	4
0	16	0	19	0.35258	0.0	0.023790	0.155300	0.0	0.0	0.0	4
0	12	0	25	0.11763	0.0	0.003550	0.098970	0.0	0.0	0.0	4
0	25	0	0	0.23354	0.0	0.144810	0.098970	0.0	0.0	0.0	4
0	15	0	26	0.23526	0.0	0.197950	0.007100	0.0	0.0	0.0	4
0	26	0	0	0.23526	0.0	0.007100	0.197950	0.0	0.0	0.0	4
0	18	0	27	0.23526	0.0	0.197950	0.007100	0.0	0.0	0.0	4
0	27	0	0	0.23526	0.0	0.007100	0.197950	0.0	0.0	0.0	4
0	21	0	28	0.23526	0.0	0.197950	0.007100	0.0	0.0	0.0	4
0	28	0	0	0.23526	0.0	0.007100	0.197950	0.0	0.0	0.0	4

0	12	0	15	0.28518	0.0	14.017300	0.186950	0.0	0.0	0.0	4
0	15	0	18	0.30918	0.0	15.294000	0.200310	0.0	0.0	0.0	4
0	18	0	21	0.30918	0.0	15.294000	0.200310	0.0	0.0	0.0	4
0	25	0	26	0.36612	0.0	4.114600	18.881700	0.0	0.0	0.0	4
0	26	0	27	0.33012	0.0	3.798100	17.740600	0.0	0.0	0.0	4
0	27	0	28	0.33012	0.0	3.798100	17.740600	0.0	0.0	0.0	4
0	30	1	34	0.07056	0.0	0.004570	0.004570	0.0	0.0	0.0	1
0	30	2	34	0.18408	0.0	0.020310	0.020310	0.0	0.0	0.0	1
0	31	2	34	0.07056	0.0	0.004570	0.004570	0.0	0.0	0.0	1
0	31	3	34	0.07056	0.0	0.004570	0.004570	0.0	0.0	0.0	1
0	32	3	34	0.07056	0.0	0.004570	0.004570	0.0	0.0	0.0	1
0	33	1	34	0.07056	0.0	0.004570	0.004570	0.0	0.0	0.0	1
0	33	3	34	0.18408	0.0	0.020310	0.020310	0.0	0.0	0.0	1
0	33	4	34	0.07056	0.0	0.004570	0.004570	0.0	0.0	0.0	1
0	16	0	36	0.62915	0.0	3.225800	5.586500	0.0	0.0	0.0	4
0	36	0	38	0.76660	0.0	3.089900	11.354000	0.0	0.0	0.0	4
0	37	0	39	3.75000	0.0	35.113000	391.000000	0.0	0.0	0.0	4
0	35	0	37	3.41700	0.0	85.141000	26.658000	0.0	0.0	0.0	4
0	13	0	35	3.06140	0.0	112.640000	1.050200	0.0	0.0	0.0	4
0	30	0	33	0.53484	0.0	2.949200	2.715880	0.0	0.0	0.0	4
0	10	0	30	0.45120	0.0	2.403480	0.027180	0.0	0.0	0.0	4
0	32	0	33	0.46565	0.0	6.229510	6.049500	0.0	0.0	0.0	4
0	31	0	32	0.20040	0.0	0.109800	0.105510	0.0	0.0	0.0	4
0	30	0	31	0.46565	0.0	6.229500	6.049500	0.0	0.0	0.0	4
0	33	0	37	0.37990	0.0	1.040570	0.004270	0.0	0.0	0.0	4
0	32	0	37	0.75261	0.0	11.258700	3.051800	0.0	0.0	0.0	4
0	30	0	35	0.37990	0.0	1.040570	0.004270	0.0	0.0	0.0	4
0	31	0	35	0.75261	0.0	11.258700	3.051800	0.0	0.0	0.0	4
0	35	0	36	0.27360	0.0	3.637310	0.008710	0.0	0.0	0.0	4
0	37	0	38	0.27360	0.0	3.637310	0.008710	0.0	0.0	0.0	4
0	22	0	23	0.20931	0.0	0.300050	0.010060	0.0	0.0	0.0	4
0	24	0	29	0.27976	0.0	1.135590	0.016560	0.0	0.0	0.0	4
0	22	0	24	0.20931	0.0	0.300050	0.010060	0.0	0.0	0.0	4
0	10	0	22	0.13988	0.0	0.008280	0.008280	0.0	0.0	0.0	4
0	13	0	24	0.15417	0.0	0.021160	0.021160	0.0	0.0	0.0	4
0	23	0	29	0.20931	0.0	0.300050	0.010060	0.0	0.0	0.0	4
0	14	0	29	0.15417	0.0	0.021160	0.021160	0.0	0.0	0.0	4

```
0 11 0 23  0.13988     0.0      0.008280  0.008280       0.0  0.0  0.0 4
0 14 0 45 .0035285     0.0      0.010652  0.296920       0.0  0.0  0.0 4
0 17 0 46 .0083089     0.0      0.052729  0.908478       0.0  0.0  0.0 4
0 20 0 47 .0081300     0.0      7.123710  0.197950       0.0  0.0  0.0 4
0 41 0 48 .0020162     0.0      7.123710  0.197950       0.0  0.0  0.0 4
0 14 0 42 .0182286     0.0      7.123710  0.197950       0.0  0.0  0.0 4
0 17 0 43 .0182286     0.0      7.123710  0.197950       0.0  0.0  0.0 4
0 20 0 44 .0182286     0.0      7.123710  0.197950       0.0  0.0  0.0 4
0 40 0 41  0.72420     0.0      3.201600  0.012450       0.0  0.0  0.0 4
0 41 0  0  0.88281     0.0      5.927700  0.012780       0.0  0.0  0.0 4
0 20 0 41  0.41355     0.0      5.761740 12.206400       0.0  0.0  0.0 4
0 19 0 40  0.35258     0.0      0.023790  0.155300       0.0  0.0  0.0 4
0 42 0 49 .0039270     0.0      2.810000  2.810000       0.0  0.0  0.0 9
0 42 0 50 .0061370     0.0      2.810000  2.810000       0.0  0.0  0.010
0 43 0 51 .0039270     0.0      2.810000  2.810000       0.0  0.0  0.0 9
0 43 0 52 .0061370     0.0      2.810000  2.810000       0.0  0.0  0.010
0 44 0 53 .0039270     0.0      2.810000  2.810000       0.0  0.0  0.0 9
0 44 0 54 .0061370     0.0      2.810000  2.810000       0.0  0.0  0.010
     0.01
0 30 1 34  0.005
0 30 2 34  0.005
0 31 2 34  0.005
0 31 3 34  0.005
0 32 3 34  0.005
0 33 1 34  0.005
0 33 3 34  0.005
0 33 4 34  0.005
0 30 0 31  0.005
0 31 0 35  0.005
0 32 0 33  0.005
0 32 0 37  0.005
0 42 0 49  0.300
0 42 0 50  0.220
0 43 0 51  0.300
0 43 0 52  0.220
0 44 0 53  0.300
0 44 0 54  0.220
```

```
 0  1 0  2    1    5 0.06340
 0  1 0  0    1    5 0.05640
 0  2 0  0    1    5 0.05640
 0  3 0  5    1    5 0.02819
 0  5 0  6    1    5 0.95100
 0  8 0  0    1    5 0.05640
 0  7 0  8    1    5 0.02819
 0  7 0  9    1    5 0.11630
 0 11 0  0    1    5 0.05640
 0 10 0 11    1    5 0.02819
 0 10 0 12    1    5 0.08809
 0 12 0  0    1    5 0.11280
 0  1 0  3    1    5 0.10220
 0  3 0  8    1    5 0.07752
 0  8 0 11    1    5 0.06732
 0  5 0  7    1    5 0.07752
 0  7 0 10    1    5 0.06732
 0 14 0  0    1    5 0.05638
 0 13 0 14    1    5 0.02819
 0 11 0 14    1    5 0.13040
 0 10 0 13    1    5 0.13040
 0 30 1 34    1    6 0.05000
 0 33 1 34    1    6 0.03008
 0 33 4 34    1    6 0.04604
 0 14 0 45    1   10 0.32500   0.0
 0 17 0 46    1   10 0.32500   0.0
 0 20 0 47    1   10 0.32500   0.0
 0 41 0 48    1   10 0.32500   0.0
 0 14 0 42    1    5 0.10000   0.0
 0 17 0 43    1    5 0.10000   0.0
 0 20 0 44    1    5 0.10000   0.0
0.0        1.00
0.325000   1.00
0.325001   0.04171934
1.00       0.04171934
2.00       0.04171934
3.00       0.04171934
```

3.150000	0.04171934
3.150001	0.26890760
4.00	0.26890760
7.00	0.26890760
0.0	1.00
0.325000	1.00
0.325001	0.04171934
1.00	0.04171934
2.00	0.04171934
3.00	0.04171934
3.150000	0.04171934
3.150001	0.26890760
4.00	0.26890760
7.00	0.26890760
0.0	1.00
0.325000	1.00
0.325001	0.04171934
1.00	0.04171934
2.00	0.04171934
3.00	0.04171934
3.150000	0.04171934
3.150001	0.26890760
4.00	0.26890760
7.00	0.26890760
0.0	1.00
0.325000	1.00
0.325001	0.04171934
1.00	0.04171934
2.00	0.04171934
3.00	0.04171934
3.150000	0.04171934
3.150001	0.26890760
3.25	0.26890760
3.50	0.26890760

42	50	43	52	44	54				
1	0	0	0	0	0	1	0	0	0
2	0	0	0	0	0	1	0	0	0

3	0	0	0	0	0	1	0	0	0
4	0	0	0	0	0	1	0	0	0
5	0	0	0	0	0	1	0	0	0
6	0	0	0	0	0	1	0	0	0
7	0	0	0	0	0	1	0	0	0
8	0	0	0	0	0	1	0	0	0
9	0	0	0	0	0	1	0	0	0
10	0	0	0	0	0	1	0	0	0
11	0	0	0	0	0	1	0	0	0
12	0	0	0	0	0	1	0	0	0
13	0	0	0	0	0	1	0	0	0
14	0	0	0	0	0	1	0	0	0
15	0	0	0	0	0	1	0	0	0
16	0	0	0	0	0	1	0	0	0
17	0	0	0	0	0	1	0	0	0
18	0	0	0	0	0	1	0	0	0
19	0	0	0	0	0	1	0	0	0
20	0	0	0	0	0	1	0	0	0
21	0	0	0	0	0	1	0	0	0
22	0	0	0	0	0	1	0	0	0
23	0	0	0	0	0	1	0	0	0
24	0	0	0	0	0	1	0	0	0
25	0	0	0	0	0	1	0	0	0
26	0	0	0	0	0	1	0	0	0
27	0	0	0	0	0	1	0	0	0
28	0	0	0	0	0	1	0	0	0
29	0	0	0	0	0	1	0	0	0
30	0	0	0	0	0	1	0	0	0
31	0	0	0	0	0	1	0	0	0
32	0	0	0	0	0	1	0	0	0
33	0	0	0	0	0	1	0	0	0
34	0	0	0	0	0	1	0	0	0
35	0	0	0	0	0	1	0	0	0
36	0	0	0	0	0	1	0	0	0
37	0	0	0	0	0	1	0	0	0
38	0	0	0	0	0	1	0	0	0
39	0	0	0	0	0	1	0	0	0

40	0	0	0	0	0	1	0	0	0
41	0	0	0	0	0	1	0	0	0
42	0	0	0	0	0	1	0	0	0
43	0	0	0	0	0	1	0	0	0
44	0	0	0	0	0	1	0	0	0
45	0	0	0	0	0	1	0	0	0
46	0	0	0	0	0	1	0	0	0
47	0	0	0	0	0	1	0	0	0
48	0	0	0	0	0	1	0	0	0
49	0	0	0	0	0	1	0	0	0
50	0	0	0	0	0	1	0	0	0
51	0	0	0	0	0	1	0	0	0
52	0	0	0	0	0	1	0	0	0
53	0	0	0	0	0	1	0	0	0
54	0	0	0	0	0	1	0	0	0
1	34	0	0	0	1	0	0		
2	34	0	0	0	1	0	0		
3	34	0	0	0	1	0	0		
4	34	0	0	0	1	0	0		
1	1	0	0						
2	1	0	0						
3	1	0	0						
4	1	0	0						
5	1	0	0						
6	1	0	0						
7	1	0	0						
8	1	0	0						
9	1	0	0						
10	1	0	0						
11	1	0	0						
12	1	0	0						
13	1	0	0						
14	1	0	0						
15	1	0	0						
16	1	0	0						
17	1	0	0						
18	1	0	0						

19	1	0	0
20	1	0	0
21	1	0	0
22	1	0	0
23	1	0	0
24	1	0	0
25	1	0	0
26	1	0	0
27	1	0	0
28	1	0	0
29	1	0	0
30	1	0	0
31	1	0	0
32	1	0	0
33	1	0	0
34	1	0	0
35	1	0	0
36	1	0	0
37	1	0	0
38	1	0	0
39	1	0	0
40	1	0	0
41	1	0	0
42	1	0	0
43	1	0	0
44	1	0	0
45	1	0	0
46	1	0	0
47	1	0	0
48	1	0	0
49	1	0	0
50	1	0	0
51	1	0	0
52	1	0	0
53	1	0	0
54	1	0	0
55	1	0	0

56	1	0	0
57	1	0	0
58	1	0	0
59	1	0	0
60	1	0	0
61	1	0	0
62	1	0	0
63	1	0	0
64	1	0	0
65	1	0	0
66	1	0	0
67	1	0	0
68	1	0	0
69	1	0	0
70	1	0	0
71	1	0	0
72	1	0	0
73	1	0	0
74	1	0	0
75	1	0	0
76	1	0	0
77	1	0	0
78	1	0	0
79	1	0	0
80	1	0	0
81	1	0	0
82	1	0	0
83	1	0	0
84	1	0	0
85	1	0	0
86	1	0	0
87	1	0	0
88	1	0	0
89	1	0	0
90	1	0	0
91	1	0	0
92	1	0	0

93	1	0	0
94	1	0	0
95	1	0	0
96	1	0	0
97	1	0	0
98	1	0	0
99	1	0	0
100	1	0	0
101	1	0	0
102	1	0	0
1	1	0	0
2	1	0	0
3	1	0	0
4	1	0	0
5	1	0	0
6	1	0	0
7	1	0	0
8	1	0	0
9	1	0	0
10	1	0	0
11	1	0	0
12	1	0	0
13	1	0	0
14	1	0	0
15	1	0	0
16	1	0	0
17	1	0	0
18	1	0	0
19	1	0	0
20	1	0	0
21	1	0	0
22	1	0	0
23	1	0	0
24	1	0	0
25	1	0	0
26	1	0	0
27	1	0	0

28	1	0	0
29	1	0	0
30	1	0	0
31	1	0	0
32	1	0	0
33	1	0	0
34	1	0	0
35	1	0	0
36	1	0	0
37	1	0	0
38	1	0	0
39	1	0	0
40	1	0	0
41	1	0	0
42	1	0	0
43	1	0	0
44	1	0	0
45	1	0	0
46	1	0	0
47	1	0	0
48	1	0	0
49	1	0	0
50	1	0	0
51	1	0	0
52	1	0	0
53	1	0	0
54	1	0	0
55	1	0	0
56	1	0	0
57	1	0	0
58	1	0	0
59	1	0	0
60	1	0	0
61	1	0	0
62	1	0	0
63	1	0	0
64	1	0	0

65	1	0	0
66	1	0	0
67	1	0	0
68	1	0	0
69	1	0	0
70	1	0	0
71	1	0	0
72	1	0	0
73	1	0	0
74	1	0	0
75	1	0	0
76	1	0	0
77	1	0	0
78	1	0	0
79	1	0	0
80	1	0	0
81	1	0	0
82	1	0	0
83	1	0	0
84	1	0	0
85	1	0	0
86	1	0	0
87	1	0	0
88	1	0	0
89	1	0	0
90	1	0	0
91	1	0	0
92	1	0	0
93	1	0	0
94	1	0	0
95	1	0	0
96	1	0	0
97	1	0	0
98	1	0	0
99	1	0	0
100	1	0	0
101	1	0	0

```
   102     1     0     0
     1     0     1     1
     3     0     1     1
     8     0     1     1
    11     0     1     1
    30     0     1     1
    33     0     1     1
    34     0     1     1
    35     0     1     1
    37     0     1     1
    45     0     1     1
    46     0     1     1
    47     0     1     1
    48     0     1     1
    50
    52
    54
END
```

REFERENCES

1. Walhout, G. J.: Crashworthiness Observations in General Aviation Accident Investigations - A Statistical Overview. Aircraft Crashworthiness, University Press of Virginia, 1975.

2. Thomson, R. G; and Goetz, R. C.: NASA/FAA General Aviation Crash Dynamics Program - A Status Report, AIAA paper 79-0780, presented at the AIAA/ASME/ASCE/AHS 20th Structure Dynamics and Harness Conference, St. Louis, Mo., April 1979.

3. Carden, H. D.; and Hayduk, R. J.: Aircraft Subfloor Response to Crash Landings, paper 810614 presented at SAE Business Aircraft Meeting and Exposition, Wichita, Ks., April 1981.

4. Cronkhite, J. D.; Haas, T. J.; Berry, V. L.; and Winter, R.: Investigation of the Crash Impact Characteristics of Advanced Airframe Structures, USARTL Technical Report 79-11, The Applied Technology Laboratory, U.S. Army Research and Technology Laboratory (AVRADCOM), Ft. Eustis, Va., September 1979.

5. Crash Survival Design Guide, USARTL Technical Report 79-22, The Applied Technology Laboratory, U.S. Army Research and Technology Laboratory (AVRADCOM), Ft. Eustis, Va., August 1980.

6. The NASTRAN User's Manual, NASA SP-222(03) National Aeronautics and Space Administration, Washington, D.C., July 1976.

7. Wittlin, G.; and Gamon, M. A.: General Aviation Airplane Structural Crashworthiness User's Manual, 3 Vols., DOT Report Number FAA-RD-77-189, U. S. Department of Transportation, Federal Aviation Administration, Systems Research and Development Service, Washington, D.C., February 1978.

8. Reilly, M. J.; and Tanner, A. E.: Development of Crashworthy Passenger Seats for General Aviation Aircraft. NASA CR-159100, 1978.

9. Military Standardization Handbook, Metallic Materials and Elements for Aerospace Vehicle Structures, MIL-HDBK-5C, 2 Vols., Department of Defense, Washington, D.C., September 1976.

10. Bruhn, E. F.: Analysis and Design of Flight Vehicle Structures, Tri-State Offset Company, June 1973.

*U.S. GOVERNMENT PRINTING OFFICE: 1982 539-007/15 1-3